

AD-A066 380

SHAPE TECHNICAL CENTER THE HAGUE (NETHERLANDS)
THE COMBINED US/NATO DIGITAL TROPOSCATTER TEST PROGRAMME OVER T--ETC(U)
DEC 78 P NIELSEN, J OSTERHOLZ, E PUSONE

F/G 17/2.1

UNCLASSIFIED

STC-CR-NICS-38

DCEC-TR-12-78

NL

1 OF 3
ADA
066380



NATO UNCLASSIFIED

LEVEL

FILE REF: 9980

SHAPE Technical Centre
Centre Technique du SHAPE

STC Consultant Report
CR-NICS-38

AD A0 66380



DCEC Technical Report
TR 12-78



DDC FILE COPY

FINAL REPORT ON THE COMBINED US/NATO
DIGITAL TROPOSCATTER TEST PROGRAMME
OVER TWO ACE HIGH LINKS

P. Nielsen
J. Osterholz
E. Pusone
I. Vogt

This document has been approved
for public release and sale; its
distribution is unlimited.

Abstract (NATO Unclassified):

The combined US/NATO Digital Troposcatter Test Programme was carried out by the Defense Communications Engineering Center (for the US) and the SHAPE Technical Centre (for NATO) between January and August 1977 over two ACE High links in Central Europe which were made available to NATO. The purpose of the tests was to obtain performance data on a multichannel digital troposcatter system using operational communications links. This report contains a description of the equipment and procedures employed, a summary of the results, and the conclusions drawn from the tests. The data obtained has been incorporated in an extensive data base held at both DCEC and STC to provide the capability for future analyses.

The Hague
Published December 1978

NATO UNCLASSIFIED

20 03 09 059

CONDITIONS OF RELEASE

With reference to NATO Documents C-M(55)15(Final) and C-M(63)5, this document is released to a NATO Government at the direction of the STC subject to the following conditions:

1. The recipient NATO Government agrees to use its best endeavours to ensure the information herein disclosed, whether or not it bears a security classification, is not dealt with in any manner (a) contrary to the intent of the provisions of the Charter of the Centre, or (b) prejudicial to the rights of the owner thereof to obtain patent, copyright or other likely statutory protection therefor.

2. If the technical information was originally released to the Centre by a NATO Government subject to restrictions clearly marked on this document the recipient NATO Government agrees to use its best endeavours to abide by the terms of the restrictions so imposed by the releasing Government.

GUIDE TO DOCUMENT LAYOUT

<i>Summary (yellow pages)</i>	<i>Page iii</i>
<i>Introduction</i>	<i>1</i>
<i>Test links</i>	<i>5</i>
<i>Digital test configurations</i>	<i>15</i>
<i>Data acquisition system</i>	<i>27</i>
<i>Methods of data collection</i>	<i>41</i>
<i>Test link predictions</i>	<i>49</i>
<i>Measured propagation characteristics</i>	<i>72</i>
<i>Digital system performance analysis</i>	<i>114</i>
<i>Digital modem performance</i>	<i>143</i>
<i>Operational experience</i>	<i>166</i>
<i>Summary and conclusions</i>	<i>190</i>
<i>Appendices</i>	<i>197 to 267</i>
<i>References</i>	<i>269</i>

280/NO/CMS

1457C- REPORT DOCUMENTATION PAGE		READ INSTRUCTIONS BEFORE COMPLETING FORM	
1. REPORT NUMBER CR-NICS-38 DCEC TR-12-78 AD-E 100 189		3. RECIPIENT'S CATALOG NUMBER	
4. TITLE (and Subtitle) FINAL REPORT ON THE COMBINED US/NATO DIGITAL TROPOSCATTER TEST PROGRAMME OVER TWO ACE HIGH LINKS.		9. TYPE OF REPORT & PERIOD COVERED Final Report.	
7. AUTHOR(s) P. Nielsen, J. Osterholz, E. Pusone, I. Vogt		6. PERFORMING ORG. REPORT NUMBER	
9. PERFORMING ORGANIZATION NAME AND ADDRESS SHAPE Technical Centre, the Hague, and the Defense Communications Engineering Center 1860 Wiehle Ave., Reston, VA 22090		8. CONTRACT OR GRANT NUMBER(s)	
11. CONTROLLING OFFICE NAME AND ADDRESS Defense Communications Engineering Center Transmission Engineering Division, R200 1860 Wiehle Ave., Reston, VA 22090		10. PROGRAM ELEMENT, PROJECT, TASK AREA & WORK UNIT NUMBERS N/A	
14. MONITORING AGENCY NAME & ADDRESS (if different from Controlling Office) N/A 12/284p.		12. REPORT DATE Dec 78	
		13. NUMBER OF PAGES 271	
		15. SECURITY CLASS. (of this report) Unclassified	
		15a. DECLASSIFICATION/DOWNGRADING SCHEDULE	
16. DISTRIBUTION STATEMENT (of this Report) Approved for public release; distribution unlimited.			
17. DISTRIBUTION STATEMENT (of the abstract entered in Block 20, if different from Report) N/A			
18. SUPPLEMENTARY NOTES Review relevance 5 years from submission date.			
19. KEY WORDS (Continue on reverse side if necessary and identify by block number) Digital Troposcatter MDTs Ace High DAR Performance Data Multichannel			
20. ABSTRACT (Continue on reverse side if necessary and identify by block number) The combined US/NATO Digital Troposcatter Test Programme was carried out by the Defense Communications Engineering Center (for the US) and the SHAPE Technical Centre (for NATO) between January and August 1977 over two ACE High links in Central Europe which were made available to NATO. The purpose of the tests was to obtain performance data on a multichannel digital tropo-scatter system using operational communications links. This report contains a description of the equipment and procedures employed, a summary of the results, and the conclusions drawn from the tests. The data obtained has			

Block 20.

been incorporated in an extensive data base held at both DCEC and STC to provide the capability for future analyses.

NATO UNCLASSIFIED

-i-

STC Consultant Report CR-NICS-38
DCEC Technical Report TR 12-78

FINAL REPORT ON THE COMBINED US/NATO
DIGITAL TROPOSCATTER TEST PROGRAMME
OVER TWO ACE HIGH LINKS

by

P. Nielsen
E. Pusone
I. Vogt

Communications Division, STC

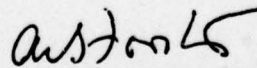
and

J. Osterholz

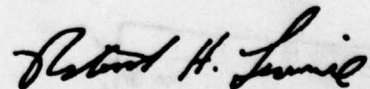
Defense Communications Engineering Center
Reston, VA., U.S.A.

A report prepared by STC under NICS Special
Project Task GEN/6 and the Defense Communica-
tions Engineering Center under a MOU between
the Defense Communications Agency and NICSMA

Approved:



A.E.T. Forster,
Acting Chief,
Communications Division



Robert H. Levine,
Deputy Director, DCEC

SHAPE Technical Centre
The Hague
Published December 1978

This document consists
of x + 271 pages
(excluding covers)

NATO UNCLASSIFIED

02 09 059

NOTE TO READERS

This report has been prepared by the SHAPE Technical Centre for the NATO Integrated Communications System Management Agency (NICSMA) under the terms of the NICS Special Project and by the U.S. Defense Communications Engineering Center for NATO under the terms of the "MOU Engineering Digital Transmission Tests on ACE High" by the Defense Communications Agency and NICSMA.

The report has neither been approved nor disapproved by NICSMA, and the contents may or may not be used as a basis for the future procurement action by that agency. Accordingly, the material contained herein cannot, unless specifically authorized by NICSMA, be utilized directly for the development of industrial responses to any NICSMA invitation for bidding action, nor can the contents of the report be used to challenge any contractual action which the agency might take in the future or to give the recipient any rights whatsoever.

ACCESSION for	
NTIS	White Section <input checked="" type="checkbox"/>
DDC	Dark Section <input type="checkbox"/>
UNANNOUNCED	
JUSTIFICATION	
BY _____	
DISTRIBUTION/AVAILABILITY CODES	
Dist.	AVAIL and/or SPECIAL
A	

SUMMARY

The combined US/NATO Digital Troposcatter Test Programme was established by a memorandum of understanding^{*} between the Defense Communications Agency (DCA) on behalf of the United States and the NATO Integrated Communication System Management Agency (NICSMA) on behalf of NATO. The purpose of the programme was to obtain performance data on a multichannel digital troposcatter system using operational communication links. More specifically, the aims were:

- To verify existing methods and, if necessary, to develop new methods for reliably predicting digital troposcatter performance on the basis of measured and predicted RF link performance.
- To provide a statistical data base to characterize digital troposcatter channels and user services.
- To gain experience with the operation of digital troposcatter links under realistic conditions.
- On the basis of the above, to confidently establish the feasibility of digital troposcatter transmission in both the Defense Communications System (DCS) and the NATO ACE High system.
- To establish a basis for additional theoretical and experimental activities concerning digital troposcatter transmission, as required.

Testing was accomplished over two ACE High links in Central Europe which were made available by NATO:

- a 170-km diffraction link located in southern Germany and operating at C-band frequencies
- the 287-km trans-horizon link between Germany and Italy, operating at UHF frequencies.

^{*}"MOU concerning combined US/NATO Digital Transmission Test Program over ACE High", Enclosure to NICSMA letter NICSMA/SPED/CPB(??) 116, dated 17 May 1977

The US provided two types of prototype digital troposcatter modem, together with associated time division multiplex (TDM) and pulse code modulation (PCM) equipments. The first type, called Megabit Digital Troposcatter Subsystem (MDTS), is based on decision directed adaptive equalization, whereas the second type, called Distortion Adaptive Receiver (DAR), uses transmitter time gating as the primary technique to combat intersymbol interference. The instrumentation required for data acquisition purposes was furnished jointly by the US and NATO. Test direction and data analysis responsibilities were shared between the Defense Communications Engineering Center (DCEC) and SHAPE Technical Centre (STC).

The tests on the UHF link were carried out during the months of January, February, April, and May 1978. No measurements could be made during March, since the link had to carry operational traffic during the WINTEX exercise. Unfortunately, the retuning of the UHF power amplifiers (to correct for the narrowband tuning during WINTEX) resulted in unsymmetrical and too narrow passbands and this affected the measurement results obtained with the MDTS modem after WINTEX.

Measurements on the C-band link were taken during the one-month period from mid-July to mid-August 1978.

The following data was collected in the form of manual test logs and also on computer-compatible digital tapes:

- (a) Received signal level (RSL) for each diversity receiver in use
- (b) Multipath dispersion
- (c) Bit error events

- (d) Loss of synchronization, separately for
- digital modem
 - Asynchronous TDM unit
 - US PCM/TDM
 - NATO PCM/TDM equipment (30/32 channels)
- (e) Modem signal-to-noise ratio (SNR) indicator voltage.

Measurements were made at data signalling rates of about 3, 6, and, for the MDTS modem, also at 9 Mbit/s; these rates correspond to the transmission of 48, 96, and 144 voice channels respectively, digitized with 64 Kbit/s PCM. Due to differences in the framing structure and in multiplexing the service channel, the actual data rates used by the MDTS and the DAR modems are not identical for the same number of voice channels.

The data collected has been analysed by STC and DCEC, working in close cooperation. In addition, the data has been incorporated in an extensive data base held at both STC and DCEC to provide the capability for future analyses.

This document is the final report on the combined test programme and is the joint responsibility of DCEC and STC. It contains a summary of all data taken during the tests, the conclusions which could be supported by the data, and the associated discussions.

A summary of the major test results relating to digital performance on the test links is given below:

MDTS modem at 6.3 Mbit/s

UHF test link

- For 90% of the time, the mean bit error rate (BER) was better than 3×10^{-8} in quadruple diversity and 4×10^{-5} in dual diversity, at a mean transmitted power of 4 kW.
- For 99% of the time, the mean BER was better than 3×10^{-5} in quadruple diversity and 2×10^{-3} in dual diversity, at a mean transmitted power of 4 kW.

- The quadruple diversity fade outage rate was zero for 95% of all the runs. The mean fade outage duration measured over all runs was 370 ms, excluding the worst-case outage (lasting approximately 20 minutes), which occurred after the WINTEX exercise. The mean fade outage duration measured before WINTEX was 100 ms or less.

C-band test link

- The mean BER was never worse than 1×10^{-6} in quadruple diversity and 3×10^{-8} in dual diversity, at a transmitted power of 50 watts.
- Fade outage occurred with negligible frequency; the duration was less than 100 ms in the C-band link in quadruple diversity.

DAR modem at 7.0 Mbit/s

UHF test link

- In quadruple diversity, the mean BER was better than 1×10^{-2} for 90% of the test runs, at a mean transmitted power of 1 kW.
- Dual diversity tests were limited by the inability of the DAR modem to accommodate the RF bandlimiting and multipath dispersion encountered on the test link.
- The quadruple diversity fade outage rate was better than 10^{-2} outages/second for 90% of the test runs. The mean outage duration was typically less than 500 ms.

C-band test link

- The mean BER was never worse than 3×10^{-7} in quadruple diversity and 2×10^{-2} in dual diversity (one measurement only, otherwise the BER was less than 10^{-3}) at a transmitted power of 50 W.
- Fade outages occurred with negligible frequency and with a typical duration of 300 ms or less on the C-band link in quadruple diversity.

Low bit error rates (10^{-10} to 10^{-8}) were achieved over the majority of the tests at 6.3 Mbit/s on the UHF link and 9.4 Mbit/s on the C-band link. However, when bit errors occurred, they occur-

red at carrier-to-noise ratios (CNR) which were significantly higher than those measured during previous media simulator and troposcatter link tests. The reasons for this discrepancy have not been identified. The most probable causes of the higher than expected error rate are various test and radio equipment problems and the mixed mode propagation encountered on the UHF link.

The maintenance of bit count integrity (BCI) is of paramount importance for the successful operation of TDM digital communications. The system test configuration employed in this programme included one level of asynchronous multiplexing and two levels of synchronous multiplexing between the radio and the voice channels terminated in the US- and NATO-supplied PCM/TDM equipment. Test results showed that, for quadruple diversity operation, loss of BCI was a very infrequent event and that, in fact, BCI losses were responsible for only an exceedingly small percentage of the total number of fade outages measured.

While the measured propagation characteristics of the C-band diffraction link agreed well with predictions, the trans-alpine UHF link was found to exhibit a mode of propagation which was unexpected. In particular, variable intensity specular signal components were received together with troposcatter components in certain diversity receivers for a substantial fraction of the test. These specular components, attributed to double knife-edge diffraction along the great circle path and off-boresight diffraction of reflections, added to the overall multipath dispersion of the UHF link.

Markedly different median signal levels on the various diversity branches were observed on both test links. Moreover, the difference between the median signal levels of any two receivers was not constant but varied over a wide range on the UHF test link. While this condition is unusual and not representative of

normal troposcatter propagation, asymmetrical propagation can occur on diffraction links with variable terrain and possibly on troposcatter links with angle diversity.

In summary, the following major conclusions were reached:

- (a) No technical difficulties are anticipated in the application of digital transmissions of up to 9.4 Mbit/s in 7 MHz of RF bandwidth to the C-band link or similar links using quadruple diversity and narrow beam antennas.
- (b) With regard to the UHF link, it is difficult to extend the test results to the performance to be expected during the entire year. However, based on the measured data, reliable transmission at 6.3 Mbit/s would probably be possible, given the continued availability of the test RF bandwidth (7 MHz) and quadruple diversity.
- (c) It is unconfirmed whether 9.4 Mbit/s could be transmitted reliably in 7 MHz on the UHF link throughout the year. The performance of this configuration varied from a generally low BER (10^{-7}) before WINTEX to a higher BER (10^{-5} to 10^{-3}) after WINTEX. It is felt that the combination of a distorted RF passband and the multipath dispersion contributed significantly to the high BER measured in the second period.
- (d) Due to the mixed-mode propagation on the UHF link, little new information was obtained for the planning of links with purely tropospheric scatter propagation. However, measured multipath dispersion data and its lack of correlation with median CNR was consistent with previous measurements on pure troposcatter links.
- (e) The test results confirmed that, for quadruple diversity, loss of BCI was a very infrequent event and that BCI losses were responsible for a very small percentage of the number of outages measured.

TABLE OF CONTENTS

	Page
1. INTRODUCTION	1
2. TEST LINKS	5
2.1 Selection of test links	5
2.2 Major characteristics of test links	8
3. DIGITAL TEST CONFIGURATIONS	15
3.1 Digital equipment configurations	15
3.2 Troposcatter modem and re-equipment configurations	21
4. DATA ACQUISITION SYSTEM	27
4.1 Selection of test observables	27
4.2 Measurement methods	27
4.3 Data recording techniques	30
4.4 Calibration procedures	38
5. METHODS OF DATA COLLECTION	41
5.1 UHF link	41
5.2 C-band link	46
6. TEST LINK PREDICTIONS	49
6.1 UHF test link	49
6.2 C-band test link	64
7. MEASURED PROPAGATION CHARACTERISTICS	72
7.1 General	72
7.2 Propagation characteristics of UHF test link	72
7.3 Propagation characteristics of the C-band link	105
7.4 Summary of propagation analysis	112
8. DIGITAL SYSTEM PERFORMANCE ANALYSIS	114
8.1 MDTS UHF test link system performance	114
8.2 DAR UHF test link system performance	131
8.3 System synchronization (UHF test link)	132
8.4 System performance observations	138
8.5 C-band test link system performance	139

TABLE OF CONTENTS (Cont'd)

	Page
9. DIGITAL MODEM PERFORMANCE	143
9.1 General	143
9.2 Average bit error description	143
9.3 Frozen-channel description	153
9.4 Analysis of MDTS modem loss of bit count integrity	161
9.5 Discussion of potential MDTS modem optimization areas	164
10. OPERATIONAL EXPERIENCE	166
10.1 General	166
10.2 Lessons learned	166
10.3 Experience with the REL 2600 troposcatter radios	168
11. SUMMARY AND CONCLUSIONS	190
APPENDIX A: DIGITAL TROPOSCATTER TRANSMISSION TECHNOLOGY	197
APPENDIX B: DIGITAL EQUIPMENT CHARACTERISTICS	221
APPENDIX C: DISPERSION MONITOR MEASUREMENT TECHNIQUE	226
APPENDIX D: DIGITAL TAPE RECORDING FACILITY	234
APPENDIX E: CCIR TROPOSCATTER PATH LOSS PREDICTIONS	243
APPENDIX F: PREDICTION OF THE DIFFRACTION LOSS ENCOUNTERED ON THE LINK IDGZ-APEZ USING A DOUBLE-EDGE APPROXIMATION FOR THE PATH PROFILE	248
APPENDIX G: SHORT-TERM DISTRIBUTION OF RSL FOR A WIDEBAND SIGNAL SUBJECT TO FREQUENCY SELECTIVE FADING	252
APPENDIX H: CCIR DIFFRACTION PATH LOSS PREDICTION FOR THE C-BAND TEST LINK	258
APPENDIX I: ON THE SEPARATION OF A RICE-FADING CHANNEL INTO A RAYLEIGH-FADING AND A NON-FADING COMPONENT	260
APPENDIX J: MULTIPATH DISPERSION FOR MIXED-MODE PROPAGATION	265
REFERENCES	269

1. INTRODUCTION

The combined US/NATO Digital Troposcatter Test Programme was established by a Memorandum of Understanding^{*} between the Defense Communications Agency (DCA) on behalf of the United States and the NATO Integrated Communications System Management Agency (NICSMA) on behalf of NATO. The purpose of the programme was to obtain performance data on a multichannel digital troposcatter system using operational communication links. More specifically, the aims were:

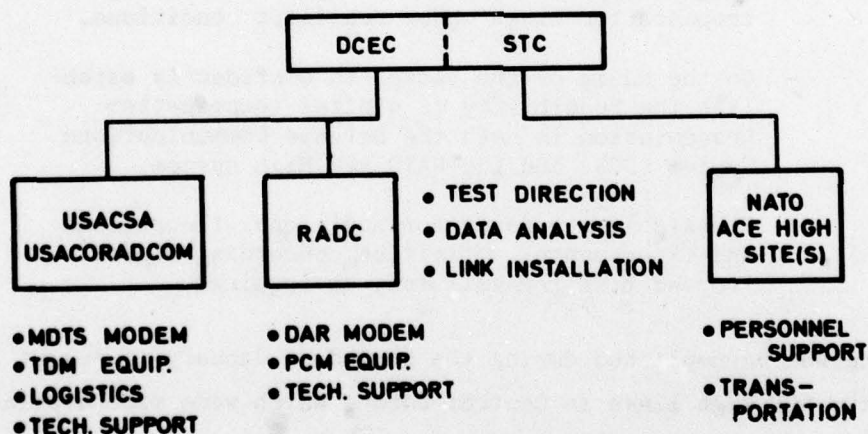
- To verify existing methods and, if necessary, to develop new methods for reliably predicting digital troposcatter performance on the basis of measured and predicted RF link performance.
- To provide a statistical data base to characterize digital troposcatter channels and user services.
- To gain experience with the operation of digital troposcatter links under realistic conditions.
- On the basis of the above, to confidently establish the feasibility of digital troposcatter transmission in both the Defense Communications System (DCS) and the NATO ACE High system.
- To establish a basis for additional theoretical and experimental activities concerning digital troposcatter transmission, as required.

Testing was accomplished during the period of January to August 1977 over two ACE High links in Central Europe which were made available by NATO. The US provided two types of prototype digital troposcatter modems, called Megabit Digital Troposcatter Subsystem

^{*}"MOU concerning combined US/NATO Digital Transmission Test Program over ACE High", Enclosure to NICSMA letter NICSMA/SPED/CPB(77) 116, dated 17 May 1977

(MDTS) and Distortion Adaptive Receiver (DAR), and the associated time division multiplex (TDM) and pulse code modulation (PCM) equipments. The instrumentation required for data acquisition purposes was furnished jointly by the US and NATO. Test direction and data analysis responsibilities were shared between the Defense Communications Engineering Center (DCEC) and the SHAPE Technical Centre (STC).

The prototype digital troposcatter modems which were tested were developed under US Department of Defense (DOD) Research and Development programmes for potential US DOD applications. The PCM and TDM equipments employed in the test are functionally similar to equipments likely to be used in US DOD digital transmission systems. Figure 1 shows the assignment of support requirements among US and NATO technical agencies. Except for minor deviations, the tests were conducted in close agreement with the test plan published prior to the tests by DCEC and STC (Ref. 1).



RADC = ROME AIR DEVELOPMENT CENTER
 USACSA = U.S. ARMY COMMUNICATIONS SYSTEM AGENCY
 USACORADCOM = U.S. ARMY COMMUNICATIONS RESEARCH AND
 DEVELOPMENT COMMAND

78134

Fig. 1 Test programme organization

Test data, collected in the form of manual test logs and also on computer-compatible digital tapes, has been analyzed by DCEC and STC in close cooperation. This document is the final report on the combined test programme and is the joint responsibility of DCEC and STC. It contains a summary of all data taken during the tests, together with those conclusions which could be supported by the data, and the associated discussions.

Additionally, data collected under this programme has been incorporated into an extensive data base maintained at STC and DCEC to provide the capability for future analyses. At STC, the raw data has been processed and stored on magnetic tapes in the form of detailed propagation and performance statistics for each 20-minute segment of the entire test period.

This report does not specifically address the utilization of the test results for systems engineering purposes. The applicability of the test results to system engineering and planning for the ACE High system will be the topic of a separate report to be issued by STC. Digital troposcatter transmission system engineering for the DCS has been addressed in DCEC TR 12-76 (Ref. 2), and in other documents (see, for example, Ref. 10).

A detailed description of the two test links is provided in Chapter 2, together with the rationale for the selection of these links. Test configurations and the interconnections with existing station equipment are described in Chapter 3. Chapter 4 contains an outline of the choice of test "observables" and a brief description of the Data Acquisition System (DAS) hardware used in the programme. Chapter 5 discusses the methods of apportioning the test time among the different test configurations, data rates, diversity configurations, etc. The test results are given in Chapters 6 to 9. Chapter 10 presents some of the lessons learned

during the test programme and examines the specific details of interfacing digital troposcatter modems with analogue radios of recent manufacture. Some overall comments and conclusions are given in Chapter 11.

2. TEST LINKS

2.1 SELECTION OF TEST LINKS

The ACE High network spans the entire ACE area from the most northern flank of NATO in Norway to the easternmost flank in Turkey. The network comprises a total of 49 over-the-horizon (O/H) links plus a comparable number of microwave line-of-sight (LOS) tail links and interconnections. The majority of the O/H links were installed in the early 1960s and operate (with one exception) in the 670-960 MHz UHF band. Seven links in the Central Region were added in 1967-68. Six of these links operate at C-band (4.4-5.0 GHz) and one in the 790-960 MHz UHF band.

Early in the planning of the test programme, all the 49 O/H links in ACE High were reviewed to assess their suitability as test links. Many factors were considered, inter alia:

- (a) the expected propagation characteristics, with special emphasis on expected multipath performance
- (b) the degree to which a given link could be considered representative of other ACE High or DCS O/H links
- (c) the intrinsic bandwidth limitations of high-power klystron amplifiers
- (d) the ease with which digital modems could be interfaced with existing station equipment
- (e) the geographical location and accessibility of the stations
- (f) the constraints imposed by the availability prime power and physical space
- (g) traffic rerouting possibilities.

As a result of this first examination, five links were identified as possible candidates:

- A. Kindsbach (ABHZ), Germany, to Feldberg (AFEZ),
Germany (C-band)
- B. Dosso dei Galli (IDGZ), Italy, to Feldberg
(AFEZ), Germany (UHF)
- C. Mosjen (NMOZ), Norway, to Trondheim (NSBZ),
Norway (UHF)
- D. Paris South (FAOZ), France, to Trier (FROZ),
France (UHF)
- E. London (UMAZ), UK, to Paris North (FFLZ),
France (UHF)

The preferred option was to test both Link A and Link B, while single-link testing of one of the Links C to E (with decreasing priority) was considered to be an acceptable alternative.

Eventually, approval was obtained from the appropriate NATO authorities to employ Link A and Link B for the test programme. The rationale behind this preferred option is given in the following paragraphs, with special reference to points (a) to (g) listed above.

The unique feature of high-speed digital troposcatter modems is their ability to combat intersymbol interference caused by multipath dispersion. A given modem can successfully handle only a certain amount of multipath delay spread, the limit depending on the transmitted data rate and the specifics of the modem design. To exercise the full capabilities of the digital modems, it was desirable to include in the tests one of the more dispersive links of ACE High. Based on predictions, Link B is among the five most dispersive links in the system.

Due to constraints of time and funds, it was not possible to perform extensive trials with digital modems over all the ACE

High or DCS O/H links. Thus it is highly desirable to be able to utilize data obtained under this test programme to aid in the assessment of digital modems on other O/H links. The great majority of the O/H links in ACE High and DCS operate either in the 670-960 MHz band (UHF) or in the 4.4-5.0 GHz band (C-band). Because of the different propagation characteristics encountered in these two frequency bands, it was considered that both bands should be included in the tests.

Data rates of the order of 6 to 7 Mbit/s were required if the tests were to be representative of actual system configurations having link cross sections up to about 100 toll-quality voice circuits. With current modem designs, this transmission rate requires a 3-dB RF bandwidth of between 7 and 10 MHz, which is difficult or impossible to achieve with some of the older types of UHF klystrons employed in ACE High. The klystrons used on Link B (Varian Type 4, KM 50000LQ) are of a more recent design and can be tuned to have the bandwidth required for the test. C-band klystrons do not present a bandwidth problem.

The digital modems provided by the US have 70-MHz IF interface connections. Old ACE High UHF radios (REL 2400) have an intermediate frequency of 24.5 MHz and require the use of fairly complex and costly interface equipment if they are to be compatible with the modems. Link B is the only ACE High UHF link which is fitted with RSL 2600 series equipment with 70-MHz IF interconnection points. All C-band links have REL 2600 equipment.

Because the test programme would require the transportation of heavy and bulky equipment to the test sites and because personnel would need to visit the stations on a regular basis, it was important to ensure that the stations selected could be accessed even during the winter months. The choice of the combination of Link A and Link B had the significant advantage that the receive

site would be common to both links and that therefore all the data acquisition equipment could remain at the AFEZ site throughout the entire test. Access to AFEZ and ABHZ was found to present no problems. Access to IDGZ is possible throughout the year, although sometimes difficulties are encountered during the winter. However, this was considered acceptable since access to the transmit sites would be required only infrequently.

Prime power and physical space were found to be adequate at all of the three stations associated with Links A and B.

Whatever test link(s) were chosen, a suitable means of rerouting the operational traffic during the test period had to be found. Unless rerouting could be done on a no-cost basis (for instance, through ACE High or DCS), the cost associated with circuit rerouting was likely to dominate the budget for the test programme. Link A and Link B are tandem links connected at a relay station (AFEZ) via a baseband bridge, and any rerouting arrangement for one of these links would therefore automatically make the other link available.

The selection of Link A and Link B was made on the basis of the considerations outlined above, after it had been ascertained that rerouting could be arranged via ACE High throughout the test period.

2.2 MAJOR CHARACTERISTICS OF TEST LINKS

A map of the ACE High regions, showing the two test links, is given in Fig. 2. Link A extends mainly over hilly woodland while Link B is a trans-alpine link. The path profiles of the two links are shown in Fig. 3 and 4, respectively. Major characteristics of the test links are given in Table 1.

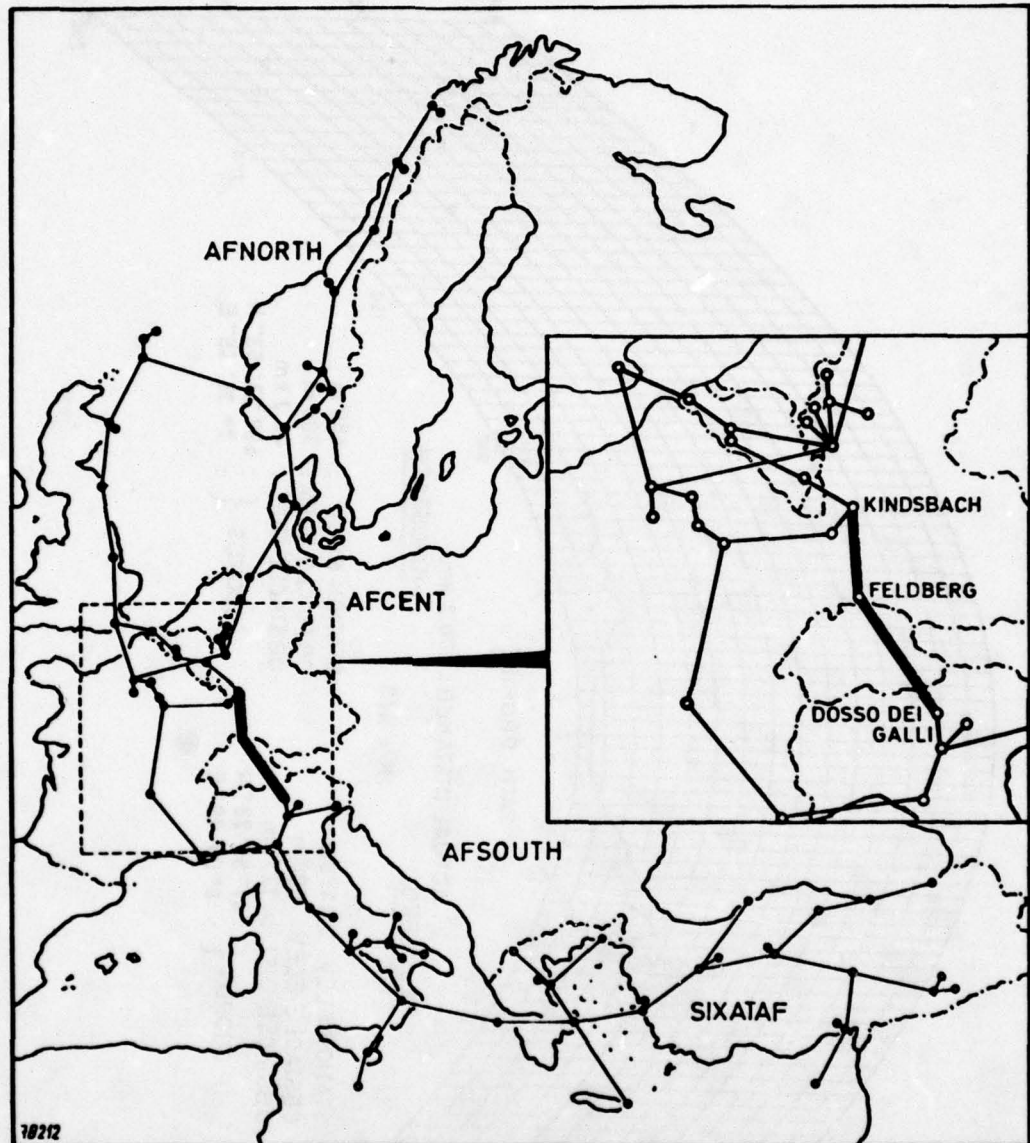


Fig. 2 ACE High system

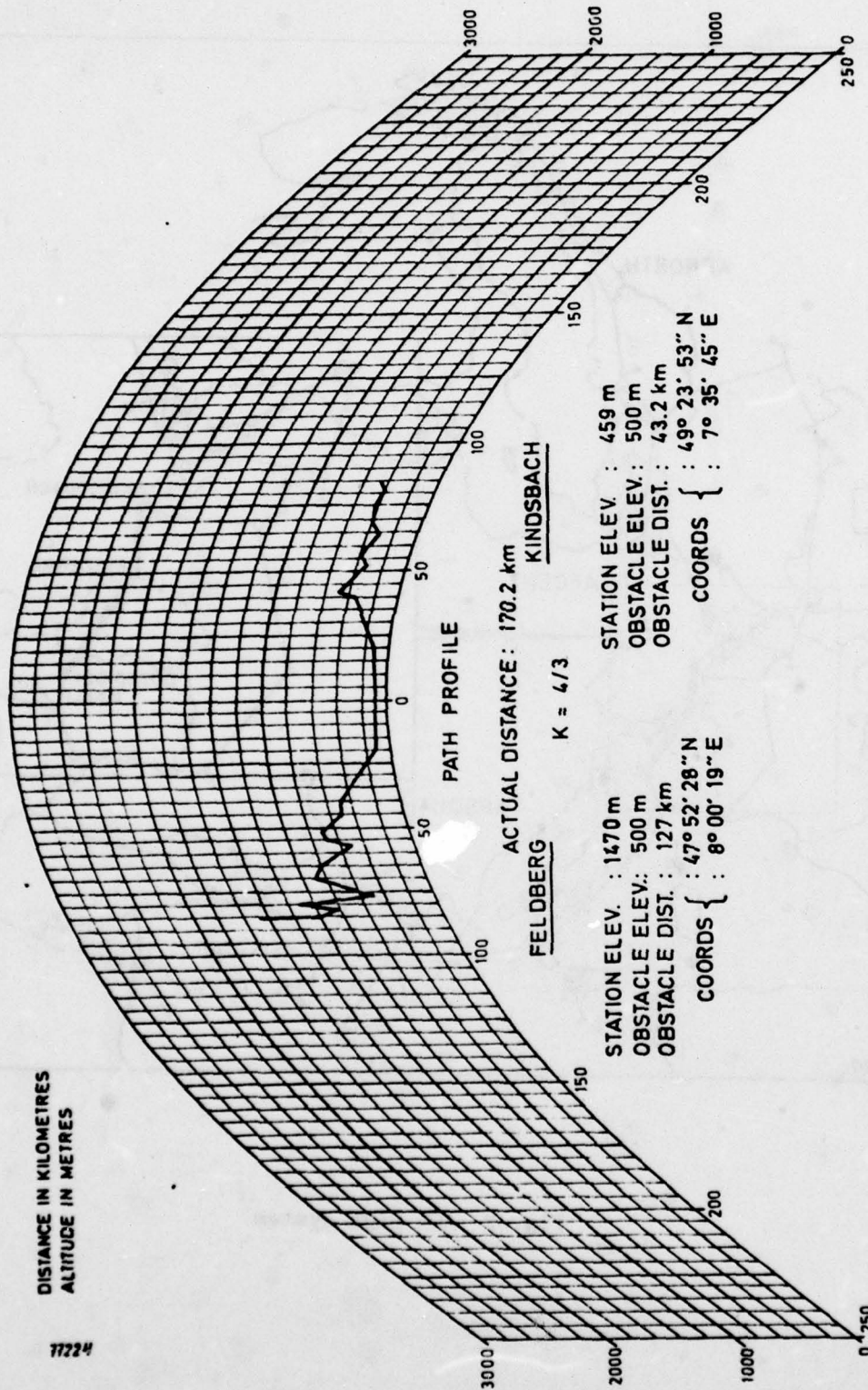


Fig. 3 Path profile of C-band link

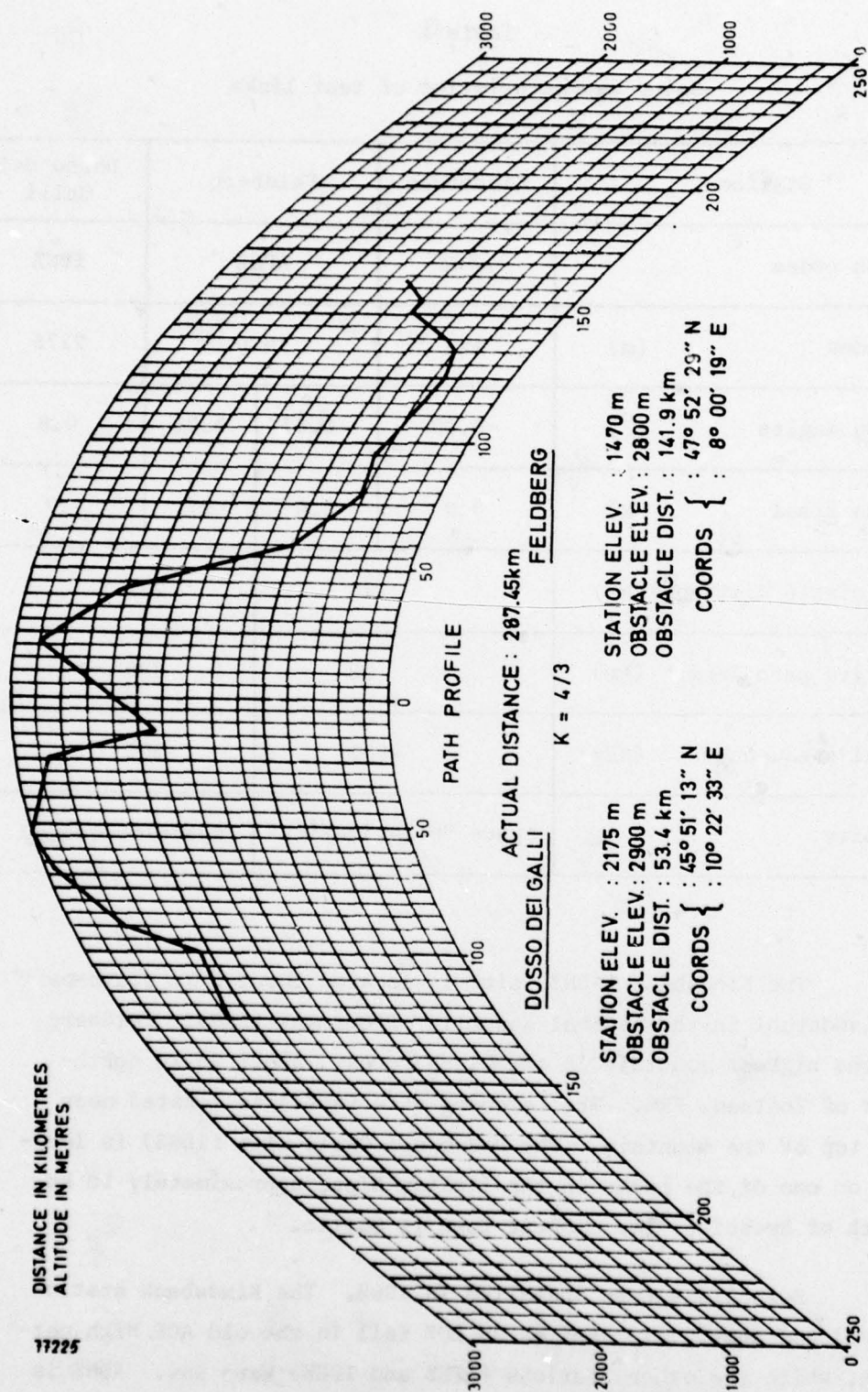


Fig. 4 Path profile of UHF link

Table 1

Major characteristics of test links

Station	Kindsbach	Feldberg		Dosso dei Galli
Station codes	ABHZ	AFEZ		IDGZ
Altitudes (m)	459	1470		2175
Horizon angles ($^{\circ}$)	-0.09	-0.87	0.06	0.6
Antenna sizes (m)	3.0	3.0	27	27
Great circle distance (km)	170		287	
Effective path length (km)	28		385	
Nominal frequency (MHz)	4500		900	
Diversity	space "polarization"		space/frequency	

The Kindsbach (ABHZ) site is located about 5 km south-east of Landstuhl in the Federal Republic of Germany (FRG). Feldberg is the highest mountain in the Black Forest, about 25 km north-east of Todtnau, FRG. The Feldberg site (AFEZ) is located near the top of the mountain. The Dosso dei Galli site (IDGZ) is located on one of the peaks in the Italian Alps, approximately 50 km north of Brescia. The closest town is Collio.

Both links were installed in 1968. The Kindsbach station (ABHZ) was previously used as an LOS tail in the old ACE High network, while the other stations (AFEZ and IDGZ) were new. ABHZ is

equipped with multiplex equipment for terminating a number of the circuits from direction AFEZ. AFEZ is a troposcatter relay station and IDGZ has through-group connections to an adjacent LOS tail.

2.2.1 Diversity configurations

The C-band test link, Link A, employs quadruple space diversity with polarization discrimination. The configuration is shown in Fig. 5(a). The UHF test link, Link B, is configured in a dual space/dual frequency diversity arrangement as shown in Fig. 5(b).

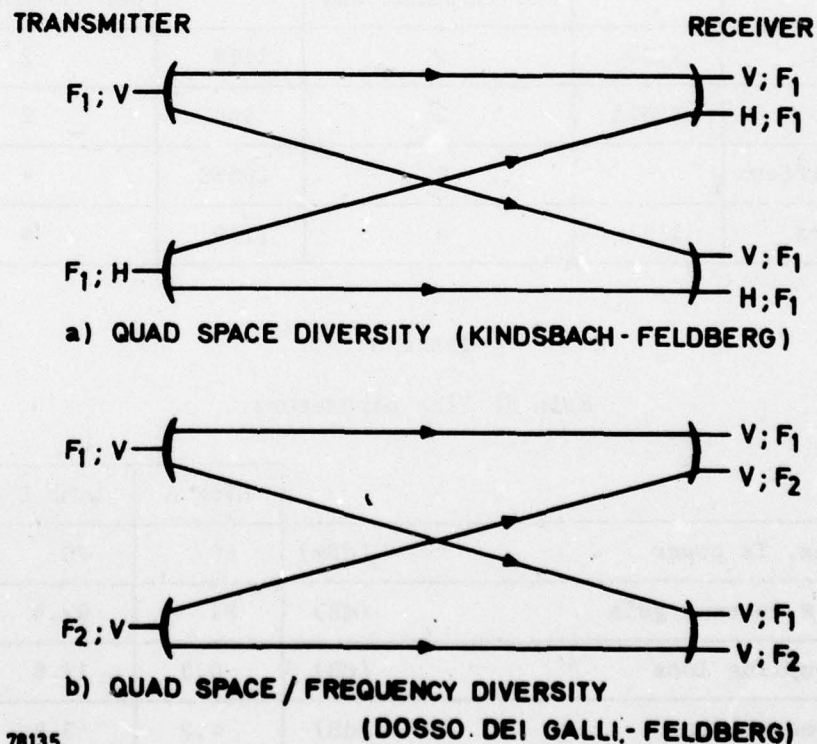


Fig. 5 Test link diversity configurations

2.2.2 RF equipment

Both links are equipped with REL 2600-series RF equipment, the main components of which are listed in Table 2. Link B is fitted with parametric preamplifiers and threshold extension units. The antennas are 3-m parabolic dishes for Link A and 27-m offset parabolic antennas for Link B. The main RF parameters of the two links are given in Table 3.

Table 2

REL 2600-series RF equipment installed

	Link A (C-band)		Link B (UHF)	
	Type no.	No. installed per terminal end	Type no.	No. installed per terminal end
Exciters	1160	2	1118	2
HPAs	1162A	2	954D	2
Preamplifiers	-	0	1055C	4
Receivers	1161	4	1119	4

Table 3

Main RF link parameters

		Link A	Link B
Max. Tx power	(dBm)	60	70
2 x antenna gain	(dB)	81	92.6
Coupling loss	(dB)	0.3	12.6
Feeder loss	(dB)	4.2	3.4
Rx noise figure	(dB)	8.0	2.0
Antenna polarization decoupling	(dB)	40	35
Half-power beamwidth	(°)	1.5	0.9

3. DIGITAL TEST CONFIGURATIONS

3.1 DIGITAL EQUIPMENT CONFIGURATIONS

The MDTS modem is based on decision-directed adaptive equalization of the troposcatter channel whereas the DAR modem uses transmitter time gating as a means of combatting intersymbol interference. A brief description of the MDTS and DAR modulation and equalizing techniques can be found in Appendix A.

Photographs of the digital equipments used during the tests are presented in Fig. 6 and 7. Relevant technical information concerning these equipments is shown in Appendix B.

Two test configurations were implemented on the test links. The first configuration, referred to as the system test configuration, included TDM and PCM equipments. In the second configuration, referred to as the link test configuration, measurements were made without any TDM or PCM equipment.

3.1.1 System tests

The system test configuration (Fig. 8) was used for system level testing with the MDTS modem only and was operated at a nominal transmitted data rate of 6.3 Mbit/s, which corresponds to 96 PCM voice channels. This configuration enabled system performance data to be collected, relating to PCM voice channel fade outage statistics and PCM/TDM synchronization stability. The transmit side of a 24-channel PCM equipment, TD-968, provided 1.544-Mbit/s NRZ data and timing signals to one of three input ports of an AN/GSC-24, asynchronous TDM. The second input port of the AN/GSC-24 accepted 2.048-Mbit/s NRZ data and timing from a simulated data source (SDS), which was used for bit error measurements.

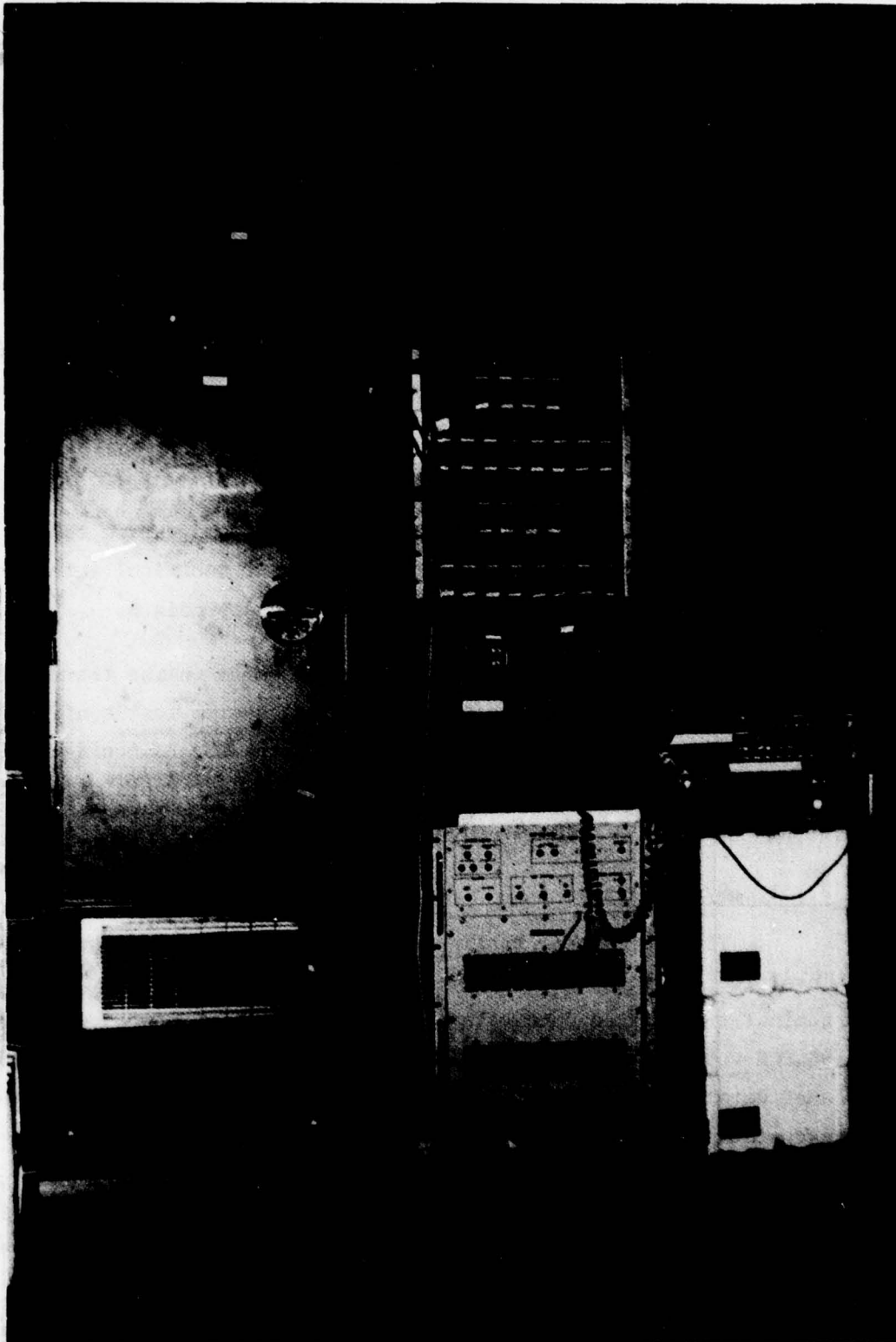


Fig. 6 Digital troposcatter system
(MDTS modem, AN/GSC-24 TDM, TD-968 PCM/TDM)

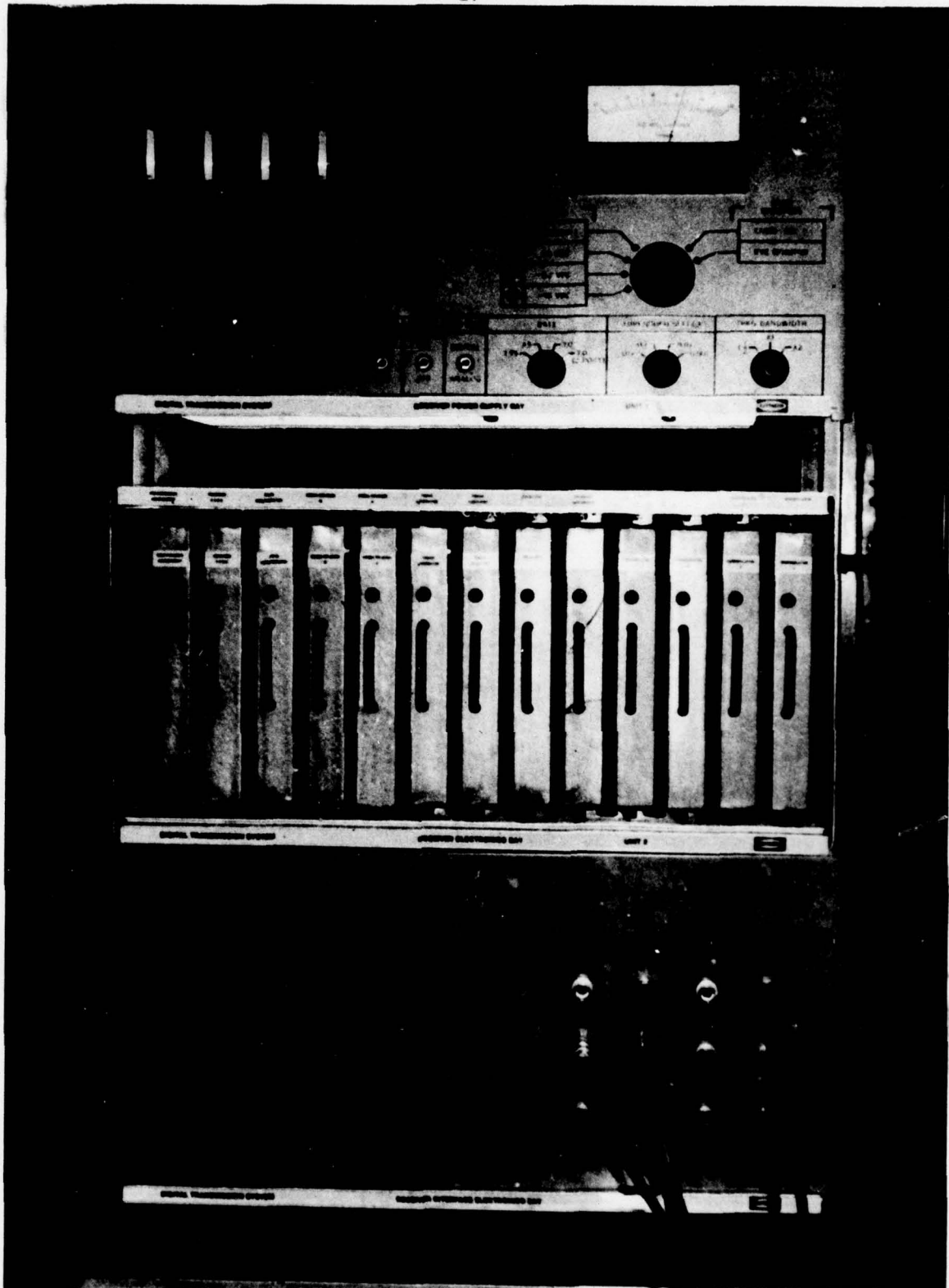


Fig. 7 DAR digital troposcatter modem

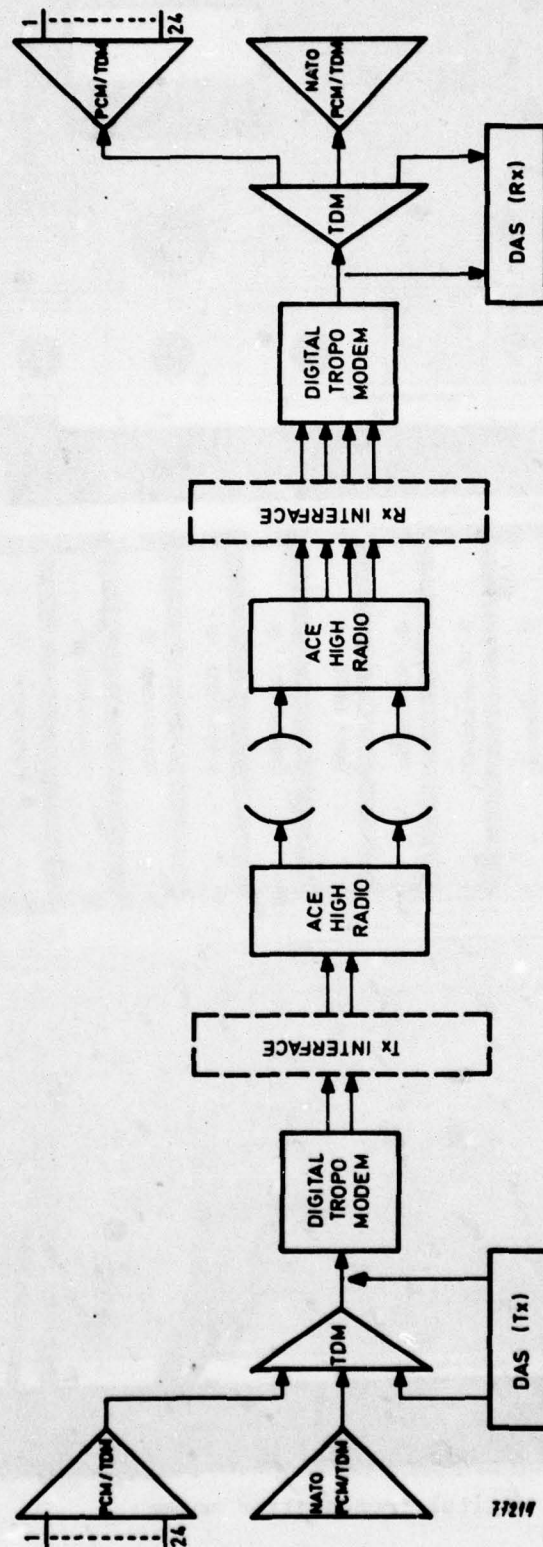


Fig. 8 System test configuration

The third AN/GSC-24 port was configured to accept another 1.544 Mbit/s input, but was left unloaded for the UHF test. For the C-band test, both the TD-968 and a CEPT standard 30-channel 2.048-Mbit/s PCM multiplex were used as inputs to the AN/GSC-24 TDM. The SDS was clocked at 1.544 Mbit/s and inserted into the third port of the TDM. The combined output rate of the AN/GSC-24 was 6.276 Mbit/s. The data output of the AN/GSC-24 along with its associated timing line was input to the MDTs modem. The MDTs modem provided a stable clock source at the combined bit rate back to the AN/GSC-24 to maintain a synchronous interface. On the distant-end receive side, the 6.276-Mbit/s recovered data and timing were provided to the demultiplexer portion of another AN/GSC-24, TDM. The demultiplexed data streams and associated timing signals were taken from the AN/GSC-24 and input to the receive sides of the distant-end TD-968 and SDS units at 1.544 Mbit/s and 2.048 Mbit/s respectively.

3.1.2 Link tests

The link test configuration (Fig. 9) was used for 3.5 and 7.0 Mbit/s DAR tests and for 3.2 and 9.4 Mbit/s MDTs tests. A 3.2 or 3.5 Mbit/s transmitted data rate is equivalent to 48 (64 kbit/s) PCM channels, 7.0 Mbit/s to 96 PCM channels, and 9.4 Mbit/s is equivalent to 144 PCM channels. In this configuration, NRZ data and timing signals from a transmit SDS unit were applied directly to the digital modems at the data rates mentioned above. On the receive side, the recovered data and timing signals were input to a receive SDS unit for error measurement.

The MDTs and DAR digital service channels were integrated into the station orderwire facilities and used throughout the programme for both test and operational ACE High system coordination purposes.

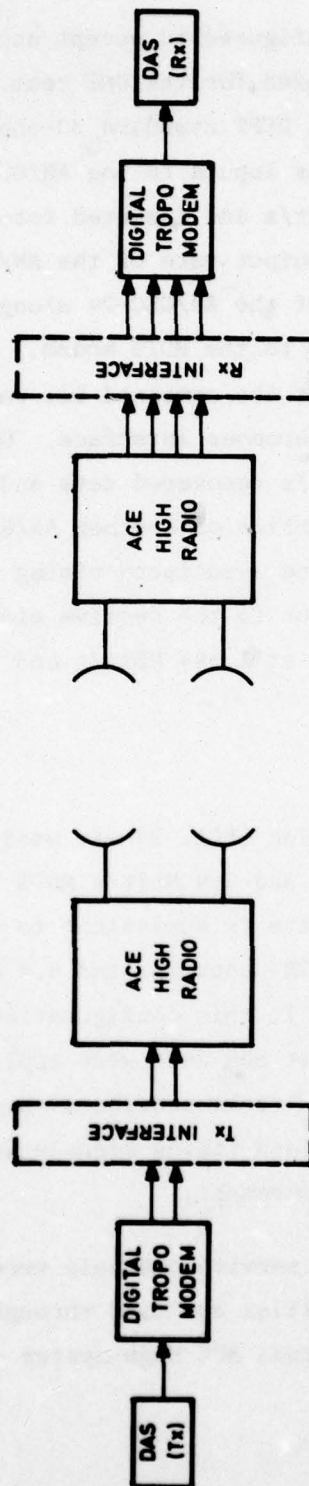


Fig. 9 Link test configuration

172/3

3.2 TROPOSCATTER MODEM AND RE-EQUIPMENT CONFIGURATIONS

Both the MDTS and DAR modems utilize Differentially Encoded Quaternary Phase Shift Keying (QPSK) as their modulation techniques. The MDTS phase-modulates a 70-MHz IF carrier over a full symbol duration, while the DAR phase-modulates a 70-MHz IF carrier over only a portion of the symbol duration, thus providing a guard time and reducing the effect of multipath induced intersymbol interference. Interfaces between the ACE High radios and the MDTS and DAR troposcatter modems were accomplished at the 70-MHz intermediate frequency of both the UHF and C-band radios. The modem/RF equipment interface is discussed in para. 3.2.1.

Bandwidth requirements imposed by the MDTS and DAR modems for the test programme are given in Table 4. Filters were used to limit the bandwidths containing 99% of the transmitted power to those given in Table 4. Table 4 reflects the fact that the DAR can operate at a maximum RF spectrum efficiency of 0.7 bit/Hz of RF bandwidth and the MDTS modem can operate at a maximum RF spectrum efficiency of 1.3 bit/Hz with a more optimum RF spectrum efficiency of 1 bit/Hz.

Table 4

Bandwidth constraints

Modem	Data rate (Mbit/s)	Bandwidth (MHz)
MDTS	3.2	3.5
	6.3	7.0
	9.4	7.0
DAR	3.5	7.0
	7.0	10.5

3.2.1 UHF radio configuration

Minor modification of the RF equipment was required for operation with the digital troposcatter modems. This modification included the replacement of the local oscillators by stable frequency synthesizers. Block diagrams of the modifications made to the UHF radio are shown in Fig. 10 and 11, and Fig. 12 is a photograph of the modified UHF radio equipment.

To limit the bandwidth of the transmitted MDTs signal to approximately 3.5 and 7 MHz, 3.1 and 6.2 MHz (3-dB bandwidths) bandpass filters were used to filter the modem IP output at 3.2 and 6.3 Mbit/s respectively. During the 9.4-Mbit/s tests, which were carried out with separate MDTs modems, the 6.2-MHz bandwidth IF filter was used to restrict the signal bandwidth to approximately 7 MHz. For the DAR tests no separate filters were used. A 3-dB hybrid power splitter was installed to split the output 70-MHz signal to drive the dual exciters.

The 70-MHz modem signal was connected to the up-converter by the connection J1 at the rear of the exciter drawer. The normal 70-MHz FDM signal was left disconnected during digital testing. To restore FDM radio operation all that was required was the interchange of 70-MHz signal cables at J1. The frequency-synthesized local oscillator signals were connected to the up-converter/exciter at a level of approximately -5 dBm. Site personnel were able to return to FDM/FM operation in approximately four minutes.

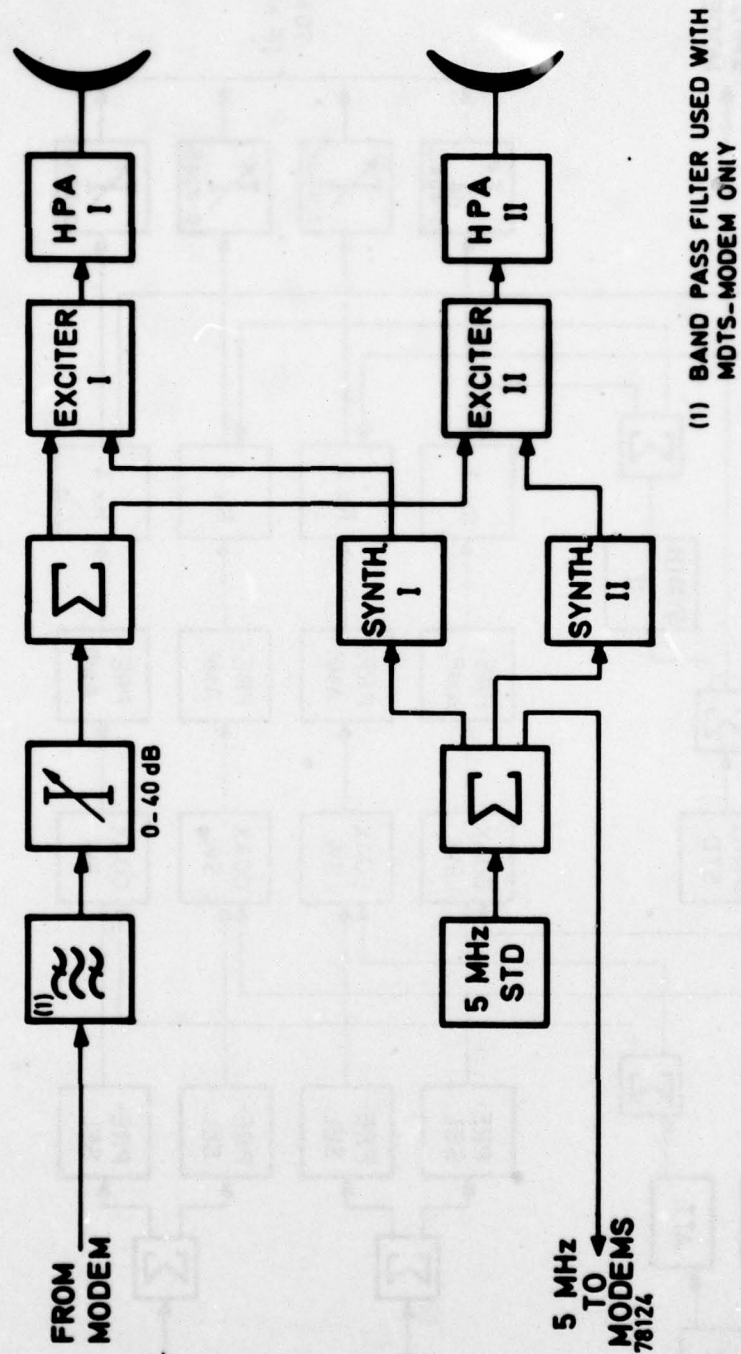


Fig. 10 UHF radio-transmitter configuration

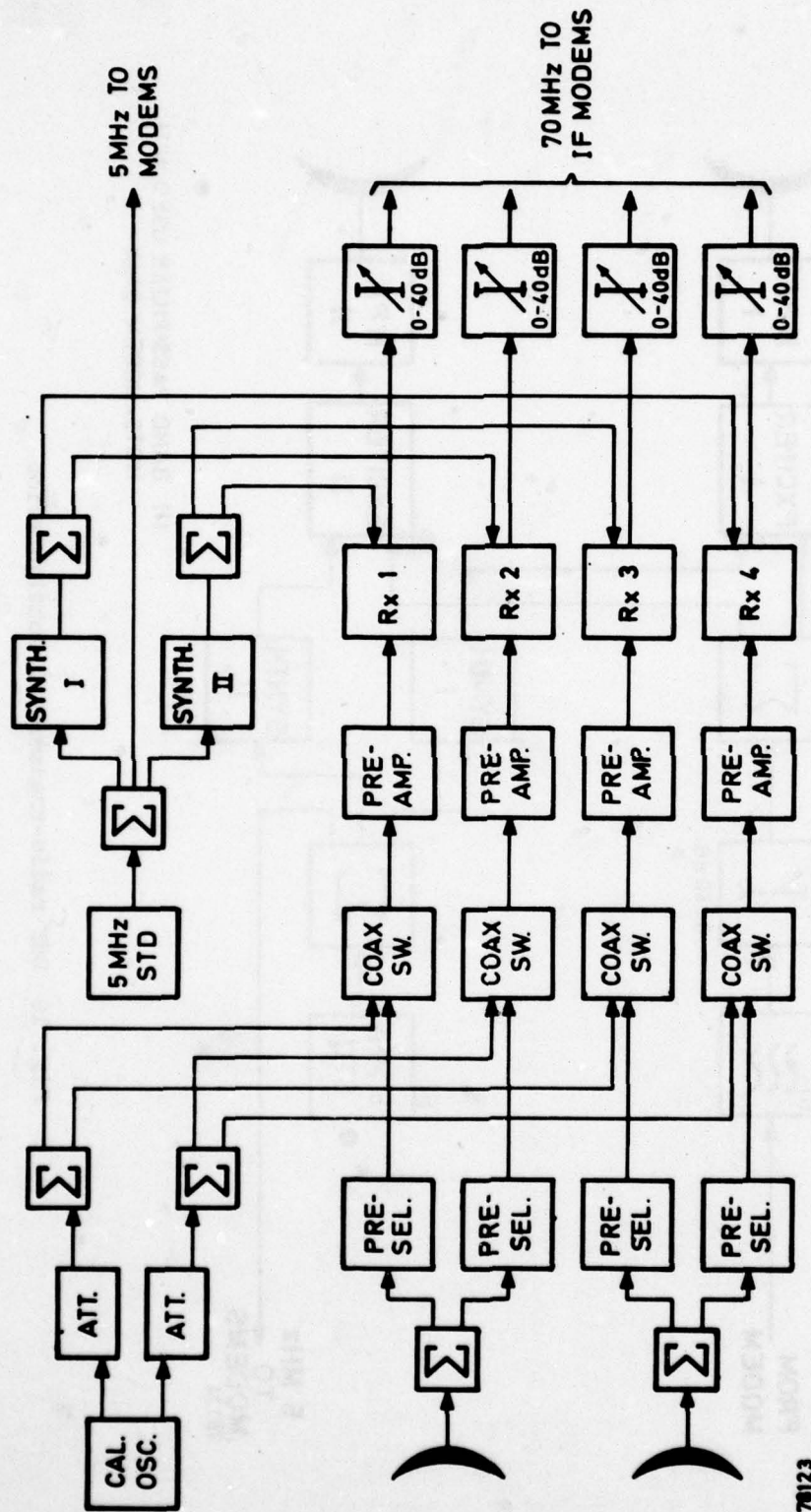


Fig. 11 UHF radio-receiver configuration

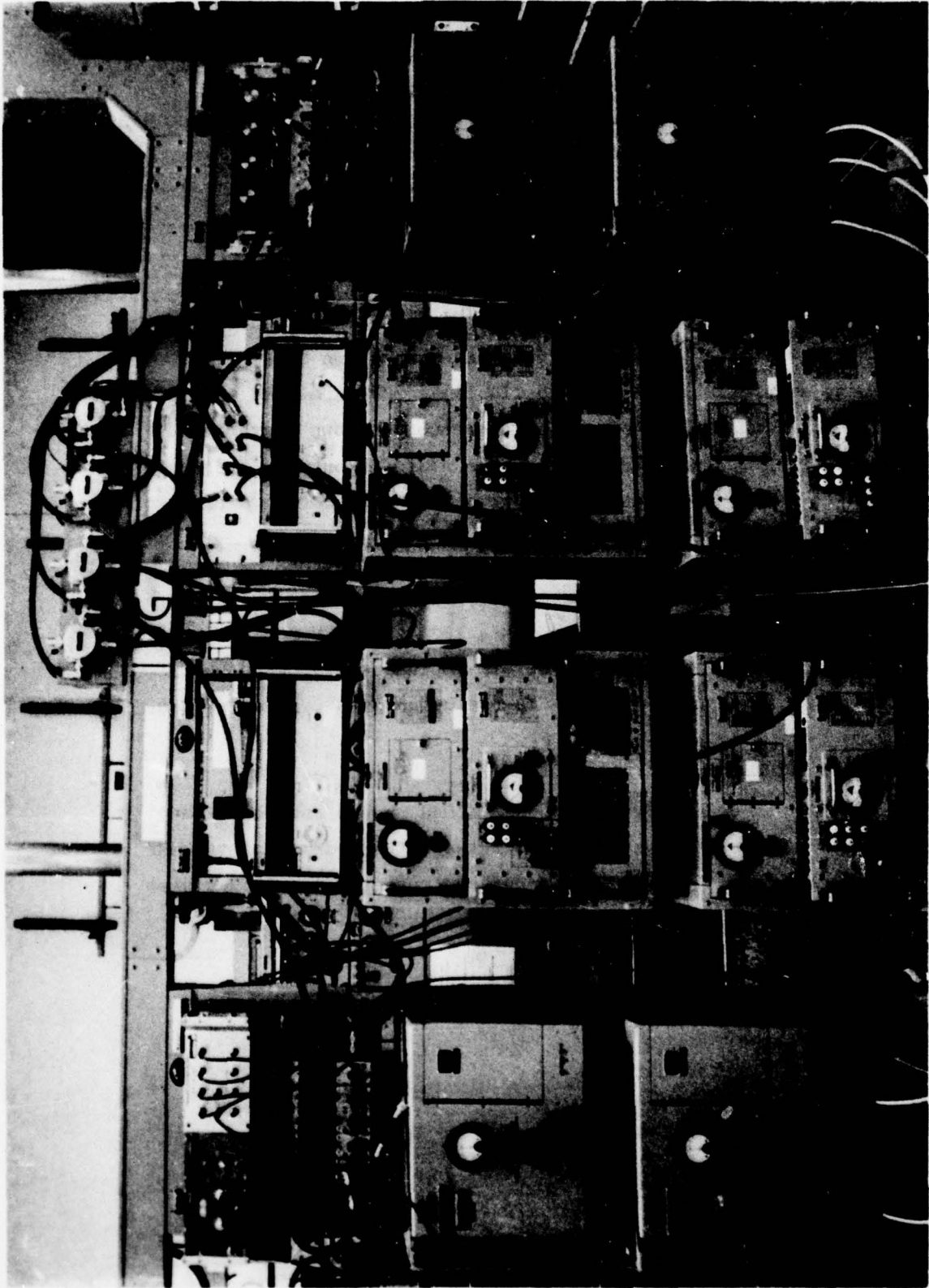


Fig. 12 UHF troposcatter radio with modifications

On the receive side, the insertion loss of the RF presel-ectors was measured and found to be approximately 2.5 dB. The parametric amplifiers were found to have 2-dB peak-to-peak gain in-stability over an hour and were replaced by low-noise transistor RF amplifiers provided by STC.

The local oscillators for the four diversity receivers were replaced by stable frequency synthesizers as shown in Fig. 11. Frequencies of 110.33333 MHz and 114.11111 MHz were used as inputs to the final multiplier stages of the receiver down converters. Attenuators were installed between the radio IF outputs and the modems to provide protection against overloading during periods of high received signal level (RSL).

A calibration unit was provided by STC to calibrate the RSL measuring equipment and was installed in the RF room. The calibration unit (described in detail in Chapter 4) could be switched on line ahead of the RF preselector by a coaxial switch.

3.2.2 C-band radio configuration

The interface between the MDTs/DAR modems and the C-band radio was similar to the interface between the modems and the UHF radios, except that different frequency synthesizer settings were used to stabilize the C-band radio local oscillator.

4. DATA ACQUISITION SYSTEM

4.1 SELECTION OF TEST OBSERVABLES

The test objectives listed in Chapter 1 required that simultaneous measurements be made of received signal level (RSL), dispersion, bit error performance, and bit count integrity (BCI). In addition, there were certain observables of secondary importance which were readily available and which might provide additional information about the performance of the digital link.

The following is a complete list of the observables used to define the requirements of the Data Acquisition System (DAS):

- (a) RSL for each diversity receiver in use
- (b) Multipath dispersion (post-combiner)
- (c) Bit-error events
- (d) Loss-of-BCI events, separately for
 - digital modem
 - asynchronous TDM unit
 - US PCM/TDM
 - NATO PCM/TDM equipment (30/32 channels)
- (e) Modem SNR indicator voltage
- (f) Subjective voice quality.

Sections 4.2 to 4.4 describe the techniques used to measure and record these observables and the necessary calibration procedures.

4.2 MEASUREMENT METHODS

Received signal levels were measured by means of a 70-MHz logarithmic IF amplifier for each diversity receiver. The inputs of these amplifiers were connected in parallel with the modem IF

inputs by a set of four two-way power splitters. The video signals from the DC-coupled outputs could be recorded by several different means, as discussed in Section 4.3. The principal characteristics of the logarithmic amplifiers used are given in Table 5.

Table 5

Principal characteristics of logarithmic IF amplifiers,
RHG Type LST 7010

Centre frequency	:	70 MHz
Bandwidth	:	10 MHz
Risetime	:	100 ns
Input range	:	-80 dBm to 0 dBm
Linearity	:	± 1 dB over input range

One question of concern was whether the amplifiers would correctly measure the level of the timegated RF waveforms employed with the DAR modem. Since the detailed characteristics of the detectors in these amplifiers were not known, a simple measurement was made to determine the performance of the amplifiers with time-gated signals. The measured characteristics for a CW signal and a gated signal with a duty cycle of 50% were compared prior to the start of testing. A 3-dB difference in average power for the same DC output voltage indicated that the logarithmic amplifiers perform peak detection rather than average detection.

The scattering function of a troposcatter channel can be determined experimentally by the measurement of the time-varying complex impulse response over a suitable period of time. Such measurements are carried out most conveniently by probing the channel with a carrier that has been PSK-modulated by a pseudo-random sequence. The principles behind such measurements and a suitable instrumentation are described in detail in Ref. 3. A multipath

analyzer based on the principles given in Ref. 3 was planned for in all the test programme, but unfortunately did not become available in time for measurements on the UHF link. Instead, real-time estimates of the channel dispersion were obtained by the use of a control voltage in the backward equalizers of the modems. Before the actual tests began, experiments with the modems operating over a troposcatter channel simulator had verified that this control voltage is monotonically related to the two sigma (2σ) multipath spread of the channel. Calibrations of the multipath dispersion indicator voltages for the MDTs and for the DAR were obtained prior to the tests (see Appendix C). It should be noted that, for the DAR, no reliable indication was obtained for multipath spreads greater than half a symbol interval, due to the time gating employed with this modem to mitigate intersymbol interference. For the MDTs, a change in the calibration of the dispersion monitor occurred on 6 April 1977 due to a modification of the backward equalizer card in that modem.

For bit-error measurements, use was made of a pseudo-random data source and a corresponding data correlator, both usually referred to as a Simulated Data Source (SDS). For link tests, the SDS units were connected to selected ports of the asynchronous time division multiplexer, AN/GSC -24. In either case, the occurrence of a bit error generated an output pulse that was used to drive various counters.

Loss of synchronization or bit count integrity (LBCI) events were signalled by the various equipments via TTL-compatible control circuits. A retriggerable monostable multivibrator (one-shot) on each circuit ensured that all indications were maintained for a minimum period of 100 ms to allow proper detection by the recording equipment.

Voice monitoring was possible in either of two ways. During system tests, one of the channels in the 24-channel PCM equipment was available for one-way speech communications. In addition, for both system and link tests, a high-quality (64 kbit/s) CVSD digital orderwire was connected to the existing ACE High radio orderwire system to permit a duplex orderwire (analogue in one direction and digital in the other) to be maintained over the link being tested.

4.3 DATA RECORDING TECHNIQUES

The data recording system required for the tests had to serve two distinct functions:

- (a) To perform mass storage of data in a form suitable for subsequent off-line processing.
- (b) To perform direct read-out and/or printing of data to allow the test operator to monitor the quality of the data continuously and to provide a first look at the performance figures obtained.

Due to the large amount of data to be collected, different instrumentations were required to perform these two basic functions. Moreover, the fact that the same data was stored by several different means resulted in a highly desirable redundancy in the test set-up. In fact, very little data was lost during the trials as a result of malfunction of elements of the data acquisition system.

Mass storage of data was performed using a computer-compatible digital tape recorder with a suitable interface unit containing A/D converters, logic for data formatting and multiplexing, a time clock, and switch arrays for labelling the data to be recorded. All the observables listed in Section 4.1, with the exception of analogue speech samples, were recorded on the digital tape. The sampling rate employed was 10 Hz, sufficient to resolve the fastest

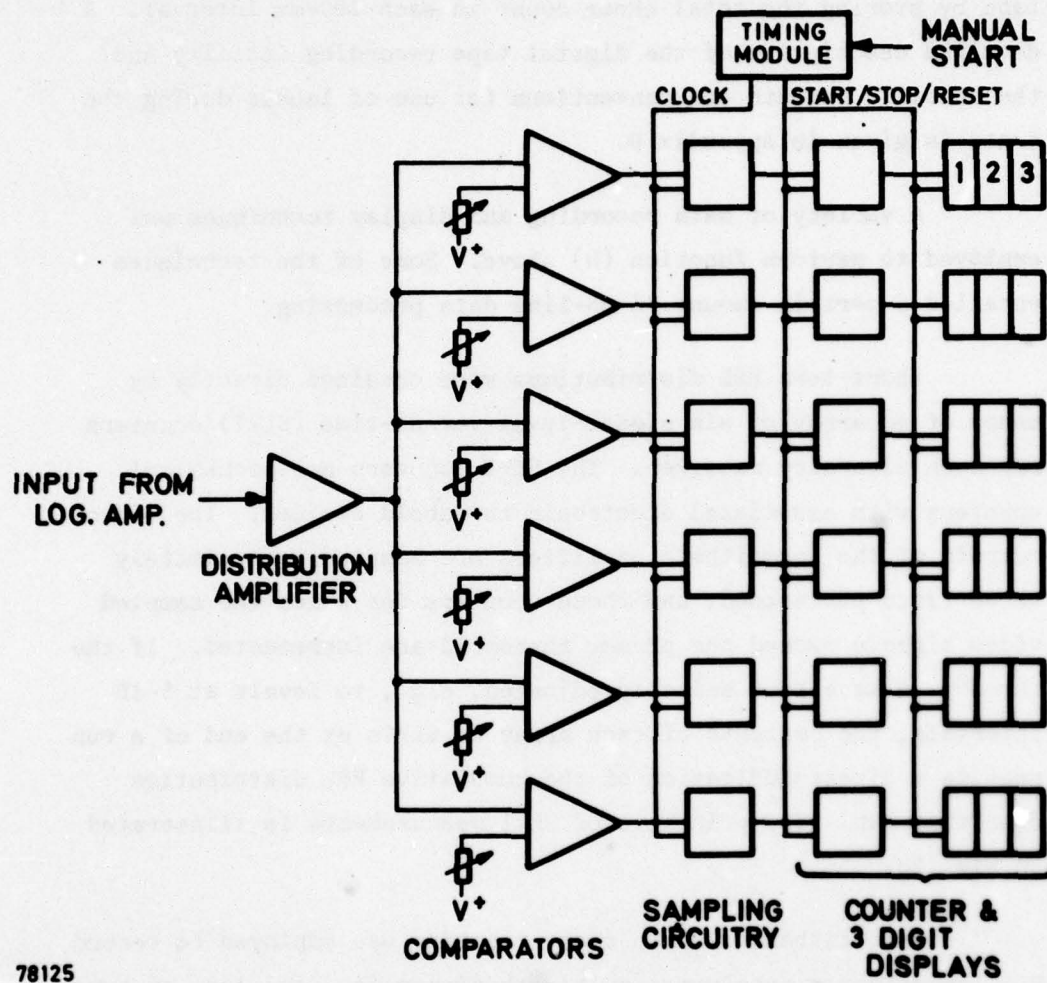
fades expected with the exception of fading caused by aircraft traversing the common volume. Error events were recorded on the tape by storing the total error count in each 100-ms interval. A detailed description of the digital tape recording facility and the specific formats and conventions for use of labels during the tests is given in Appendix D.

A variety of data recording and display techniques was employed to perform function (b) above. Some of the techniques entailed a certain amount of on-line data processing.

Short-term RSL distributions were obtained directly by means of an array of six signal-level-versus-time (SLVT) counters for each diversity receiver. The SLVT counters are mechanical counters with associated electronic threshold devices. The video outputs of the logarithmic amplifiers are sampled approximately three times per second, and those counters for which the sampled video signals exceed the preset threshold are incremented. If the thresholds have been suitably adjusted, e.g., to levels at 5-dB intervals, the contents of each array of SLVTs at the end of a run provide a direct indication of the cumulative RSL distribution over that run. The principle of SLVT measurements is illustrated in Fig. 13.

A multichannel strip chart recorder was employed to record RSL for selected receivers, multipath dispersion, and loss of synchronization events.

In addition to the error counter used with the digital tape recorder, two more counters were used for the direct processing and display of error events. One of these counters simply totaled the errors over a run. The other counted errors over one-second intervals and fed these counts to the Error Distribution Analyzer (EDA) for limited on-line processing. The EDA comprises an array



78125

Fig. 13 SLVT block diagram

of counters, one of which is incremented based on the one-second error count. Each counter has an associated range of error counts:

<u>Counter No.</u>	<u>Error count range</u>
1	0
2	1 to 9
3	10 to 99
:	:
k	10^{k-2} to $10^{k-1} - 1$
:	:
10	Greater than 10^8

At the completion of a run, the contents of the counters are automatically printed on a digital printer, thus giving the distribution of one-second error counts over the run.

Overall block diagrams and a photograph of the DAS are given in Fig. 14 to 16.

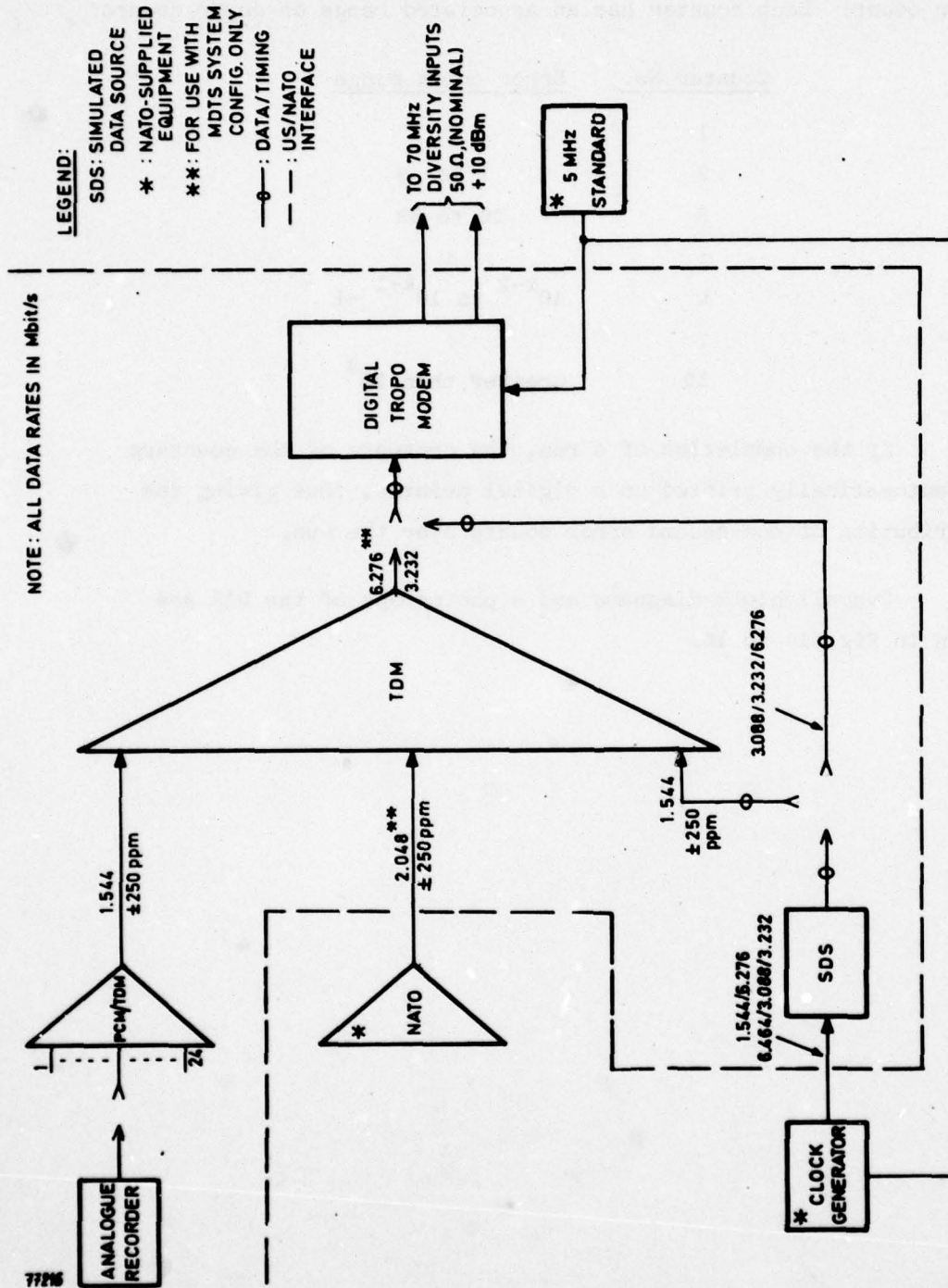
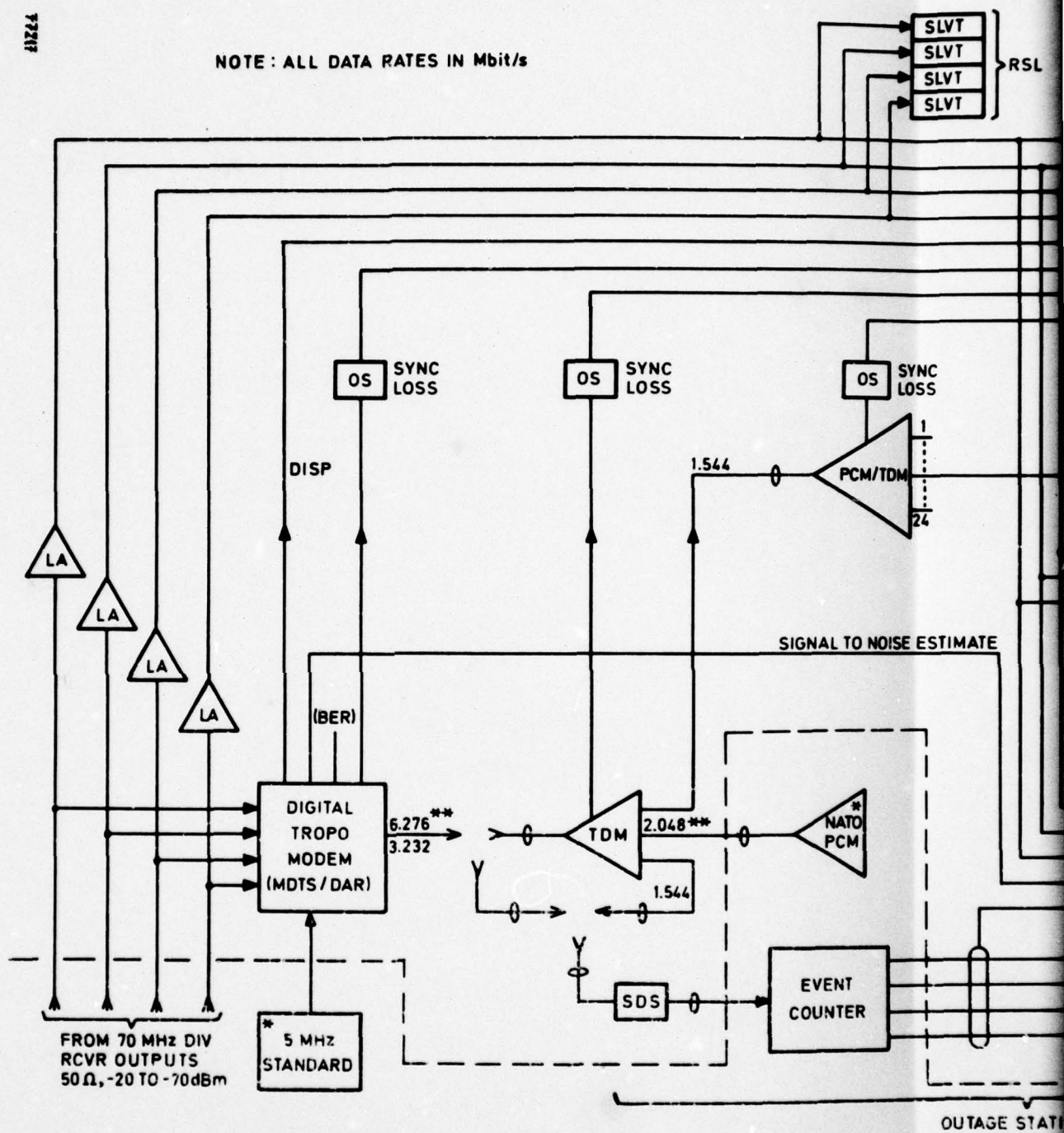


Fig. 14 Data acquisition system (TX)

41224

NOTE: ALL DATA RATES IN Mbit/s



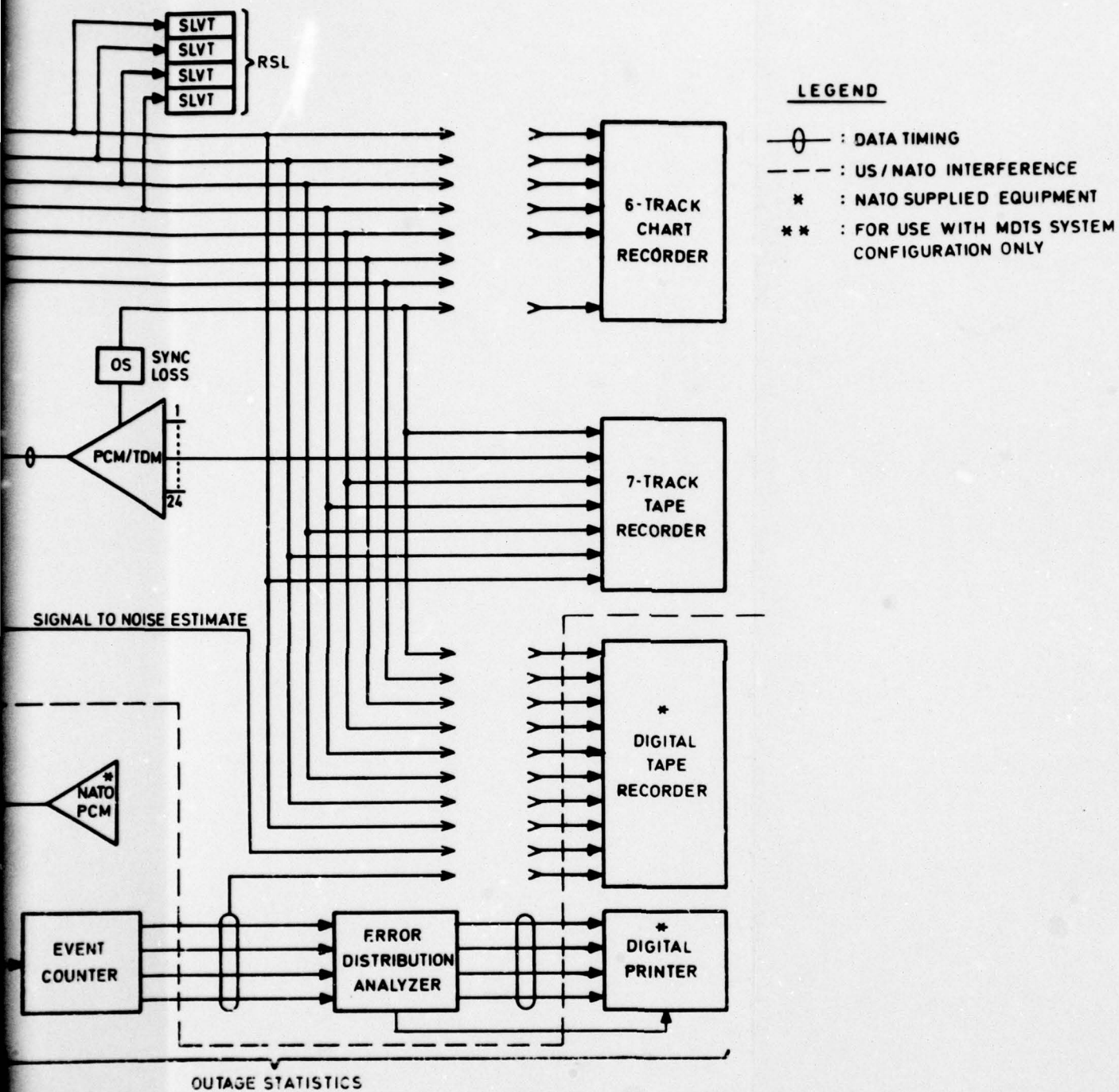


Fig. 15 Data acquisition system (Rx)

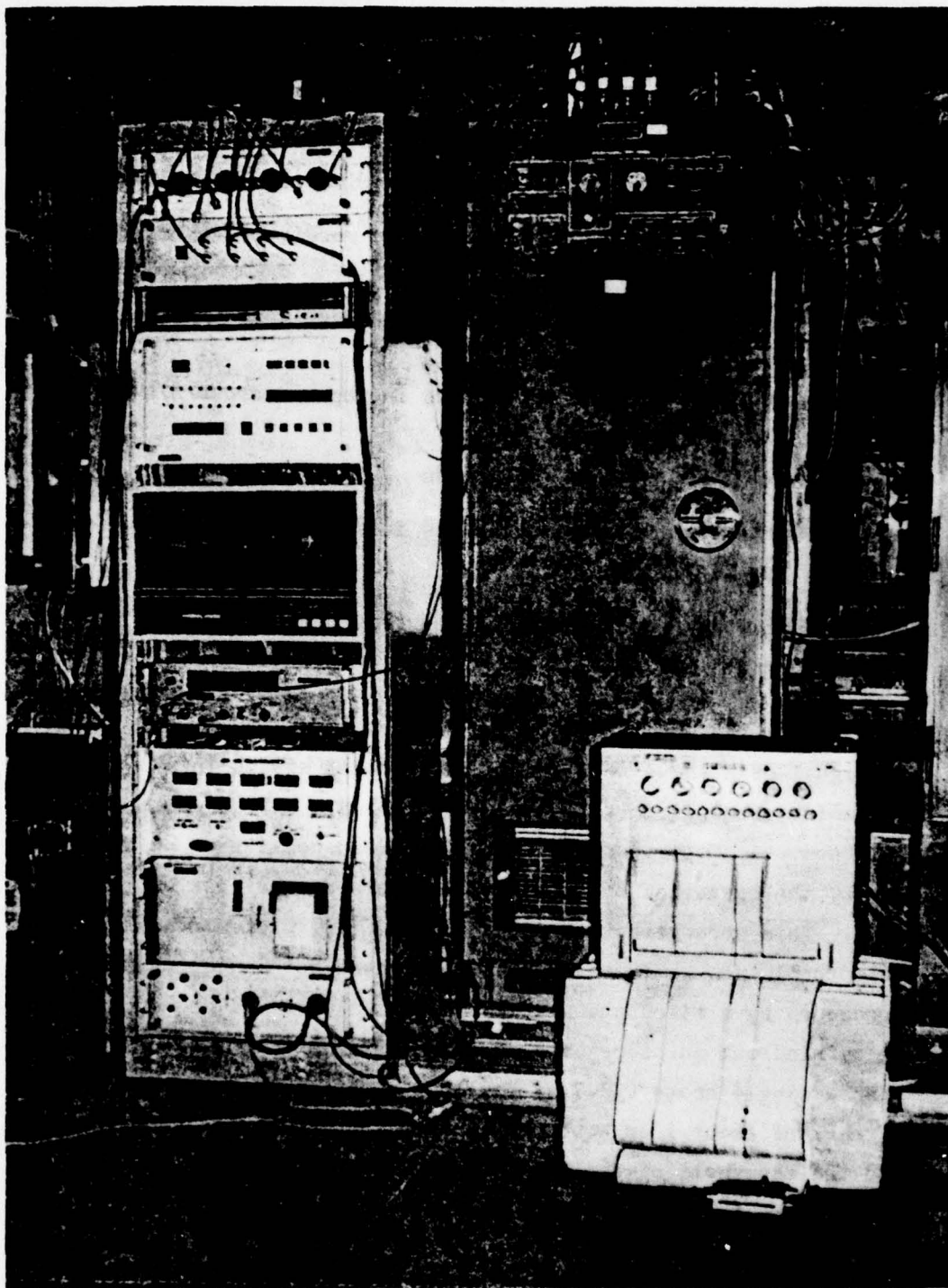


Fig. 16 Data acquisition system (DAS)

4.4 CALIBRATION PROCEDURES

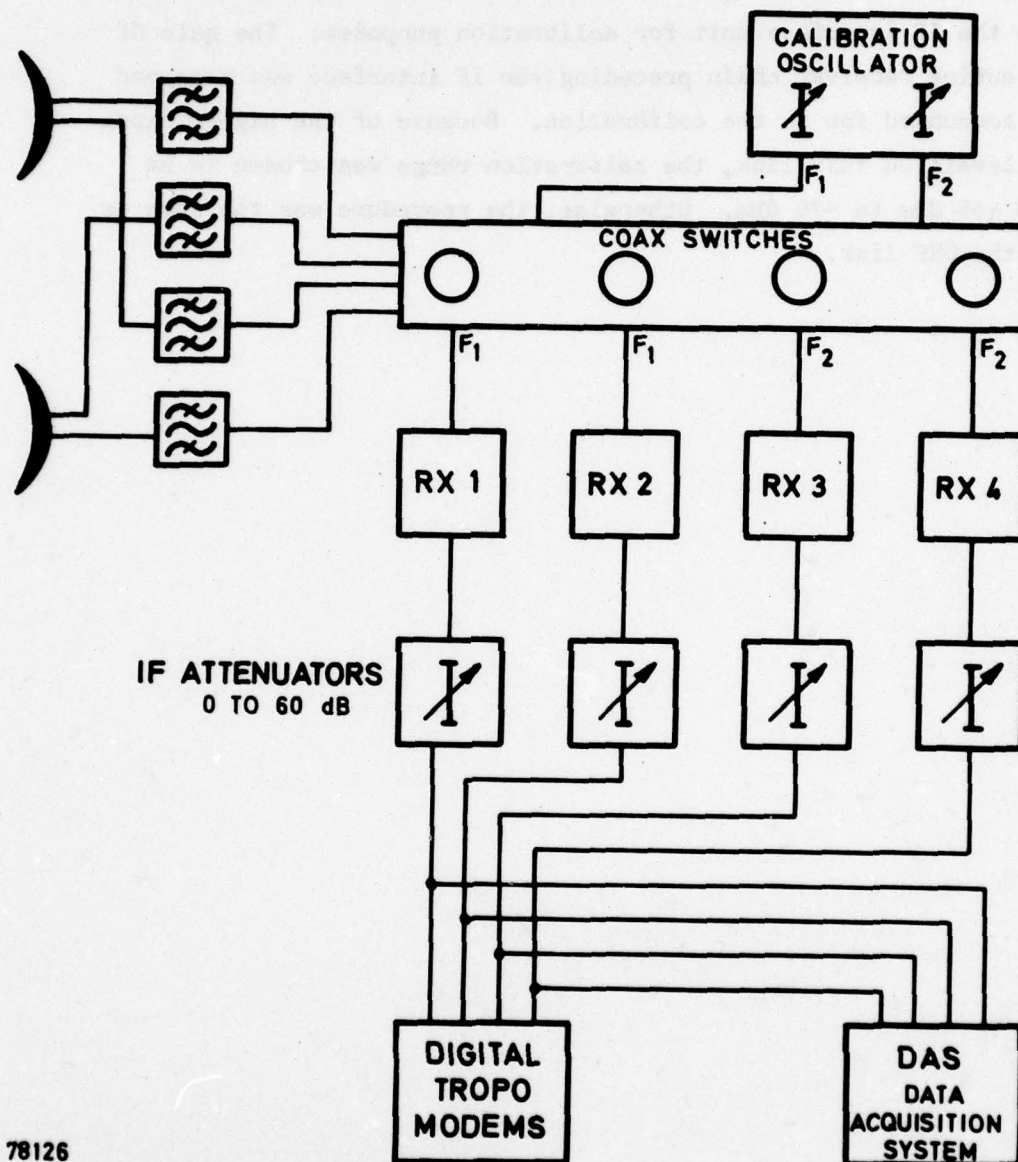
In the Data Acquisition System described in the preceding paragraphs, only the RSL measurements required frequent calibrations. The following sources of inaccuracies were identified:

- (a) Gain variations in diversity receivers (from RF inputs to 70-MHz IF outputs)
- (b) Gain and bias variations in logarithmic amplifiers
- (c) Gain and bias variations in tape recorder A/D converters
- (d) Drift in SLVT thresholds
- (e) Gain and bias variations in strip chart recorder.

Ideally, a calibration procedure should compensate for all these errors.

For the UHF link, a procedure was established by which an RF signal of a known level could be injected at the input of the low-noise preamplifiers by the operation of a set of coaxial switches. A complete range of calibrations could then be carried out by the operation of the IF attenuators in the test equipment rack. This arrangement is shown in Fig. 17. Diplexer and pre-selector losses were measured and accounted for in the calibration procedure by a fixed amount. A typical calibration sequence would be carried out in steps of 5 dB from -65 dBm to -105 dBm; for each step a single frame (12.7 s) would be recorded on the digital tape, a track of about 1 cm would be recorded on the strip chart recorder, and the threshold of the appropriate SLVTs would be adjusted to the point where the counters just began to increment.

The above procedure was difficult to adapt to the C-band link, primarily because all the RF input circuitry is implemented



78126

Fig. 17 Calibration arrangement

with waveguides. It was therefore decided to use IF calibration only, i.e., a 70-MHz signal of a known level was injected directly into the IF interface unit for calibration purposes. The gain of the entire receiver chain preceding the IF interface was measured and accounted for in the calibration. Because of the higher expected levels on this link, the calibration range was chosen to be from -35 dBm to -75 dBm. Otherwise, the procedure was the same as for the UHF link.

5. METHODS OF DATA COLLECTION

As there were a large number of combinations of transmitted data rate and diversity configurations which were of interest, an overall data-collection method was developed to ensure that sufficient time would be available in each transmission configuration of interest to maximize the statistical confidence in the test data. Figure 18 shows the general allocation of test time between the two test links.

5.1 UHF LINK

Much of the first period of the three UHF test periods was allocated to non-diversity and dual-diversity performance testing at all data rates. This was done to ensure that some bit error activity was observed and also to explore the performance sensitivity of the modems to diversity configuration. The second UHF test period emphasized quadruple-diversity testing, to provide information on modem and digital system performance in an operational type of transmission configuration. Unfortunately, after a lightning storm at Dosso dei Galli in the middle of the second test period, transmitter 1 exhibited fast dips in the output power which were reflected in degraded performance on receivers 1 and 3. Only data taken in dual diversity by receivers 2 and 4 were reliable until transmitter 1 was repaired prior to test period 3. Thus, in the second period of UHF link testing, dual-diversity data predominated. A detailed allocation of test time on the UHF link is provided in Tables 6 to 8.

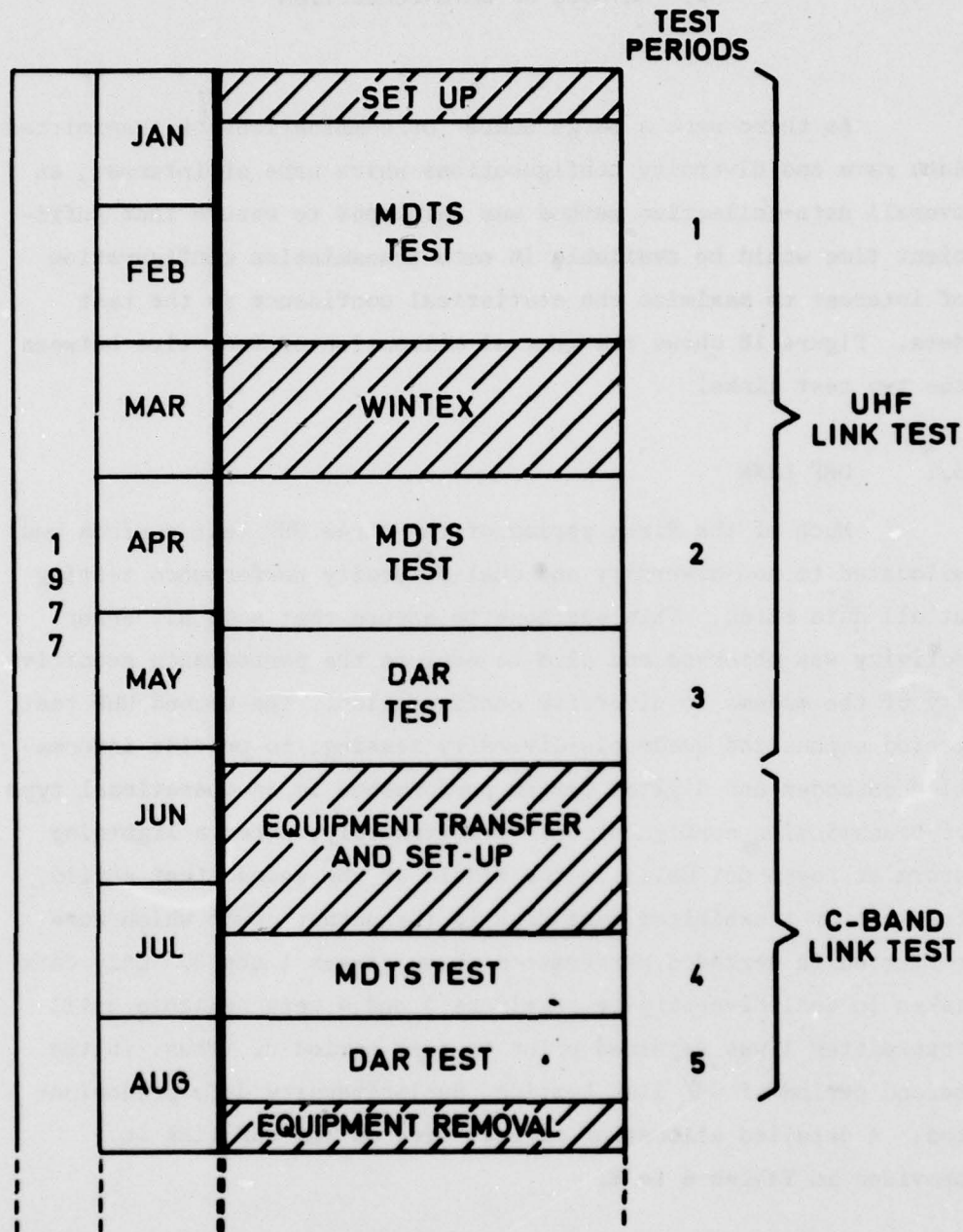


Fig. 18 Test programme structure

Table 6

Summary of short test runs (20 min), January to February 1977

Diversity	No. of runs				
	Data rate (Mbit/s)			Total runs	Percentage
	3.1	6.3	9.6		
Quadruple	51	54	9	114	23
Dual (Rx1 + Rx3)	22	40	6	299	61
Dual (Rx2 + Rx4)	56	149	26		
None (Rx1)	9	8	1	77	16
None (Rx2)	1	10	2		
None (Rx3)	3	6	2		
None (Rx4)	12	21	2		
Others	0	0	3	3	0
Total runs	154	288	51	493	100
Percentage	31	59	10	100	100

Table 7

Summary of test runs, 1 April to 4 May 1977
(MDTS modem UHF link tests)

Note: Because of the malfunctioning of one of the high power amplifiers, certain runs had to be discarded; only those numbers of runs shown in brackets were taken into account in the evaluation of the test data.

Summary of short test runs (20 min), 2 April to 4 May 1977

Diversity	No. of runs			
	Data rate (Mbit/s)		Total runs	Percentage
	3.1	9.6		
Quadruple	105(69)	20	125	62.5
Dual (Rx1 + Rx2)	12(1)	2(0)	14	7
Dual (Rx2 + Rx4)	49	10	59	29.5
Others	2	0	2	1
Total runs	168	32	200	100
Percentage	84	16	100	100

Summary of long test runs (about 15 hr), 1 April to 4 May 1977

Diversity	No. of runs			
	Data rate (Mbit/s)		Total runs	Percentage
	3.1	9.6		
Quadruple	12(5)	3	15	53.6
Dual (Rx1 + Rx3)	3(1)	0	3	10.7
Dual (Rx2 + Rx4)	7	1	8	28.6
Others	2	0	2	7.1
Total runs	24	4	28	100
Percentage	85.7	14.3	100	100

Table 8

Summary of test runs, 16 May to 5 June 1977
(DAR modem UHF band tests)

Summary of short runs (20 min), 16 May to 5 June 1977

Diversity	No. of runs			
	Data rate (Mbit/s)		Total runs	Percentage
	3.5	7.0		
Quadruple	44	21	65	54
Dual (Rx1 + Rx3)	32	4	36	30
Dual (Rx2 + Rx4)	15	0	15	12
Others	3	2	5	4
Total runs	94	27	121	100
Percentage	78	22	100	100

Summary of long runs (about 15 hr), 16 May to 5 June 1977

Diversity	No. of runs			
	Data rate (Mbit/s)		Total runs	Percentage
	3.5	7.0		
Quadruple	3	0	9	43
Dual (Rx1 + Rx3)	7	0	7	33
Dual (Rx2 + Rx4)	5	0	5	24
Others	0	0	0	0
Total runs	21	0	21	100
Percentage	100	0	100	100

5.2 C-BAND LINK

The data collection accomplished on the C-band link was evenly divided between periods of quadruple-diversity and dual-diversity testing. A detailed breakdown of C-band test time is given in Tables 9 and 10. The total test time spent on the C-band link was considerably less than that spent on the UHF test link. This was initially unplanned. Fabrication difficulties in preparing the DAR modem resulted in an extension of the MDTS UHF test period and a subsequent shortening of the C-band test period since the overall test length was fixed. Nevertheless, it is felt that adequate time was spent on the C-band link to gain a satisfactory understanding of DAR and MDTS performance on this type of link.

Table 9

Summary of test runs, 15 July to 29 July 1977
(MDTS modem C-band tests)

Summary of short runs (20 min), 15 July to 29 July 1977

Diversity	No. of runs			
	Data rate (Mbit/s)		Total runs	Percentage
	6.4	9.6		
Quadruple	61	100	161	64
Dual (Rx1 + Rx3)	21	6	27	11
Dual (Rx2 + Rx4)	43	7	50	20
Others { Non diversity No SLVT	0	8	8	3.1
	2	3	5	1.9
Total runs	127	124	251	100
Percentage	50.6	49.4	100	100

Summary of long runs (about 15 hr), 15 July to 29 July 1977

Diversity	No. of runs			
	Data rate (Mbit/s)		Total runs	Percentage
	6.4	9.6		
Quadruple	4	6	10	66.9
Dual (Rx1 + Rx3)	1	0	1	7.7
Dual (Rx2 + Rx4)	2	0	2	15.4
Others	0	0	0	0
Total runs	7	6	13	100
Percentage	54	46	100	100

Table 10

Summary of test runs, 1 August to 14 August 1977
(DAR modem C-band tests)

Summary of short runs (20 min), 1 August to 14 August 1977

Diversity	No. of runs			
	Data rate (Mbit/s)		Total runs	Percentage
	3.5	7.0		
Quadruple	9	135	144	49.1
Dual (Rx1 + Rx3)	4	65	69	23.5
Dual (Rx2 + Rx4)	4	63	67	22.9
Others { Non diversity No SLVT	4	5	9	3.1
	2	2	4	1.4
Total runs	23	270	293	100
Percentage	7.8	92.2	100	100

Summary of long runs (about 15 h), 1 August to 14 August 1977

Diversity	No. of runs			
	Data rate (Mbit/s)		Total runs	Percentage
	3.5	7.0		
Quadruple	0	7	7	54
Dual (Rx1 + Rx3)	0	2	2	15
Dual (Rx2 + Rx4)	0	4	4	31
Others	0	0	0	0
Total runs	0	13	13	100
Percentage	0	100	100	100

6. TEST LINK PREDICTIONS

Propagation and performance predictions were made for the UHF and C-band test links to provide a framework against which to discuss the measured data and the sufficiency of available prediction techniques. Digital performance predictions for the MDTS and DAR modems, at 6.3 and 7.0 Mbit/s respectively, were made for both test links and were based on the propagation predictions discussed below.

6.1 UHF TEST LINK

6.1.1 Received-signal-level predictions

There are two widely-used methods by which a distribution of short-term median received signal levels (RSLs) can be obtained. The first method was developed by the US National Bureau of Standards (NBS) and is described in NBS Technical Note 101 (Ref. 4). The other method is recommended by the CCIR (Ref. 5). The CCIR method is based on that given in NBS Technical Note 101, but is considerably easier to use. The predicted distribution of median RSLs for the UHF test link is shown in Fig. 19 for both the NBS and CCIR methods. A transmitter output power of 4 kW has been assumed. Details of the CCIR calculations are given in Appendix E. In general, the CCIR method predicts a somewhat higher long-term median RSL and a lower standard deviation than the NBS method. This is seen clearly in Fig. 19, although the NBS prediction, computed at a service probability of 0.5, compares moderately well with the CCIR method. However, for the performance predictions in the subsequent sections the more pessimistic assumption of a service probability of 0.95 was used.

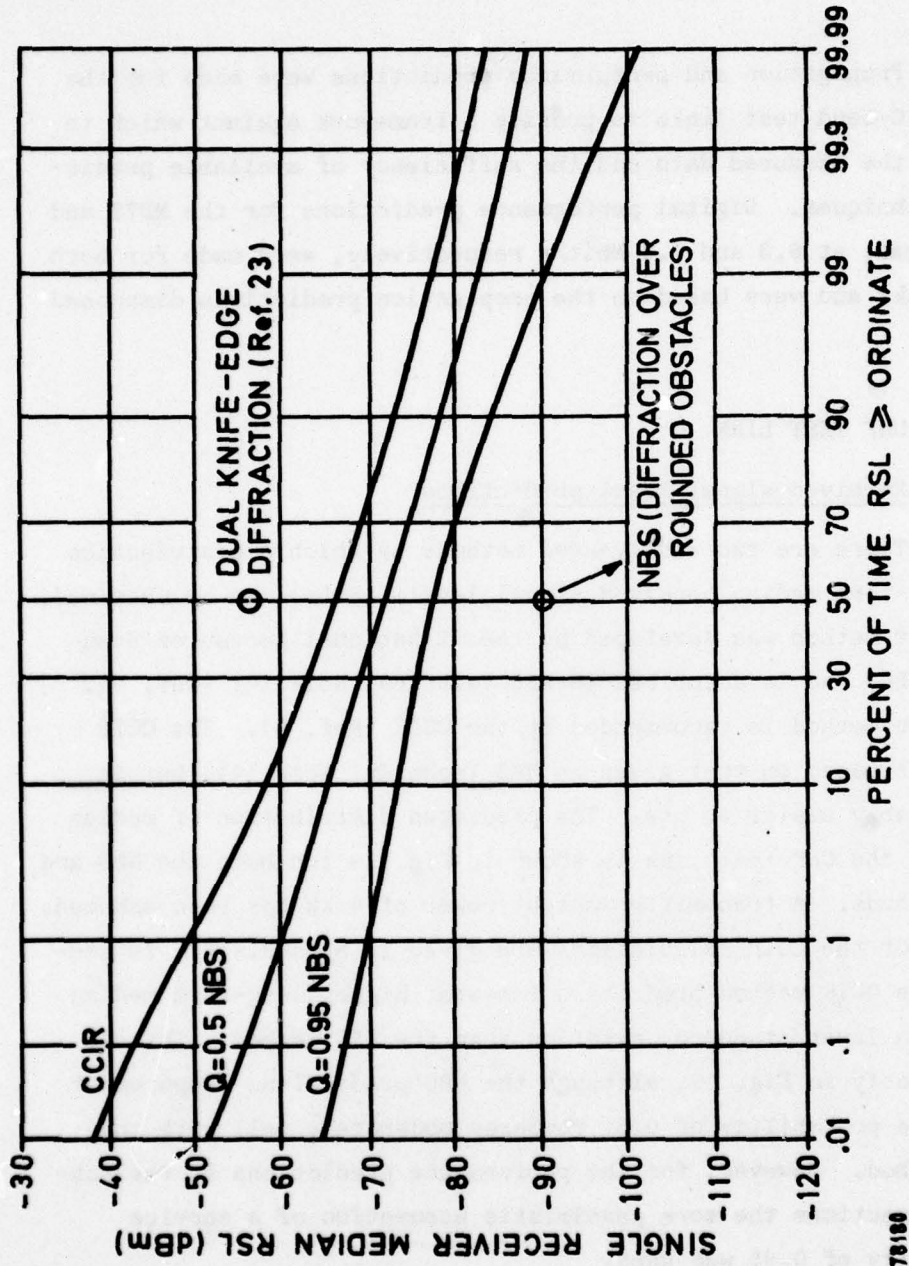


Fig. 19 Predicted RSL distribution (UHF test link)

In addition to troposcatter propagation, a multiple-edge diffraction signal could propagate on the UHF test link, depending on the fine structure of the horizon obstacles shown in Fig. 4. If multiple-edge diffraction were to occur, it would alter the expected RSL distribution considerably. For diffraction paths, the long-term median RSL is typically 20 dB above the scatter level and deviates from the median with a significantly reduced standard deviation, typically less than 2 dB. An RSL calculation based on double knife-edge diffraction was made using CCIR procedures and is detailed in Appendix F. The result of this calculation is noted in Fig. 19 as a single point.

It should be noted that the UHF path profile shown in Fig. 4 does not directly support the hypothesis of knife-edge diffraction. A diffraction calculation using the path profiles of Fig. 4 indicated that the diffraction component would be at least 18 dB below the scatter component power. This calculation, made with a computer program available at DCEC, was based on diffraction over irregular terrain and the gain due to knife-edge obstacles was therefore not considered.

Given the expected distribution of median RSLs, there remains the question of the expected short-term distribution of the RSL about a particular median value. For narrowband troposcatter propagation, the behaviour of short-term RSL is accurately described by Rayleigh statistics. However, because of frequency selective fading, the short-term RSL statistics measured with a wideband signal may deviate from a Rayleigh distribution: a deep fade in only a portion of the transmitted bandwidth of the wideband signal would reduce the total signal level much less than would a corresponding fade in a narrowband signal. Thus, the resultant RSL statistics measured for a wideband signal under frequency selective fading are different from the RSL statistics measured with a narrowband signal, which would be fading in a non-frequency selective manner. The effect of frequency selective fading on RSL statistics is discussed in more detail in Appendix G.

However, for the purposes of prediction, it is assumed that fading on the UHF test link would be sufficiently non-frequency selective and that a correction for selective fading would not be required.

If, as proposed earlier in this section, a diffraction signal were also to be propagated on this link, then the resultant short-term RSL distribution would be Rician rather than Rayleigh.

6.1.2 Dispersion predictions

There are several models by which the 2σ or double-sided RMS dispersion for a troposcatter path can be computed. Early models were developed by S.O. Rice (Ref. 6) and E.D. Sunde (Ref. 22).

More recently, two other troposcatter dispersion models have been developed which utilize various atmospheric parameters to derive delay power spectra. These models were derived by Bello (Ref. 7) and Parl (Ref. 8). The reader is referred to the references for specific mathematical details. Both of these models predict a delay power spectrum which is defined as the ensemble average of the time-varying troposcatter channel impulse response. The basic shape of the delay power spectra derived by both models indicates a gradual decrease in scatter power as a function of path delay. This is in contrast to the abrupt fall-off of received power with increasing path delay described by the Sunde model. For the purpose of developing dispersion predictions for the test links, only the models developed by Bello and Parl will be employed. A quantity, called δ_s , which is the 2σ value of the delay power spectrum, will be used to characterize the dispersion of the test links, i.e.,

$$\delta_s = 2 \left[\int \tau^2 Q(\tau) d\tau - \left(\int \tau Q(\tau) d\tau \right)^2 \right]^{\frac{1}{2}}$$

where $Q(\tau)$ is the normalized delay power spectrum.

The Bello model approximates $Q(\tau)$ as a two-dimensional scatter integral while the Parl model considers scattering in three dimensions.

The delay power spectrum $Q(\tau)$ is in itself a time-varying quantity and a function of large-scale meteorological conditions. The two factors which cause the delay power spectrum to vary are:

- changes in the effective earth radius, Ka , (where a is the actual earth radius) and
- changes in the distribution of refractive-index irregularities in the common volume.

The second factor can be taken into account in the calculation of dispersion by changing the scatter angle exponent, ν , in the Bello model and the slope, n , of the refractive index spectrum in the Parl model. It is shown in Ref. 16 that $\nu = n + 1$.

For the calculation of the median value of dispersion, the standard values $K = 4/3$ and $n = 11/3$ have been assumed. To predict the largest value of δ_s which is likely to occur, estimates had to be made for the worst combination of K and n . Panter (Ref. 9) gives a value of $K = 0.6$ for the European area as a worst-month median for high-altitude scatter paths (see Table 11). It should be pointed out that this data was obtained on the basis of tropo-scatter pathloss measurements which explained all loss variations as resulting from changes in K factor. On the other hand, radio-sonde measurements made in Germany (Ref. 14 and 15) show that a value of $K \leq 1$ does not occur more frequently than 0.1% of the time. A value of $K = 0.66$ was finally selected for the calculation of the worst-hour δ_s . It is estimated that a value of $K = 0.66$ would not occur more frequently than 0.01% of the time.

Table 11

European area K values

	<u>Annual median</u>	<u>Worst-month median</u>
Overland	K = 1.33	K = 0.95
Oversea path	1.90	1.20
High-altitude path (scatter volume at an altitude of 400 m or more)	1.00	0.60
Overland path > 55° lat.	K = 1.33	K = 0.75
Oversea path > 55° lat.	1.90	1.20

With regard to the slope of the refractive index spectrum, a value of $n = 1$ was taken for the calculation of the largest value of δ_s . Based on Ref. 16, this value is exceeded for about 98% of the time.

The results of the dispersion calculation using the models developed by Bello and Parl are shown in Table 12.

6.1.3 UHF link digital performance predictions

Performance predictions for the MDTs and DAR modems were generated as part of the test programme. Because of time limitations, predictions were made on the basis of troposcatter propagation only. Therefore, the effect of other potential propagation modes (e.g., diffraction) is discussed only qualitatively in this section. Short-term and long-term performance predictions of both mean bit error rate (BER) and fade outage rate (see Ref. 2 and 10) were made and are presented in this section as functions of single-receiver median RSL and of time availability respectively.

MDTS modem

The predicted BER performance of the MDTs modem on the UHF test link is shown in Fig. 20 as a function of single receiver median RSL in quadruple diversity. The three curves represent BER

Table 12

Predicted dispersion

Model	K-factor	Elev. angle [*] (°)	Dispersion (ns)
Bello	1.33	0	111
	0.66	0	198
Parl	1.33	0	104
		0.25	137
		0.50	178
	0.66	0	185
		0.25	242
		0.50	304

(a) UHF test link

Model	K-factor	Elev. angle [*] (°)	Dispersion (ns)
Bello	1.33	0	2.3
	0.66	0	34.5
Parl	1.33	0	5.0
	0.66	0	80.0

(b) C-band test link

^{*}Elevation angle of the antennas in beamwidths above the standard radio horizon

predictions for three combinations of antenna elevation angle, K factor, and spectrum slope which bound the conditions which were expected to occur on this link. The rapid fall-off of BER with RSL seen in this figure is partly due to the quadruple diversity configuration and partly due to a slight degree of inband or implicit diversity predicted for this link on the basis of troposcatter propagation.

Figure 21 shows the predicted fade outage probability as a function of single receiver median RSL for the UHF test link. This curve was obtained by the methods derived in Ref. 10 and shows a rapid fall-off in fade outage probability very similar to that seen in Fig. 20.

Figures 22 and 23 show the expected long-term statistics of BER and fade outage rate under the assumption of troposcatter propagation. The calculations are based on the NBS method of prediction for a service probability of 95%. It is worthwhile to consider the effect of other propagation modes on these distributions. As an example, the presence of a significant diffraction component should result in a BER measured at the higher percentiles which would be better than predicted. A diffraction component of significant power should also affect the fade outage probability distribution in essentially the same way.

Further, it should be pointed out that Fig. 22 and 23 show near-error-free or fade-outage-free operation for about 70% of the test period. In practice, random errors can occur due to station power transients and therefore the percentage of time over which the system will operate totally error-free cannot be predicted exactly. The percentage of time over which the system will operate without fade outage should, however, be predictable with greater precision, since random bit errors will generally not occur with sufficient density to cause the recording of a fade outage (i.e., a BER of 10^{-4} measured over a 100-ms interval).

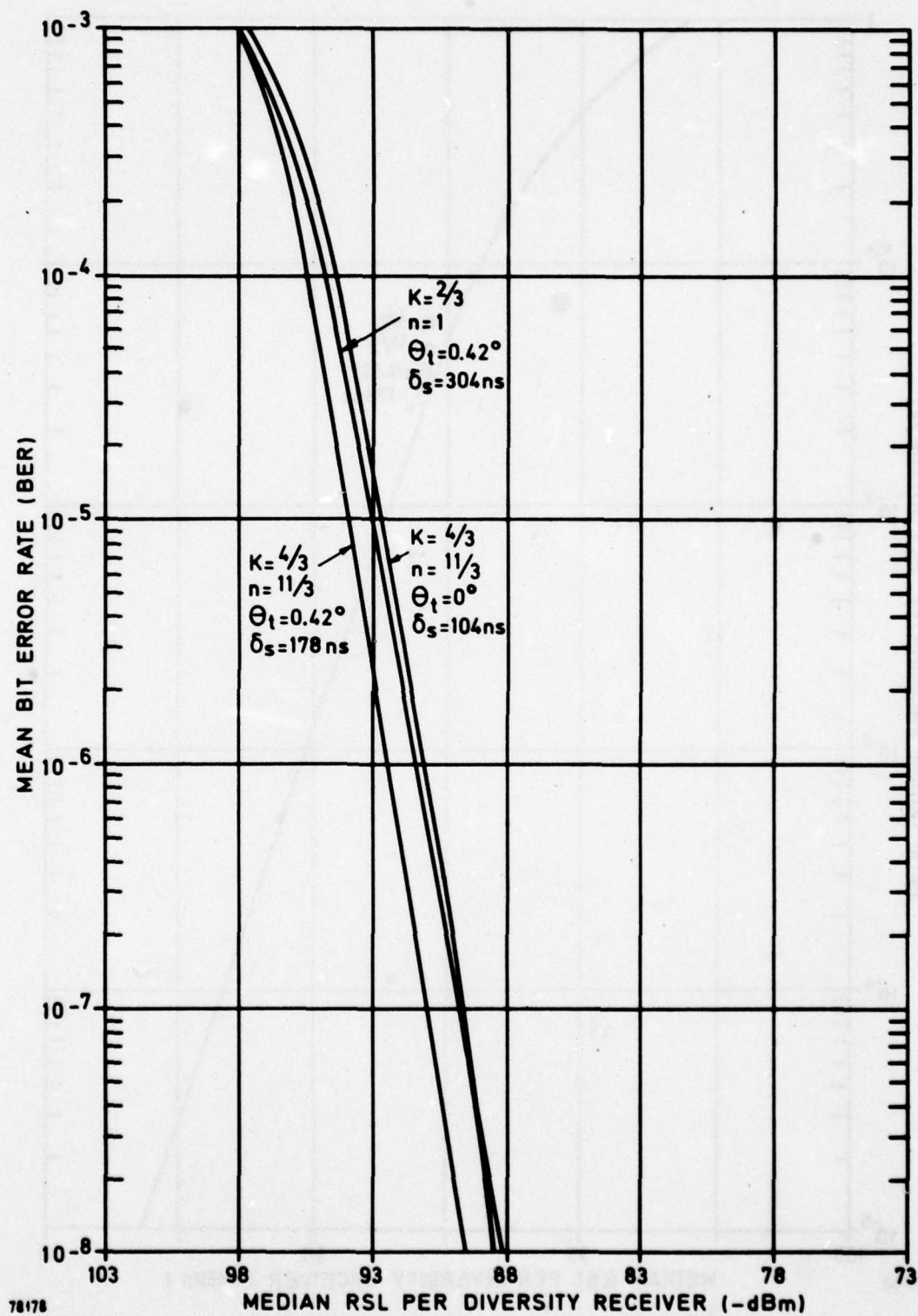


Fig. 20 Predicted MDTs modem performance (quadruple diversity, 6.3 Mbit/s, UHF test link)

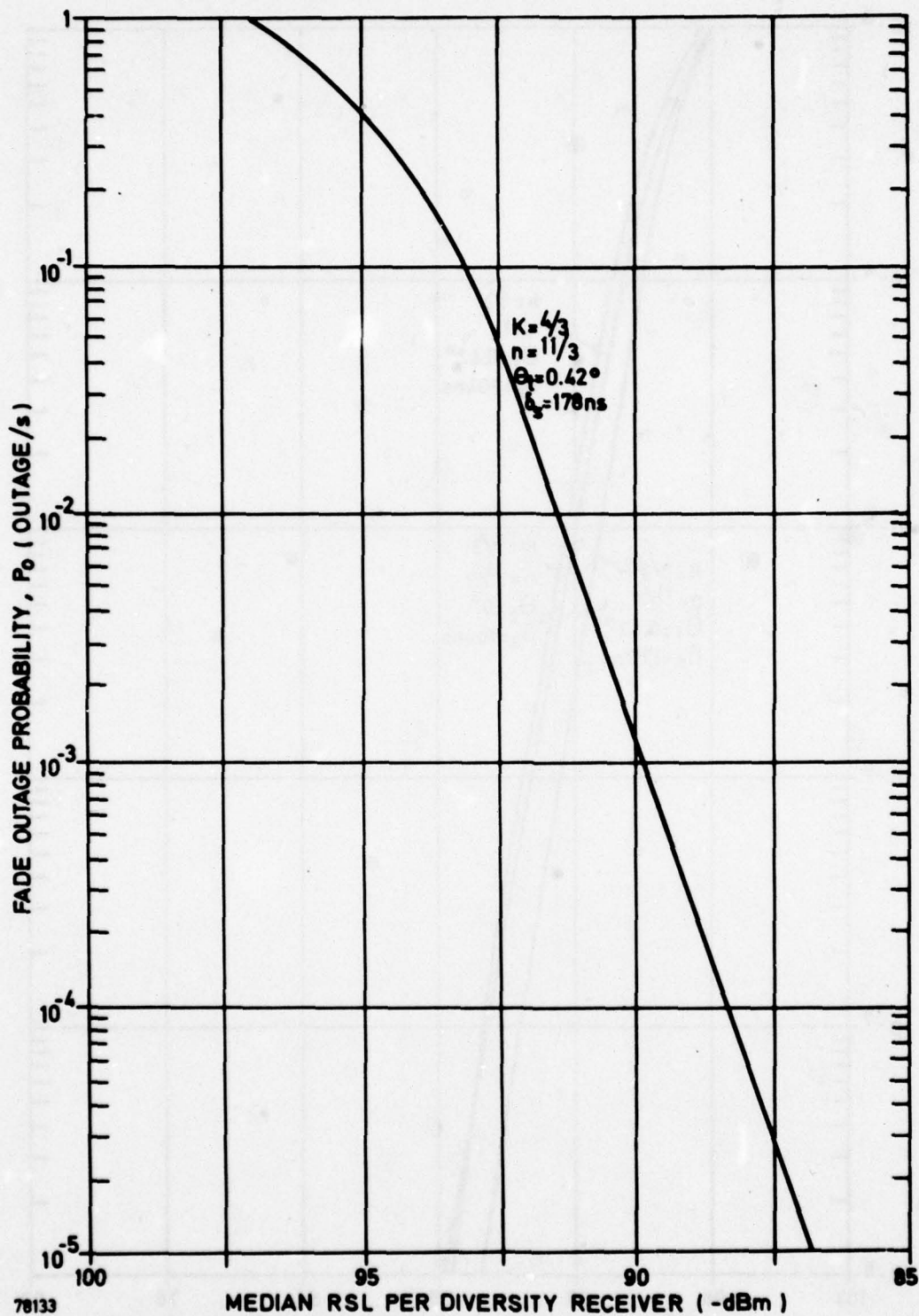


Fig. 21 Predicted fade outage probability MDTs modem
(quadruple diversity, 6.3 Mbit/s, UHF test link)

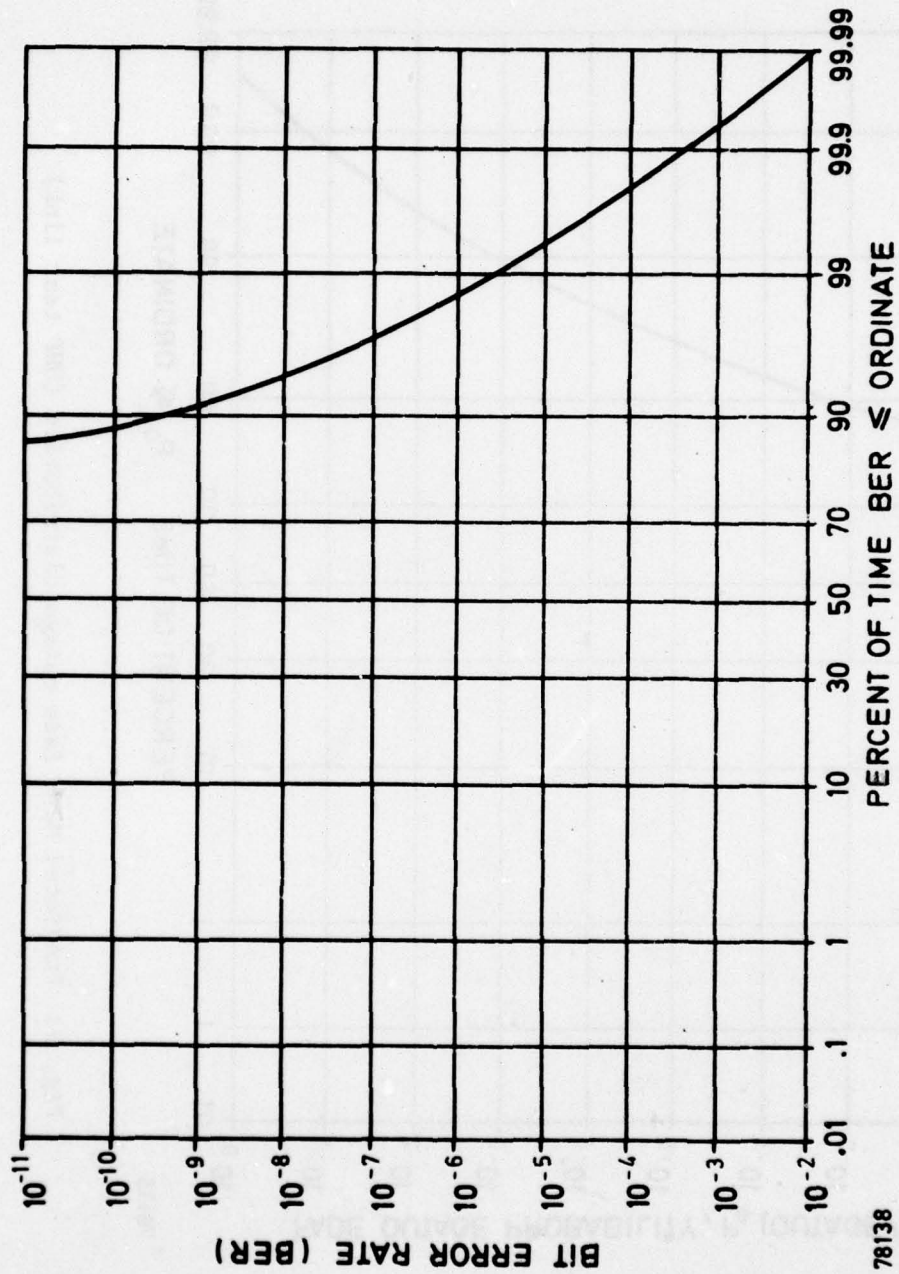


Fig. 22 Predicted MDTs BER distribution (UHF test link)

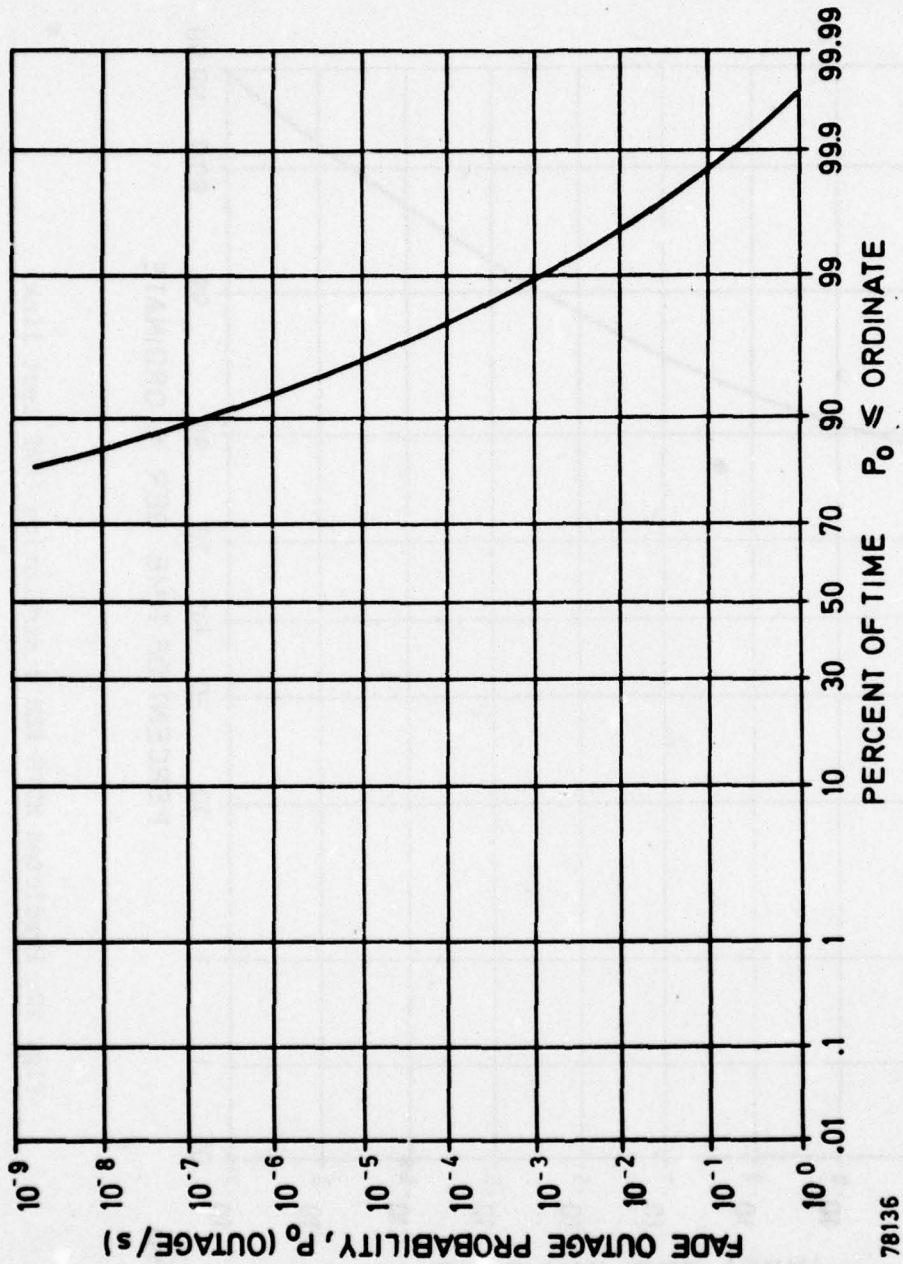


Fig. 23 Predicted MDTs fade outage distribution (UHF test link)

DAR modem

The dispersion handling capability of the DAR modem is more limited than that of the MDTs and therefore assumptions as to the prediction of dispersion on the UHF test link are very important. Figure 24 shows the BER performance of the DAR as a function of single receiver median RSL for values of δ_s encompassing expected conditions. It should be noted that, for the range of predicted median values of δ_s (100-150 ns), the DAR is expected to perform close to its optimum capability. However, for predicted values expected for the smaller percentages of time, the DAR modem may exhibit an irreducible bit error rate caused by dispersion. In fact, at a δ_s of 190 ns, an irreducible bit error rate of approximately 1×10^{-5} is predicted.

The prediction of fade outage probability under the conditions where DAR is within its dispersion handling capability can be obtained by the method described in Ref. 10 and the curve is essentially the same as that shown in Fig. 21 for the MDTs modem. However, the model described in Ref. 10 assumes a negligible multipath dispersion penalty and therefore a prediction of fade outage probability for dispersion-limited performance is not currently available. However, it may be argued that if the DAR modem exhibited a high irreducible bit error rate (true dispersion limited performance), then the probability of "fade" outage might have little significance since dispersion and not fading would cause bit errors. Under this condition, the mean BER rather than fade outage rate might be the most relevant indicator to assess.

Three predicted long-term BER distributions were generated for the DAR modem: for the case where the dispersion is as predicted under nominal conditions and for cases where the dispersion is 190 and 280 ns. The distributions are shown in Fig. 25. A long-term prediction of fade outage probability for the DAR was not made because the fade outage probability under dispersion-limited conditions could not be predicted with any accuracy.

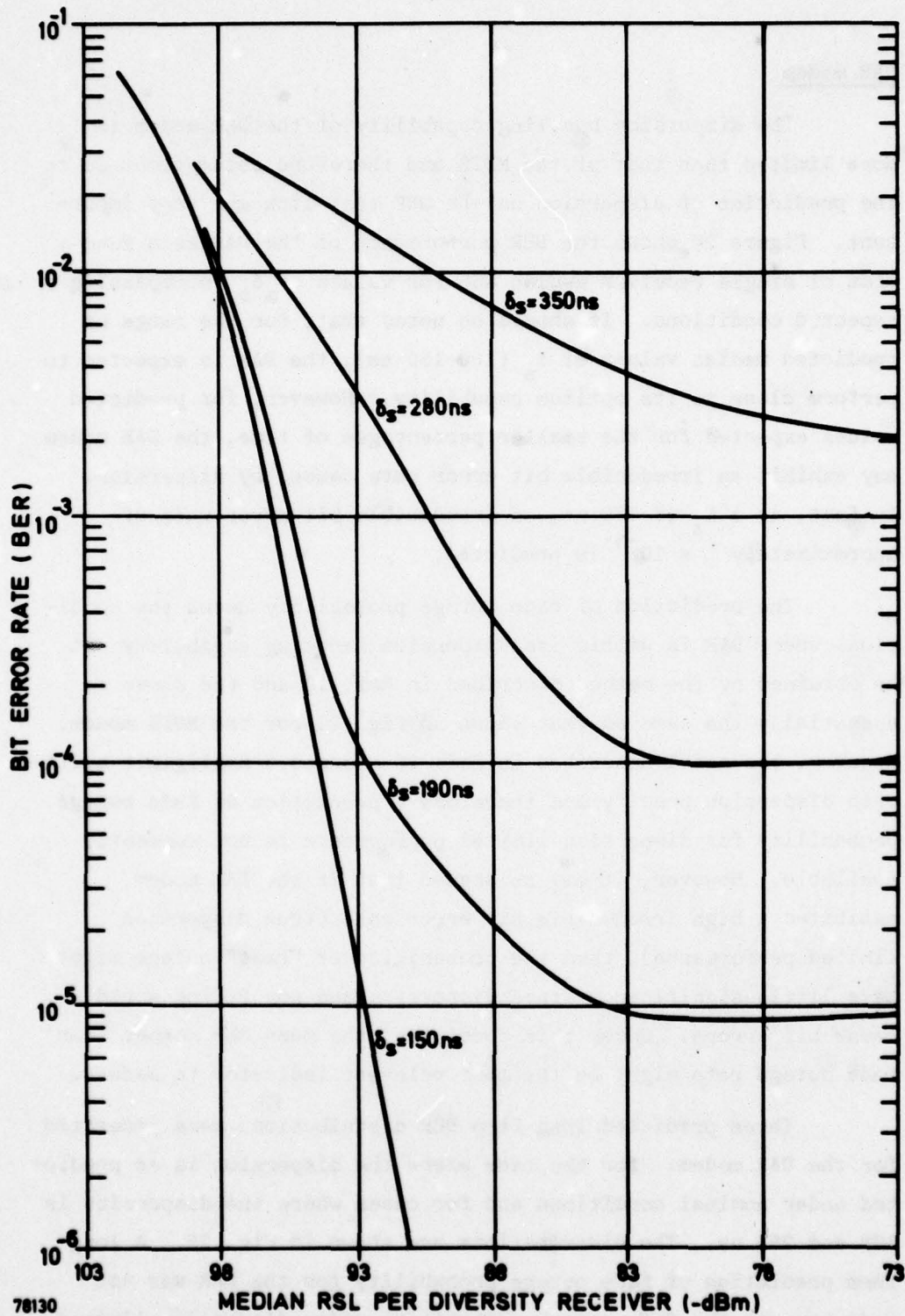


Fig. 24 Predicted DAR modem performance (quadruple diversity, 7.0 Mbit/s, UHF test link)

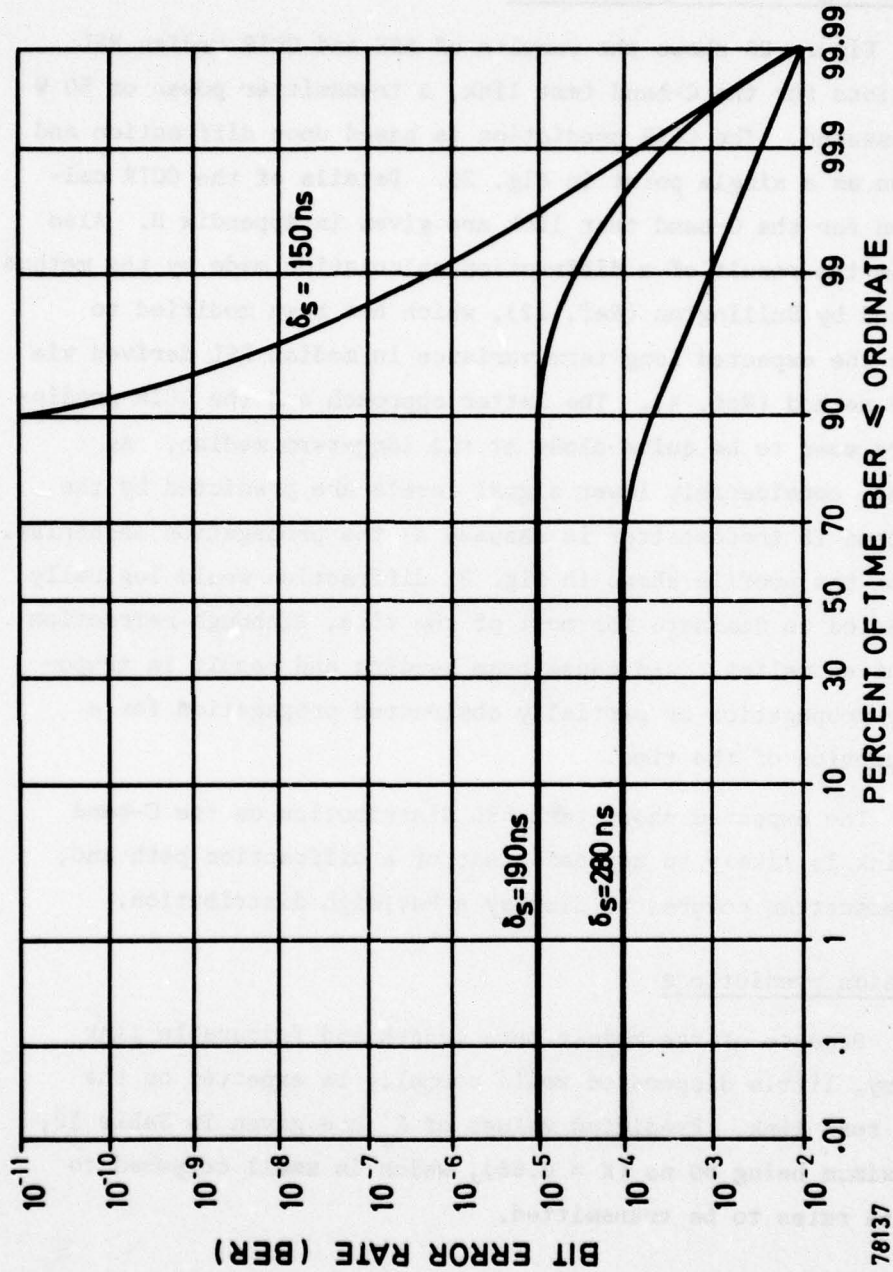


Fig. 25 Predicted DAR BER distributions (UHF test link)

6.2 C-BAND TEST LINK

Received signal level predictions

Figure 26 shows the results of NBS and CCIR median RSL predictions for the C-band test link, a transmitter power of 50 W being assumed. The CCIR prediction is based upon diffraction and is shown as a single point in Fig. 26. Details of the CCIR calculation for the C-band test link are given in Appendix H. Also shown is the result of a diffraction calculation made by the method described by Bullington (Ref. 12), which has been modified to include the expected long-term variance in median RSL derived via the NBS method (Ref. 4). The latter approach and the CCIR prediction are seen to be quite close at the long-term median. As expected, considerably lower signal levels are predicted by the NBS method if troposcatter is assumed as the propagation mechanism. Based on the profile shown in Fig. 3, diffraction would logically be expected to dominate for most of the time, although refraction gradient anomalies could cause beam bending and result in troposcatter propagation or partially obstructed propagation for a small portion of the time.

The expected short-term RSL distribution on the C-band test link is likely to approach that of a diffraction path and, if troposcatter occurs, to display a Rayleigh distribution.

Dispersion predictions

Because of the modest path length and favourable link geometry, little dispersion would normally be expected on the C-band test link. Predicted values of δ_s are given in Table 12, the maximum being 80 ns ($K = 0.66$), which is small compared to the data rates to be transmitted.

Performance predictions

The low dispersion and elevated RSL expected on the C-band path make the prediction of MDTs and DAR performance straightforward.

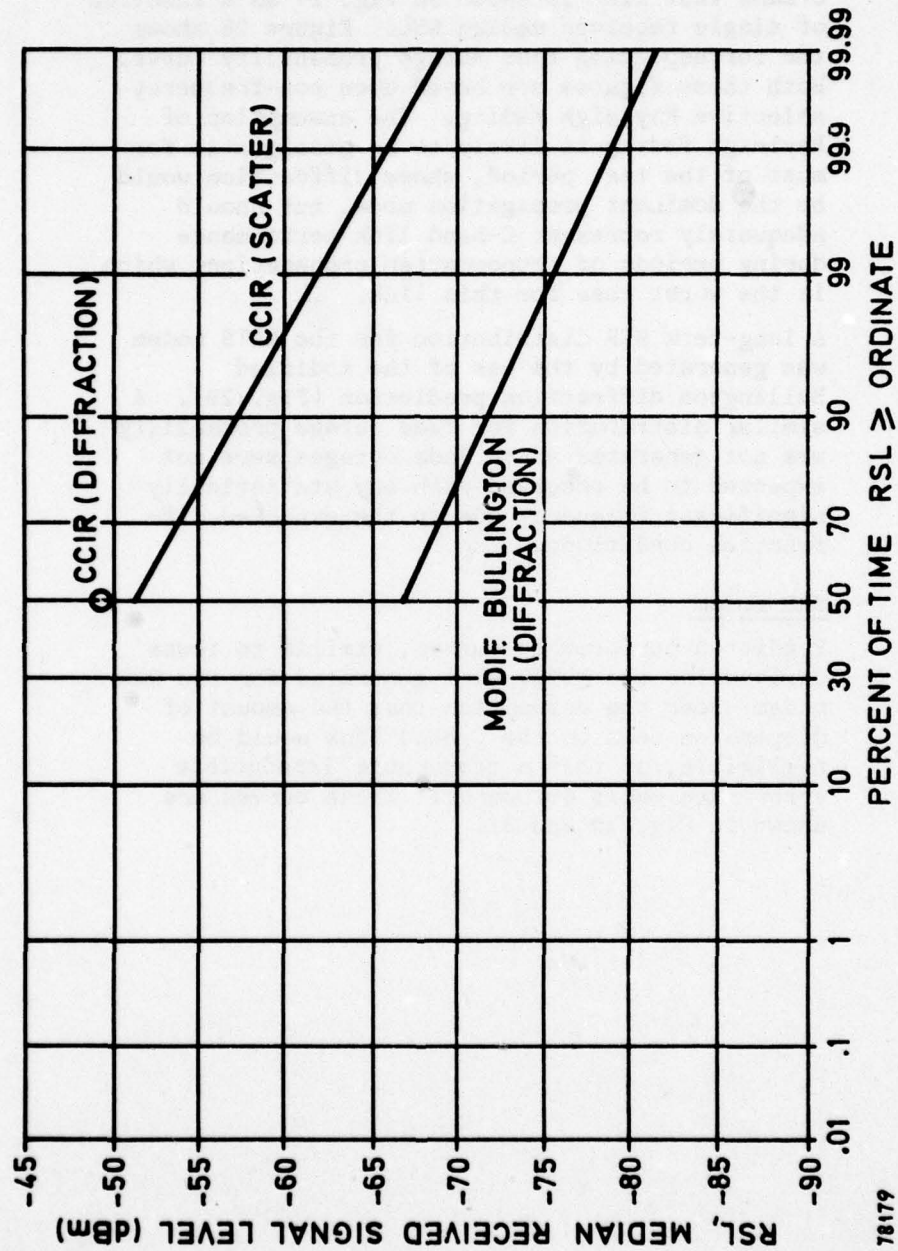


Fig. 26 Predicted RSL distributions (C-band test link)

- MDTS modem

The predicted BER performance of the MDTS on the C-band test link is shown in Fig. 27 as a function of single receiver median RSL. Figure 28 shows the corresponding fade outage probability curve. Both these figures are based upon non-frequency selective Rayleigh fading. The assumption of Rayleigh fading is likely to be pessimistic for most of the test period, where diffraction would be the dominant propagation mode, but should adequately represent C-band link performance during periods of troposcatter propagation, which is the worst case for this link.

A long-term BER distribution for the MDTS modem was generated by the use of the modified Bullington diffraction prediction (Fig. 29). A similar distribution for fade outage probability was not generated since fade outages were not expected to be observed with any statistically significant frequency due to the expected diffraction conditions.

- DAR modem

Predicted performance curves, similar to those derived for the MDTS, were generated for the DAR modem under the assumption that the amount of dispersion seen on the C-band link would be negligible, so that a measurable irreducible error rate would not occur. These curves are shown in Fig. 30 and 31.

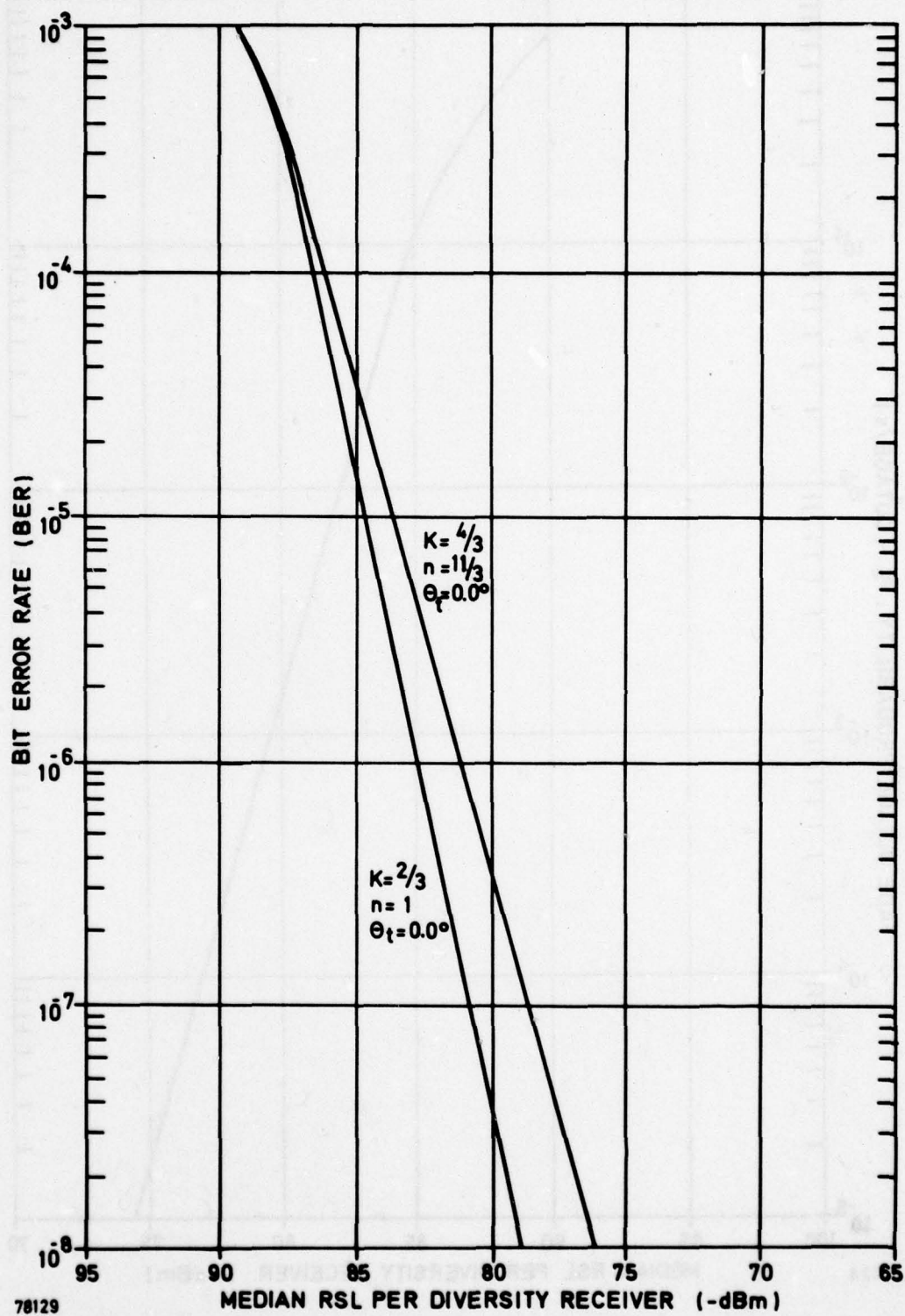


Fig. 27 Predicted MDTS modem performance (quadruple diversity, 6.3 Mbit/s, C-band test link)

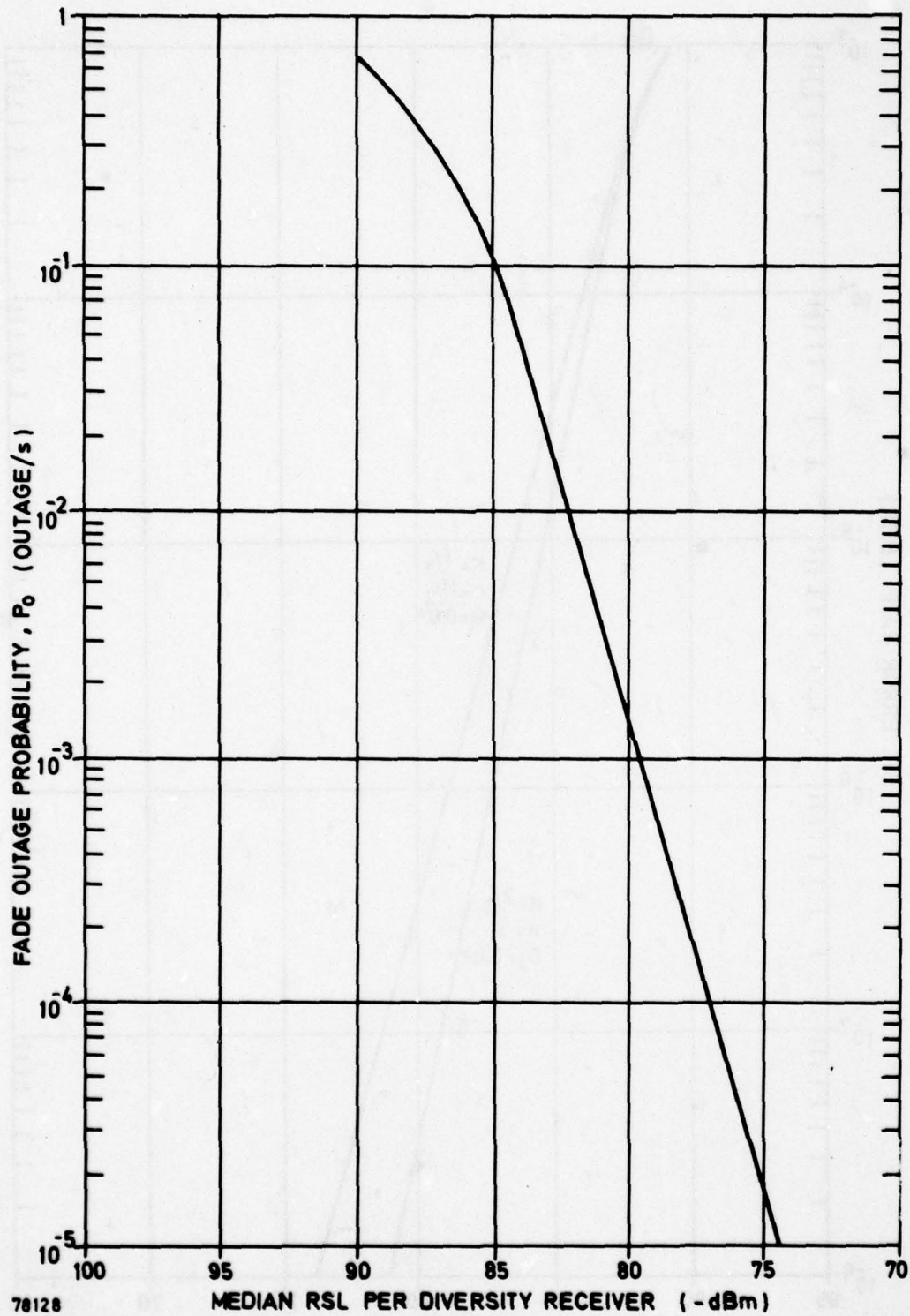


Fig. 28 Predicted MDTs fade outage probability (C-band test link)

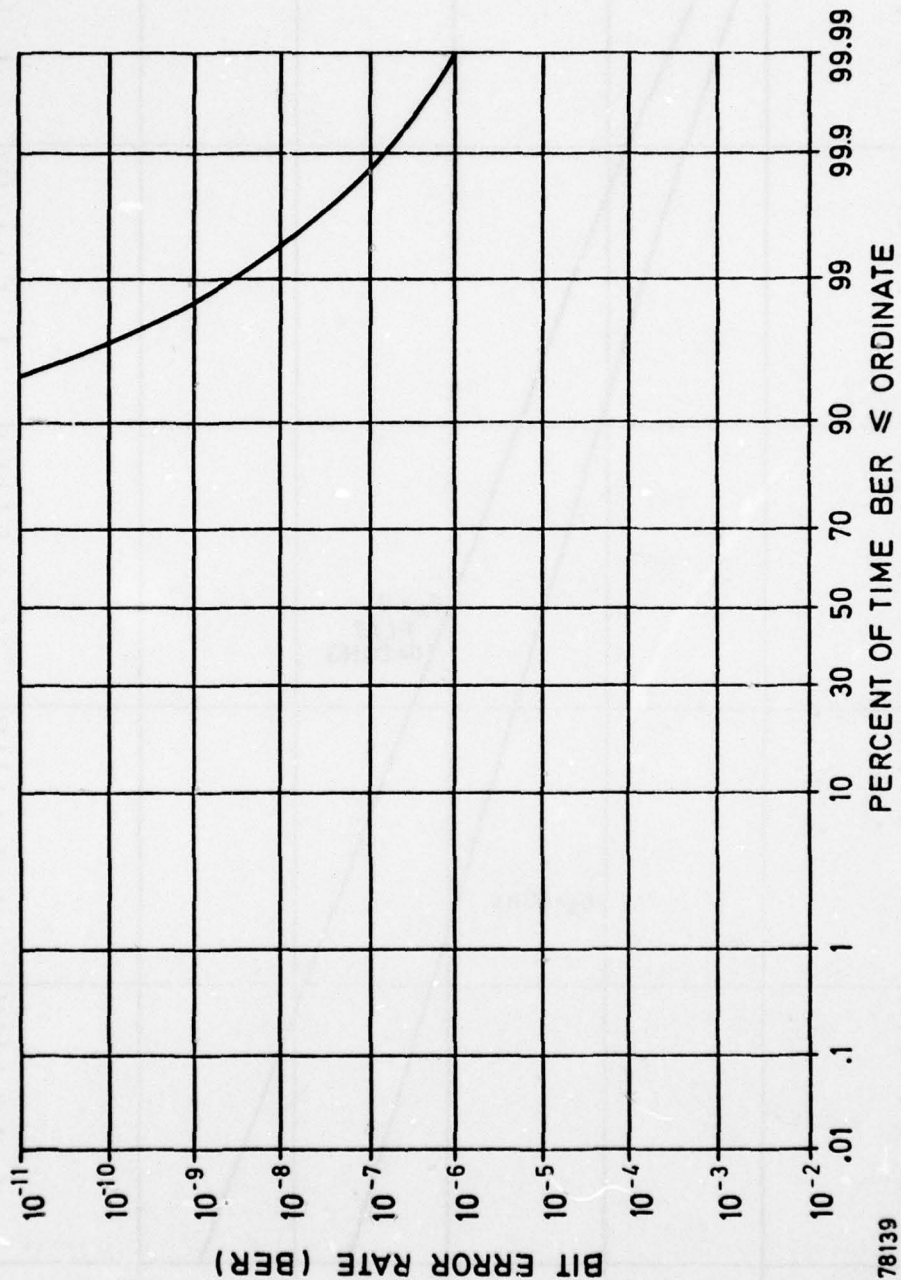


Fig. 29 MDTs predicted BER distribution (C-band test link)

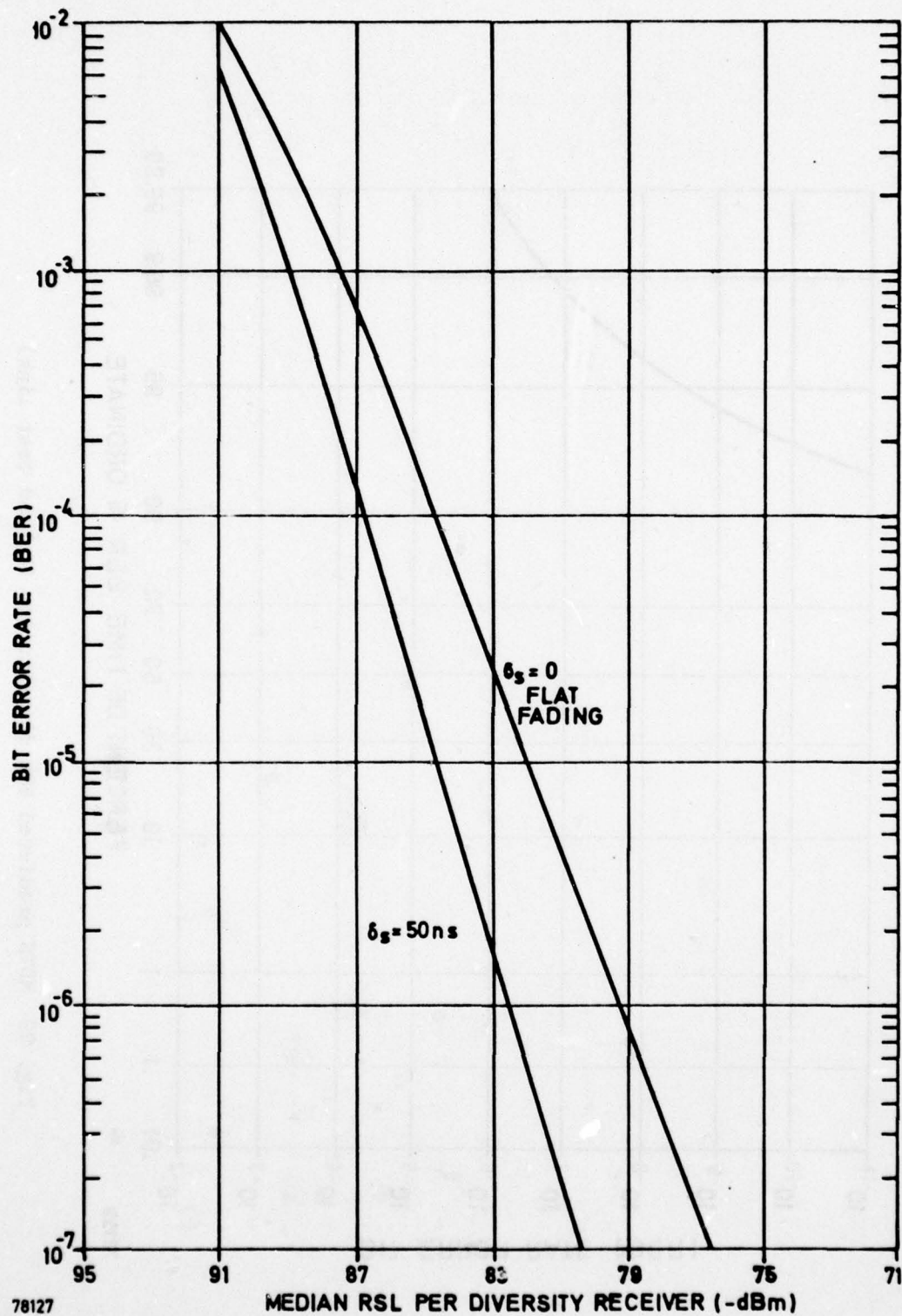


Fig. 30 Predicted DAR modem performance (quadruple diversity, 7.0 Mbit/s, C-band test link)

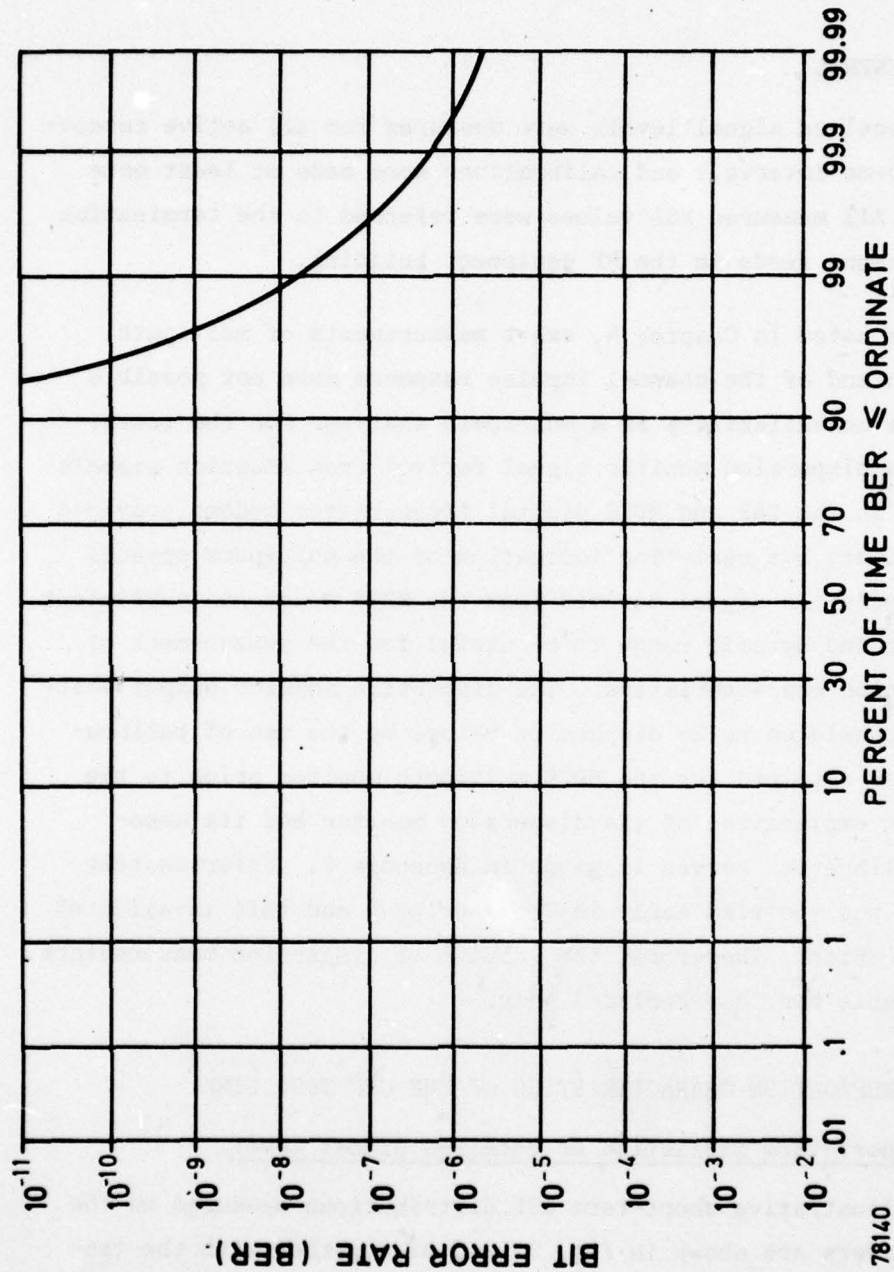


Fig. 31 Predicted DAR BER distribution (C-band test link)

7. MEASURED PROPAGATION CHARACTERISTICS

7.1 GENERAL

Received signal levels were measured for all active receivers at 100-ms intervals and calibrations were made at least once per day. All measured RSL values were referred to the termination of the antenna feeds in the RF equipment building.

As noted in Chapter 4, exact measurements of multipath dispersion and of the channel impulse response were not possible due to the unavailability of a multipath analyzer for the tests. However, a dispersion monitor signal derived from adaption signals contained in the DAR and MDTS digital troposcatter modems provided an approximate but real-time indication of the multipath spread. However, only the signal derived from the MDTS modem had sufficient resolution and dynamic range to be useful for the measurement of 2σ dispersion characteristics. The dispersion monitor output voltage was translated to 2σ dispersion values by the use of calibration curves obtained for the MDTS multipath monitor prior to the tests. An explanation of the dispersion monitor and its associated calibration curves is given in Appendix C. Unfortunately the modem was modified early in Test Period 2 and this invalidated the calibration. Therefore, the results of dispersion measurements are available for Test Period 1 only.

7.2 PROPAGATION CHARACTERISTICS OF THE UHF TEST LINK

7.2.1 Short-term statistics of received signal level

Illustrative short-term RSL distributions measured on the four receivers are shown in Fig. 32 and 33 together with the theoretical distribution for a Rayleigh fading signal. In Fig. 32, which was obtained during an active fading period, the distribution of the signal level measured in Rx 4 agrees moderately well with the Rayleigh distribution, except at the higher percentages.

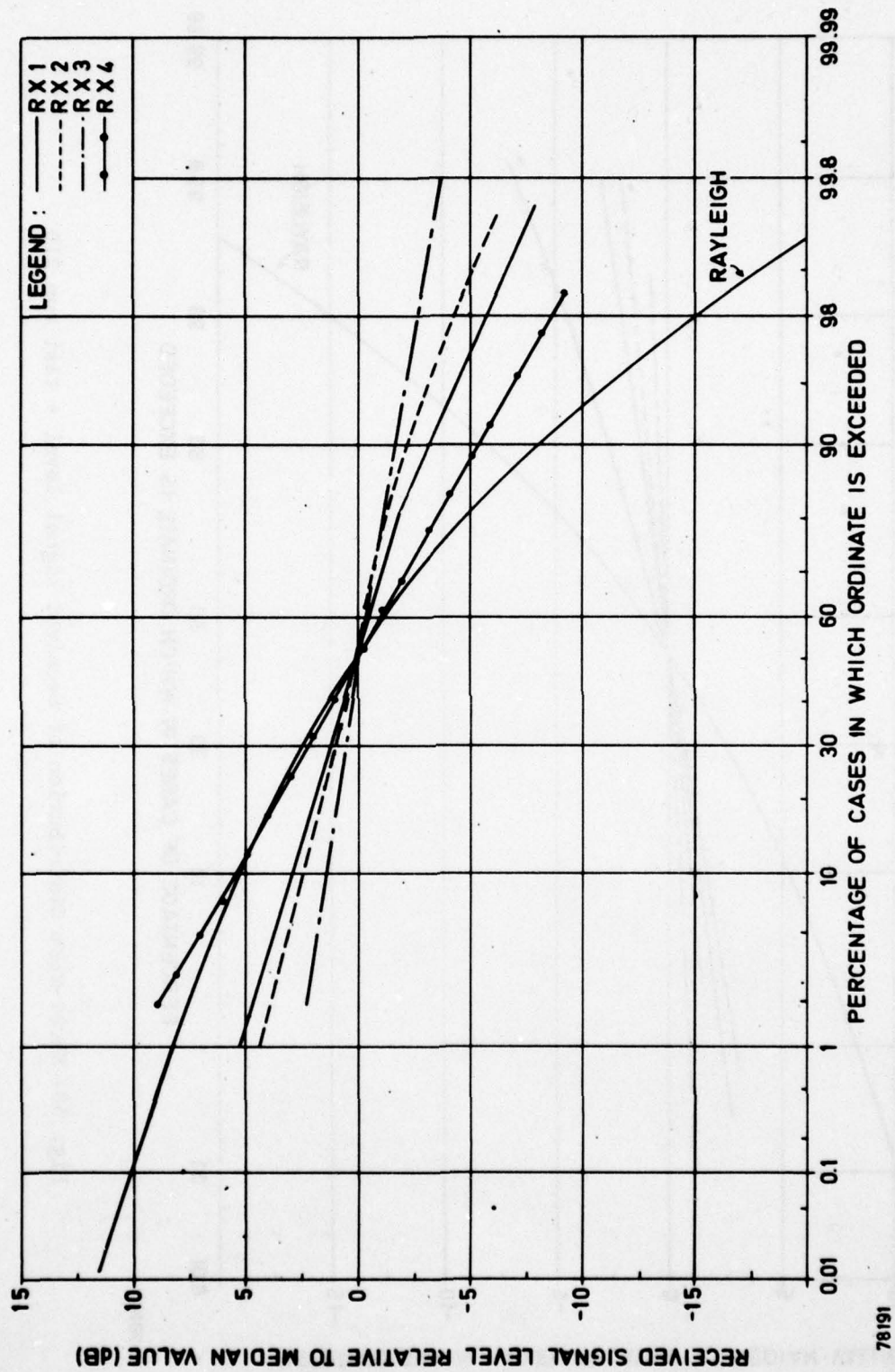


Fig. 32 Short-term distribution of received signal level - test run 257

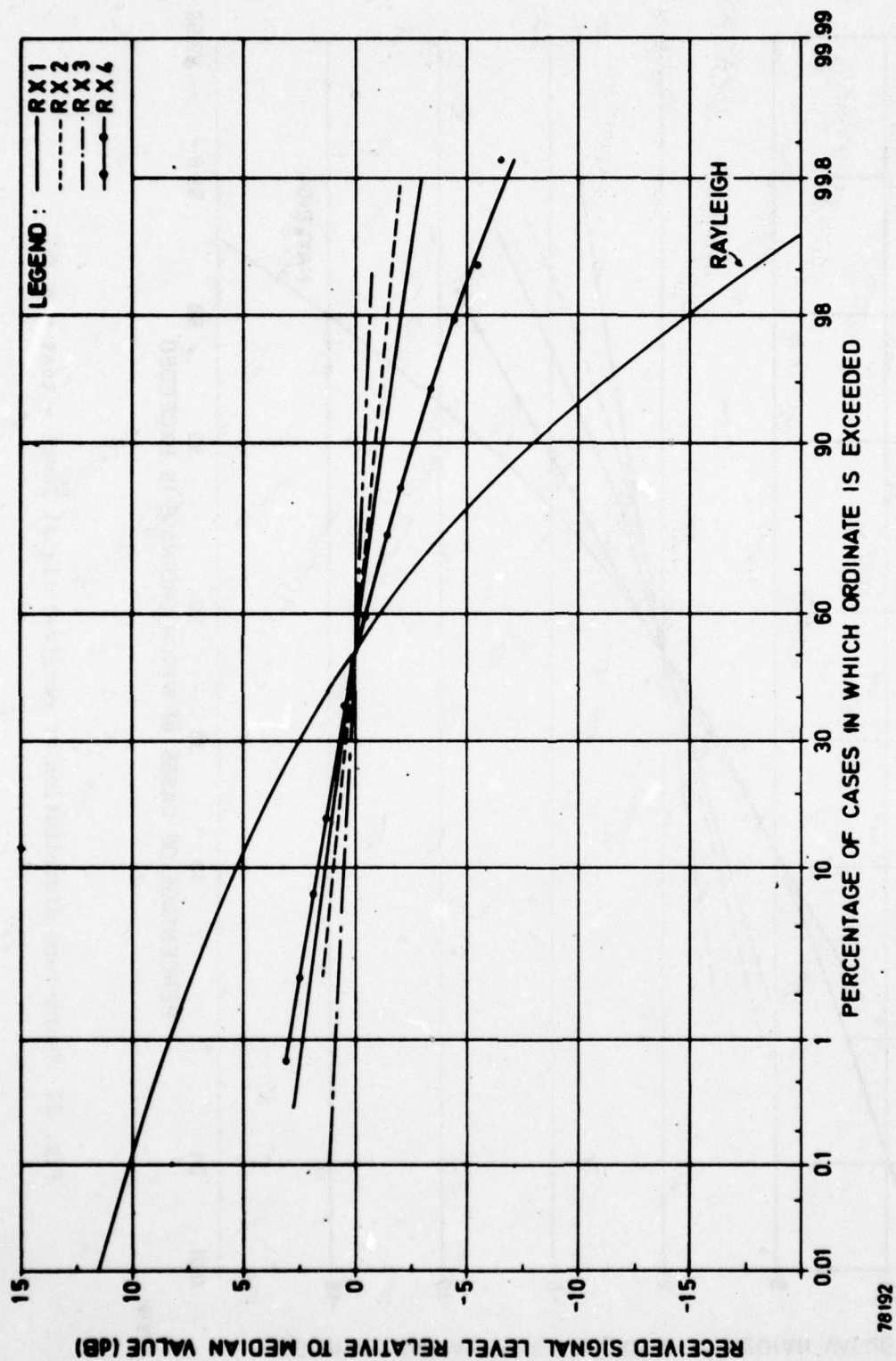


Fig. 33- Short-term distribution of received signal level - test run 219

However, the fading range of the other receivers is much smaller than expected for a scatter signal. In Fig. 33, which was obtained during one of the more frequent shallow fading periods, the fading range of all four receivers is significantly less than that of the Rayleigh distribution. The large deviation from a Rayleigh distribution cannot be explained by the reduction of the fading range due to selective fading of wide-band signals (see para. 6.1.1). Rather, they indicate the presence of a strong specular component, particularly so for Rx 3.

To isolate the propagation mechanism affecting the UHF link, it was necessary to eliminate the effects of frequency selective fading. This was accomplished by transmitting a narrow-band FM signal and recording the signals received on Rx 2 and Rx 4 for about 20 hours on 6 and 7 May. The short-term distribution of this signal still deviates considerably from the Rayleigh distribution, as shown by the example in Fig. 34. It is therefore reasonable to assume that the received signal consists of a specular component and a scatter component. The envelope of such a signal has a Rician probability distribution (Ref. 17). For Rician fading, the power ratio between the two components can be determined from the ratio of the standard deviation to the mean of the received signal power, as shown in Appendix I. Since the total received power is known, it is also possible to calculate the received powers for the specular and scatter components separately. This procedure was accomplished for the 20 hours of narrow-band recordings. The result is shown in Fig. 35.

As seen in Fig. 35, the power of the specular component in Rx 2 ranged from 6 to 12 dB higher than the power of the scatter component. The level of the scatter component was about the same for both Rx 2 and Rx 4. The specular component of the signal received by Rx 4 was highly variable, ranging from -78 to -88 dB.

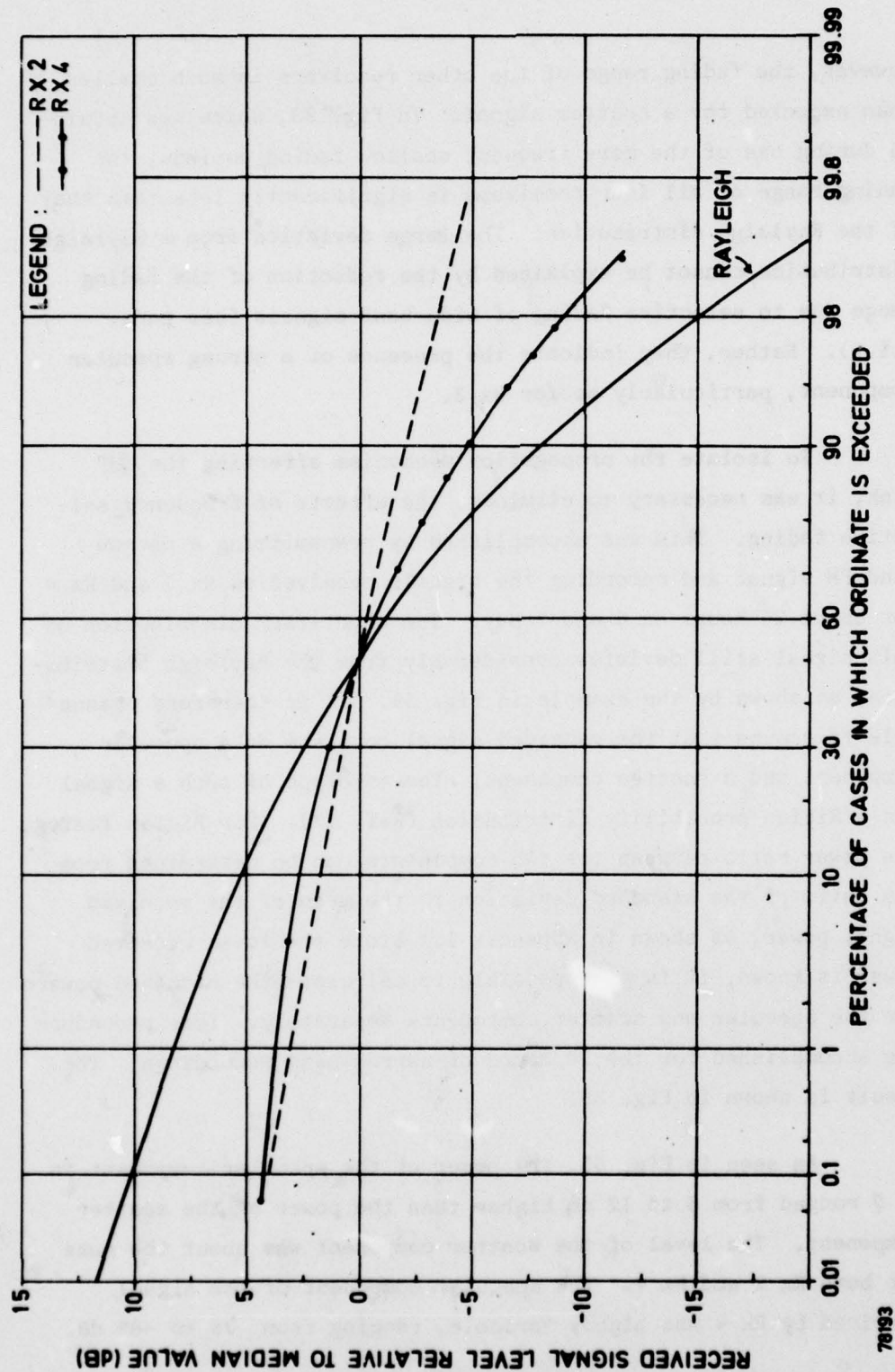


Fig. 34 Short-term distribution of received signal level - narrow-band transmission

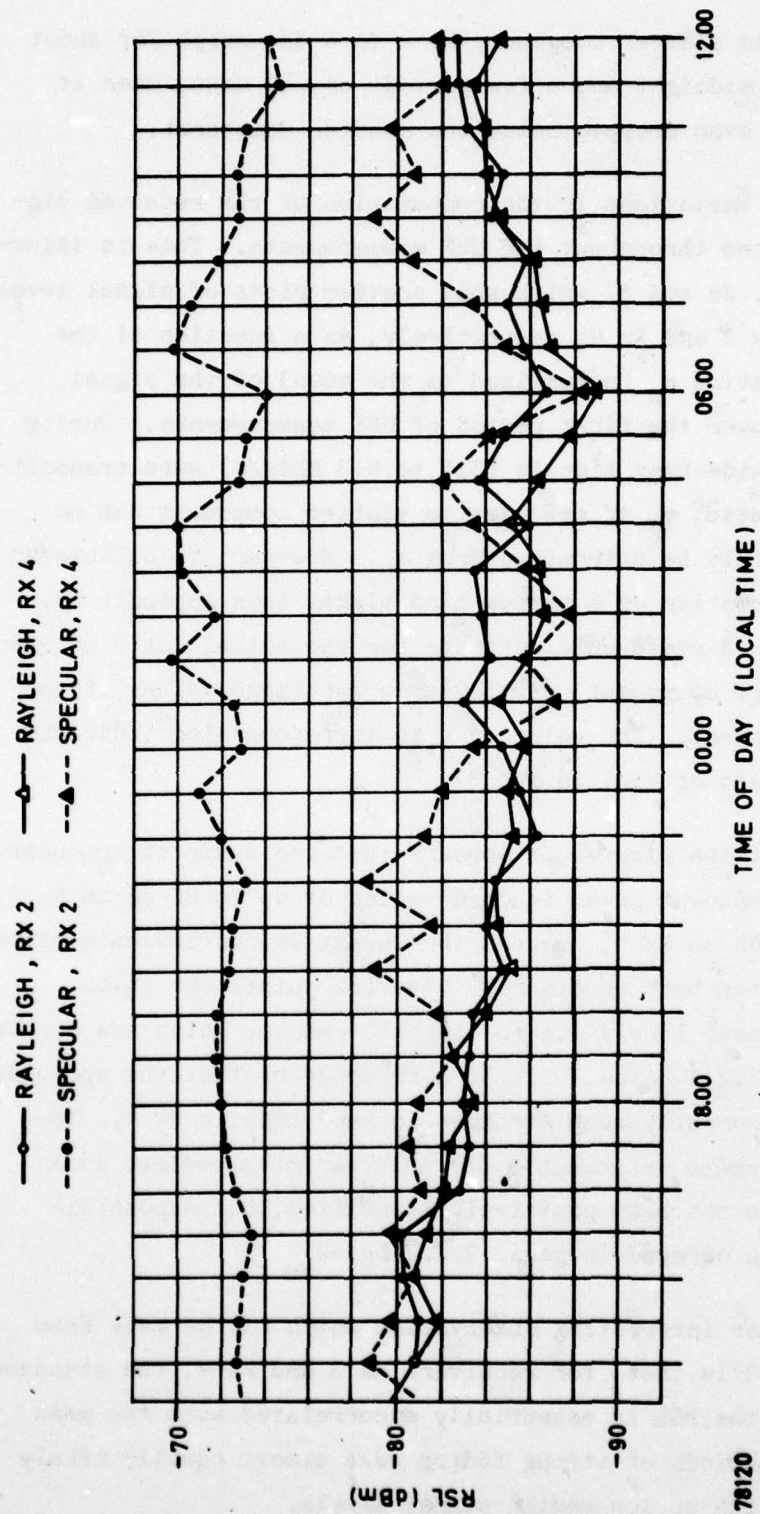


Fig. 35 Diurnal variations of specular and scatter components - 6 and 7 May

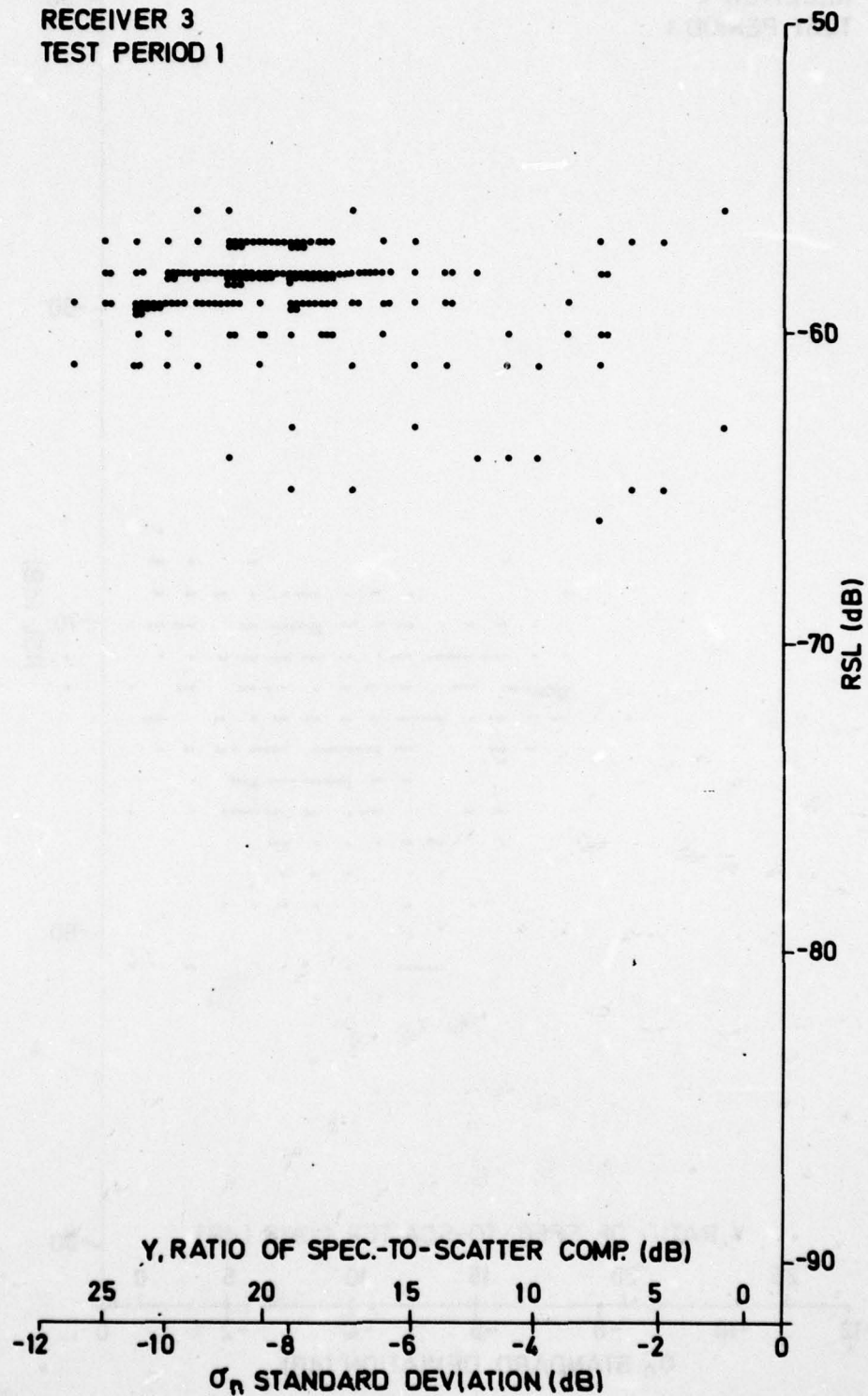
It exceeded the scatter component by 2 to 6 dB except for about 2 hours after midnight and a few periods around dawn, when it approached or even dropped below the scatter component.

Large variations in the composition of the received signal were noticed throughout the UHF measurements. This is illustrated in Fig. 36 and 37 which show scatter plots of signal level received on Rx 3 and Rx 4, respectively, as a function of the standard deviation σ_n (normalized to the mean) of the signal distribution over the first period of UHF measurements. During this period, wide-band signals (3.5 to 6.3 Mbit/s) were transmitted and the ratio, y , of specular to scatter component can no longer accurately be determined from σ_n . However, y , calculated under the assumption of a narrow-band signal (see Appendix I), still provides a reasonable estimate for the actual ratio of specular to scatter component, particularly for large values of the specular component. The value of y is therefore also indicated on the abscissae of Fig. 36 and 37.

From these figures it appears that the ratio of specular to scatter component power reached values of up to 26 dB on Rx 3, and up to 20 dB on Rx 4, whereas the lowest values indicate almost pure scatter for both receivers. (The few points for which $y > 0$ dB are most likely due to aircraft passes, which are discussed in para. 7.2.7 below.) It is also apparent that the specular component is normally much stronger in Rx 3 than in Rx 4. The physical phenomena responsible for this rather anomalous link behaviour have not been positively identified, but a possible explanation is offered in para. 7.2.7 below.

Another interesting observation which can be made from Fig. 36 and 37 is that, for receivers Rx 3 and Rx 4, the standard deviation of the RSL is essentially uncorrelated with the mean RSL. Thus, periods of strong fading were almost equally likely to occur at high or low median signal levels.

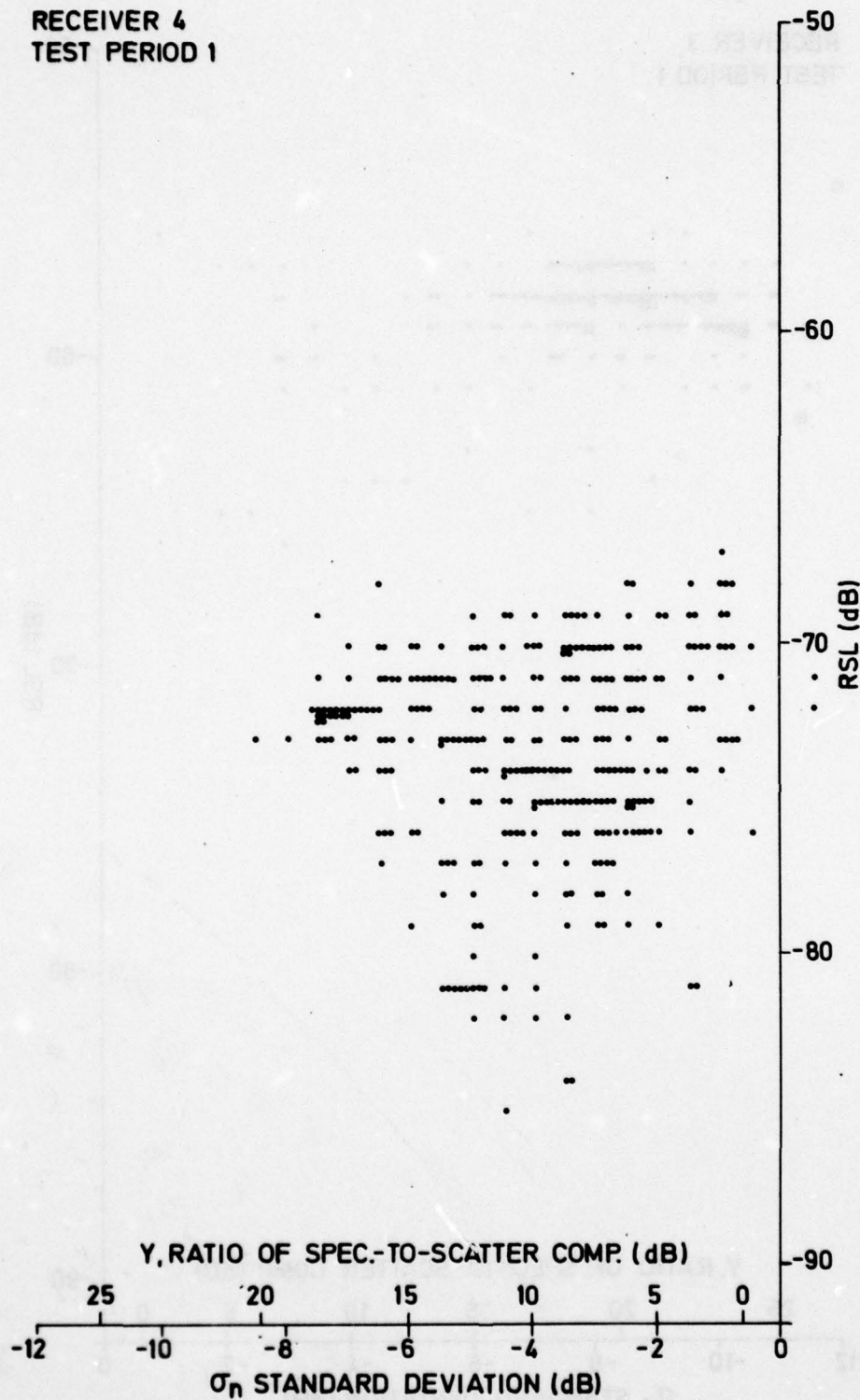
RECEIVER 3
TEST PERIOD 1



78186

Fig. 36 Scatter plot of received signal level
- as a function of standard deviation (Rx 3)

RECEIVER 4
TEST PERIOD 1



78187

Fig. 37 Scatter plot of received signal level
- as a function of standard deviation (Rx 4)

7.2.2 Fade rate

Mean fade rate^{*} data as measured over nominal 20-min runs in the first period are shown in Fig. 38 and 39 for all four receivers. Figure 38 presents this data as a histogram which has been smoothed for illustrative purposes. Of interest in this figure are the observations that, for all receivers, there were long periods with virtually no fading and also that the distributions for Rx 2 and Rx 4 show two peaks. This is most apparent for Rx 4. This distribution is seen to have a primary peak near 0.0 Hz and a secondary peak at approximately 0.2 Hz. This further supports other measured data which indicate that Rx 4 (and possibly Rx 2) received both scatter and specular components. These components alternately dominate at various times during the tests. The curves for Rx 1 and Rx 3 indicate that essentially specular signals were observed in these receivers throughout the first UHF measurement period. In Fig. 39, these measurements are presented as cumulative distributions. It is seen that median values for the fade rate range from 0.2 Hz for Rx 4 to essentially 0.0 Hz for Rx 3. For Rayleigh fading channels, it is possible to estimate the RMS doppler spread by multiplying the mean fade rate by 1.4 (Ref. 11), resulting in a median RMS doppler spread of 0.28 Hz for Rx 4. This value is consistent with the value of RMS doppler measured on other UHF troposcatter paths of similar length (Ref. 11).

In addition to the normally observed range of fade rates, periods of faster fading occurred. These periods were ascribed to signals which were reflected from aircraft traversing the scattering volume. This subject is discussed in more detail in para. 7.2.7.

^{*}The mean fade rate is defined as the average numbers of times, per second, the signal level passes through its mean value with positive slope, as determined over a 20-min interval.

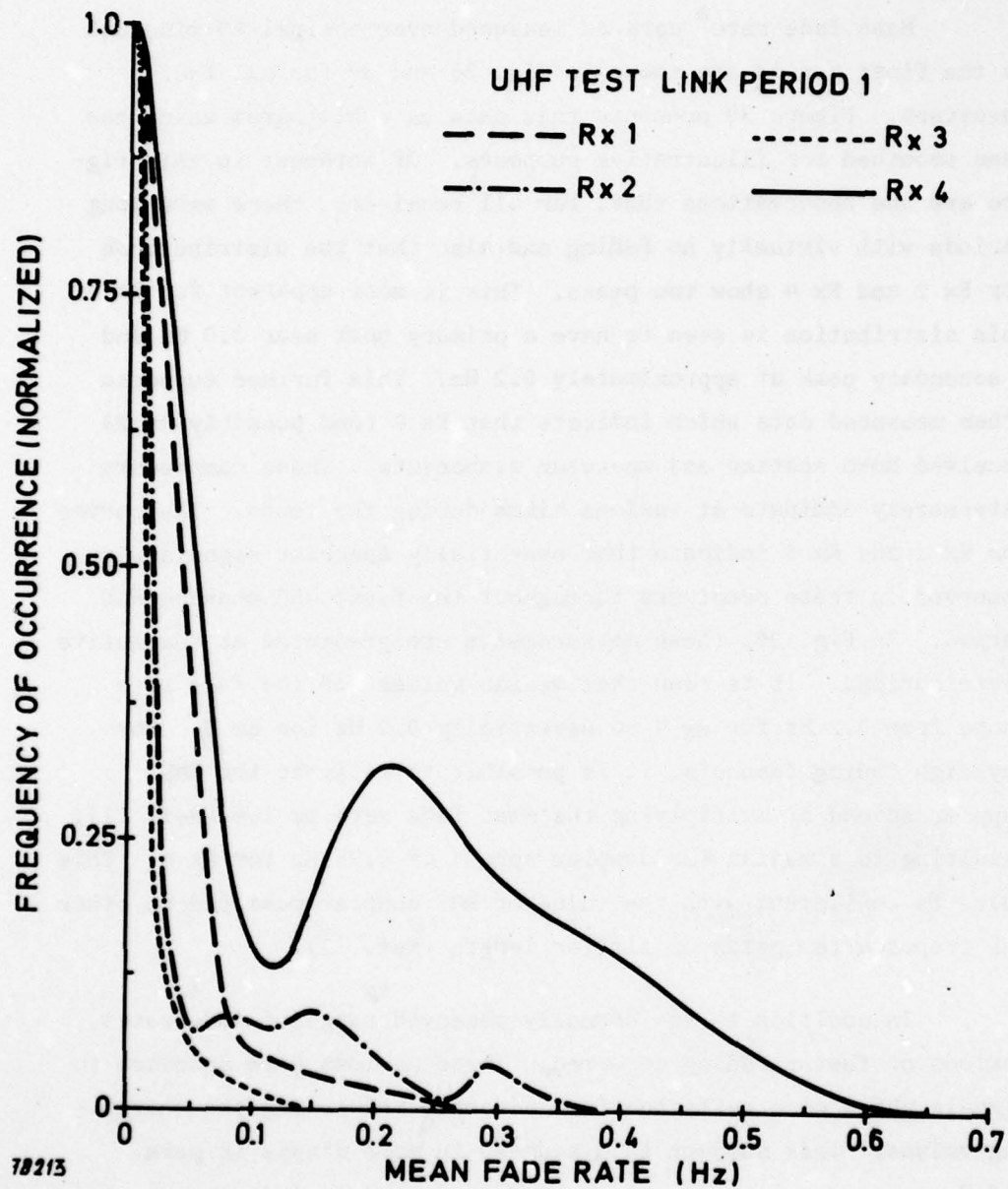


Fig. 38 Density distribution of fade rate

AD-A066 380

SHAPE TECHNICAL CENTER THE HAGUE (NETHERLANDS)
THE COMBINED US/NATO DIGITAL TROPOSCATTER TEST PROGRAMME OVER T--ETC(U)

F/G 17/2.1

DEC 78 P NIELSEN, J OSTERHOLZ, E PUSONE

UNCLASSIFIED

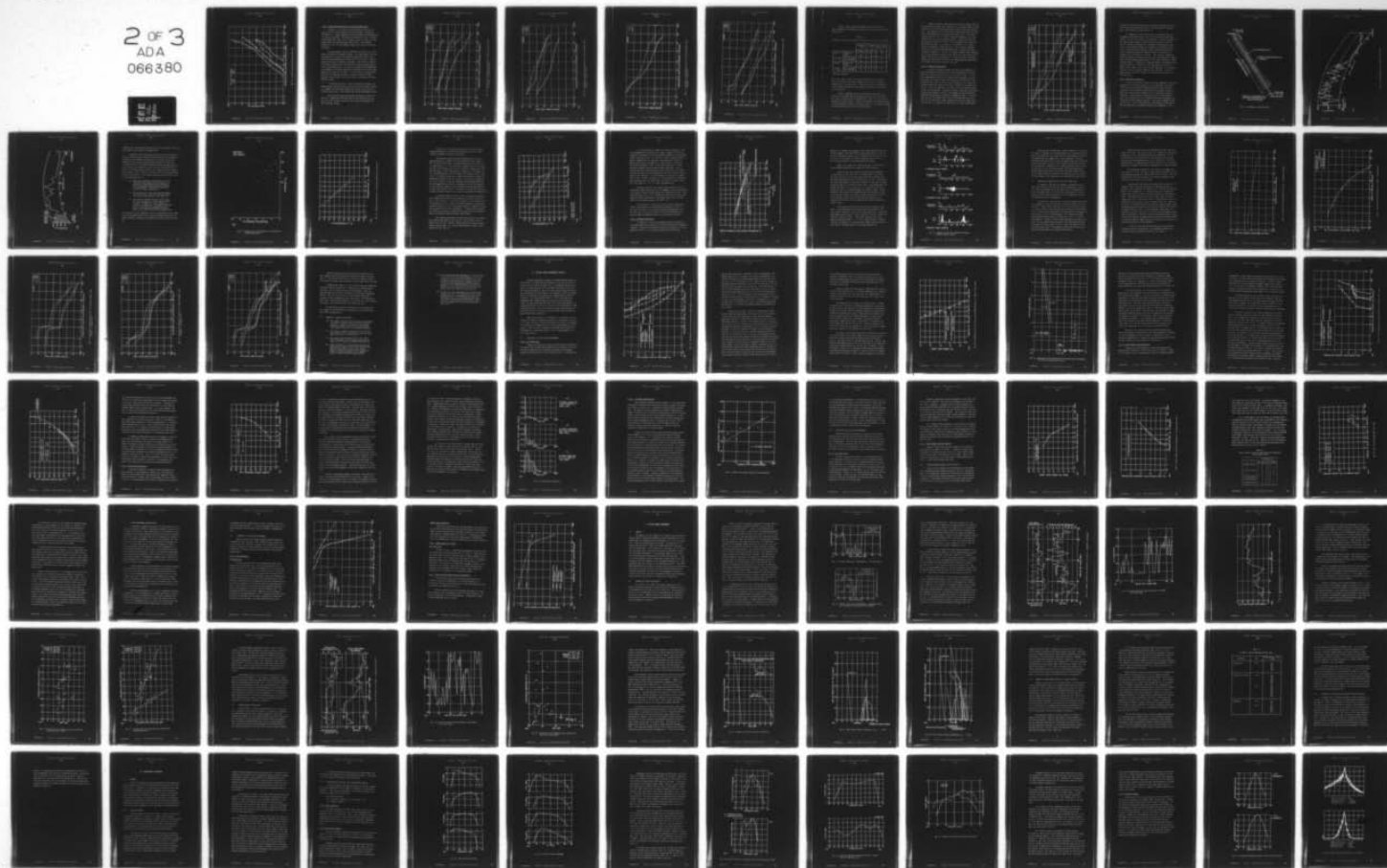
STC-CR-NICS-38

DCEC-TR-12-78

NL

2 OF 3
ADA
066380

10/1



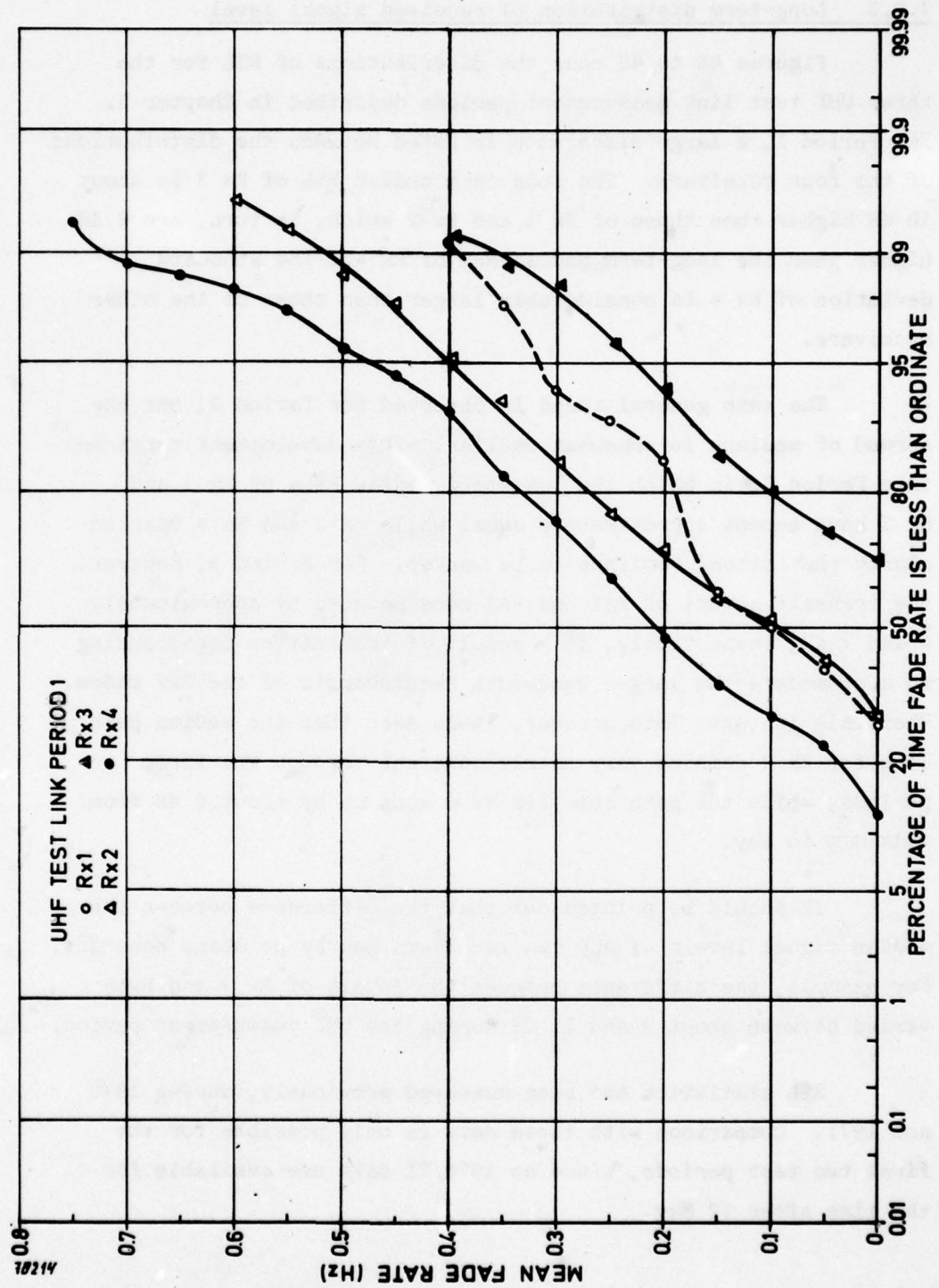


Fig. 39 Cumulative distribution of fade rate

7.2.3 Long-term distribution of received signal level

Figures 40 to 43 show the distributions of RSL for the three UHF test link measurement periods described in Chapter 5. For Period 1, a large difference is noted between the distributions of the four receivers. The long-term median RSL of Rx 3 is about 10 dB higher than those of Rx 1 and Rx 2 which, in turn, are 6 dB higher than the long-term median RSL of Rx 4. The standard deviation of Rx 4 is considerably larger than those of the other receivers.

The same general trend is observed for Period 2, but the spread of medians is somewhat smaller. This development continues into Period 3, in which the long-term median RSLs of Rx 1 and Rx 3 have become approximately equal while Rx 2 and Rx 4 (particularly the latter) continue to be weaker. For Period 3, however, the transmit powers of PA1 and PA2 were reduced by approximately 4 and 7 dB, respectively, as a result of transmitter broadbanding to accommodate the larger bandwidth requirements of the DAR modem. When this is taken into account, it is seen that the median path loss for Rx 4 remains very nearly constant through the three periods, while the path loss for Rx 3 went up by about 6 dB from February to May.

It should be pointed out that the difference between the median signal levels of any two receivers was by no means constant. For example, the difference between the levels of Rx 3 and Rx 4 varied between about 0 and 25 dB during the UHF measurement period.

RSL statistics had been measured previously, during 1970 and 1971. Comparison with these data is only possible for the first two test periods, since no 1970/71 data are available for the time after 12 May.

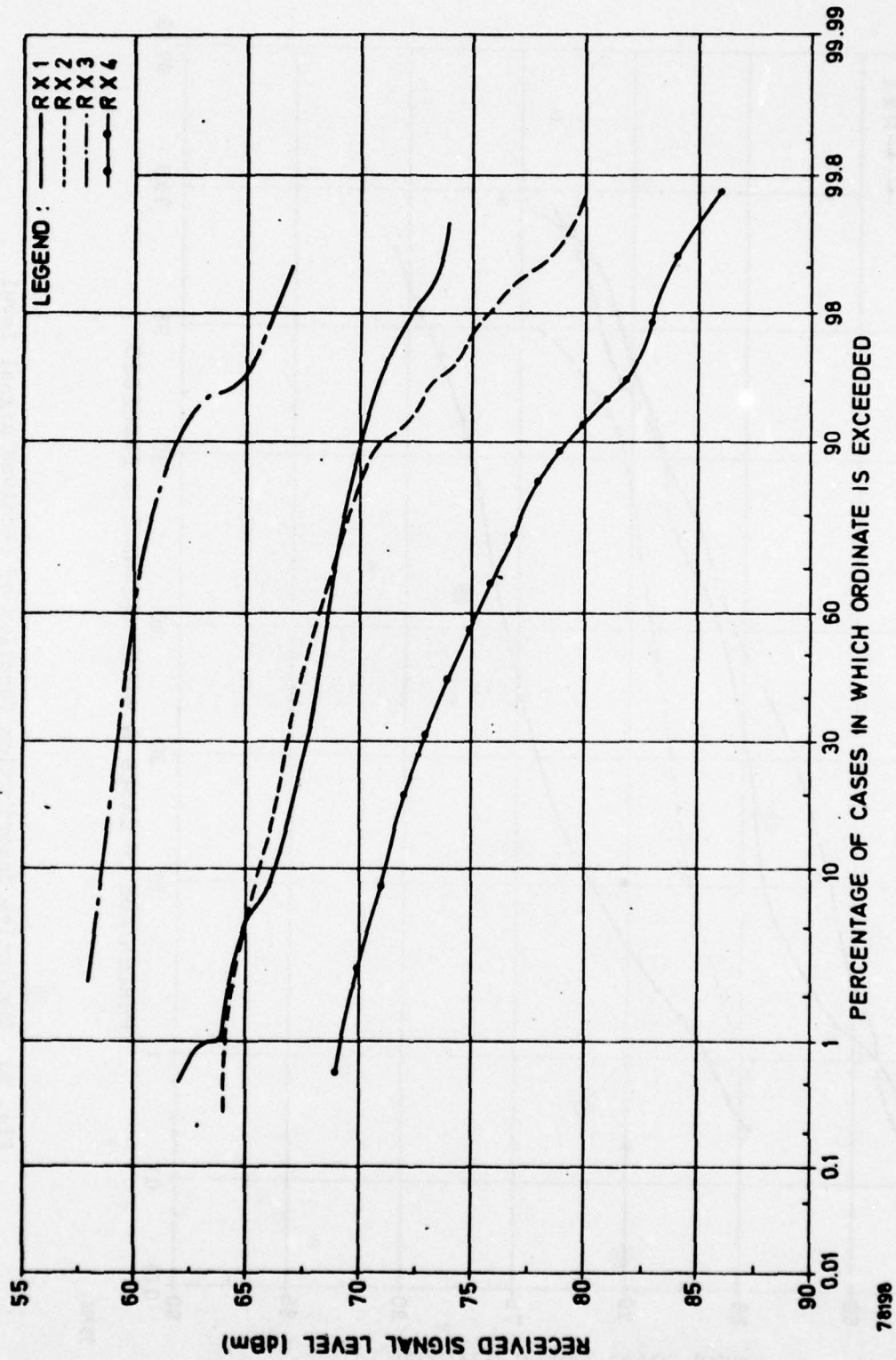


Fig. 40 Cumulative distribution function of received signal level
(24 January - 25 February 1977)

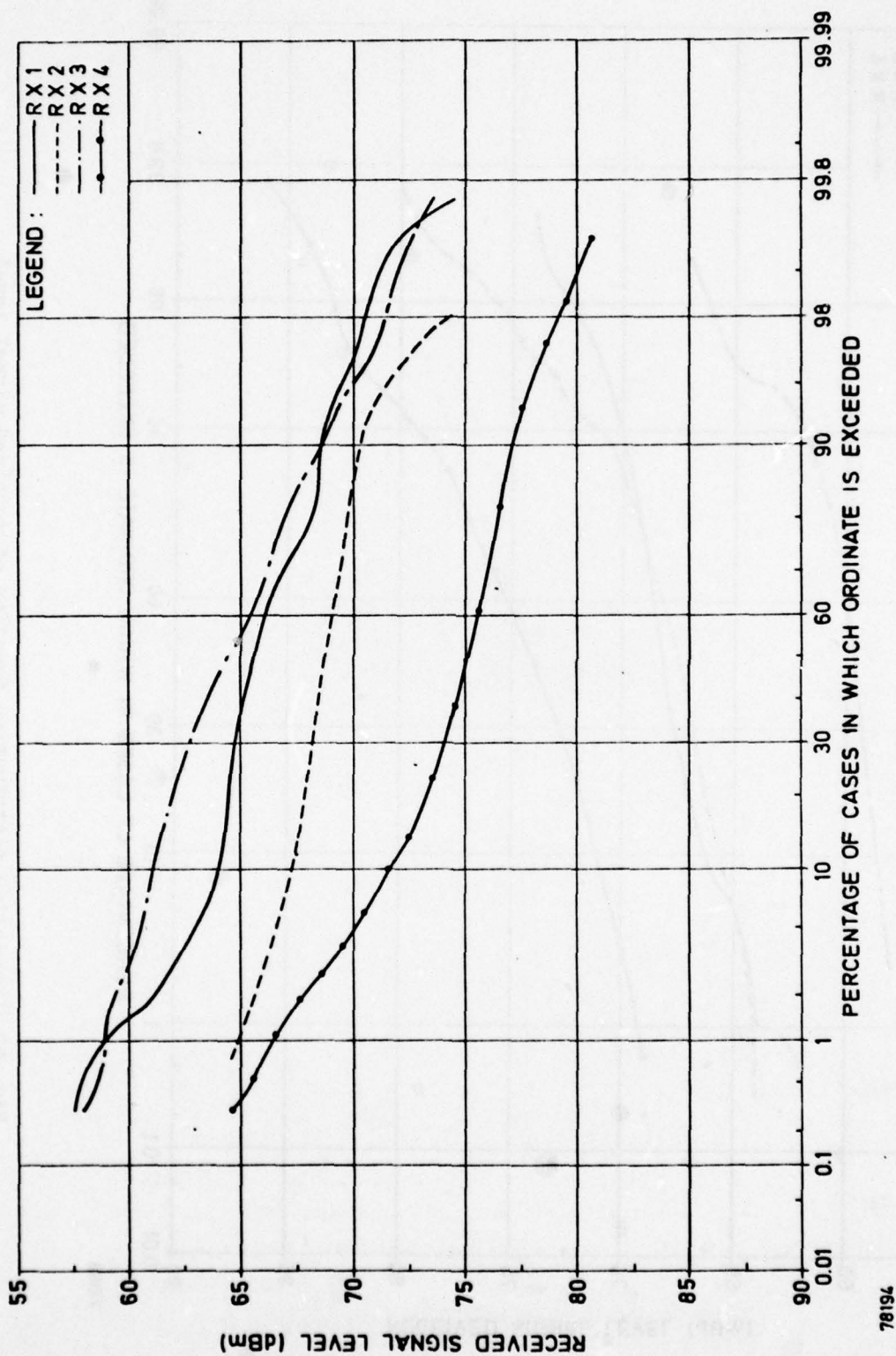


Fig. 41 Cumulative distribution function of received signal level
(2 April - 13 April 1977)

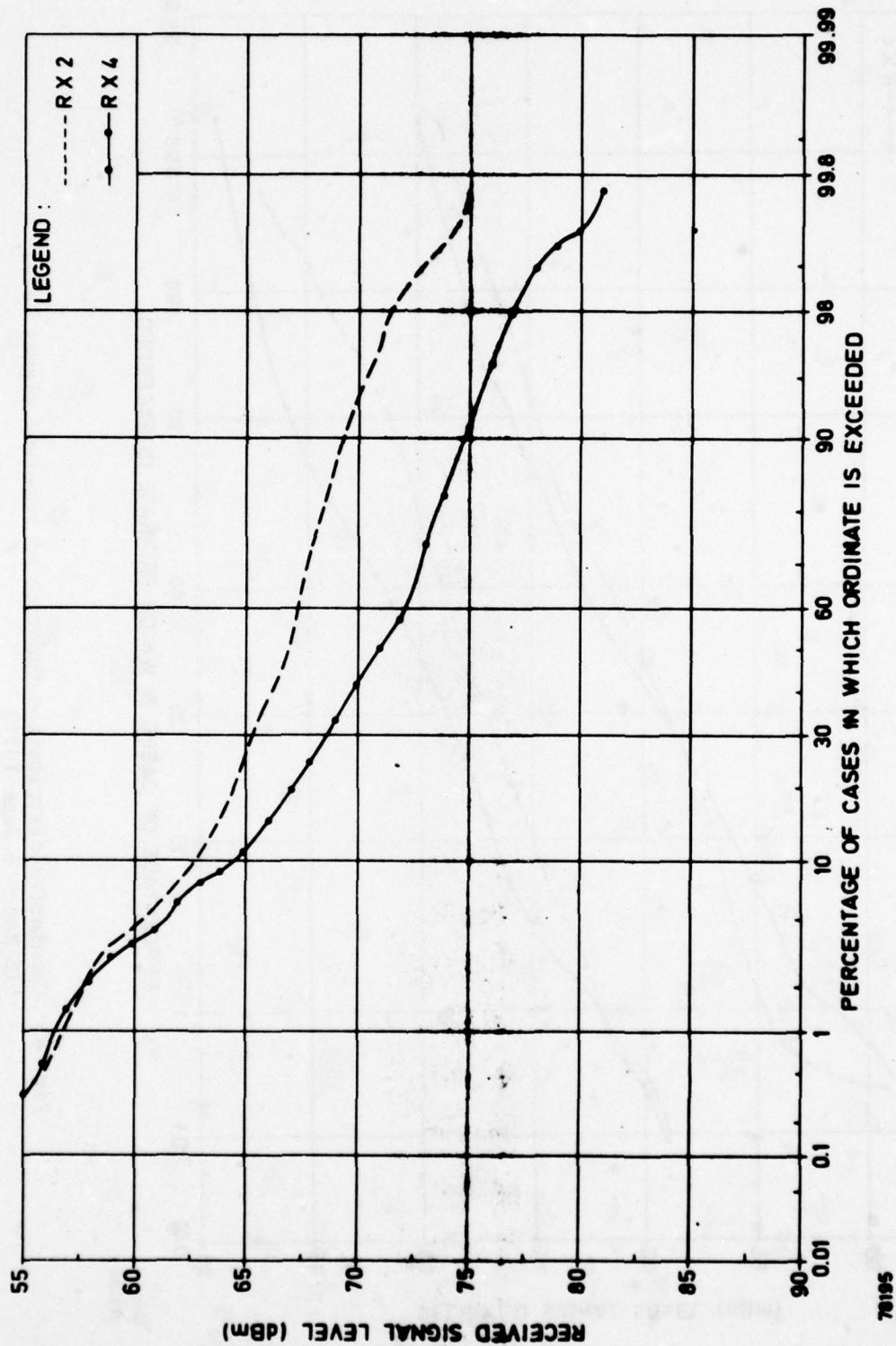


Fig. 42 Cumulative distribution function of received signal level
 (13 April - 4 May 1977)

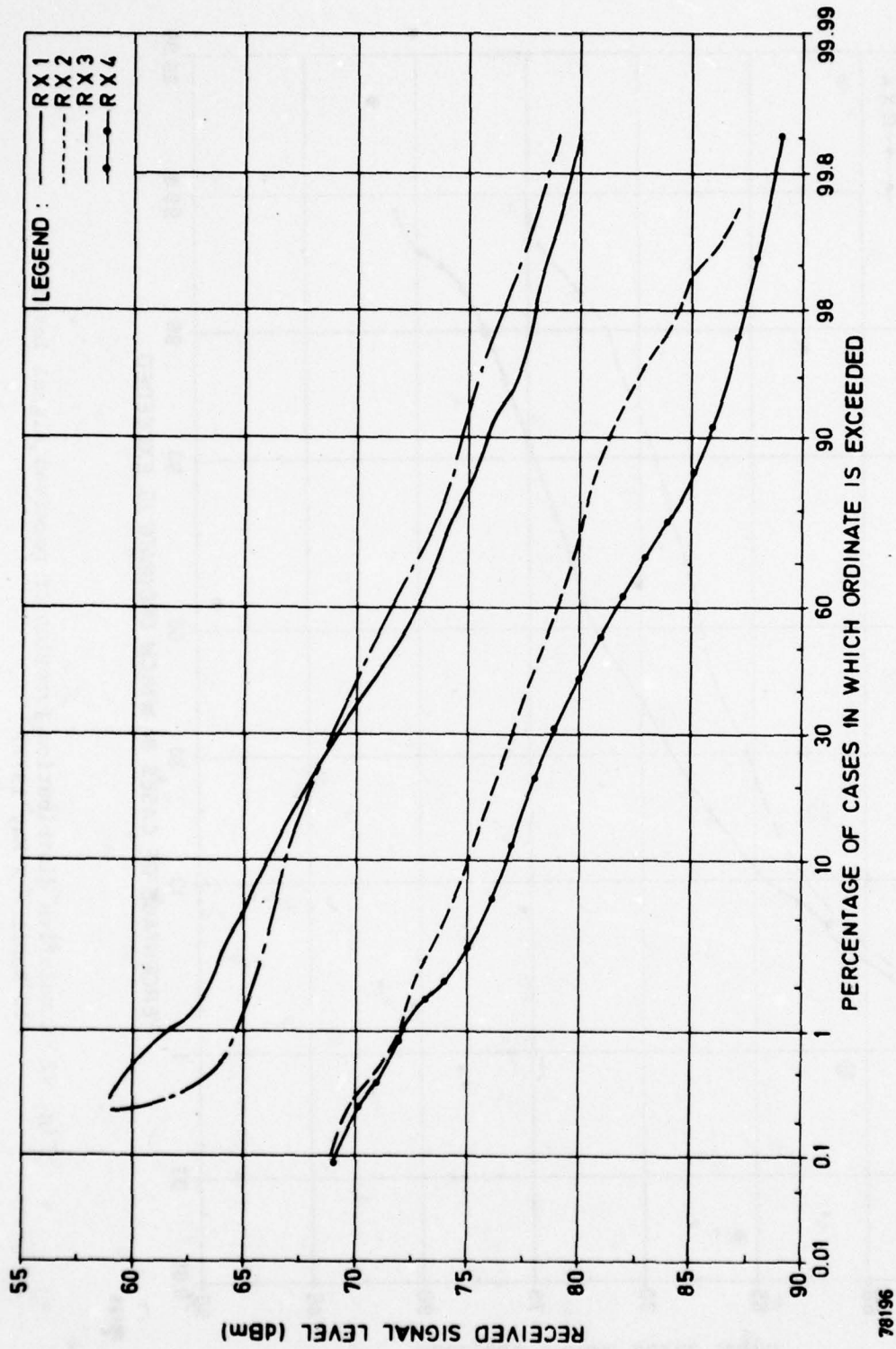


Fig. 43 Cumulative distribution function of received signal level
(16 May - 5 June 1977)

Table 13 shows the RSL exceeded for 50% and 99% of the time as measured at Feldberg in 1977 and in 1970, and at Dosso dei Galli in 1971.

Table 13

Comparison of RSL level statistics measured in 1970, 1971, and 1977

		Feldberg 1977		Feldberg 1970		Dosso dei Galli 1971
		Rx 1	Rx 4	Rx 1	Rx 4	Rx 3
Period 1	Median RSL (dBm)	-67	-72	-69	-72	-74
(February)	RSL exceeded for 99% (dBm)	-73	-84	-72	-84	-84
Period 2	Median RSL (dBm)	-65	-71	★	-73	★
(April/ May)	RSL exceeded for 99% (dBm)	-72	-79	★	-79	★

★ No data available

The values shown in Table 13 have been normalized to transmit a power of 4 kW and it has been assumed that a power of 5 kW was transmitted in 1970 and 1971. It can be seen that corresponding values measured during the three different years are all within 3 dB of each other.

The fair agreement between the different measurements indicates that the RSL statistics measured at Dosso dei Galli from July 1970 to February 1971 and reproduced in Ref. 1 may be taken to determine the worst months. These were September and October, when the RSL exceeded for 99% of the time was some 10 to 15 dB lower than that measured during the tests described herein.

Figure 44 shows the RSL statistics for the complete measurement period on the UHF link, normalized to a transmit power of 4 kW, together with the statistics predicted using the NBS and CCIR methods. Close agreement is noted between the NBS predictions for 50% service probability and the signal received by Rx 4. The median signal levels of Rx 1 to 3 are in reasonable agreement with CCIR predictions, but their standard deviation is much less than that predicted by either CCIR or NBS. This strengthens the conjecture put forward in para. 7.2.1 above for the presence of a strong specular component on these receivers. This specular component may be due to double-knife edge diffraction, as previously hypothesized in Chapter 6. In fact, the highest signal levels measured on all four receivers are about the same as the level predicted for double diffraction (see Appendix F). However, double knife-edge diffraction alone does not explain the large measured differences in the RSLs of the four diversity receivers.

7.2.4 Path profile analysis

To obtain a greater insight into UHF link propagation, a much more detailed description of the path geometry was required than was available from the path profile shown in Fig. 4. This was accomplished by the use of computerized topographic data for the great circle path between the transmitter and receiver sites as well as for areas to either side of the great circle path subtended by the major lobes of the link antennas, as illustrated in Fig. 45. With this approach, the great circle path profile shown in Fig. 46 was derived. The profile reveals a greatly varying fine structure not apparent in Fig. 4 and suggests that double knife-edge diffraction may be a realistic propagation mode. It follows from Fig. 46 that significant terrain variations may also occur over a cross section of terrain subtended by the main beam of the link antenna. To explore the significance of this, another path

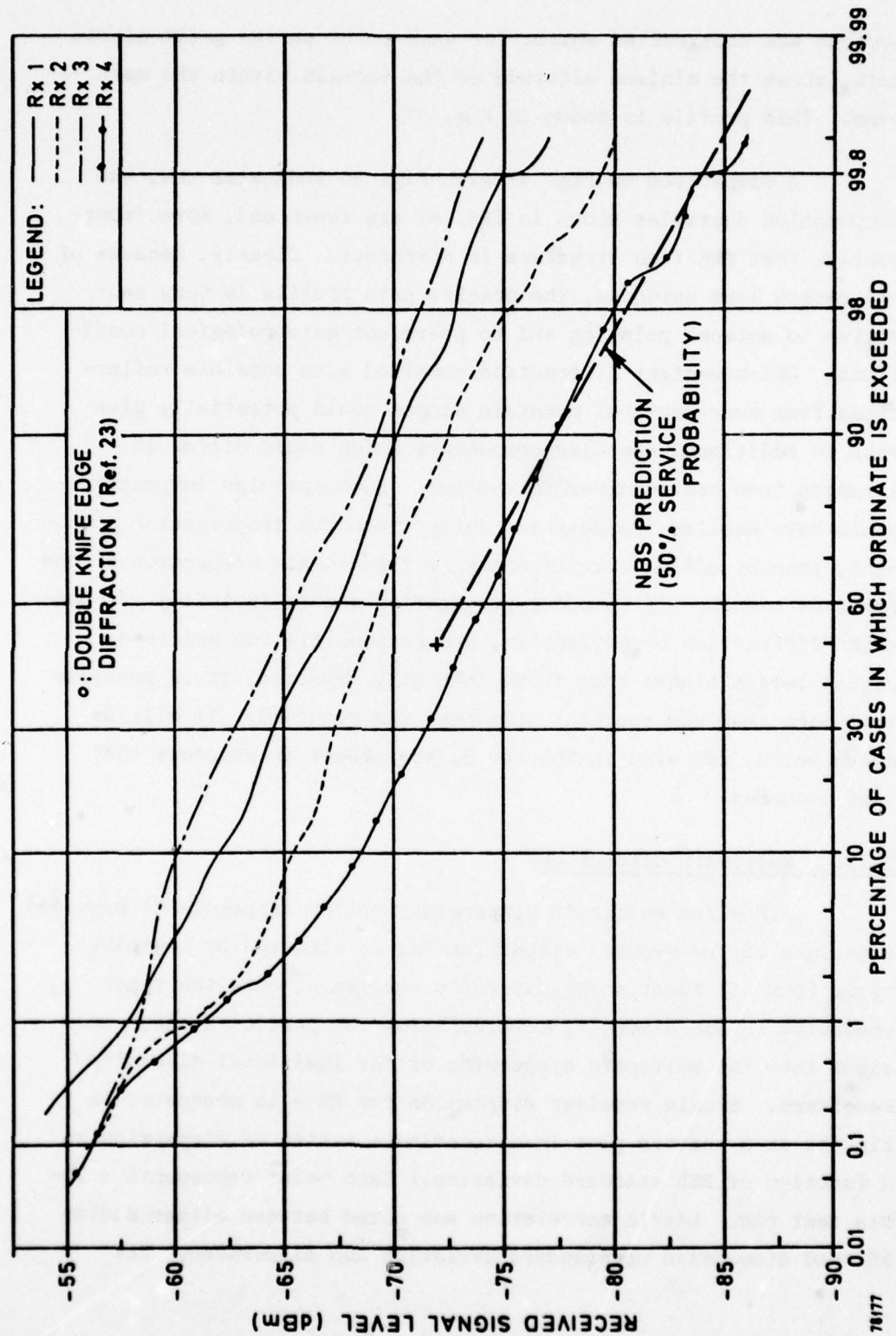


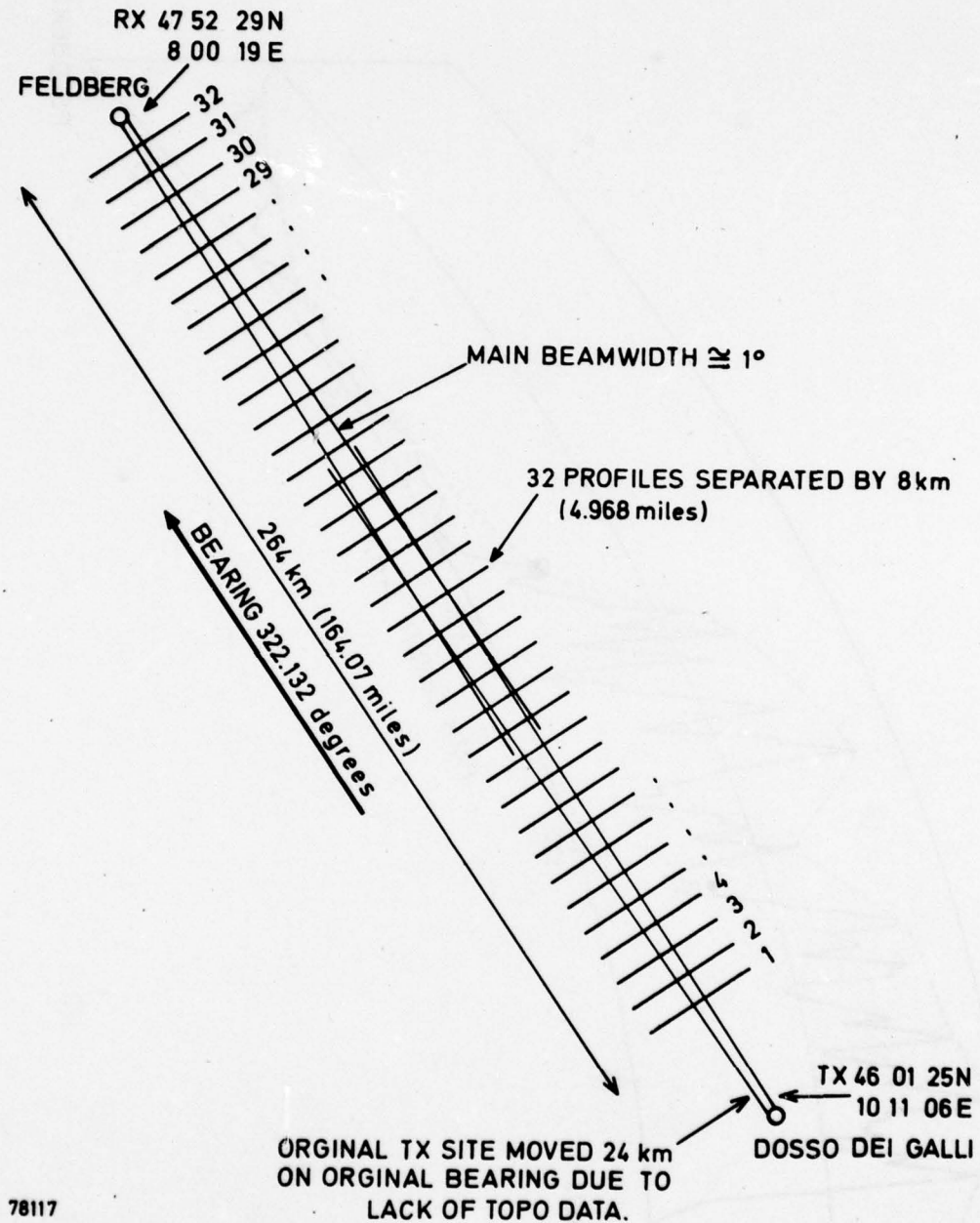
Fig. 44 Cumulative distribution function of received signal level
(24 January - 5 June 1977)

profile was constructed which, for each point on the great circle path, shows the minimum altitude of the terrain within the main beam. This profile is shown in Fig. 47.

A comparison of Fig. 47 with Fig. 46 indicates that the propagation obstacles shown in Fig. 47 are fewer and, more importantly, that the fine structure is different. Clearly, because of the narrow beam antennas, the precise path profile is very sensitive to antenna pointing and to prevalent meteorological conditions. Off-boresight diffraction combined with possible reflections from near-vertical mountain slopes could potentially give rise to additional specular components which could differ in strength from one receiver to another. Such specular components would have smaller transmission delays than the troposcatter component, thereby adding significantly to the overall dispersion of the received signal. If specular propagation modes, including off-boresight diffraction or reflection, are responsible for received signal levels higher than those initially expected, it is possible that more than one specular component was received. It will be shown below, and also in Chapter 9, that there is evidence that this occurred.

7.2.5 Multipath dispersion

Since the multipath dispersion monitor (Appendix C) provides a measure of the overall dispersion and is affected by contributions from all functioning diversity receivers, only the tests conducted in non-diversity configuration can provide a clear insight into the multipath dispersion of the individual diversity receivers. Single receiver dispersion for Rx 4 is presented in Fig. 48 as a scatter plot in a coordinate system of dispersion as a function of RSL standard deviation. Each point represents a 20-min test run. Little correlation was noted between either median RSL and dispersion or standard deviation and dispersion. For



78117

Fig. 45 Topographic analysis method

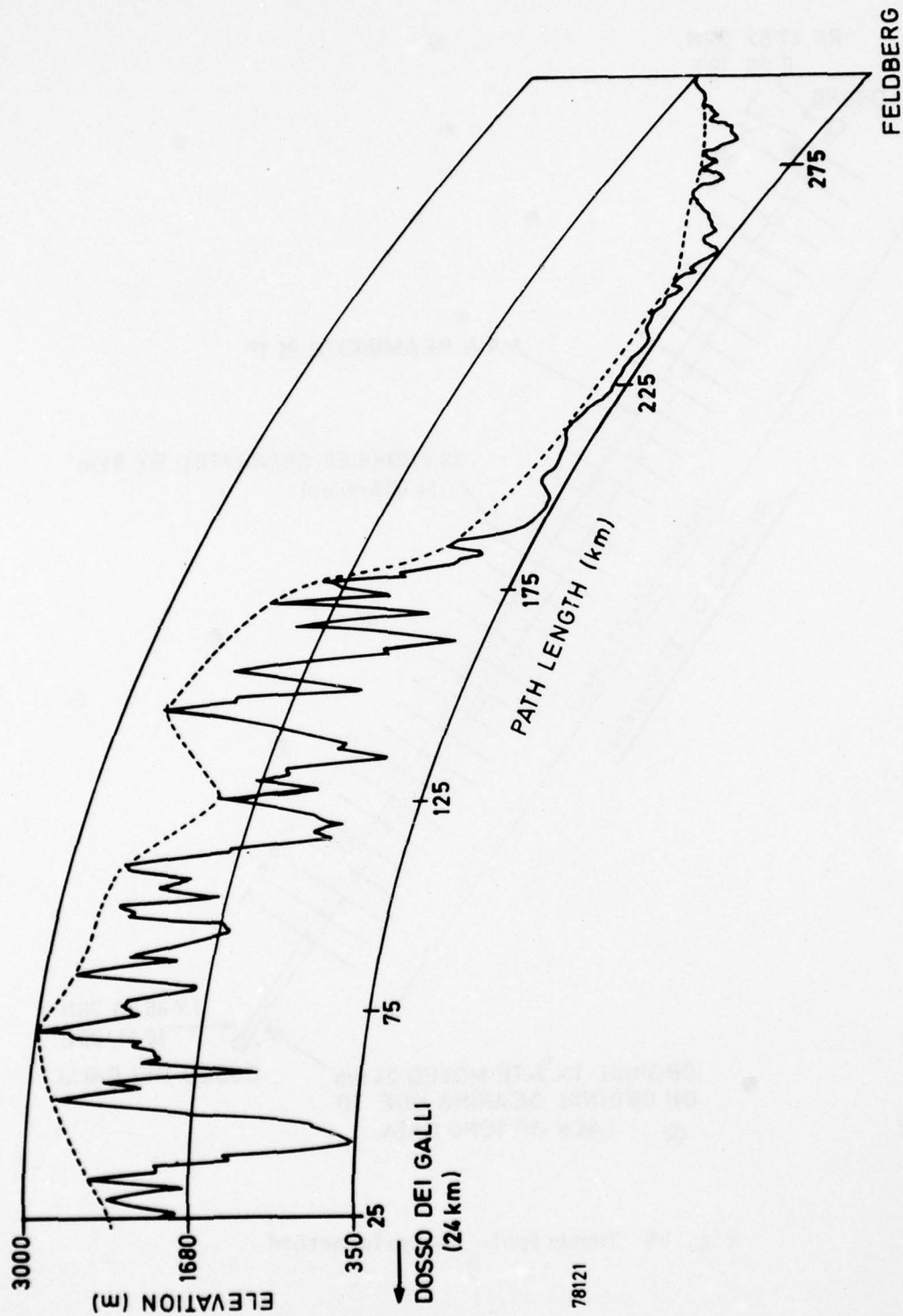


Fig. 46 Detailed great circle profile (UHF link)

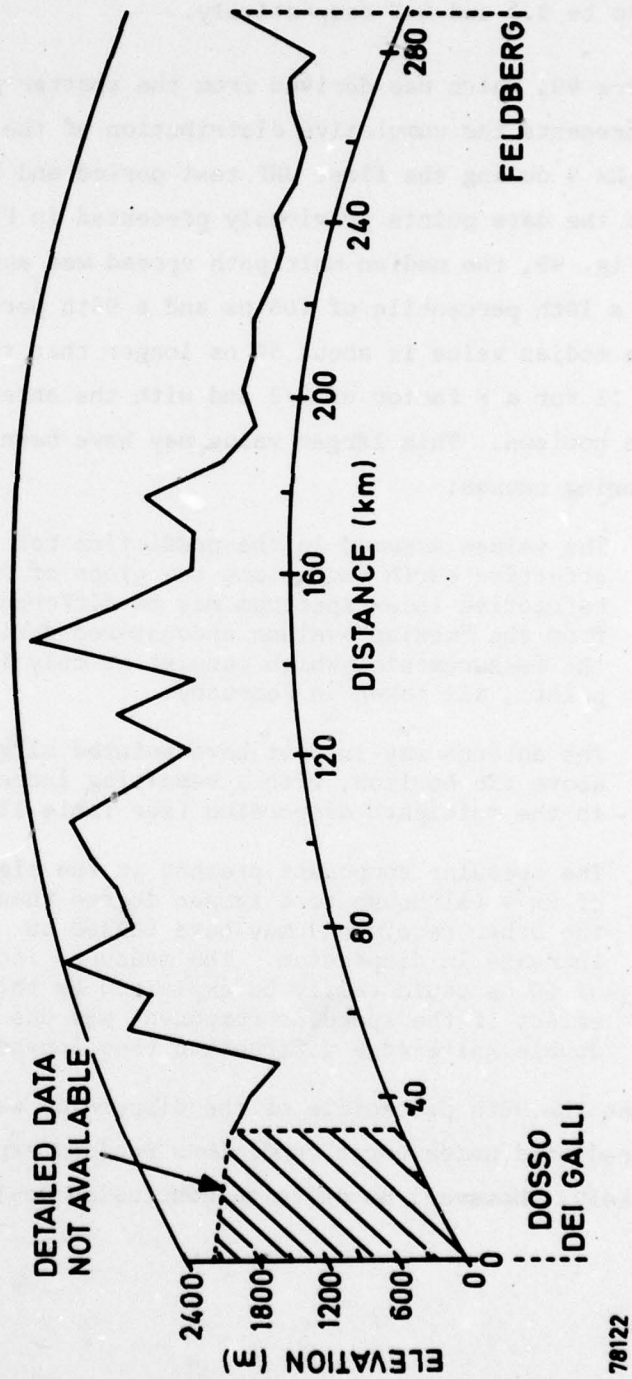


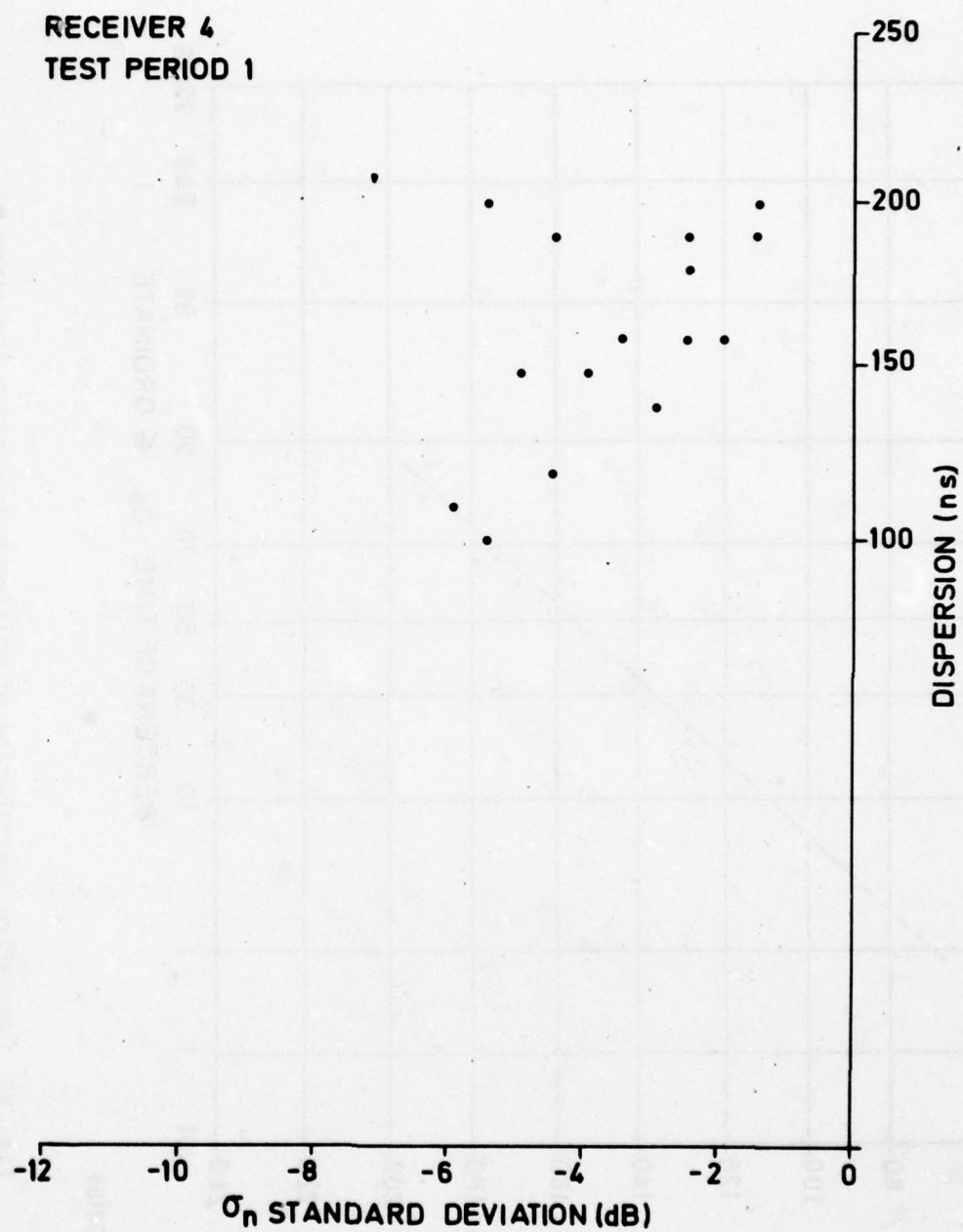
Fig. 47 Profile of lowest main beam elevation (UHF link)

example, the correlation coefficients for the data shown in Fig. 48 were found to be 0.3 and 0.2 respectively.

Figure 49, which was derived from the scatter plot shown in Fig. 48, represents the cumulative distribution of the dispersion measured in Rx 4 during the first UHF test period and has been derived from the data points previously presented in Fig. 48. As seen in Fig. 49, the median multipath spread was approximately 155 ns with a 10th percentile of 105 ns and a 90th percentile of 200 ns. The median value is about 50 ns longer than that predicted in Table 11 for a K factor of 4/3 and with the antenna pointing at the radio horizon. This larger value may have been due to one of the following causes:

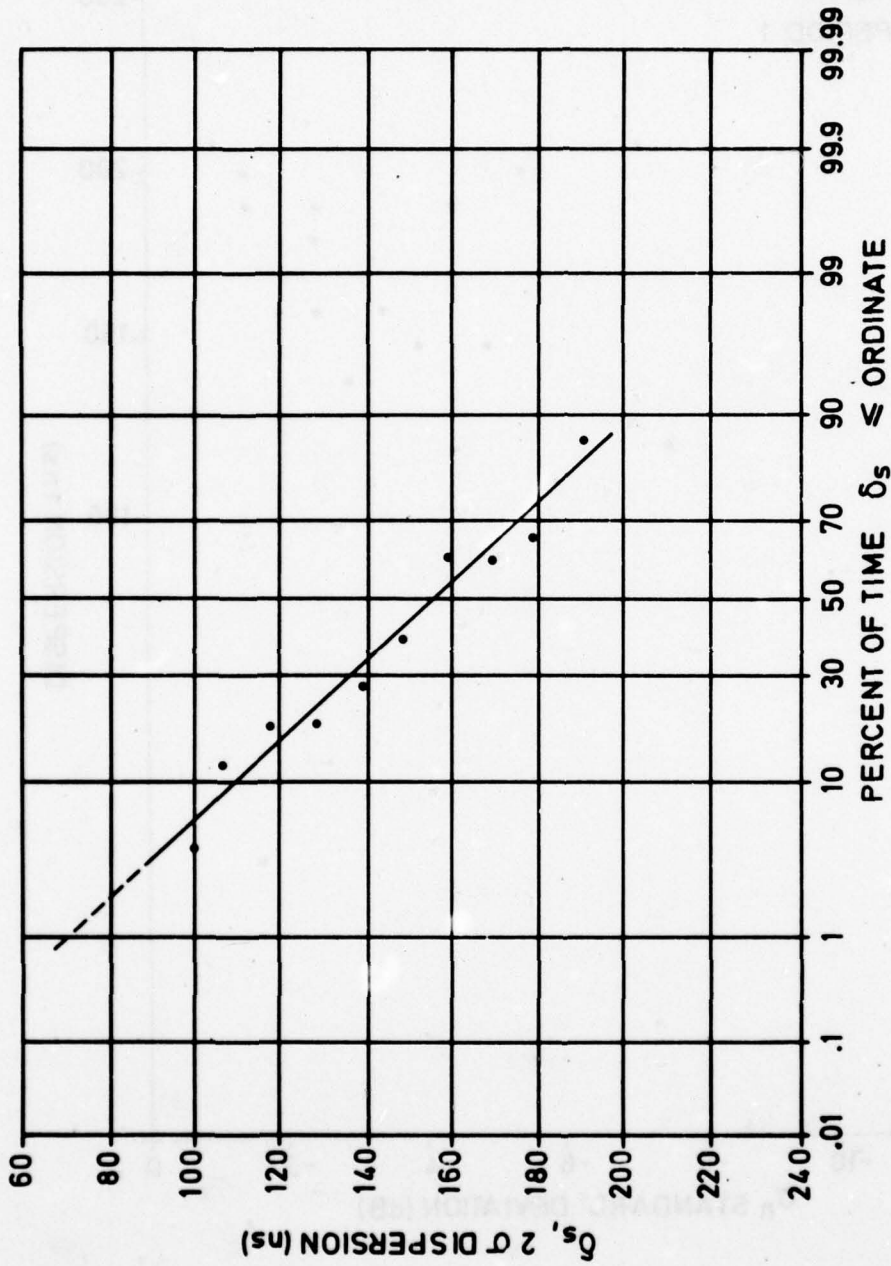
- (a) The values assumed in the prediction for the effective earth radius and the slope of the refractive index spectrum may be different from the "median" values encountered during the measurements, which consist of only 17 points, all taken in February.
- (b) The antenna may in fact have pointed slightly above the horizon, with a resulting increase in the multipath dispersion (see Table 11).
- (c) The specular component present in the signal of Rx 4 (although to a lesser degree than on the other receivers) may have caused an increase in dispersion. The measured increase of 50 ns could easily be explained by this effect if the specular component was due to double knife-edge diffraction (see Appendix J).

The fact that the 90th percentile of the dispersion was also larger than that predicted under worst conditions renders explanation (a) rather unlikely. However, no definite conclusion could be arrived at.



78185

Fig. 48 Scatter plot of dispersion as a function of standard deviation



78188

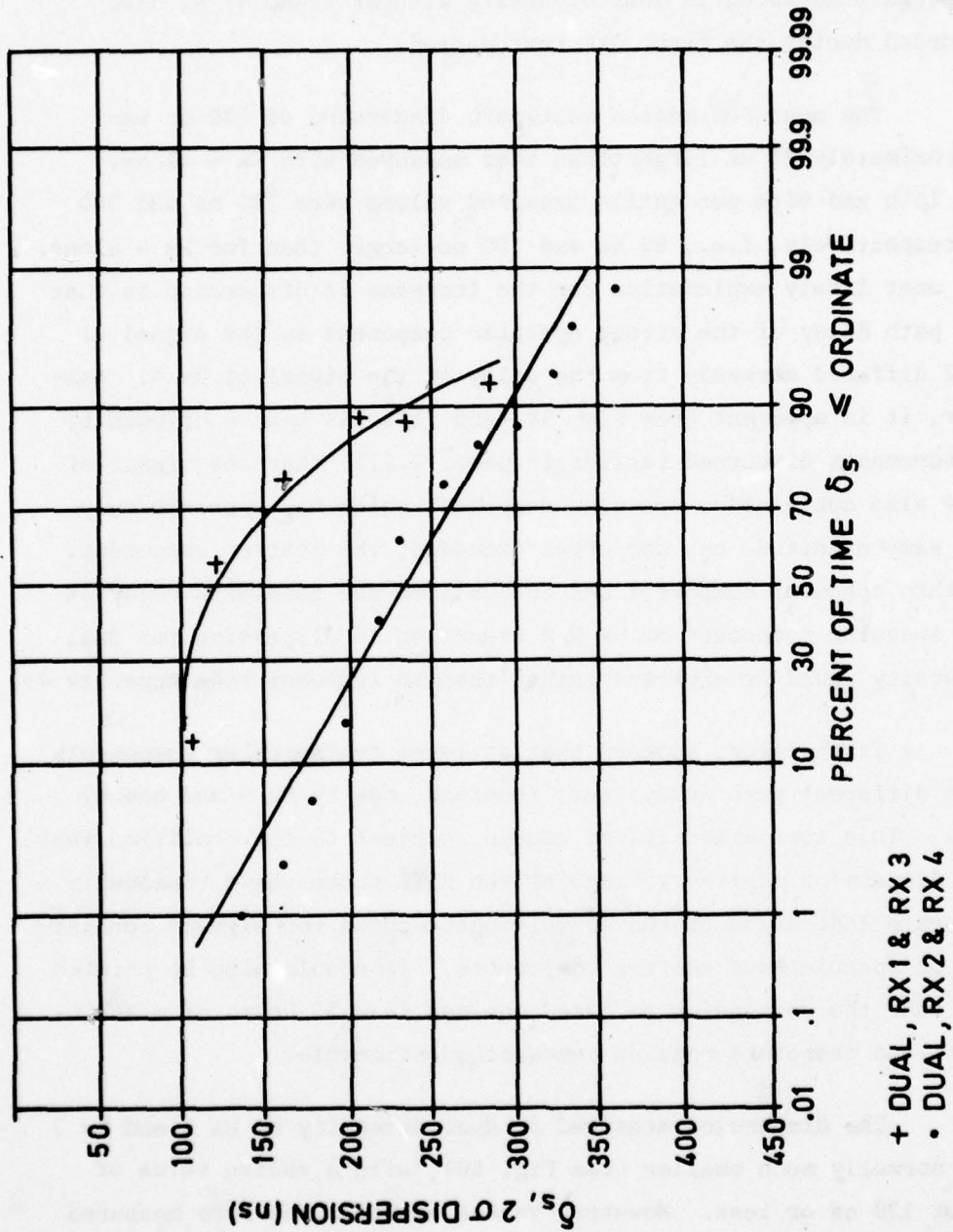
Fig. 49 Cumulative distribution of multipath dispersion (receiver 4)

Figure 50 is a cumulative distribution of the multipath dispersion measured in dual diversity with Rx 2 and Rx 4, also recorded during the first UHF test period.

The measured median multipath dispersion of 230 ns was approximately 75 ns larger than that measured with Rx 4 alone. The 10th and 90th percentile measured values were 185 ns and 300 ns respectively, i.e., 80 ns and 100 ns larger than for Rx 4 alone. The most likely explanation for the increase in dispersion is that the path delay of the strong specular component in the signal of Rx 2 differed markedly from the delay of the signal of Rx 4. However, it is apparent from Fig. 48 (and this has been confirmed by measurements discussed earlier in para. 7.2.1) that the signal of Rx 4 also contained a specular component which had approximately the same magnitude as, and often exceeded, the scatter component. If this specular component had encountered the same path delay as the specular component of Rx 2 a reduction in dispersion for dual diversity would be expected rather than an increase (see Appendix J).

It therefore appears that at least two specular components with different path delays were received, one by Rx 4 and one by Rx 2. This conclusion is, of course, subject to the condition that the dispersion monitor voltage of the MDTS modem was a reasonably accurate indication of the 2 σ multipath spread for signals consisting of specular and scatter components. It should also be pointed out that the conclusion is based on less than 25 hours of measurement, and therefore remains somewhat questionable.

The dispersion measured in dual diversity on Rx 1 and Rx 3 was normally much smaller (see Fig. 50), with a median value of about 120 ns or less. However, values up to 310 ns were measured during a few periods, i.e., values approaching the larger values measured on Rx 2 and Rx 4.



78189

Fig. 50 Cumulative distribution of dual diversity multipath dispersion

It is interesting to compare the results obtained in this test programme with the results of others. Figure 51 shows the cumulative distributions of the multipath dispersion obtained from the Rx 4 and dual (Rx 2 + Rx 4 and Rx 1 + Rx 3) diversity measurements, together with the cumulative distributions obtained on another test link at 900 MHz and 4.7 GHz (see Ref. 11 and 13). The curves portrayed in Fig. 51 have been normalized to their respective median values to permit direct comparison. The variances about the normalized median value for each of the curves is about the same with the exception of the dual diversity measurements on Rx 1 and Rx 3. The 99th percentile values of δ_s range from 1.5 to 1.8 times the median δ_s . An extrapolation of measured data indicates that a δ_s measured at the 99.9th percentile would be of the order of 1.7 to 2.0 times the median value.

The small spread of the cumulative distributions for all cases where troposcatter played a role suggests that the variations in δ_s shown in Fig. 51 may be typical for troposcatter links. However, this would have to be confirmed by other data since the only long-term direct measurements of multipath dispersion are those taken on the Youngstown-Verona link (Ref. 11).

In conclusion, it may be said that it was not possible to confirm the accuracy of the predictions presented in Table 12. This was due mainly to the unusual mixed-mode propagation on the UHF test link. On the other hand, no striking discrepancy was found between the measured values of δ_s and those predicted.

7.2.6 Aircraft reflections

In addition to the major propagation modes displayed by the trans-alpine link, periods of very rapid fading were frequently observed. The fade rates observed were well in excess of 10 Hz as opposed to the 0.1 to 1 Hz normally measured during fading.

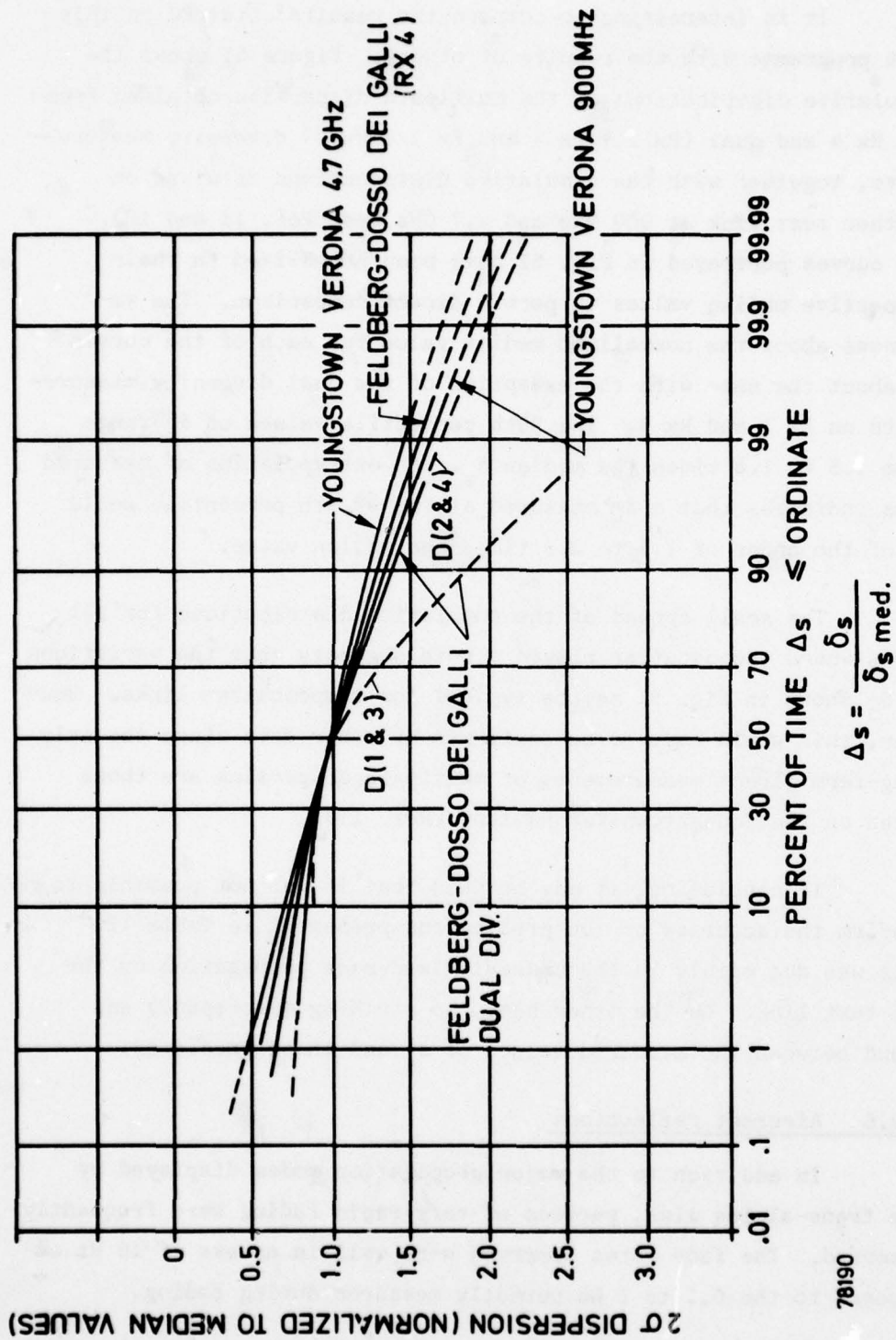


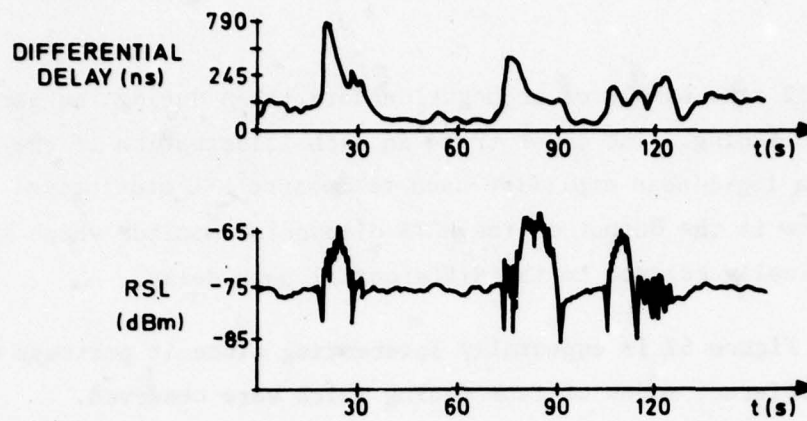
Fig. 51 Cumulative distribution functions of normalized multipath dispersion

Figure 52 is a sample of propagation data taken during the periods of rapid fading. The lower trace in each illustration is the output of a log-linear amplifier used to measure RSL statistics. The top trace is the output of the MDTs dispersion monitor which is monotonically related to the differential path delay.

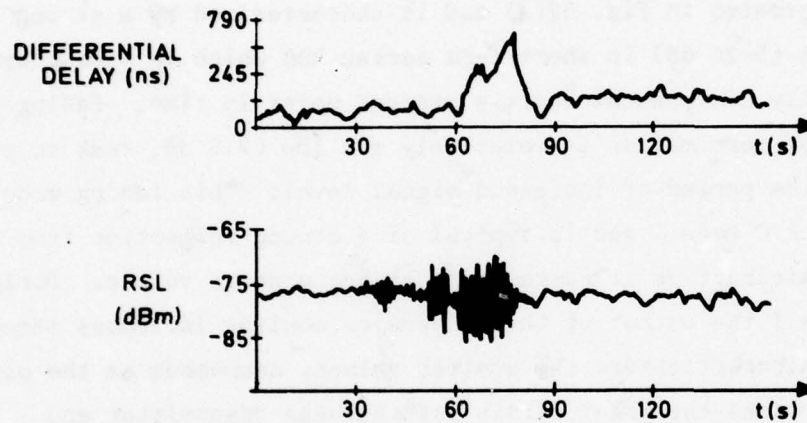
Figure 52 is especially interesting since it portrays the three different modes of fast fading which were observed.

The first and most frequently observed fast-fading mode is illustrated in Fig. 52(a) and is characterized by a strong increase (5-20 dB) in short-term median RSL which is almost symmetrically distributed about a central point in time. Fading about the short-term median is relatively shallow (2.5 dB, peak to peak) during the period of increased signal level. This fading mode was denoted A/C Mode I and is typical of a strong reflection from a single aircraft as it passes through the scatter volume. During A/C Mode I the output of the dispersion monitor increases steeply as the aircraft enters the scatter volume, decreases as the aircraft crosses the great circle path between transmitter and receiver, and finally increases again as the aircraft leaves the common volume.

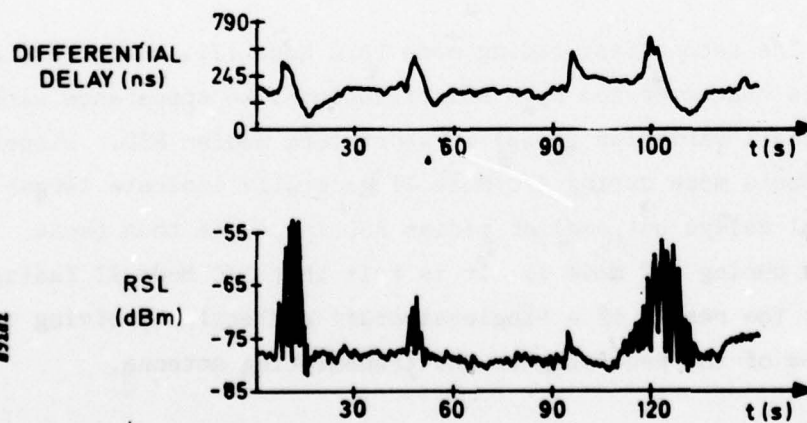
The second fast-fading mode (A/C Mode II), shown in Fig. 52(b), is characterized by a scintillation-like appearance with only a small variation (5 dB) in short-term median RSL. Dispersion measurements made during A/C Mode II generally indicate larger differential delays but smaller median RSL increases than those measured during A/C Mode I. It is felt that A/C Mode II fading could be the result of a single-aircraft reflection arriving via a side lobe of the receiving or the transmitting antenna.



a: AIRCRAFT PASS - MODE I



b: AIRCRAFT PASS - MODE II



c: AIRCRAFT PASS - MODE III

Fig. 52 Examples of RSL and dispersion measured during aircraft passes

The third fast fading mode, called A/C Mode III, is seen in Fig. 52(c). A/C Mode III is characterized by a strong increase in short-term median RSL (10-15 dB) and fast, deep fading (10-20 dB). Two explanations are suggested for these phenomena. The first explanation postulates one or more near-equal-intensity reflections from a region which is within line of sight of both the aircraft and the antenna in addition to the signal reflected directly from the aircraft to the receiving antenna. The second explanation proposes reflections from two aircraft within the common volume. As the common volume was located in the vicinity of Zurich International Airport, this explanation is considered the more likely.

7.3 PROPAGATION CHARACTERISTICS OF THE C-BAND LINK

As expected, the mode of propagation observed on the C-band link for most of the time was due to diffraction. However, for a small percentage of the time there was a considerable decrease in signal level and an increase in fading rate. This indicates that the obstacle gain was lost and troposcatter became the predominant mode of propagation.

In addition to the periods of low RSL caused by troposcatter propagation, even greater drops in RSL were observed on a few occasions. These events lasted for only a few seconds and therefore did not affect in the measured distribution of 20-min median RSLs. The most likely explanation for these periods of exceptionally low RSL (-95 to -105 dBm) appears to be obstacle blockage resulting from super-refraction conditions, i.e., $K \gg 1.33$ or even negative. However, further upward bending of the beam could result in very large troposcatter path loss, although extremely low values of K would have to occur to cause this effect on the relatively short path. These periods of very low RSL were only observed during periods of thunderstorm activity.

Figures 53 and 54 show two representative short-term distributions of RSL. The curve in Fig. 53 is typical for the shallow fading seen on the link during diffractive conditions. On the other hand, Fig. 54 represents the short-term distribution generally seen during fading periods on the C-band link. The close agreement with the Rayleigh distribution indicates that no specular diffraction component was present during periods of intense fading.

The fading rate observed on the C-band link ranged from less than 0.1 to 1 Hz. Periods of rapid fading resulting from aircraft passages through the common volume were not noted. This was expected since the link was short and therefore propagation was confined to relatively low altitudes.

Long-term RSL distributions are presented in Fig. 55 to 57. Figures 55 and 56 show the distributions measured during Test Periods 4 and 5 respectively, whereas Fig. 57 includes all measurements on the C-band link. It should be noted that transmitter output power of only 60 watts was used during the C-band measurements. The signal levels on receivers 2 and 4 were in general larger than those on receivers 1 and 3. This difference was more pronounced in July (Fig. 55) than in August (Fig. 56). Large variations in the difference between the 20-min median signal levels simultaneously measured in any two diversity branches were noticed throughout Periods 4 and 5. Such variations, which were also observed on the UHF link, seem to be typical for propagation paths where diffraction is involved. Digital troposcatter modems should therefore be capable of operating effectively with markedly different median diversity signal levels, particularly if utilization on diffraction paths is to be considered.

In Fig. 57, RSL distribution predicted by the modified Bullington method is also shown. Good agreement between this distribution and the measured values will be noted.

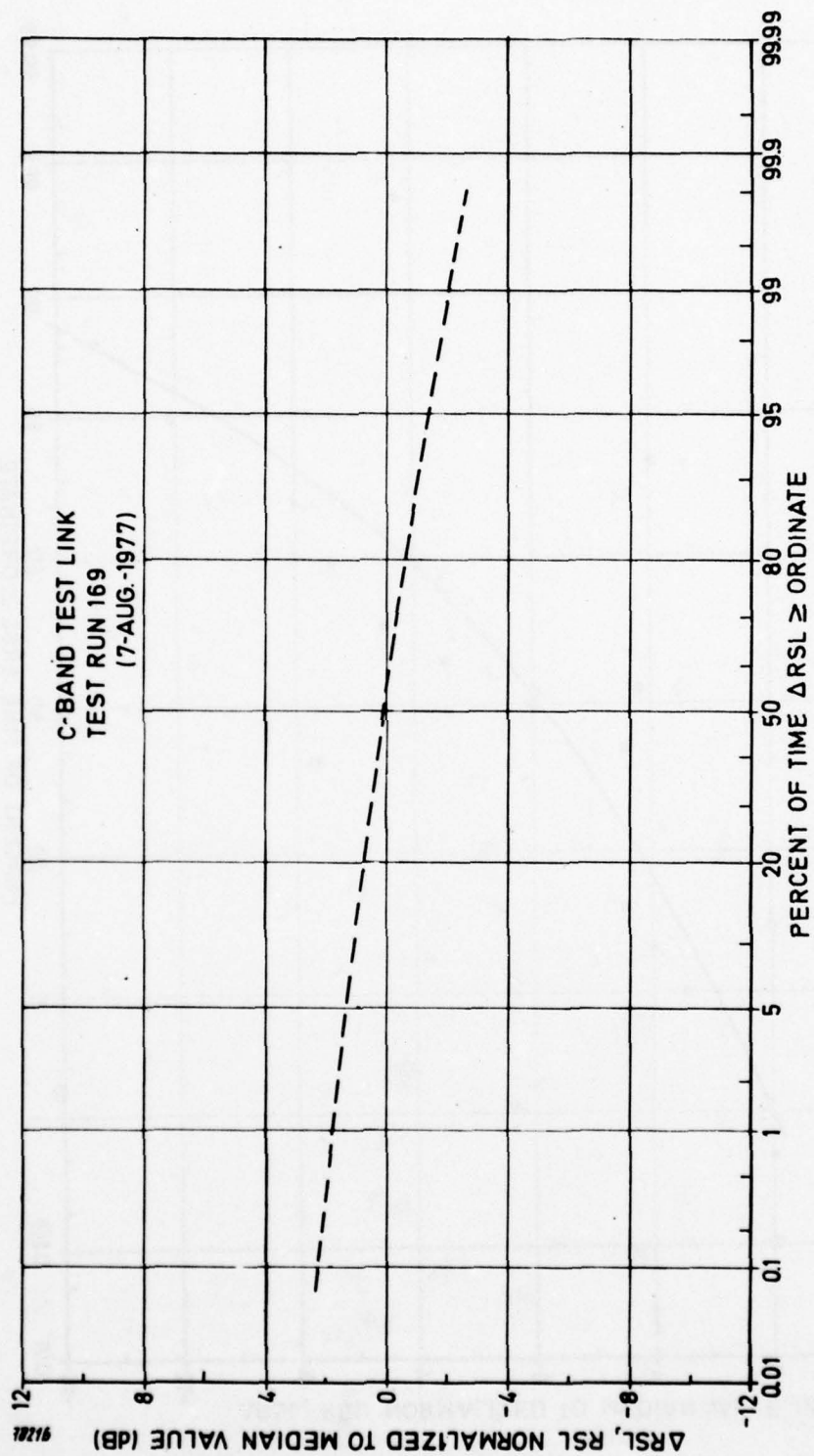


Fig. 53 Short-term RSL distribution (C-band): diffraction signal

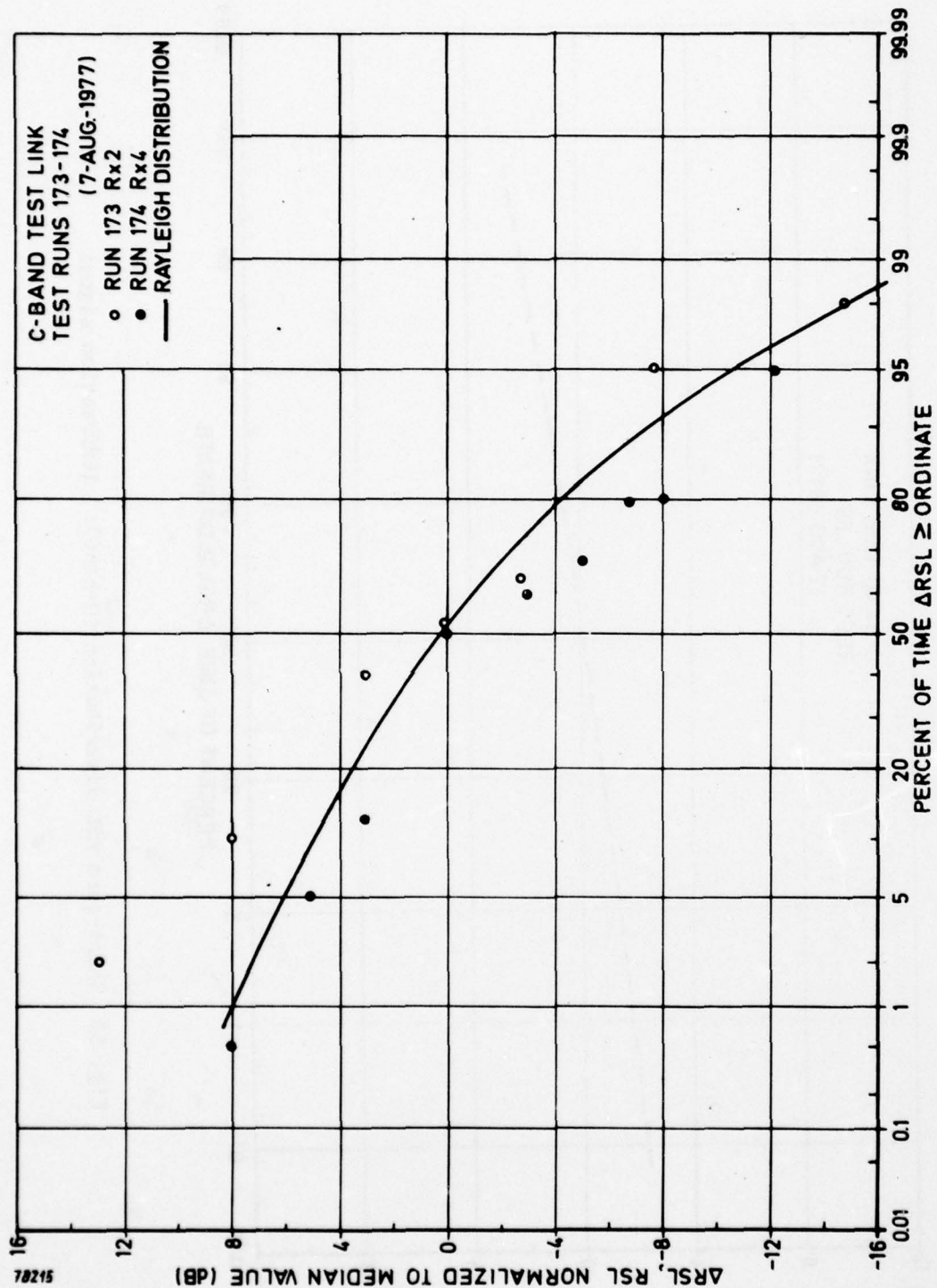


Fig. 54 Short-term RSL distribution (C-band): fading period

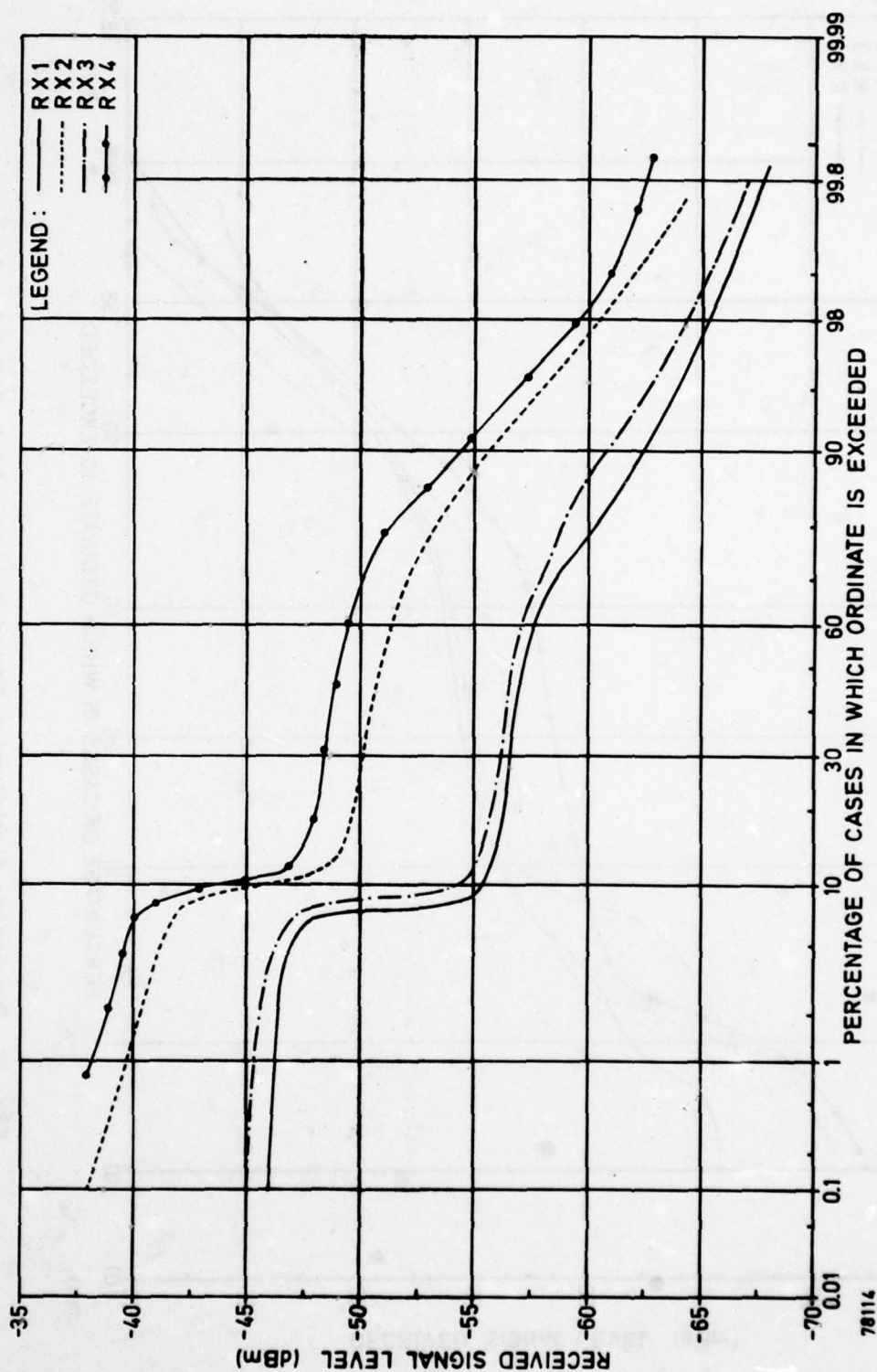


Fig. 55 Cumulative distribution function of received signal level
(15 July - 1 August 1977)

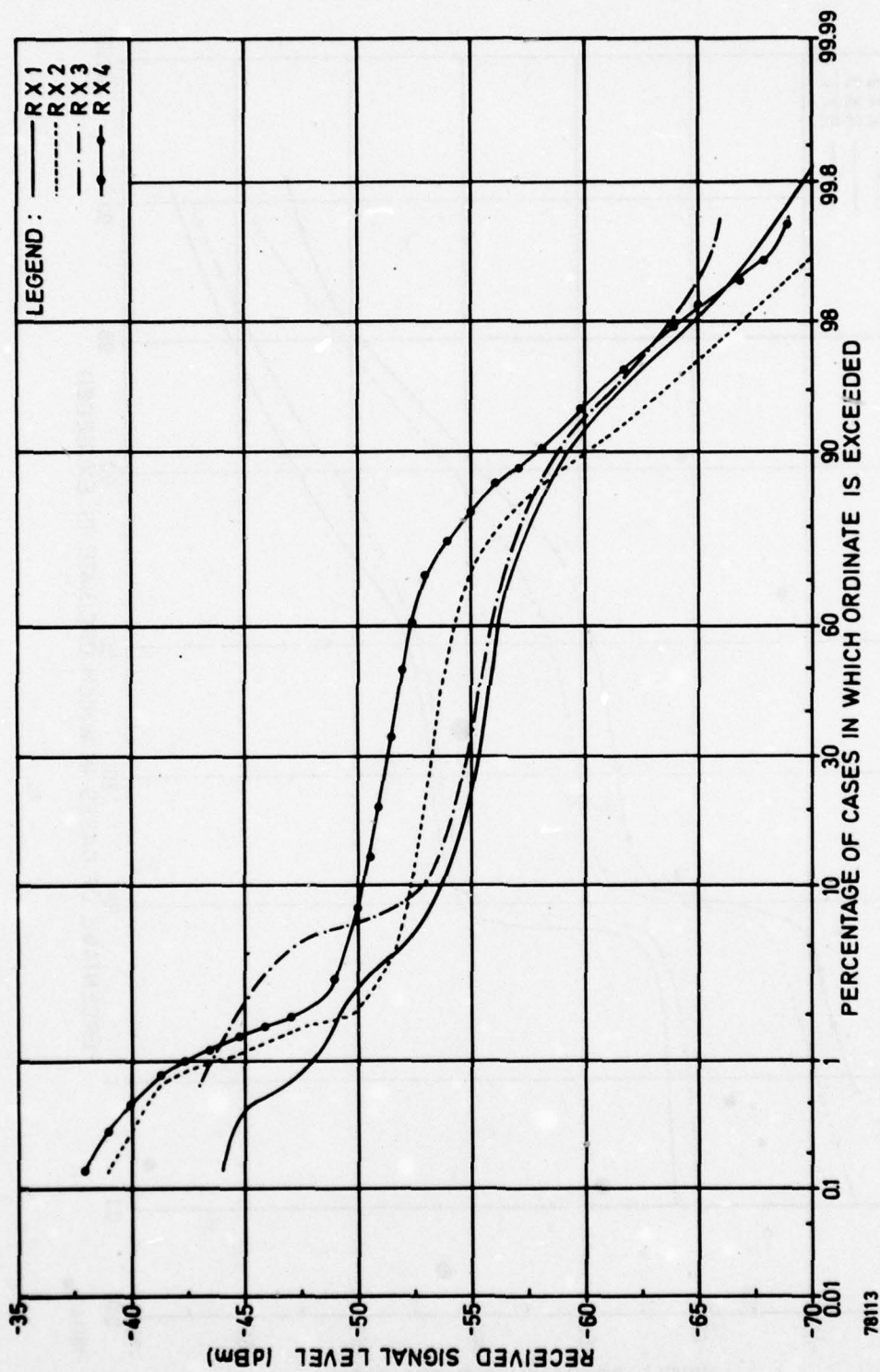


Fig. 56 Cumulative distribution function of received signal level
(1 August - 14 August 1977)

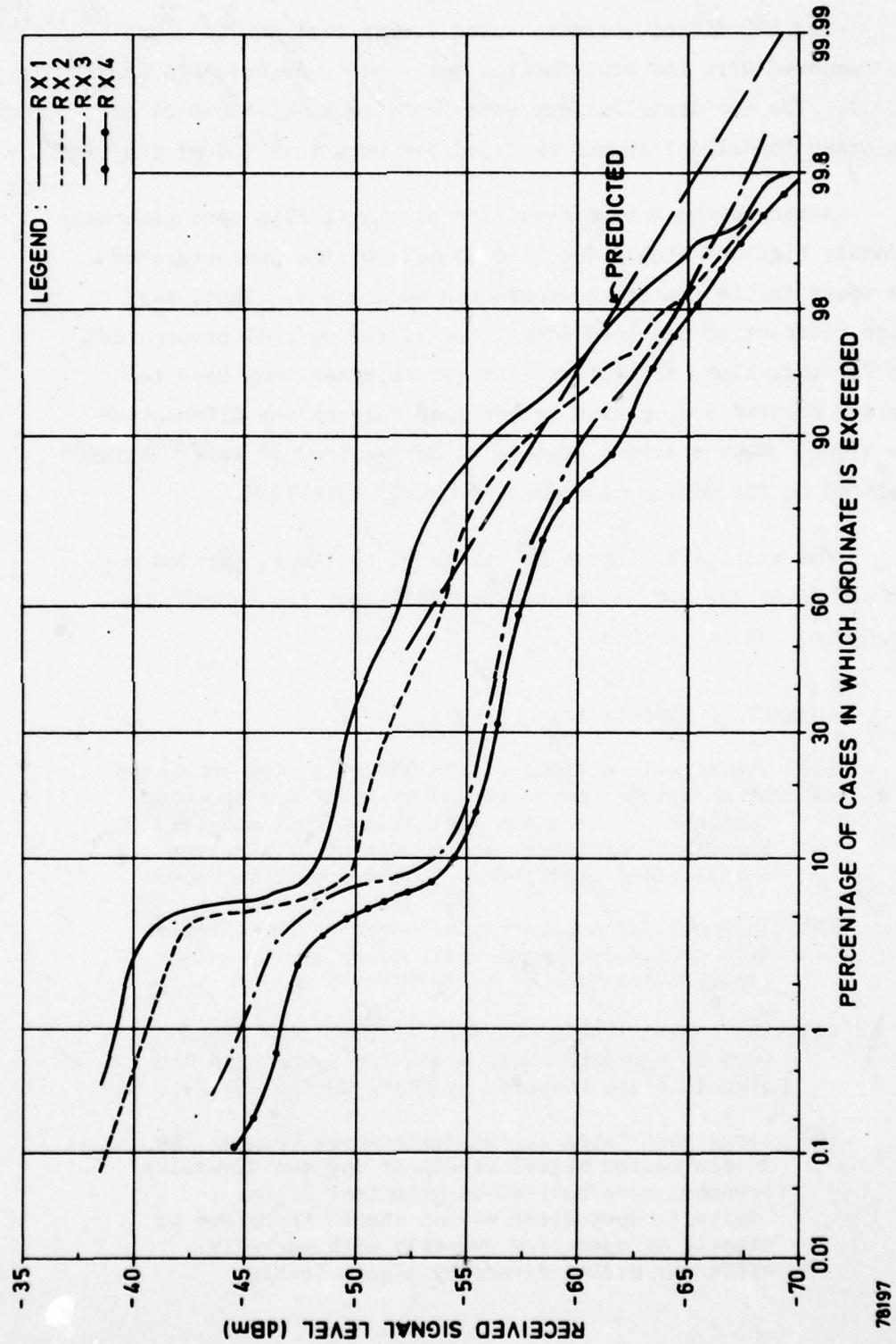


Fig. 57 Cumulative distribution function of received signal level
(15 July - 14 August 1977)

The RSL distribution measured during Test Period 5 was also compared with the distribution measured in August 1970 (see Ref. 1). The two distributions were found to be within 3 dB of each other for signal levels exceeded for more than 50% of the time.

Although the C-band test link diversity RSLs were generally extremely high and stable due to diffraction, the percentage of time spent in the scatter mode was non-negligible. Thus, even though diffraction has been identified as the nominal propagation mode for this link, any future link refurbishment may have to consider scatter propagation rather than rely on the diffraction mode alone. Beam steering appears to be required if total reliance is placed on the diffraction for the C-band test link.

The multipath dispersion indicated by the dispersion monitor signal of the MDTs modem was negligible on the C-band link, even during fading periods.

7.4 SUMMARY OF PROPAGATION ANALYSIS

- (a) The signal received on the UHF test link consisted of a scatter component and at least one specular component. There are indications that several specular components with different path delays occasionally contributed to the signal received.
- (b) The specular components measured on the UHF link were caused by double-diffraction and/or off-bore-sight diffraction or reflections.
- (c) The signal levels measured on both test links were in agreement with predictions and with the signal levels measured by SHAPE during 1970/71.
- (d) Large variations in the differences between the 20-min median signal levels of any two diversity branches were noticed on both test links. Digital troposcatter modems should therefore be capable of operating properly with markedly different median diversity signal levels.

- (e) Due to the mixed-mode propagation on the UHF link, to the relatively few measurements, and to the unavailability of a multipath analyzer, it was not possible to confirm the accuracy of predictions of the multipath dispersion. However, the variations of dispersion measured on the UHF link appeared to be consistent with data measured on other links where variations of up to twice the median multipath dispersion were observed.
- (f) Periods of scatter propagation were noted on the C-band test link. The occurrence of scatter and possibly obstructed propagation on such a short diffraction link is interesting and indicates that beam steering may be advantageously used to avoid the system gain required for pure tropo-scatter propagation and currently maintained on this link.

8. DIGITAL SYSTEM PERFORMANCE ANALYSIS

Digital performance testing of the MDTs and DAR modems was carried out on the UHF link from January to June and on the diffraction link in July and August 1977. Performance data was analysed to provide mean bit error rate (BER) statistics, short-term bit error distributions, and voice-channel fade outage statistics. The probability of fade outage is the probability that the performance of a digitized voice channel will degrade below a specific threshold. An "instantaneous" BER of 1×10^{-4} was chosen as a reasonable fade outage threshold at which bit errors would be likely to begin affecting 8-bit PCM voice channel performance. An observation period of 100 ms was chosen for the compilation of fade outage statistics, since voice channel outages with durations of less than 100 ms are likely to be unnoticed by a user unless outages become highly repetitive.

While the mean BER is not sufficient to describe the performance of digital transmission systems, it nonetheless can serve as a coarse indicator of system performance as long as the propagation mechanism is understood and a suitable measurement period is chosen. Consistent with established procedures for troposcatter measurements, a measurement period or run of approximately 17 to 20 min was chosen.

8.1 MDTs UHF TEST LINK SYSTEM PERFORMANCE

8.1.1 Bit error rate

Figure 58 represents a compilation of bit error performance data taken with the MDTs modem operating at 6.3 Mbit/s in the system test configuration and includes the effects of occasional modem and TDM losses of bit count integrity (BCI). The error rate

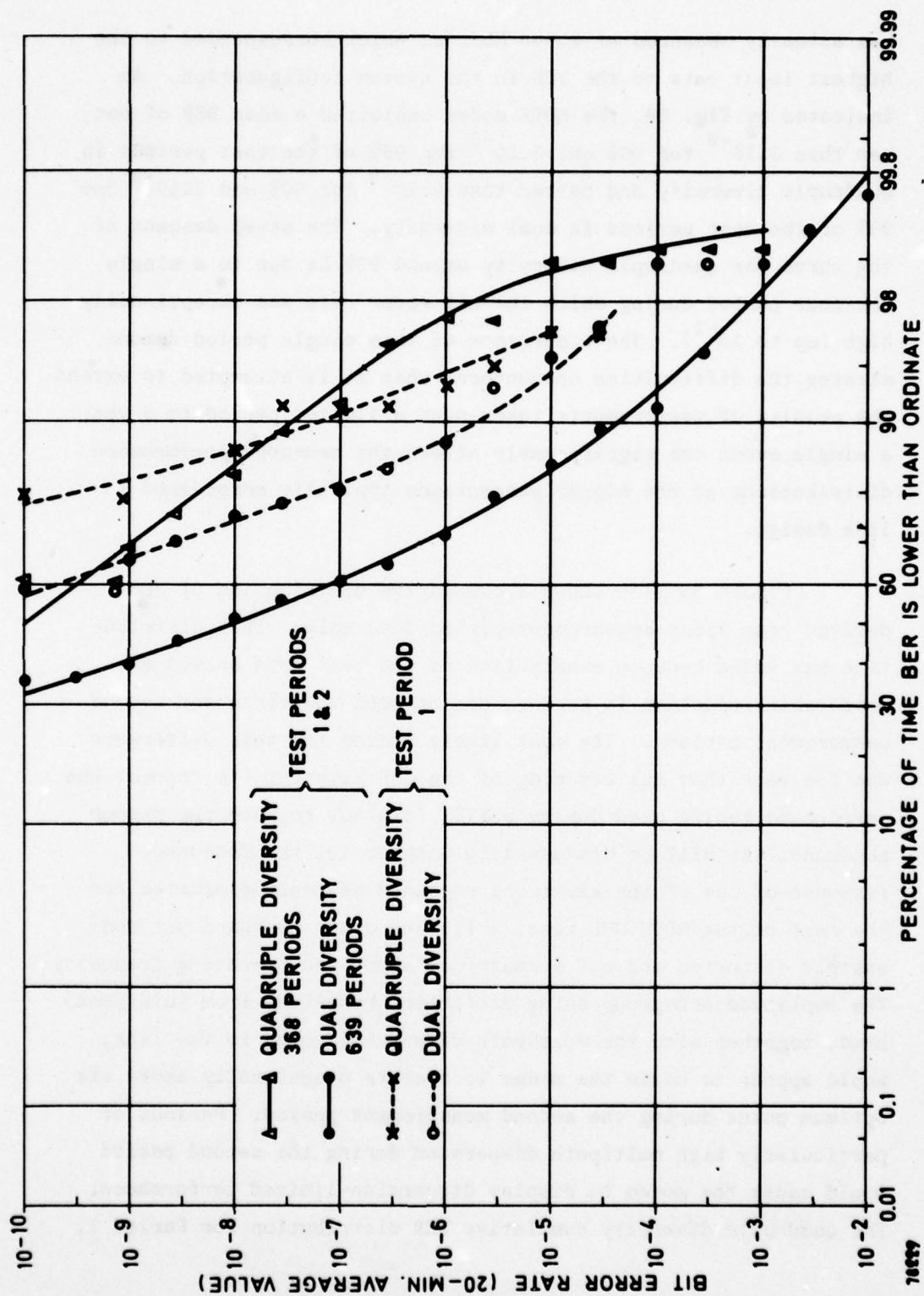


Fig. 58 Distribution of bit error rate for MDTs modem at 6.3 Mbit/s (UHF link)

was actually measured at 2.048 Mbit/s, which corresponded to the highest input rate to the TDM in the system configuration. As indicated by Fig. 58, the MDTS modem exhibited a mean BER of better than $3 \cdot 10^{-8}$ for 90% and $3 \cdot 10^{-5}$ for 99% of the test periods in quadruple diversity and better than $4 \cdot 10^{-5}$ for 90% and $2 \cdot 10^{-3}$ for 99% of the test periods in dual diversity. The steep descent of the curve for quadruple diversity around 99% is due to a single one-hour period during which the bit error rate was exceptionally high (up to 10^{-2}). The occurrence of this single period demonstrates the difficulties encountered when it is attempted to extend the results of measurements taken over a limited period to a year: a single event can significantly affect the measured performance distributions at the higher percentages typically considered in link design.

Figure 58 also shows a cumulative distribution of BER derived from first-measurement-period data only. This distribution was added because examination of the test data showed a measurable reduction in performance between the first and second measurement periods. The most likely reason for this difference was the fact that the retuning of the UHF klystron (to correct the narrowband tuning used during WINTEX) did not restore the proper passband. As will be discussed in Chapter 10, the frequency response of one of the klystrons remained severely distorted for the rest of the MDTS UHF test, while the other passband was moderately distorted and not symmetrical about the operating frequency. The amplitude and group delay distortion resulting from this passband, together with the multipath dispersion found in the link, would appear to cause the modem to operate occasionally above its optimum point during the second measurement period. Periods of particularly high multipath dispersion during the second period would cause the modem to display dispersion-limited performance. The quadruple diversity cumulative BER distribution for Period 1,

while slightly worse than the distribution for both periods, displays a different trend. The Period 1 distribution for dual diversity shows generally lower bit error rates than the overall distribution, although considerably more measurement points are included in the latter.

Figure 59 shows the distribution of MDTS BER data taken at 9.4 Mbit/s as transmitted in a 7.0-MHz RF bandwidth (i.e., approximately 1.3 bit/Hz at RF) using the link test configuration. It should be noted that the total test time spent at 9.4 Mbit/s was relatively small.

The combination of transmitter filtering used to confine 9.4 Mbit/s into 7 MHz and the multipath dispersion encountered on the UHF test link was expected to cause degradation in performance relative to the more optimally designed 6.3-Mbit/s configuration. Transmitter filtering will cause a lessening of the range of differential delay over which the MDTS equalizer circuitry can operate without a significant intersymbol interference penalty resulting in higher error rates. This effect is responsible for the BER behaviour indicated by Fig. 59. Detailed analysis of bit error events indicated that periods of concurrent fading and high dispersion resulted in the highest bit error rates.

In Figure 60 the measured mean BER is plotted as a function of carrier-to-noise ratio (CNR) together with the curves for the predicted 6.3-Mbit/s modem BER performance previously shown in Fig. 20. Two observations can be made from Fig. 60. Firstly, the combined CNR ranged from about 30 dB to more than 40 dB, which was typical for the measurements on the UHF link. Secondly, a large difference of about 10 to 20 dB may be noted between the measured and predicted performance whenever bit errors occurred (in approximately 40% of the tests). This is rather unexpected, since good

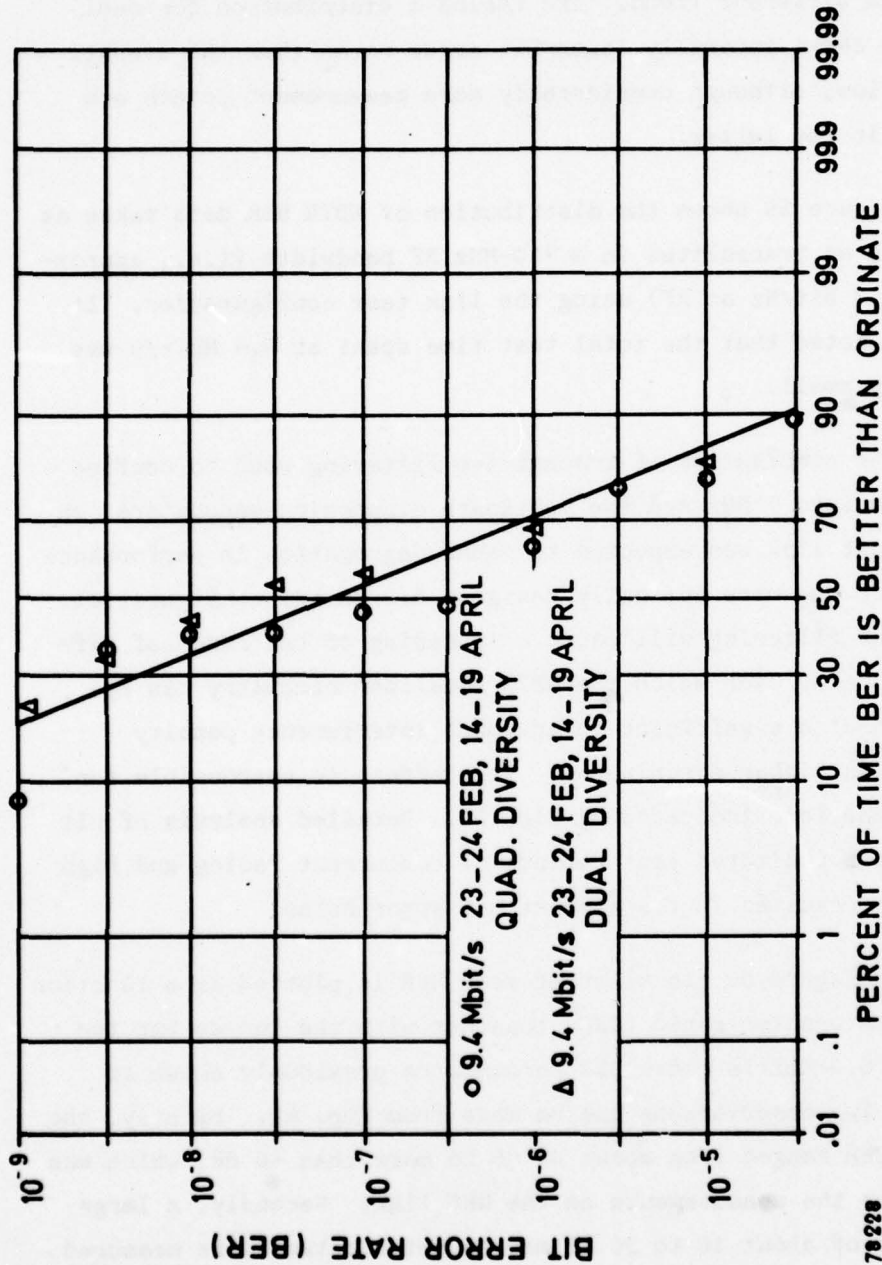


Fig. 59 Distribution of bit error rate for MDTs modem at 9.4 Mbit/s (UHF link)

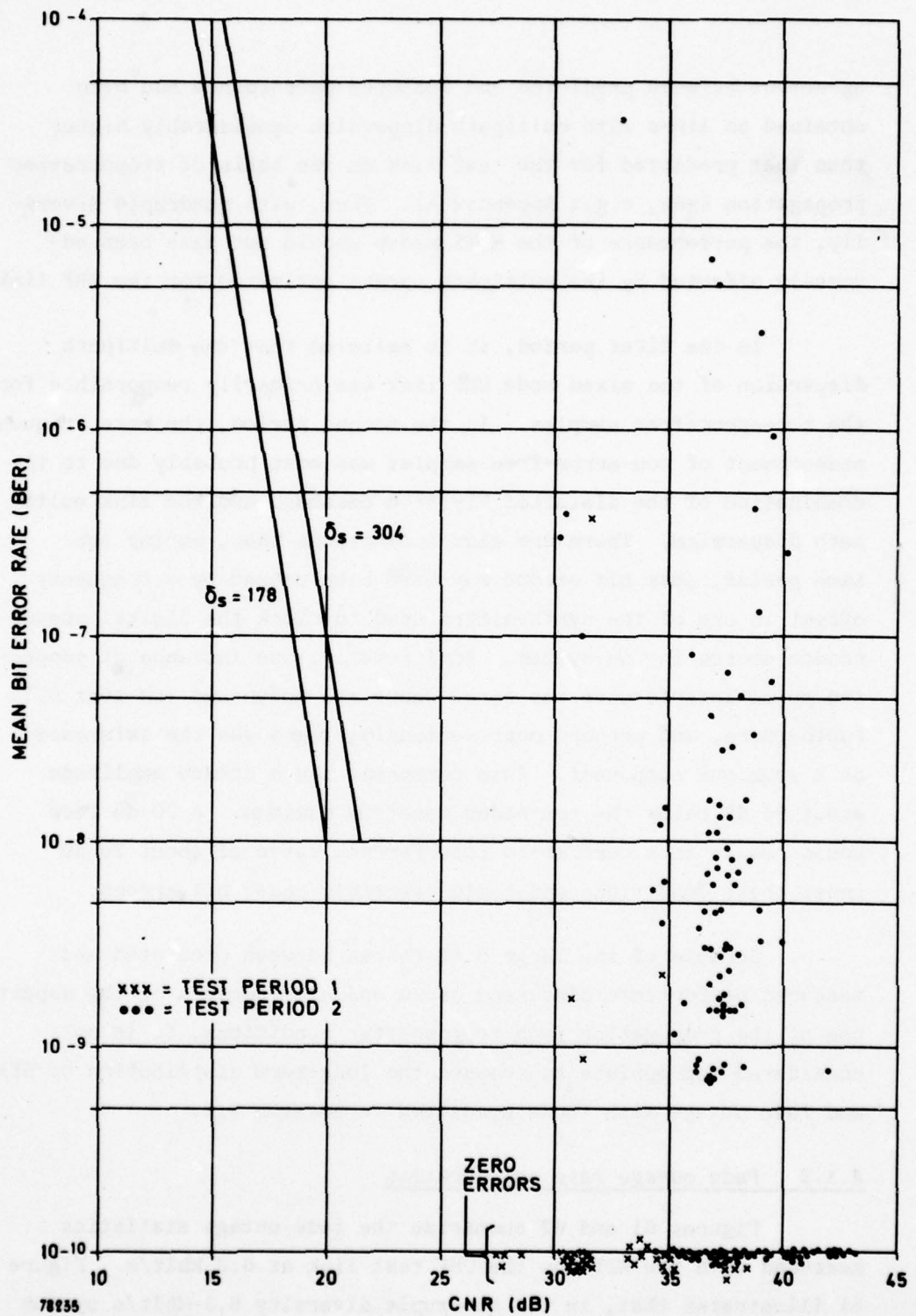


Fig. 60 Comparison between predicted and measured MDTs performance at 6.3 Mbit/s quadruple diversity

agreement between predicted and measured performance had been obtained on links with multipath dispersion considerably higher than that predicted for the test link on the basis of troposcatter propagation (see, e.g., Appendix A). Thus, with quadruple diversity, the performance of the MDTs modem should not have been adversely affected by the multipath spread estimated for the UHF link.

In the first period, it is believed that the multipath dispersion of the mixed mode UHF link was primarily responsible for the non-error-free samples. In the second period, the more frequent measurement of non-error-free samples was most probably due to the combination of the distorted klystron passband and the link multipath dispersion. There are also indications that, during the same period, some bit errors may have been caused by a frequency offset in one of the synthesizers used to clock the digital pseudorandom source in the system. Additionally, one instance of suspected pulse interference was noted where the modem and TDM lost BCI. Furthermore, and perhaps most seriously, there was the existence of a spurious component. This component had a steady amplitude about 90 dB below the non-faded spectrum maximum. A 20-dB fade would result in a carrier-to-interference ratio of about 20 dB under these conditions and could certainly cause bit errors.

Because of the large differences between predicted and measured performance discussed above and also because of the departure of the propagation from troposcatter conditions, it is not considered appropriate to compare the long-term distribution of BER and fade outage with those predicted in Section 6.1.

8.1.2 Fade outage rate and duration

Figures 61 and 62 summarize the fade outage statistics measured with the MDTs on the UHF test link at 6.3 Mbit/s. Figure 61 illustrates that, in the quadruple diversity 6.3-Mbit/s system

configuration, fade outages were observed in only about 5% of all test runs. The worst short-term measured fade outage rate was about one outage per second in quadruple diversity; the mean outage duration was 370 ms excluding the longest outage, which lasted 20 min. Of the 5% of the quadruple diversity test runs having fade outages, the majority of the fade outages were less than 20 ms in duration, further diminishing their impact on voice channel quality.

As mentioned earlier, the 6.3-Mbit/s fade outage data was measured at the 2.048-Mbit/s port side of the AN/GSC-24 TDM and thus included the effects of occasional modem and TDM synchronization losses. However, the latter were found to represent a negligible contribution to the overall fade outage probability of the system as long as quadruple diversity transmission was employed.

As could be expected, dual diversity MDTs testing on the UHF link provided more fade outage data than quadruple diversity tests. Fade outages were observed in 42% of the dual diversity test runs. The mean fade outage duration compiled over all dual diversity tests was about 750 ms. To compare predicted and measured fade outage statistics on a short-term basis, a number of dual diversity runs with approximately the same fade rate were selected. The mean fade outage duration for these runs was about 490 ms (see Fig. 62). An expression for predicting mean fade outage duration for diversity QPSK in a fading channel has previously been developed and is derived in Ref. 10. Taking a mean fade rate of 0.1 Hz, an estimated mean CNR of 26 dB, and an implementation loss of 3 dB from ideal performance, a predicted mean outage duration of 415 ms was calculated. Although this prediction is in good agreement with the measured value of 490 ms, it is useful to review the possibilities for prediction and measurement error. First, in the theoretical expression for mean outage duration, negligible intersymbol interference was assumed, whereas unusually high multipath dispersion occurred in dual diversity on the UHF test link. Secondly,

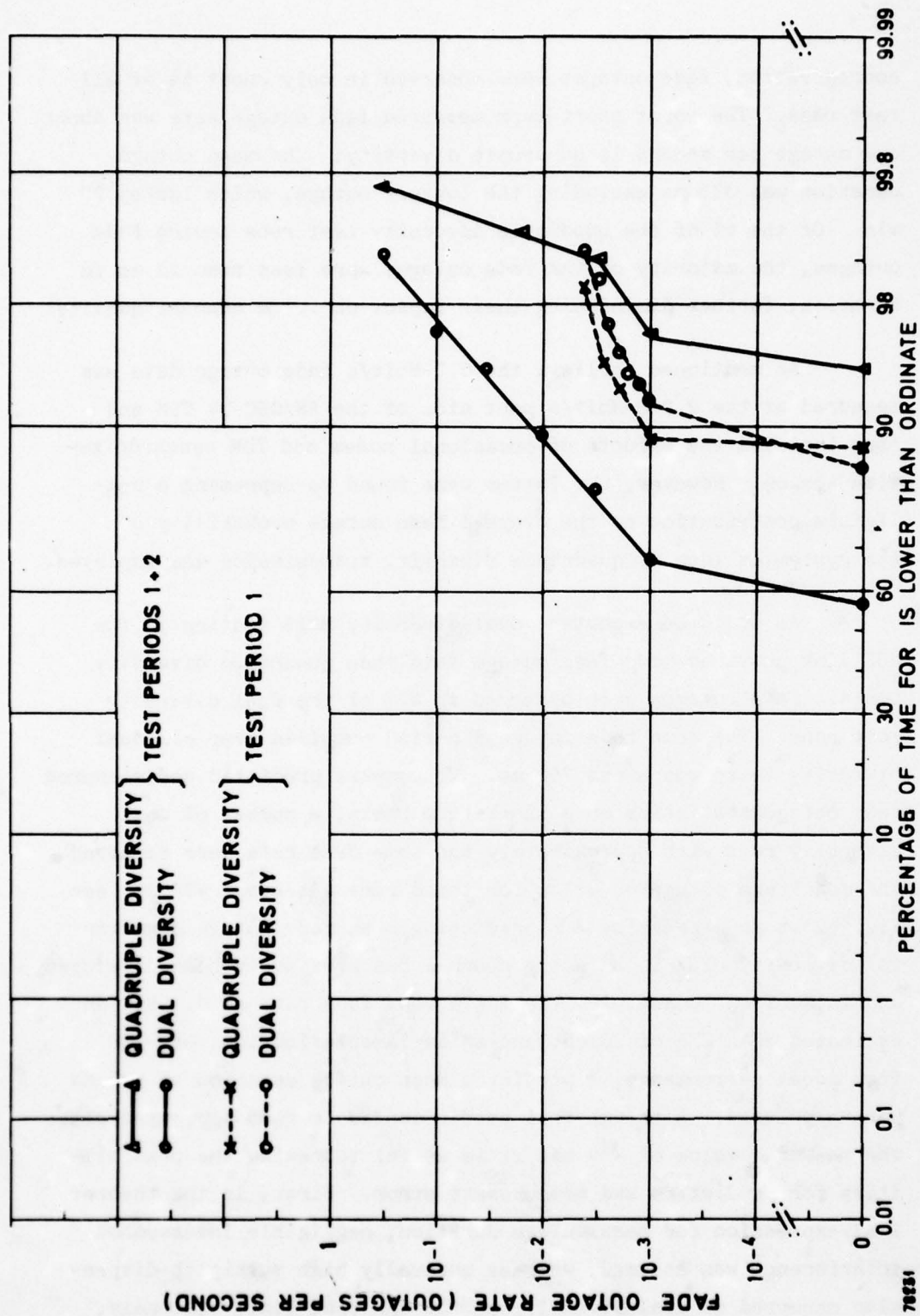


Fig. 61 Fade outage rate (FOR) for MDTs at 6.3 Mbit/s (UHF link)

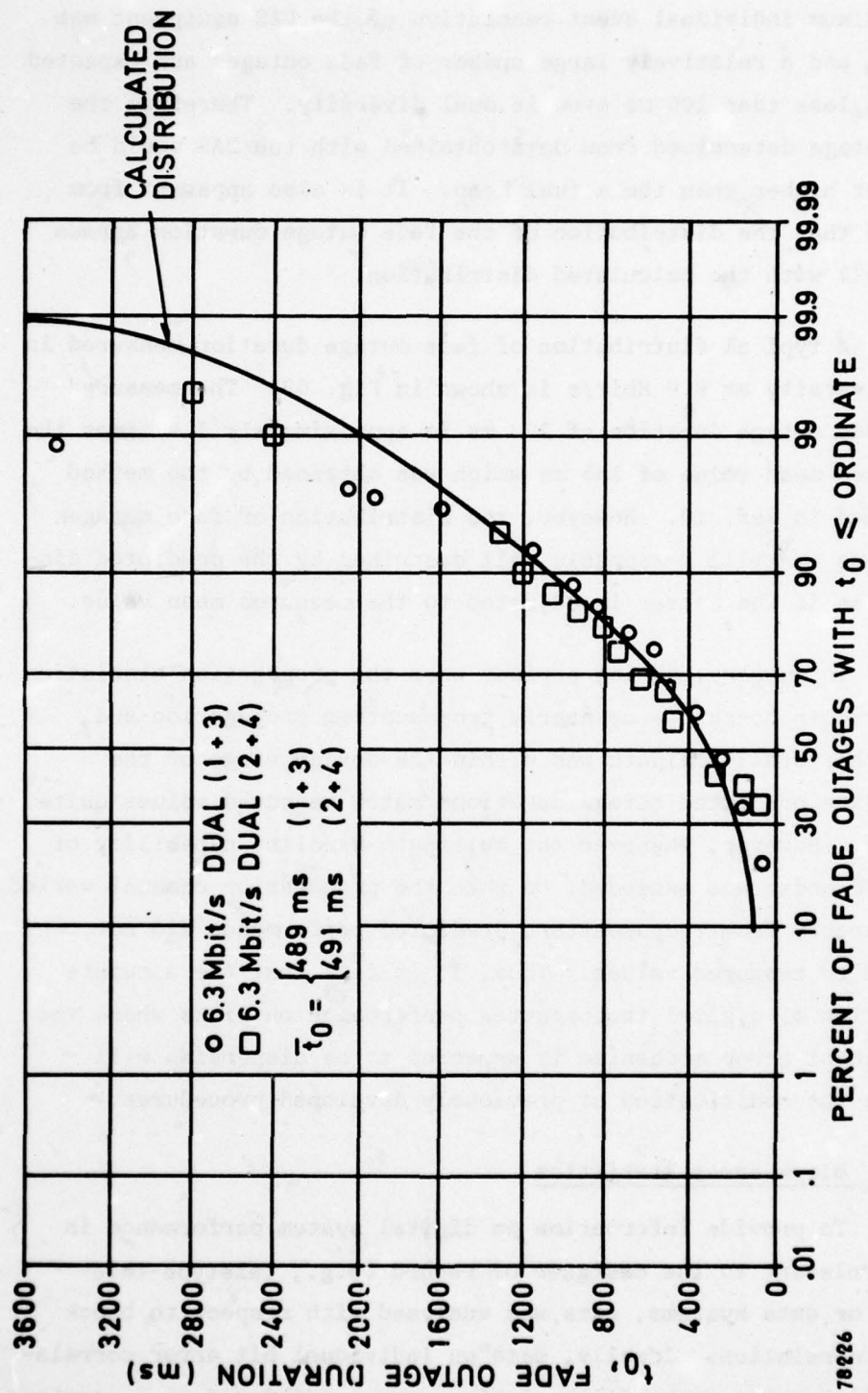


Fig. 62 Distribution of fade outage duration: comparison of measured and calculated values

the minimum individual event resolution of the DAS equipment was 100 ms, and a relatively large number of fade outages are expected to span less than 100 ms even in dual diversity. Therefore the mean outage determined from data obtained with the DAS would be somewhat higher than the actual mean. It is also apparent from Fig. 62 that the distribution of the fade outage duration agrees very well with the calculated distribution.

A typical distribution of fade outage duration measured in dual diversity at 9.4 Mbit/s is shown in Fig. 63. The measured mean fade outage duration of 224 ms is approximately 1.4 times the predicted mean value of 155 ms which was obtained by the method described in Ref. 10. However, the distribution of fade outage durations is still reasonably well described by the predicted distribution if the latter is adjusted to the measured mean value.

In summary, during periods when the propagation statistics indicated troposcatter or nearly troposcatter propagation and where the total multipath was within the design range of the modem, the predicted outage durations match measured values quite closely. However, whenever the multipath handling capability of the MDTs modem was exceeded, or when the propagation channel varied considerably from troposcatter, predicted performance did not correspond to measured values. Thus, it is felt that the accurate prediction of digital troposcatter performance on links where the predominant error mechanism is expected to be dispersion will require the modification of previously developed procedures.

8.1.3 Block error statistics

To provide information on digital system performance in terms relevant to the designer of record (e.g., teletype-telegraph) or data systems, data was analysed with respect to block error correlation. Ideally, data on individual bit error correlations (i.e., the probability of bit error conditioned on a previous

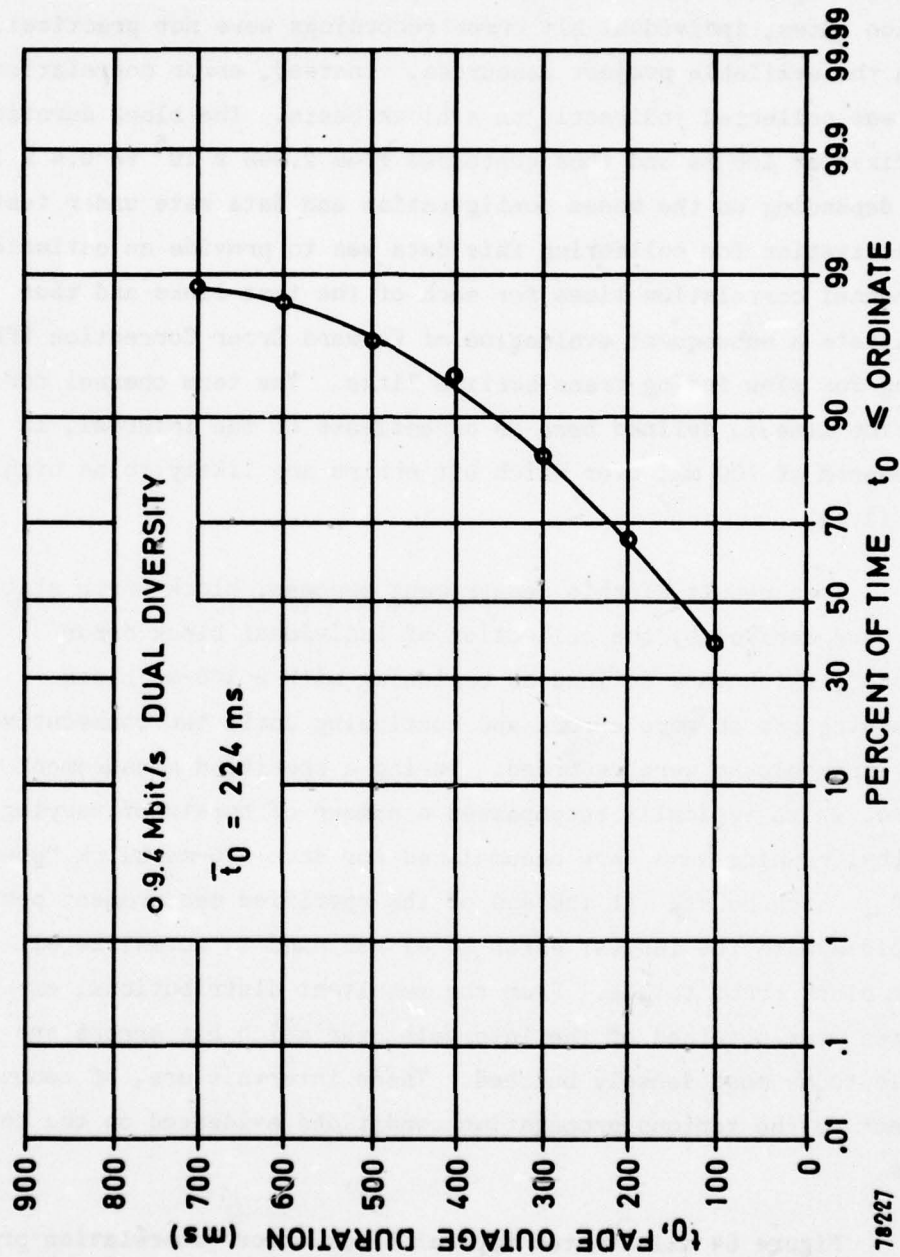


Fig. 63 Typical distribution of fade outage duration

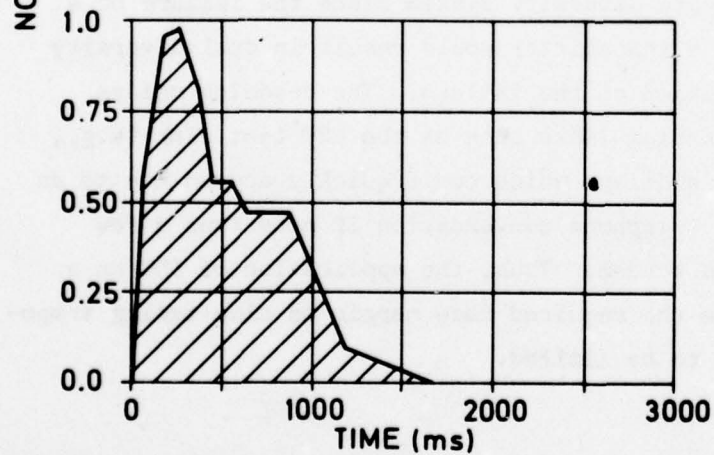
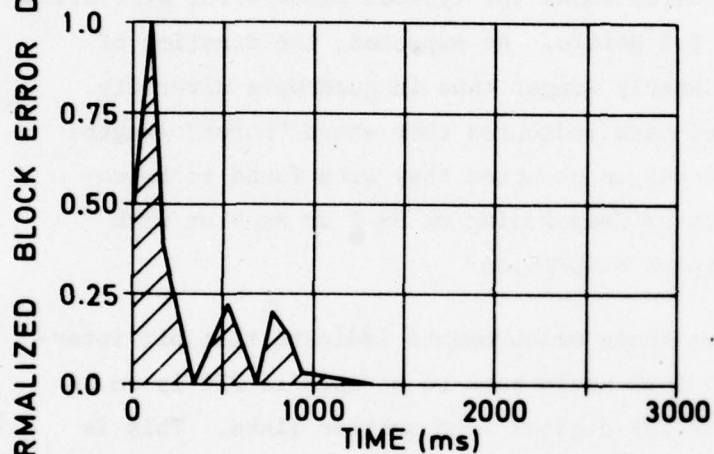
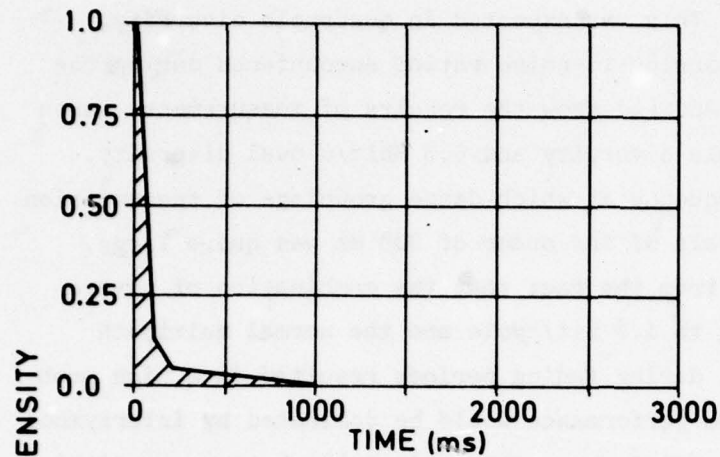
bit error) is generally considered the most desirable for use in data system design and analysis. However, due to the megabit transmission rates, individual bit error recordings were not practical, given the available project resources. Instead, error correlation data was collected indirectly on a block basis. The block duration was fixed at 100 ms and thus contained from 2.048×10^5 to 9.4×10^5 bits depending on the modem configuration and data rate under test. The motivation for collecting this data was to provide an estimate of channel correlation times for each of the test links and thus facilitate a subsequent evaluation of Forward Error Correction (FEC) coding for slow fading trans-horizon links. The term channel correlation time is defined here as an estimate of the interval, in increments of 100 ms, over which bit errors are likely to be highly correlated.

As a result of this measurement process, block error statistics were derived by the collection of individual block error "bursts", which were defined as beginning with a 100-ms block containing one or more errors and continuing until two consecutive error-free blocks were recorded. During a specified measurement period, which typically encompassed a number of bursts of varying lengths, running sums were accumulated for each 100-ms block "position" in each burst. At the end of the specified measurement period, the block with the largest error total was used to normalize all other block error totals. From the resultant distributions, estimates were obtained of the intervals over which bit errors are likely to be most densely bunched. These intervals are, of course, subject to the various propagation conditions evidenced on the test links.

Figure 64 illustrates typical block error "correlation profiles" calculated from the MDTs UHF test link data. Figure 64(a) is typical of measurements taken at 6.3 Mbit/s in quadruple diversity and indicates that most bit errors were confined to bursts of 100 ms

in duration or less. This was expected in quadruple diversity, particularly at the carrier-to-noise ratios encountered during the test. Figures 64(b) and (c) show the results of measurements taken at 9.4 Mbit/s quadruple diversity and 6.3 Mbit/s dual diversity. At 9.4 Mbit/s the frequency at which dense groupings of transmission errors spanned intervals of the order of 300 ms was quite large. This can be expected from the fact that the combination of severe transmitter filtering to 1.3 bit/cycle and the normal multipath spread of the channel during fading periods resulted in a high probability that the modem performance would be dominated by intersymbol interference. Figure 64(c) shows the typical block error statistics for dual diversity at 6.3 Mbit/s. As expected, the duration of error bursts is considerably longer than in quadruple diversity. The 6.3-Mbit/s measured data indicates that where "burst" lengths typically spanning 300-400 ms occurred they were found to be coincidental with periods of deep fading on Rx 2 or Rx 4 or with periods of large multipath dispersion.

The results of these measurements indicate that bit interleaving over roughly 400 ms would have to be used if FEC is to be employed effectively on UHF digital troposcatter links. This is true even for a quadruple diversity system since the failure of a key component such as a transmitter would result in dual diversity operation for the duration of the failure. The decoding delays associated with slow fading links such as the UHF test link (e.g., 400 ms) would result in delays which could quickly accumulate to an intolerable level for telephone conversation if more than a few links are traversed in tandem. Thus, the application of FEC on a bulk basis to decrease the required fade margin on slow-fading troposcatter links appears to be limited.



78234

Fig. 64 Block error statistics

8.1.4 Aircraft fading effects

The occasional periods of fast fading (> 10 Hz), which were attributed to aircraft passes through the scatter volumes as discussed earlier in Section 6.3, occasionally affected digital performance. The degree to which performance was affected depended on a number of factors such as diversity configuration, aircraft velocity, ambient received signal levels, and multipath dispersion. In most cases, digital performance was unaffected by aircraft passage since most aircraft passages resulted in enhanced RSLs and only a moderate increase in dispersion due to off-boresight reflection. Quadruple diversity measured performance of the MDTS modem was essentially unaffected by aircraft fading.

However, in dual diversity, periods occurred where concentrated numbers of bit errors, associated with aircraft passage events, were measured. It is considered that these bit errors resulted from intersymbol interference caused by large differential path delays between the troposcatter signal and the signal reflected by the aircraft as it passed through the common volume. Bit errors measured during aircraft passage events were typically confined to one or two bursts occurring sometimes during the first seconds and most often during the last seconds of the aircraft passage event, when the largest differential path delay between scatter and aircraft reflected signals will normally occur, as noted previously in Section 6.3. Figure 65 is based on 6.3 Mbit/s dual diversity data taken during a two-hour period of repeated aircraft crossings and illustrates the dependence of bit errors on differential path delay. The left-hand ordinate of Fig. 65 represents 100 ms estimates of the differential path delay values provided by the modem backward equalizer control voltage. An exact calibration of the dispersion monitor based on a two-component differential delay was not accomplished and thus the delay values shown are only approximate. The abscissa represents the bit error recorded in the same 100-ms inter-

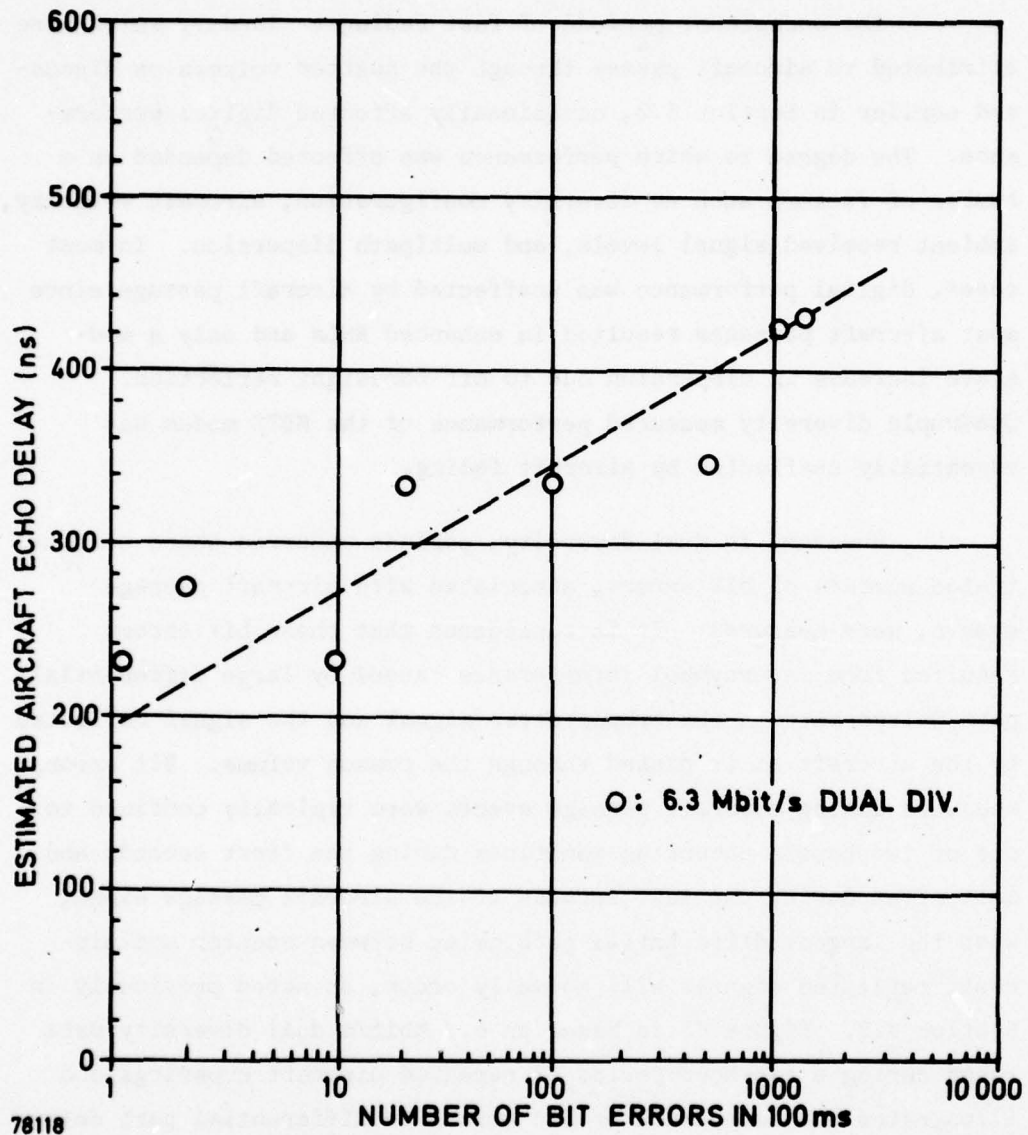


Fig. 65 Effect of aircraft passes in dual diversity

val as the delay measurement. As indicated by the large occasional differential path delays of the order of two to three times the normal troposcatter multipath delay were measured. While this phenomena has caused little concern in narrowband analogue systems, the wider bandwidth digital systems would potentially be affected by aircraft fading. Aircraft passage through digital troposcatter links can markedly increase channel dispersion and is a factor which must be considered. However, sufficient capability was provided in the MDTS modem to prevent aircraft fading effects on the UHF test link from measurably degrading system performance as long as quadruple diversity transmission was employed.

8.2 DAR UHF TEST LINK SYSTEM PERFORMANCE

DAR modem digital performance on the UHF test link was measured over a one-month period between 4 May and 6 June 1977. The DAR performance data collected was derived only from the link test configuration. Dynamic range limitations reduced the usefulness of the DAR dispersion monitor circuit which was implemented similarly to that in the MDTS modem. Thus, dispersion monitor data which coincides with periods of DAR testing was not available.

8.2.1 Bit error rate

As will be discussed in Chapter 10, bandlimiting effects in the high-power klystron resulted in a loss of dispersion handling capability in the DAR and in a modem performance which was highly dependent on the multipath dispersion on the test link. At 7.0 Mbit/s, which is the highest data rate of the DAR modem, digital performance ranged from a mean BER of 1×10^{-7} during shallow fading periods to nearly 1×10^{-2} during periods when the link was actively fading. As was the case with the MDTS modem, all DAR modem test runs were accomplished at relatively high median RSLs, typically in the -60 to -80 dBm range.

Figure 66 summarizes the BER performance of the DAR on the UHF link at 7.0 Mbit/s. The two-state performance of the DAR on this link is apparent. A significantly strong correlation was noted between the DAR modem BER and the standard deviation of the RSL measured in Rx 4 during periods when the RSL for Rx 4 was within 6 dB of the other diversity channels. This means that when the composite quadruple diversity channel became dispersive, the effective multipath capability of the DAR was insufficient to span the overall dispersion of the channel.

The 7.0-Mbit/s DAR performance is not unlike that observed during 9.4-Mbit/s MDTs tests (Fig. 59). In Fig. 59 the 9.4-Mbit/s performance is also seen to take on a two-state appearance, which resulted from an inability to accommodate simultaneously the intersymbol interference resulting from the 7-MHz imposed transmitted bandwidth constraint and the dispersive propagation mode of the UHF test link.

8.2.2 Fade outage rate and duration

Figure 67 illustrates the fade outage rate distribution measured with the DAR at 7.0 Mbit/s. In general, outage rates measured with the DAR modem were about one to two orders of magnitude greater than those measured with the MDTs. Mean outage durations ranged from 100 ms under shallow fading conditions to over 5 s under severe fading conditions.

8.3 SYSTEM SYNCHRONIZATION (UHF TEST LINK)

The bit count integrity (BCI) performance of the system test configuration was measured indirectly, but on a continuous basis. The measurement consisted of observing and recording the loss of synchronization signals generated in each of the digital equipments. Measurements obtained this way are considered pessimistic since, in actuality, not all synchronization losses

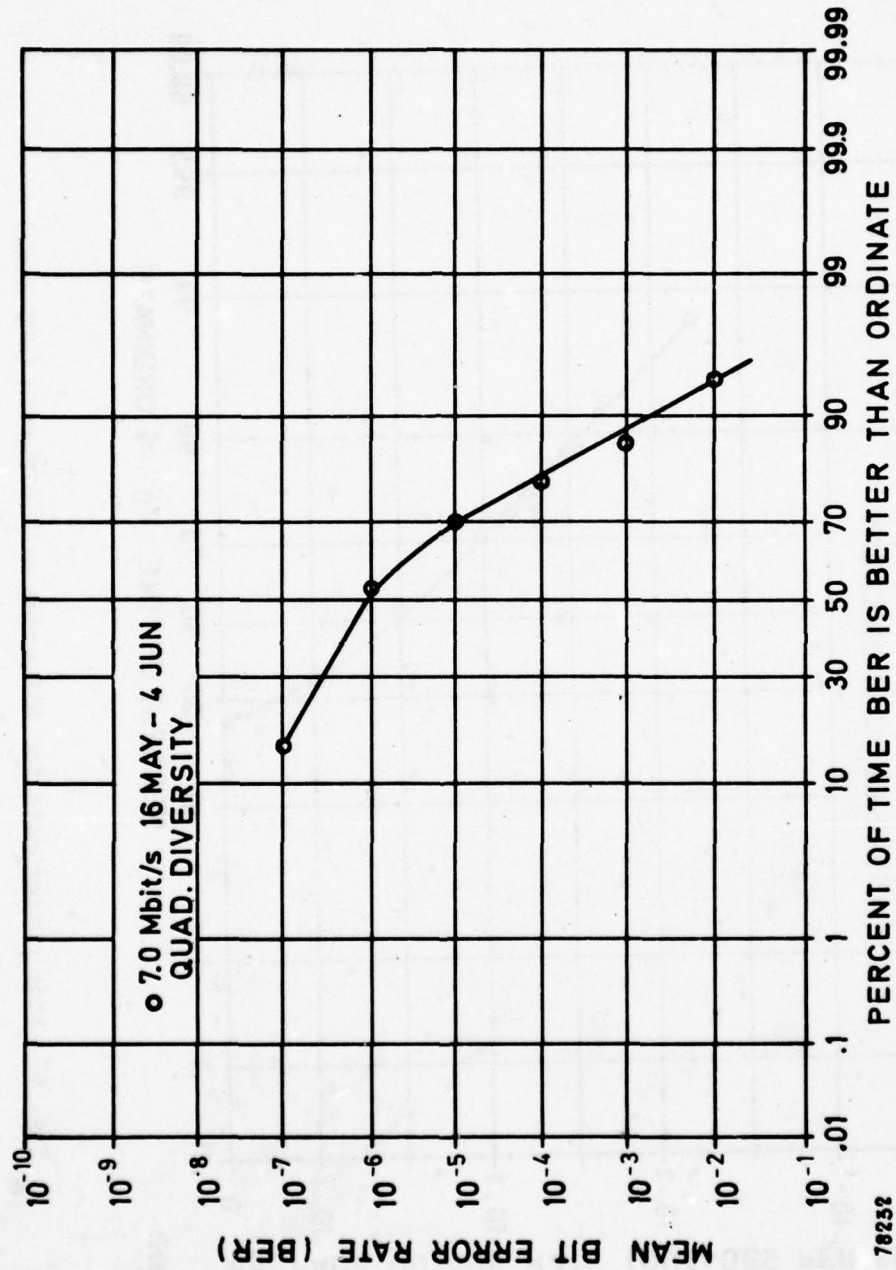


Fig. 66 Distribution of bit error rate for DAR modem at 7.0 Mbit/s (UHF link)

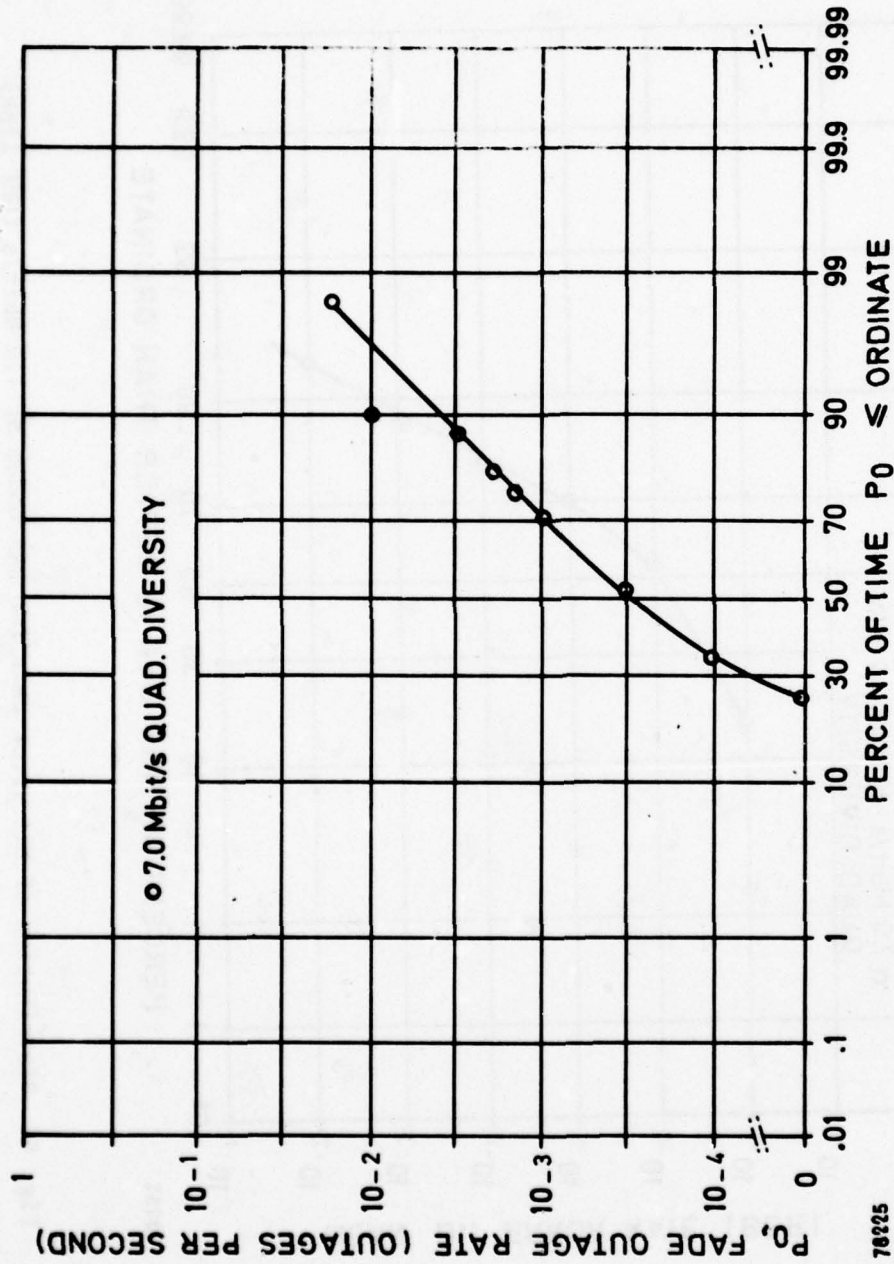


Fig. 67 Fade outage rate for DAR modem at 7.0 Mbit/s (UHF link)

will result in loss of BCI (LBCI). A cumulative summary of the data obtained is presented in Fig. 68 for dual and quadruple diversity in the 6.3-Mbit/s system tests. In quadruple diversity, LBCI events were observed in less than 2% of the test runs. BCI losses were caused only once by the MDTS modem. In dual diversity, modem LBCI events were noted in less than 9% of the 6.3 Mbit/s test runs.

It is interesting to note the effect of cascading resynchronizations of the MDTS modem, TDM, and PCM/TDM in both quadruple and dual diversity in the 6.3 Mbit/s system test configuration. Table 14 contains typical measurements of modem, TDM, and PCM/TDM resynchronization times which represent occasional periods when channels traversing the link would be unusable. It is seen that, in quadruple diversity, resynchronization of both TDM and PCM/TDM occur almost simultaneously and within 200 ms of the initial declaration of LBCI. Most often, complete system resynchronization occurred in no more than 100 ms. Analysis of error rate measurements indicates that in many cases modem resynchronization was achieved within about 20 ms at 6.3 Mbit/s.

Table 14
Typical digital system resynchronization statistics
(trans-alpine link)

Run	Configuration	Resynchronization time (x 100 ms)		
		MDTS modem	TDM	PCM/TDM
207	Non diversity	≤ 1	2	-
		0	6	-
		≤ 1	4	25
		2	10	-
218	Dual diversity	≤ 1	3	18
		2	2	3
		2	2	3
		2	6	18
248	Dual diversity	0	0	1
255	Dual diversity	≤ 1	0	1
258	Quad diversity	0	0	1
		0	0	2
268	Quad diversity	0	1	1
		0	0	2

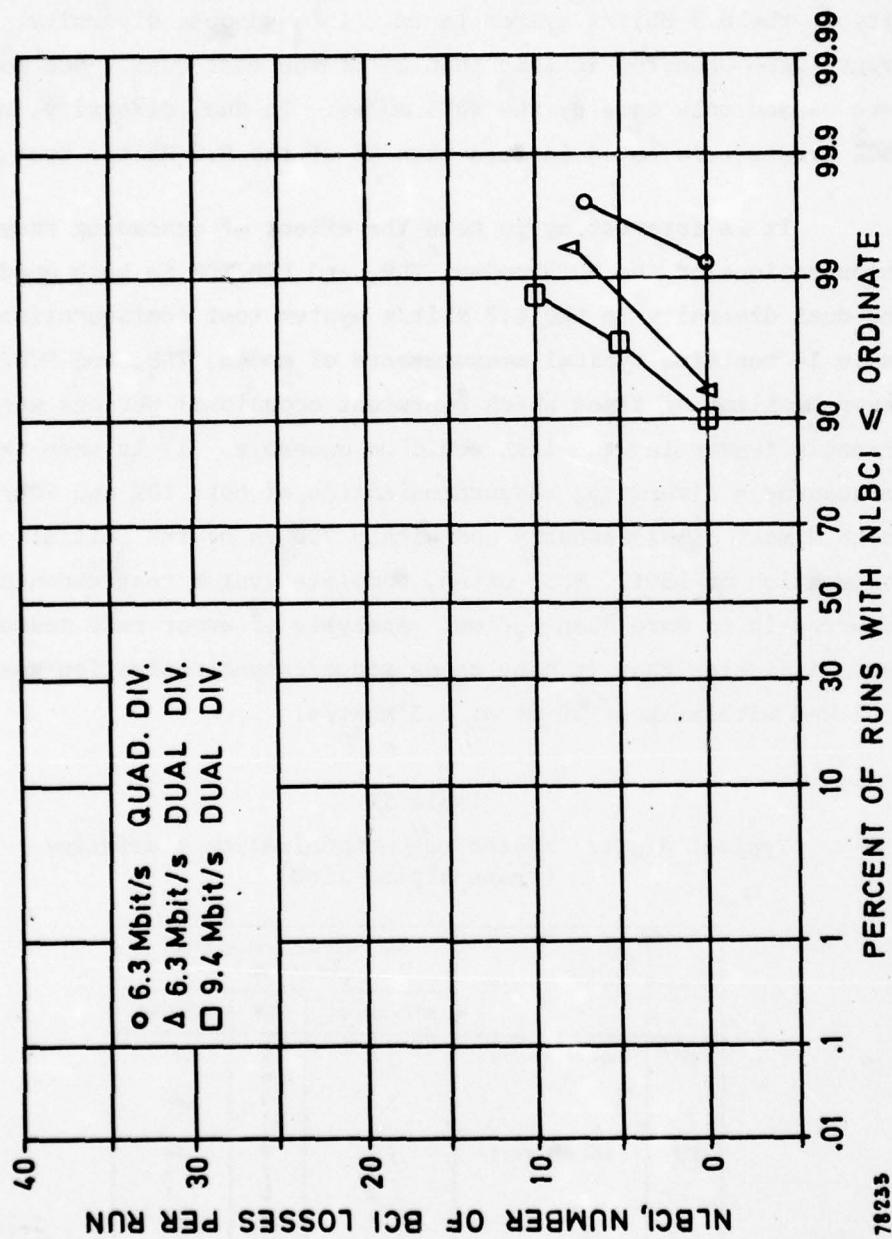


Fig. 68 BCI losses distribution (UHF link)

As illustrated in Table 14, the effect of cascading resynchronizations is more apparent in dual diversity. Normally, the MDTS modem regained BCI within 200 ms, and the TDM regained BCI within 100 ms, while the PCM/TDM remained out for up to 2.5 s with a mean time to resynchronize of 1.3 s. The reasons for the generally-longer resynchronization times measured in dual diversity stems primarily from the loss of diversity improvement relative to quadruple diversity, but periods of excessive multipath dispersion may also have contributed to this effect.

Aircraft fading events caused LBCI in the MDTS modem in dual and non-diversity on a few occasions. In all cases where aircraft fading events were correlated with LBCIs in the MDTS modem, the fading mode was identified as A/C Mode III (see Fig. 52). LBCI indications were generally coincident with a period of rapid change in path dispersion and only infrequently with peak values of dispersion itself. This appears to indicate that the rate sensitivity in the MDTS time tracking circuitry could be changed to improve low density LBCI.

Based on the above data it is considered that the more typical utilization of quadruple diversity on digital troposcatter links should result in negligibly infrequent LBCIs. When a LBCI occurs, modem resynchronization will probably take place in 100 ms or less. In TDM and TDM/PCM equipment similar to that used in the tests, complete resynchronization would occur in less than 500 ms. It should be noted that the frame synchronization algorithm for the PCM/TDM equipment used in the tests was based on a commercial design and was not specifically developed for fading channel applications. It is felt that system synchronization times could be further improved by the use of a more robust PCM/TDM frame acquisition algorithm, possibly based on parallel rather than on sequential frame searching. LBCI is not therefore expected to be a significant source of system degradation.

8.4 SYSTEM PERFORMANCE OBSERVATIONS

In summary, a number of observations can be made about the expected behaviour of digital troposcatter systems on the basis of the UHF link test data. Most importantly, it is necessary to have knowledge of the various propagation modes which can be reasonably expected to exist on a particular link. As discussed in Chapter 7, the actual mode of propagation on the UHF link differed from that predicted on the basis of the initially-available topographic profile. It was not until after a detailed topographic analysis using additional data was carried out that the propagation data derived from the UHF test link could be correlated with both physical expectations and theory. While a very detailed topographic analysis may not be required in every case (e.g., on smooth earth or over water paths), a fundamental judgement must be made by the system designer as to the "normality" of the path so that the most effective design can be proposed.

Secondly, digital system performance over properly-designed forward scatter paths will be characterized by large periods of little or no bit error activity interspersed with periods where denser bit error groupings and sometimes brief (100-300 ms) fade outages will occur. While this type of communications channel poses no fundamental difficulty to a voice or data user, system management and control procedures must be developed which consider this behaviour as normal and not necessarily as an indication of impending system degradation.

Thirdly, the maintenance of bit count integrity is generally important to the performance of a digital system and is particularly critical in the performance of a military communications system. The results of tests on the UHF link confirm data taken in other test programmes (see, e.g., Ref. 18) that show that loss of BCI will be very infrequently experienced in operational

configurations (e.g., quadruple diversity). However, uncontrollable occasional LBCI may occur even in quadruple diversity due to gross variation in path delay caused by changes in propagation mode.

8.5 C-BAND TEST LINK SYSTEM PERFORMANCE

Digital system tests using the MDTs and DAR modems were undertaken on the C-band test link during the last two weeks of July and the first two weeks of August 1977, respectively. Each modem was installed for approximately two weeks, with appropriate proportions of quadruple, dual and non-diversity testing being accomplished.

8.5.1 DAR performance

Bit error rate

The DAR displayed none of the degradations which were observed on the UHF test link. This was attributed to the increased bandwidth of the C-band RF equipment and the lack of significant multipath dispersion on the C-band test link. Figure 69 illustrates the BER distributions measured with the DAR on the C-band test link in both dual and quadruple diversity configurations. Although some periods of relatively high BER were noted in dual diversity, DAR performance was generally excellent considering that the link was operated at a transmitter power of approximately 50 watts. Fade outages occurred with almost negligible frequency; less than ten percent of the runs had fade outage events. The maximum measured short-term fade outage rate in any quadruple diversity run was approximately 2×10^{-2} outages per second, which occurred when the DAR lost BCI during a particular 16-hour run (this run is not included in the data presented in Fig. 69).

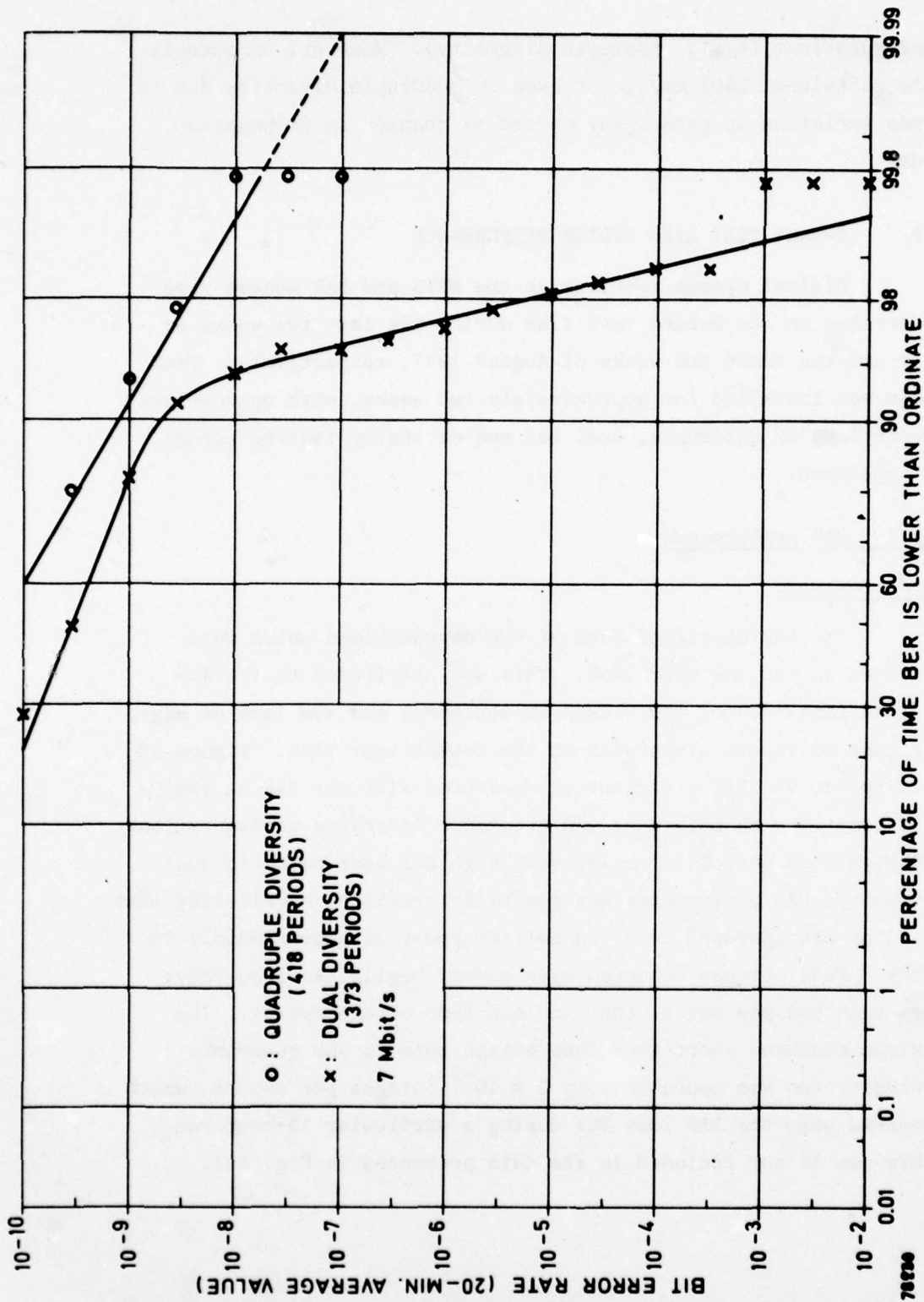


Fig. 69 Distribution of bit error rate for DAR modem at 7.0 Mbit/s (C-band link)

Block error statistics

Block error burst data for the DAR modem on the C-band link was normally uninteresting in that most errors were confined within single 100-ms intervals with the density of errors in these intervals typically ranging between 10^{-5} and 10^{-4} . During rare periods when link fading activity was particularly great, transmission errors were observed during dual diversity tests to span 300-400 ms.

8.5.2 MDTs system performance

Bit error rate

As noted in Fig. 70, MDTs BER performance was characterized by continually low BER measurements (10^{-9} to 10^{-7}). There was only one fade outage recorded during 336 hours of MDTs testing on the C-band test link: this outage lasted less than 200 ms. Although the BER was certainly low, an irreducible bit error rate of 1×10^{-9} was noted. As a result of an exhaustive equipment checkout, it is believed that this effect resulted from a faulty frequency synthesizer at the Kindsbach site which caused a small amount of incidental FM to be added to the transmitted signal.

8.5.3 MDTs and DAR synchronization performance

There were no losses of MDTs modem synchronization at 9.4 Mbit/s either with quadruple or with dual diversity. At 6.3 Mbit/s, LBCI was noted during one run, when the modem lost synchronization in quadruple diversity.

The bit timing loop in the DAR modem unlocked on at least two occasions, once in quadruple and once in dual diversity. Proper bit timing had to be restored manually. During one of these events, modem LBCI was also noted.

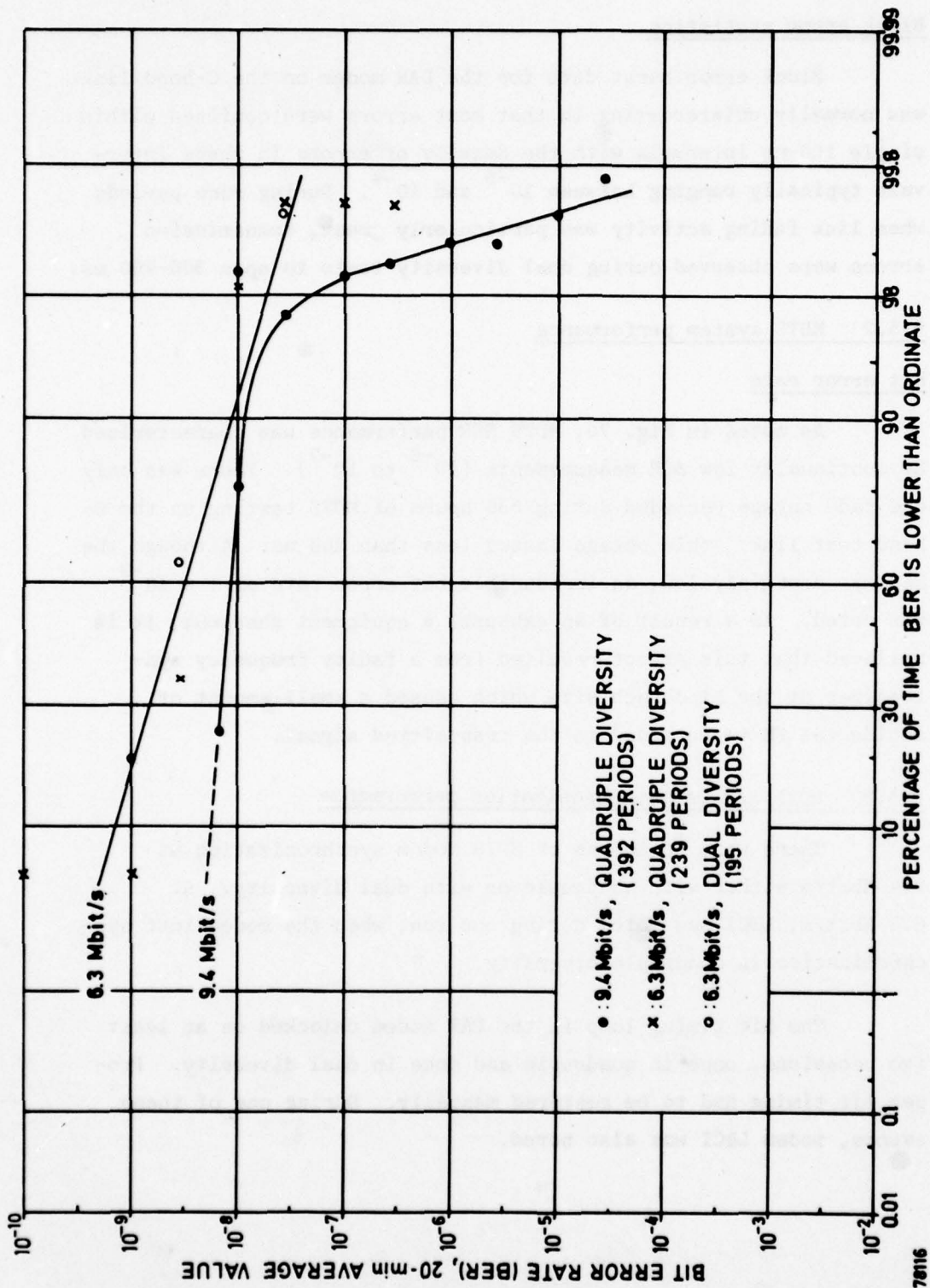


Fig. 70 Distribution of bit error rate for MDTs modem (C-band link)

9. DIGITAL MODEM PERFORMANCE

9.1 GENERAL

The purpose of this Chapter is to discuss the relationships between digital troposcatter modem bit error performance and the fluctuations of propagation path observables, i.e., RSL and dispersion. This can be approached in two ways. One approach is to relate mean BER over a 20-min run to mean CNR and 2σ dispersion over the same period. If the channel is stationary and its statistics are known, such a description provides considerable insight into the modem performance. A more general approach would be to relate "instantaneous" measures of both CNR and dispersion. This is a viable approach because troposcatter channel fluctuations are extremely slow when compared to the transmitted symbol rate. Both approaches have been pursued in the following sections. Only MDTs modem performance data taken on the UHF test link will be presented here since no usable indication of the multipath dispersion was available during DAR tests and since the propagation characteristics of the C-band test did not generally affect MDTs performance in any way that was peculiar to troposcatter transmission.

9.2 AVERAGE BIT ERROR DESCRIPTION

At 6.3 Mbit/s, the MDTs will suffer a measurable inter-symbol interference penalty in a dual diversity configuration with a 2σ dispersion of the order of 200 ns (Ref. 18). As discussed in Section 7.2, 2σ dispersions of 200 ns and greater were measured on the link at times. Therefore results of dual diversity measurements provided a basis for studying modem performance under relatively dispersive conditions.

Figures 71 and 72 illustrate the typical, largely diurnal variation in performance measured with MDTs in dual diversity D(Rx 2 + Rx 4) during Period 1. Figure 71 shows mean BER as measured periodically over an 8-hour period starting approximately at midnight. Here the BER is seen to vary from 10^{-8} to 10^{-10} and back to 10^{-8} again as the night progressed into sunrise and early morning. Figure 72 shows the variations in two performance descriptive parameters over the same period of time. The right-hand ordinate is the average standard deviation of the dual diversity RSLs in dB and reflects the overall fading intensity occurring during the observation period. The left-hand ordinate represents the correlation coefficient between outputs of the dispersion and signal-to-noise ratio (SNR) monitor voltages. The SNR monitor voltage derived in the modem is a measure of the effective SNR which includes the effects of multipath dispersion as well as thermal noise. A strong negative correlation implies that an increase in dispersion was reflected in a decrease in effective SNR, implying dispersion-limited performance. This would be expected to result in an increased BER. On the other hand, a positive correlation indicates that increased dispersion was reflected in an increase in SNR resulting from an implicit diversity improvement. Thus a lowering of the BER during periods of positive correlation between dispersion and SNR would be expected.

A comparison of Fig. 71 and 72 shows that periods of relatively high BER (10^{-8} to 10^{-9}) were coincident with moderate to strong negative correlations between SNR and multipath dispersion, implying that most transmission errors in dual diversity at 6.3 Mbit/s resulted from periods where the dispersion was slightly greater than the design range of the MDTs equalizer; of interest is the observation that periods of high channel activity generally coincided with increased dispersion. A particularly interesting observation can be made by comparing the curves in Fig. 71 and 72

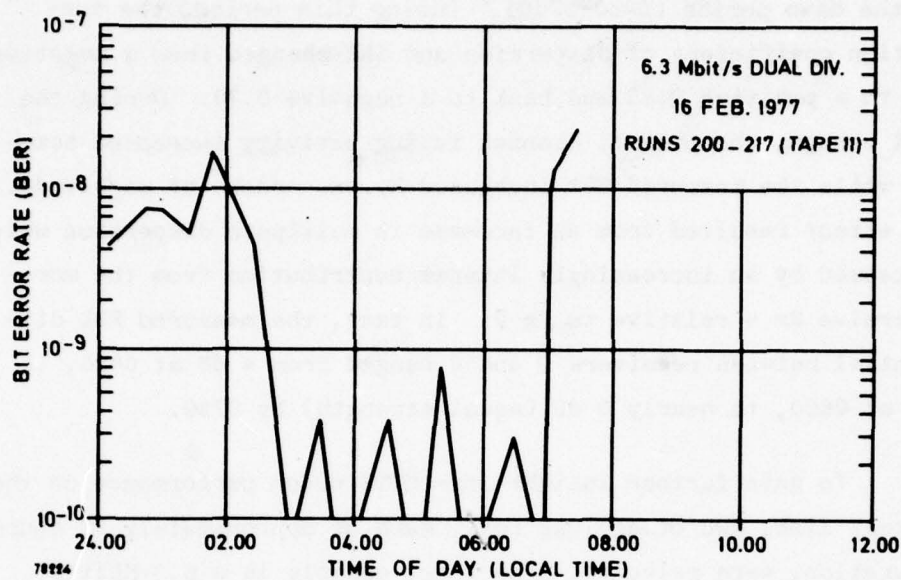


Fig. 71 Diurnal variation of performance - bit error rate

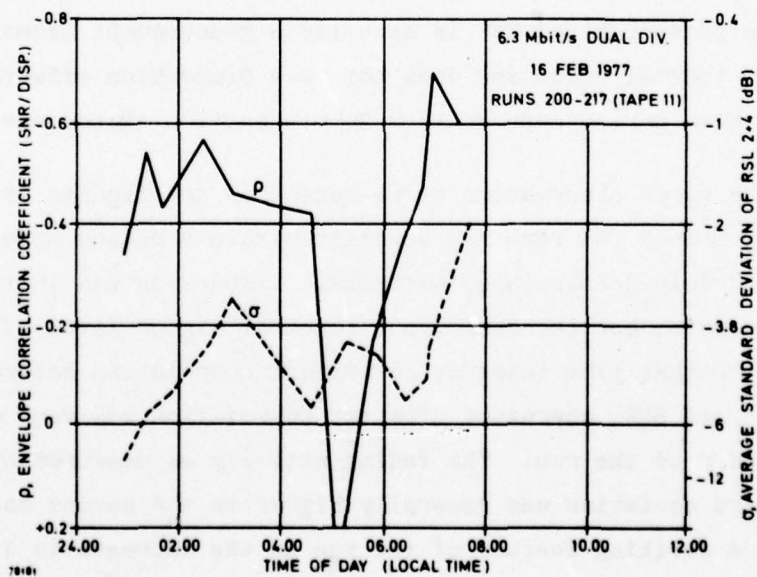


Fig. 72 Diurnal variation of performance - fading activity and correlation between SNR and dispersion

for the dawn period (0400-0700). During this period, the correlation coefficient of dispersion and SNR changed from a negative 0.44 to a positive 0.35 and back to a negative 0.70. During the final change, the overall channel fading activity increased somewhat while the measured BER increased by two orders of magnitude. This effect resulted from an increase in multipath dispersion which was caused by an increasingly intense contribution from the more dispersive Rx 4 relative to Rx 2. In fact, the measured RSL differential between receivers 2 and 4 ranged from 4 dB at 0400, to 8 dB at 0600, to nearly 0 dB (equal strength) by 0730.

To gain further insight into MDTs modem performance on the UHF test link, two other long runs, each of approximately 20 hours in duration, were selected. The first example is a 6.3-Mbit/s dual diversity run D(Rx 1 + Rx 3) made during Period 2 on 3-4 April 1977. In Fig. 73 to 75, the measured BER is plotted as a function of time together with post-combined CNR, dispersion, standard deviation of Rx 1, and correlation between the RSLs of Rx 1 and Rx 3. The post-combined CNR is actually a measurement based solely on RSL and thermal noise and does not take dispersion effects into account. Each period represents a 20-min section of the run.

The first observation to be made from the figures is that the post-combined CNR remained constant within 4 dB and appeared to be completely decorrelated with BER. Dispersion was initially low to moderate, but increased to a somewhat higher level at about 2300. Up to that time there is no evident correlation between dispersion and BER, whereas a distinct correlation was seen during the remainder of the run. The fading activity as measured by the RSL standard deviation was generally higher in the second half of the run. A striking feature of the run is the increase in diversity RSL correlation around 2300 and the unusually high level of correlation (0.6) maintained throughout the night (Fig. 75).

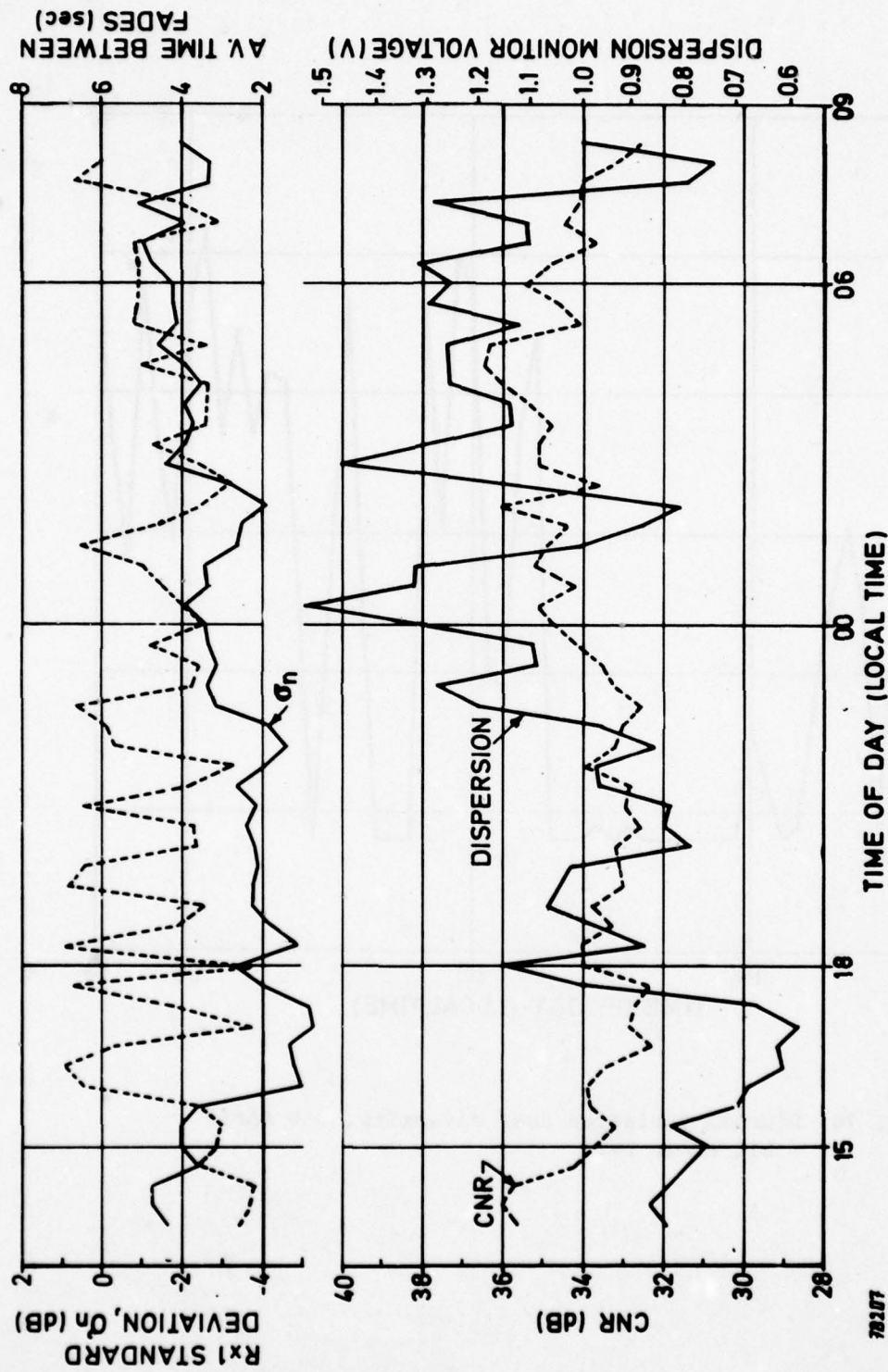


Fig. 73 Diurnal variation dual diversity, 3-4 April - propagation parameters

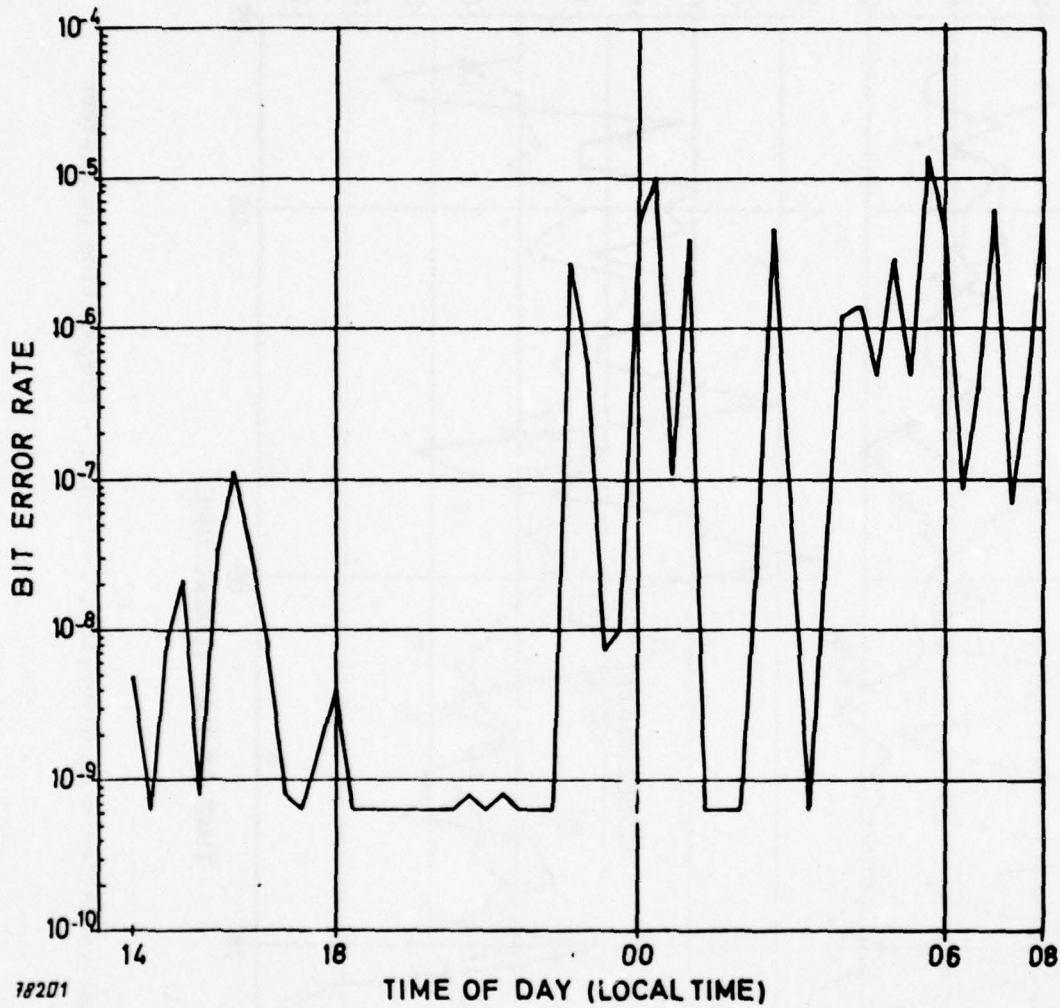


Fig. 74 Diurnal variation dual diversity, 3-4 April
- bit error rate

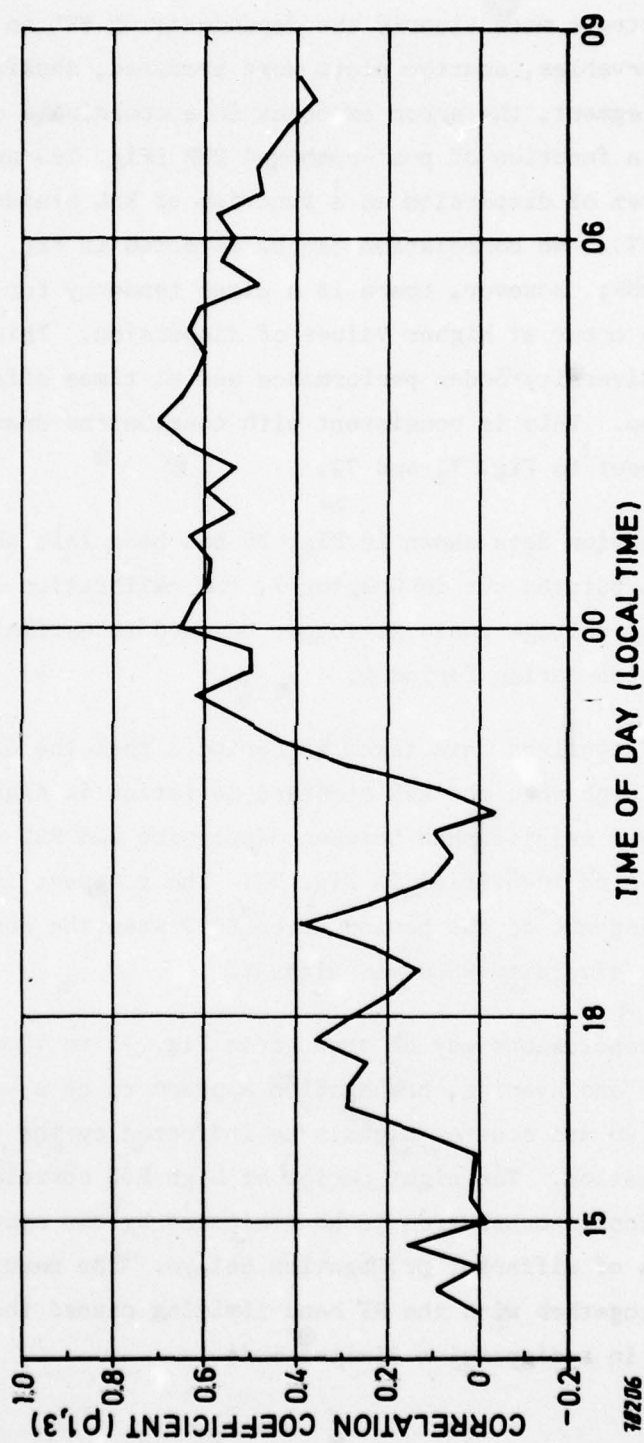


Fig. 75 Diurnal variation dual diversity, 3-4 April - correlation coefficient between RSLs of Rx 1 and Rx 3

To demonstrate more clearly the dependence of BER on the various path observables, scatter plots were produced, showing, for each 20-min segment, the error exponent in a coordinate system of dispersion as a function of post-combined CNR (Fig. 76) and in a coordinate system of dispersion as a function of RSL standard deviation (Fig. 77). No correlation can be detected in Fig. 76 between BER and CNR; however, there is a clear tendency for higher error rates to occur at higher values of dispersion. This means that dual diversity modem performance was at times affected by high dispersion. This is consistent with conclusions drawn earlier with respect to Fig. 71 and 72.

The dispersion data shown in Fig. 76 has been left as a voltage since, as pointed out in Chapter 7, the calibration of the dispersion monitor voltage could no longer be used to estimate multipath dispersion during Period 2.

Figure 77 confirms data taken in Period 1 that the dispersion tends to be high when the RSL standard deviation is high. Two modes of linear relationship between dispersion and RSL standard deviation can be identified in Fig. 77. The steepest line essentially corresponds to the period after 2300 when the correlation between dual diversity RSLs was highest.

Certain conclusions may be drawn from Fig. 71 to 77. During the afternoon and evening, propagation appears to be a varying mixture of specular and scatter signals as indicated by the changing standard deviation. The night period of high RSL correlation and high dispersion is considered to be dominated by two specular signal components of different propagation delays. The resulting high dispersion together with the RF band-limiting caused the modem to perform in a dispersion limited mode.

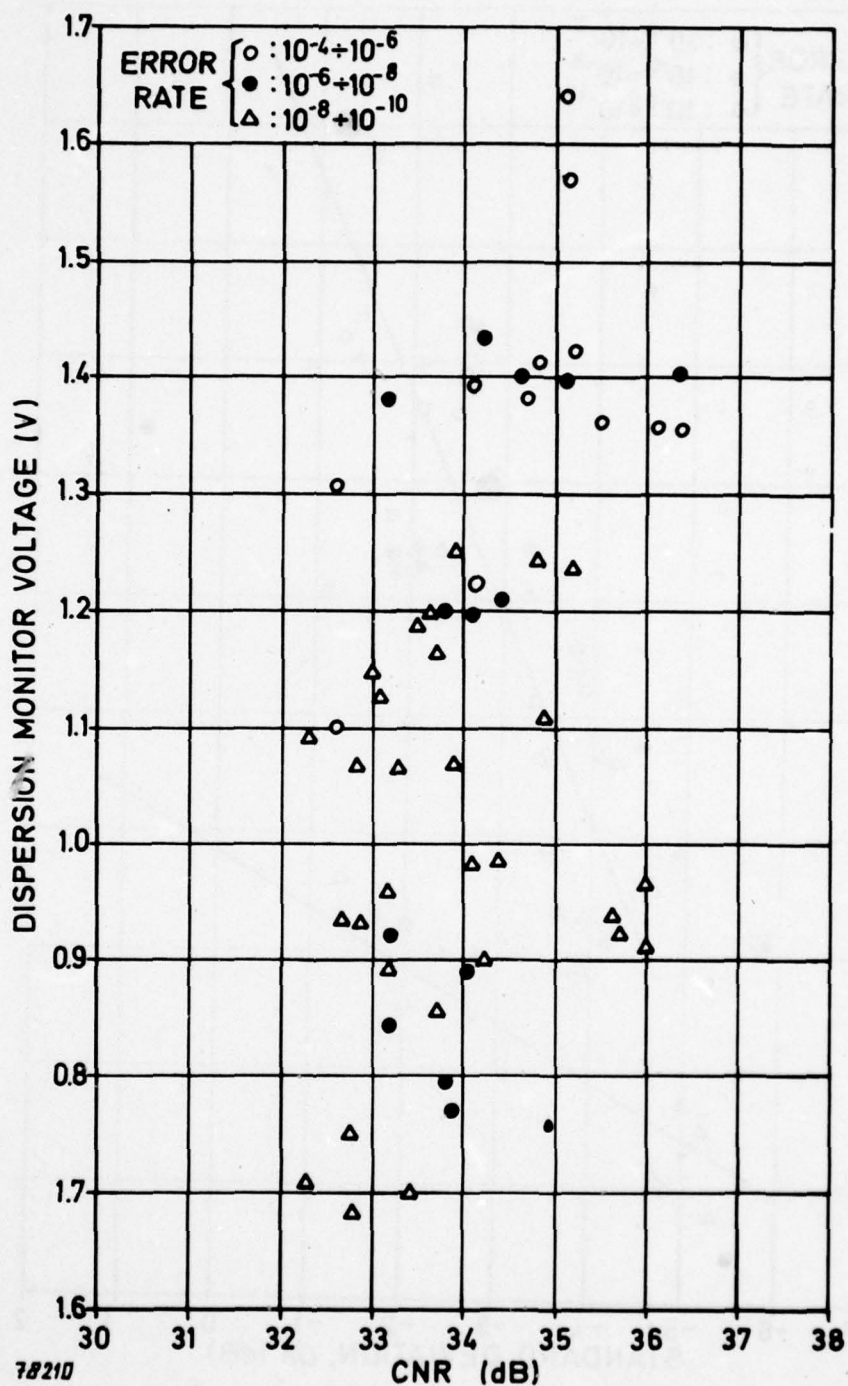


Fig. 76 Scatter plot of dispersion as a function of carrier-to-noise ratio

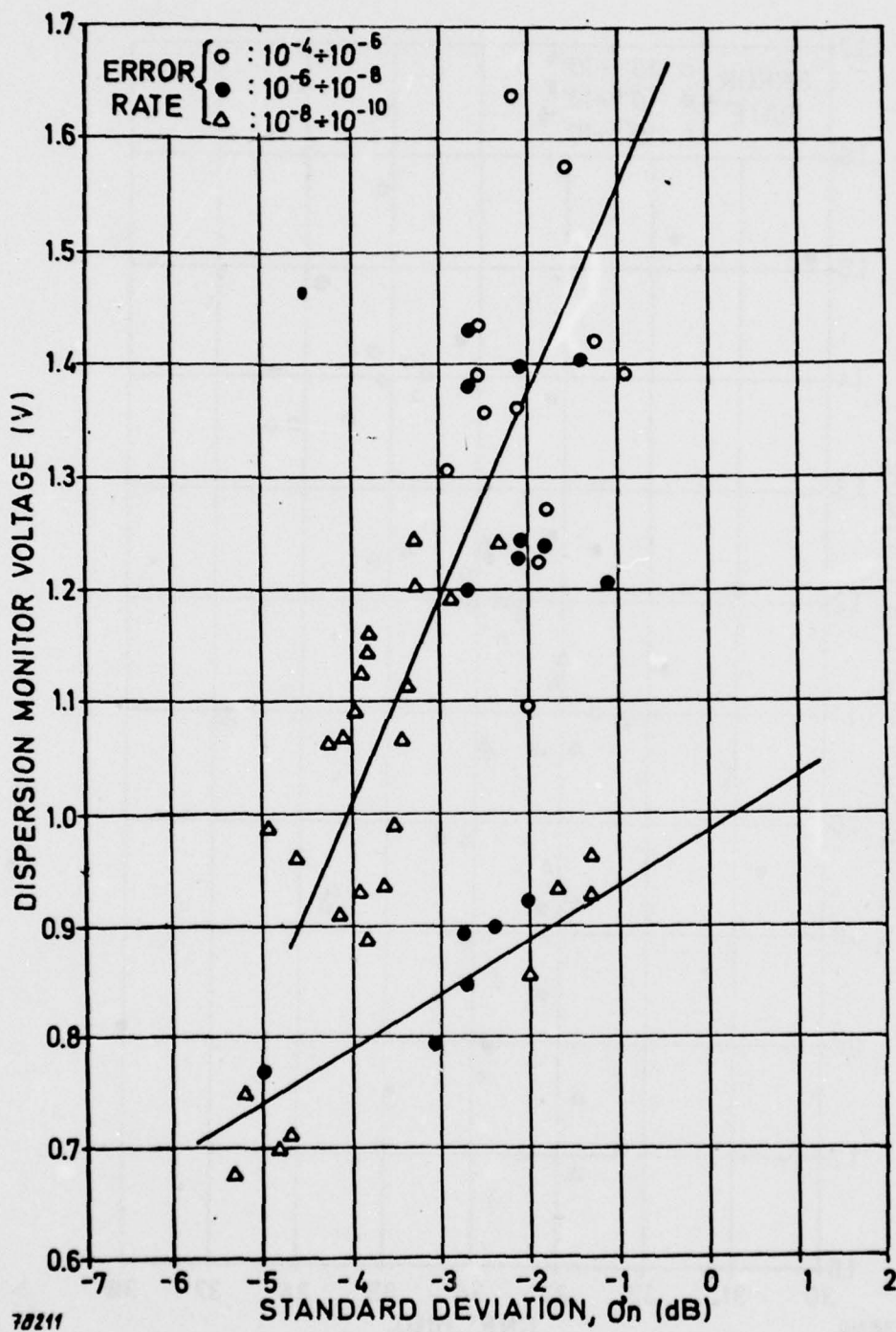


Fig. 77 Scatter plot of dispersion as a function of standard deviation

A second example is presented in Fig. 78 to 70. This is another 6.3 Mbit/s dual diversity run, D(Rx 2 + Rx 4), taken on 22 and 23 April 1977. For this run, the post-combined CNR varies over a large range, approximately between 30 dB and 50 dB, while the correlation between RSL of the two receivers is uniformly low. The measured dispersion is fairly low, except for a short period around sunrise. From the scatter plot presented in Fig. 80, the BER is seen to exhibit some correlation with both post-combined CNR and dispersion, although there is still a large amount of scatter.

The examples shown in Fig. 76 and 80 clearly demonstrate the difficulties encountered in an attempt to establish a single-values relationship between the mean BER and the mean post-combined CNR and 2σ dispersion for the UHF test. In fact, no such relationship could be established, either for dual diversity or for quadruple diversity tests, where the BER appeared to be completely uncorrelated with the CNR and no definite indication of dispersion limited operation could be found (see Chapter 8). It is therefore most likely that some of the errors observed both in dual and quadruple diversity were caused by other than low CNR or excessive dispersion, as already discussed in Chapter 8.

9.3 FROZEN-CHANNEL DESCRIPTION

The description of digital performance under "frozen channel" conditions (i.e., where the channel is viewed as an ensemble of bandlimited additive noise channel snapshots) can provide significant insight into the design sensitivities of the modem signal processing. The Data Acquisition System (DAS) was designed with a relatively high sampling rate (10 Hz) and this permitted the collection of frozen-channel snapshots of modem performance and channel conditions in the form of bit errors, received signal

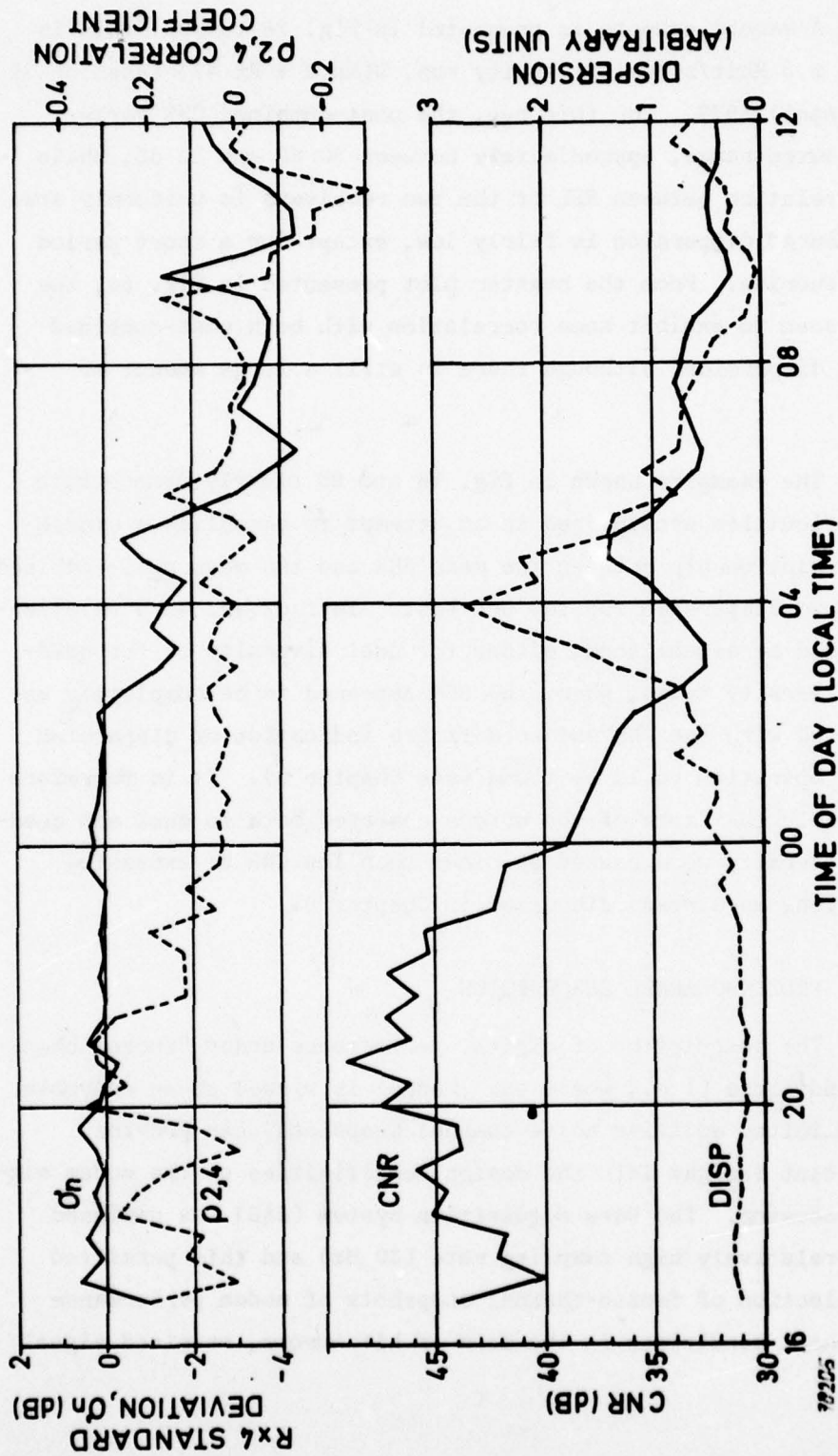


Fig. 78 Diurnal variation dual diversity, 22-23 April - propagation parameters

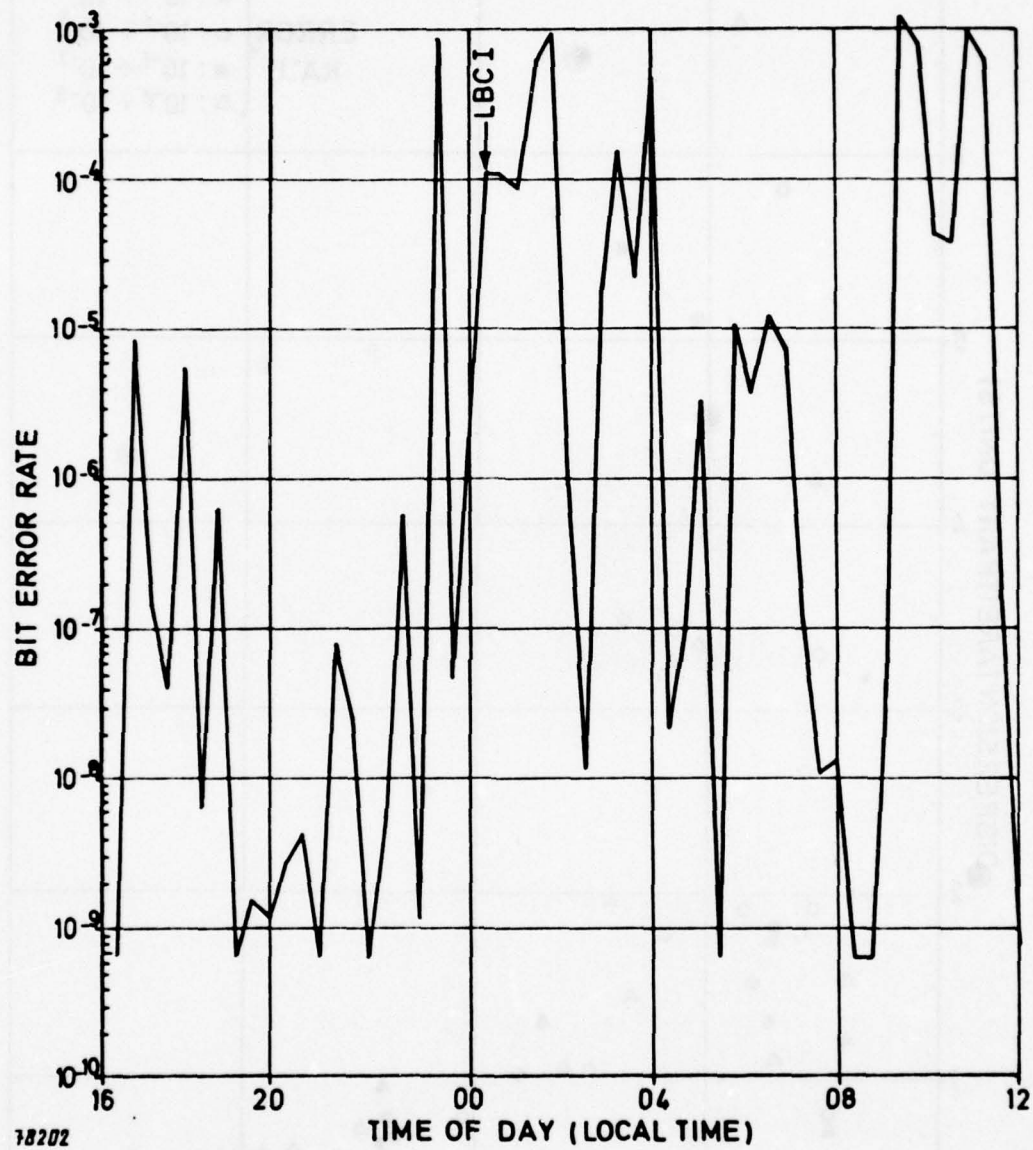


Fig. 79 Diurnal variation dual diversity, 22-23 April
- bit error rate

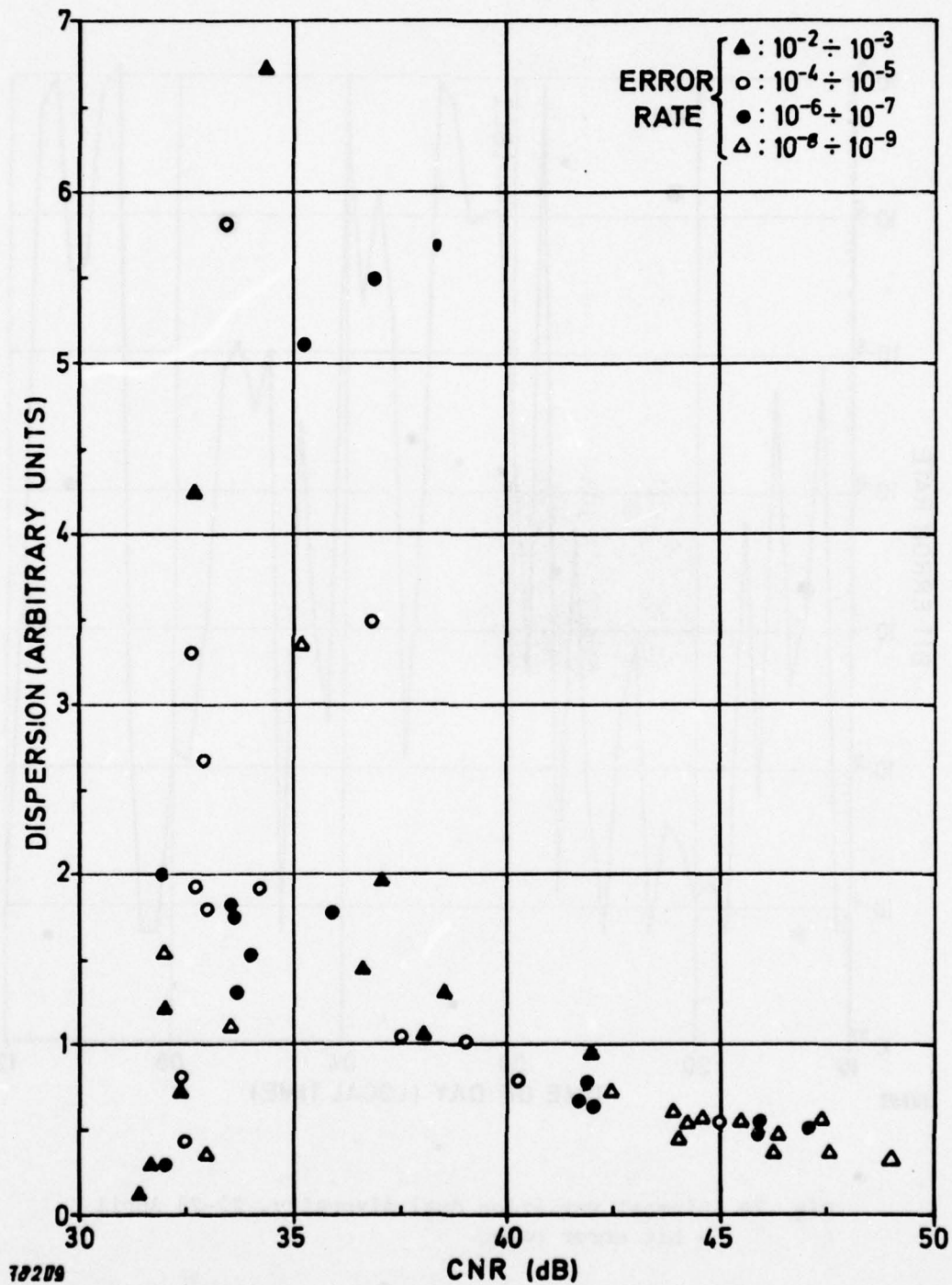


Fig. 80 Scatter plot of dispersion as a function of carrier-to-noise ratio

levels, and dispersion. From these snapshots, it was hoped that a series of modem performance contours could be generated which would uniquely relate values of "instantaneous" signal level and dispersion to values of short-term bit error rate. The performance of a modem under frequency selective fading conditions could then be represented as an ensemble of the performance obtained from each of the snapshots. Since a multipath analyzer was unavailable, it was hoped that the multipath dispersion indicator in the MDTs modem would provide the capability to collect frozen-channel statistics.

Unfortunately, the multipath dispersion monitor proved more useful for collecting longer-term statistics and its utility for frozen-channel modem characterization was marginal. Figure 81 shows a typical frozen-channel performance representative of the MDTs modem performance during Period 2. The two runs shown in Fig. 81 are presented in only two dimensions (short-term BER and post-combined SNR) - that is, the effect of dispersion has been integrated out. These measurements were made at 6.3 Mbit/s in dual diversity. The difference between the theoretical curve calculated under the assumption of negligible dispersion and the measured curve is of the order of 15 to 20 dB. This is about the same difference as shown in Fig. 60 for quadruple diversity operation.

To eliminate any adverse effects which may have been caused by the mistuned klystrons during Test Period 2, data taken during Test Period 1 are presented in Fig. 82 and 83. Figure 82 shows the frozen-channel dual diversity performance under conditions of essentially no fading - that is, the standard deviation indicated that each of the two receivers had estimated specular-to-scatter power ratios of the order of 10 dB or more. The majority of samples have zero errors, as would be expected under the higher CNRs. The occasional samples with bit errors may have been caused by random events not related to propagation. In Fig. 83, the same

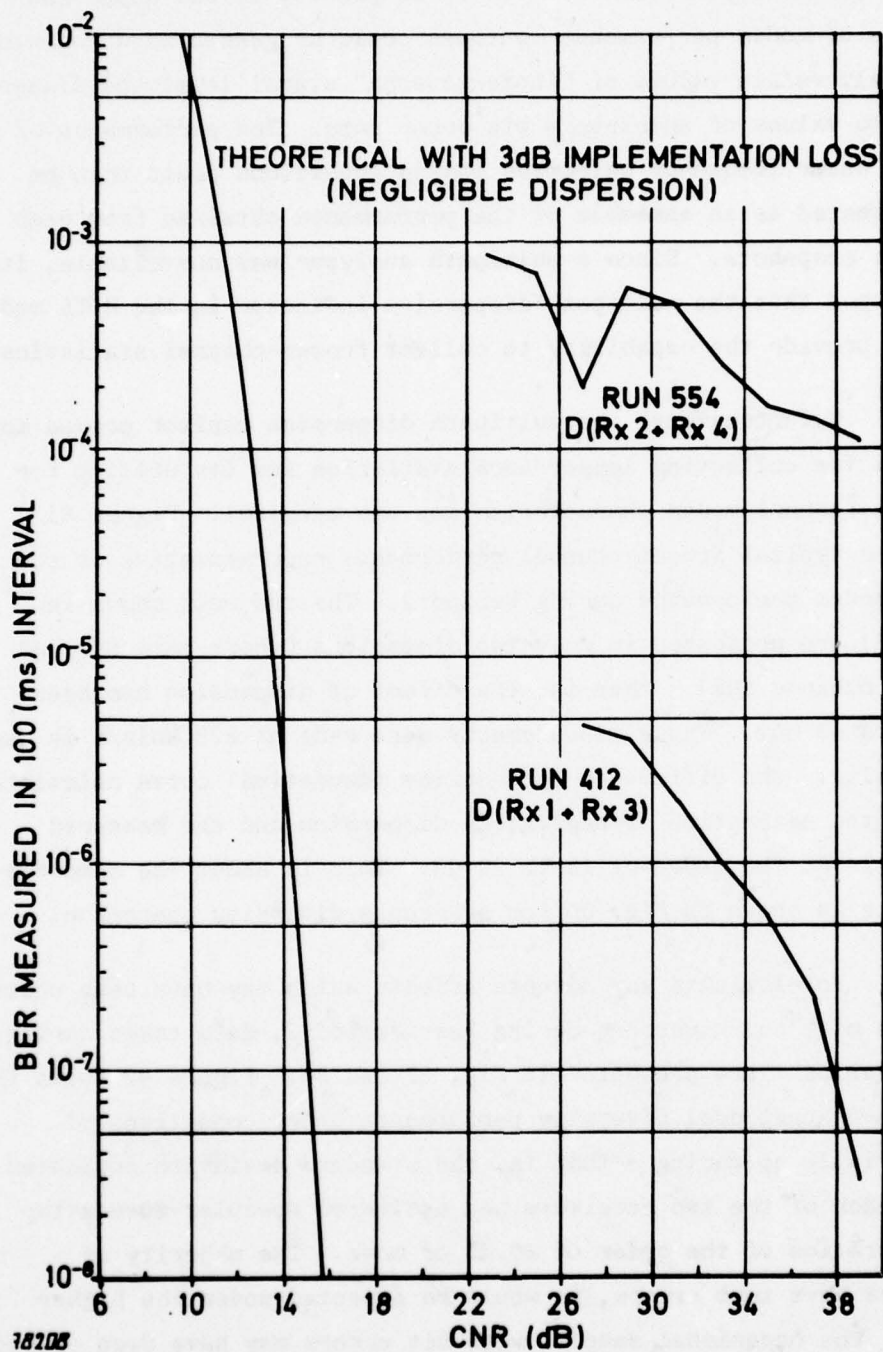


Fig. 81 Example of "frozen-channel" performance

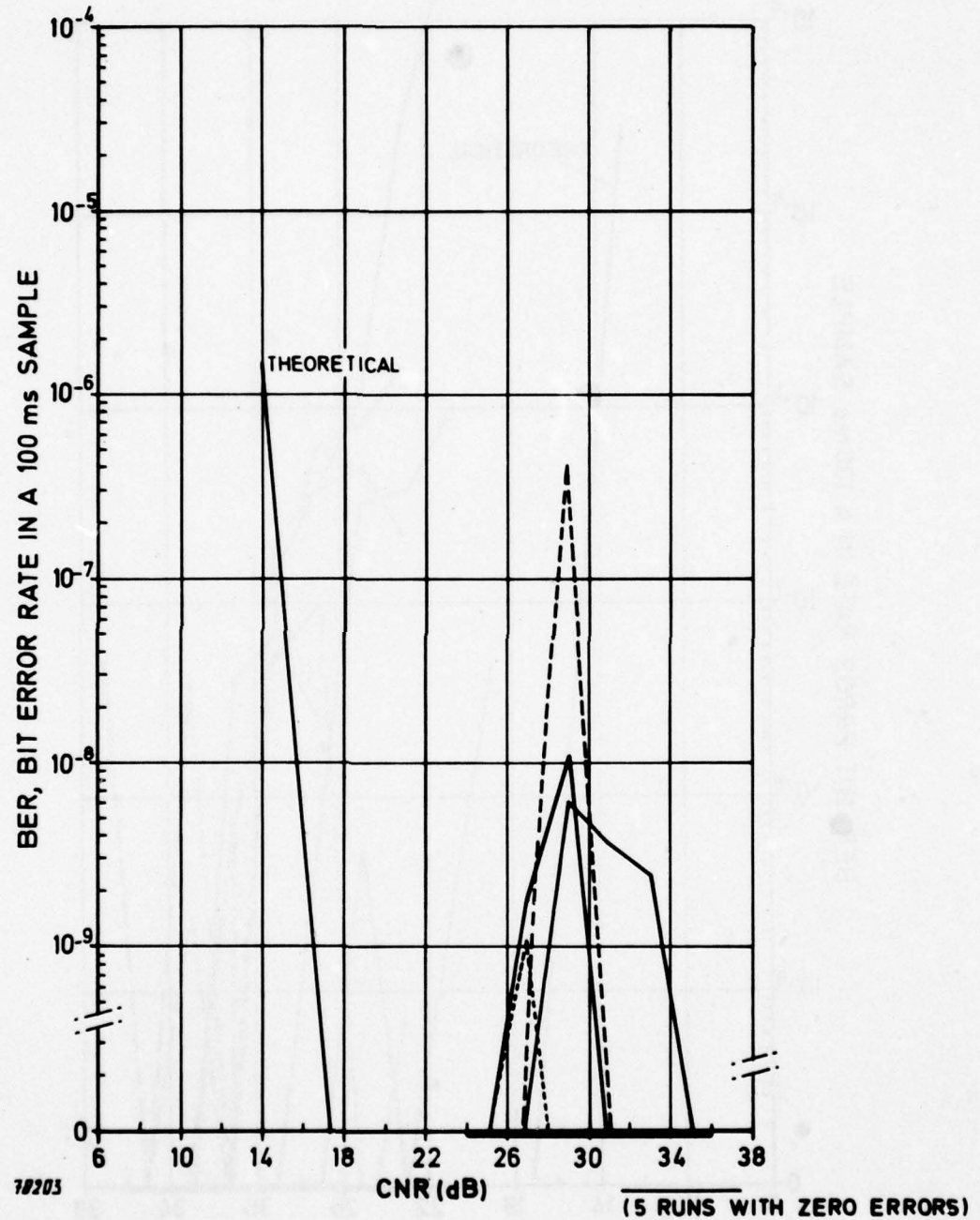


Fig. 82 MDTs frozen channel performance ($\sigma_n < -4$ dB)

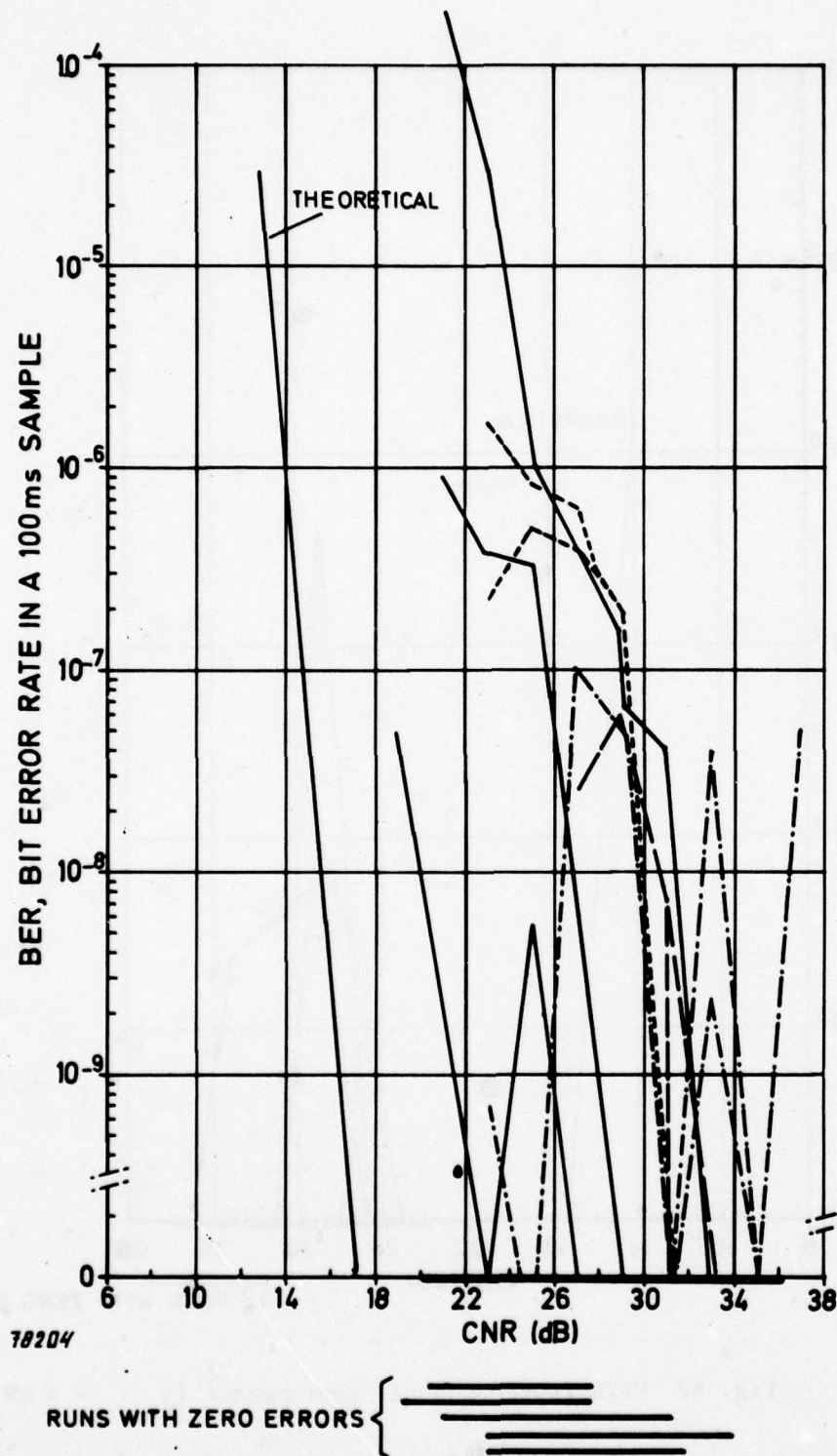


Fig. 83 MDTs frozen channel performance ($\sigma_n > -4$ dB)

types of curve are shown. However, in this case, Period 1 data with standard deviations indicating fading are plotted. Since moderate to strong correlation was noted between dispersion and fading intensity, it is believed that these points would be representative of significant multipath dispersion in Period 1. In Fig. 83, the frequency of low density error samples (10^{-7} and less) increased significantly and occasional higher density error samples (10^{-7} and above) were measured. It is felt that these error samples were caused primarily by dispersion since the RF passband was optimally tuned and no other error-causing mechanism could be identified; some of the error samples are probably not due to propagation.

9.4 ANALYSIS OF MDTs MODEM LOSS OF BIT COUNT INTEGRITY

Frequent loss of bit count integrity (LBCI) can have potentially serious implications for a digital system where encryption is employed. Thus, the ability to predict and control the rate of occurrence of such events is of considerable importance in system engineering. One potential source of LBCI can be attributed to loss of symbol synchronization in the timing recovery loop of the digital troposcatter modem. In an actual system, BCI can be lost in other digital equipment such as the TDM and encryption devices. System-level BCI statistics were presented and discussed in Section 8.4. This section will complement the previous discussions and concentrate on those LBCI events which occurred in the modem and their relationship to measured propagation parameters.

Non-diversity operation usually entailed a substantial number of LBCI events caused by deep fades or rapid changes in the channel response. However, only LBCI events associated with dual or quadruple diversity were considered of interest from a system engineering viewpoint. The following discussion relates to the UHF link only. No LBCI events were observed for the MDTs modem when operating in the C-band link.

At 3.2 Mbit/s, the only LBCI event that was observed occurred during dual diversity operations, D(Rx 2 + Rx 4). At 6.3 Mbit/s, a single modem LBCI event occurred in quadruple diversity. This event was positively identified as resulting from an aircraft fade of the type termed A/C Mode III (see Section 8.3). Apart from this event, all MDTs modem LBCI events for diversity operation at 6.3 Mbit/s occurred for dual diversity operation D(Rx 2 + Rx 4). In dual diversity, modem LBCI events were observed in 46 out of over 500 twenty-minute test runs.

MDTS modem BCI losses were more frequent at 9.4 Mbit/s and were observed in approximately 5% of the 9.4 Mbit/s quadruple diversity tests, excluding those during Test Period 2 when one of the transmitters exhibited intermittent operation. The increased BCI loss observed at 9.4 Mbit/s was undoubtedly due to the significant intersymbol interference suffered in that configuration. As seen in Table 15, MDTs resynchronization times in the 9.4-Mbit/s link configuration generally were greater than the 6.3-Mbit/s modem resynchronization times presented in Table 14 for dual and quadruple diversity. The longest modem resynchronization times at 9.4 Mbit/s were noted in quadruple diversity. This rather odd behaviour is possibly due to an overall increase in intersymbol interference caused by a greater proportional multipath spread (at 9.4 Mbit/s) and the addition of a second transmitter which was more severely band-limited (i.e., provided more intersymbol interference) than the first.

The fact that modem LBCI occurred with significantly greater frequency during 9.4-Mbit/s D(Rx 2 + Rx 4) operation suggests that the combination of intersymbol interference caused by band limiting to 7 MHz and multipath dispersion caused by the mixture of two different propagation modes in Rx 2 and Rx 4 made it more difficult for the modem to maintain stable timing recovery than in

Table 15

9.4 Mbit/s modem resynchronization times

Diversity	Run	Modem resync. time ≤ (ms)
None (Rx 4)	350	100
		100
		200
		100
		100
Dual (Rx 2 + Rx 4)	336	100
		100
		100
		100
		100
	337	100
		100
		100
		100
		100
Quadruple	339	100
		100
	365	300
		600
		300
		700
		500

the more optimally configured 6.3-Mbit/s mode. If it is assumed that Rx 2 is usually dominated by a specular signal while Rx 4 receives a strongly fading troposcatter signal having a longer transmission delay, the modem would be dominated alternately by two signals at different delays. If the multipath delay difference rapidly changed over a range comparable to a symbol interval (213 ns at 9.4 Mbit/s), LBCI could result.

Aircraft fading events caused loss of BCI in the MDTs modem in dual and non-diversity on a few occasions. In all cases of LBCI the aircraft fading mode was identified as A/C Mode III. Modem LBCI events were generally coincident with a period of rapid change in path dispersion and only infrequently with peak values of dispersion itself. In other words, LBCI occurred during periods when the differential path delay appeared to change rapidly over some range. This tends to indicate that a change of the rate sensitivity in the MDTs time tracker circuitry may improve synchronization performance in low-order diversity applications.

9.5 DISCUSSION OF POTENTIAL MDTs MODEM OPTIMIZATION AREAS

It appears that the mixed propagation modes experienced on the UHF link caused a degradation from optimum MDTs performance for two reasons. First, the asymmetry in median RSLs for the four diversity receivers often exceeded the dynamic range capability of the forward equalizer circuits. This resulted in a discrimination against Rx 4 (and occasionally against Rx 2) since Rx 4 and Rx 2 normally had the lowest powers. By virtue of their more dispersive nature, these channels may, if used, contribute to modem performance. Secondly, in low-order diversity configurations and under certain dynamic situations, the timing recovery loop of the modem appeared unable to follow the symbol timing variations caused by alternations between two signal components propagated at different

delays. If consideration is given to the possible occurrence of mixed propagation modes during the modem design stage, the performance of the modem on such channels might be further improved, particularly in low-order diversity configurations. Whether this effort is warranted, of course, depends on the system requirements and particularly on the range of channels over which digital transmission is required.

10. OPERATIONAL EXPERIENCE

10.1 GENERAL

Some of the problems encountered and some of the experience gained during the test did not manifest themselves directly in the test results. In general, the observations contained in this chapter relate specifically to the test programme itself and should not be taken as being necessarily indicative of the situation that might be expected in an operational digital troposcatter system. One exception, however, is the experience obtained in interfacing the digital troposcatter modems with the ACE High radio equipment: experience gained in this area may influence the ultimate specification of new radio equipment for both ACE High and DCS applications.

10.2 LESSONS LEARNED

The test schedule as set out in Ref. 1 called for the tests to end about June 1977. A number of transportation problems relating to equipment and personnel movement caused a six-week delay in the completion of the programme and this meant that the C-band tests had to be reduced to two weeks per modem. (The transportation problems resulted primarily from heavy snow conditions at Dosso dei Galli in January and from customs difficulties.)

Although the two test links had been made fully available to the test programme, SHAPE required that the normal duplex link orderwire circuits should be maintained while tests were in progress. To achieve this, the orderwire in the Dosso dei Galli to Feldberg direction was digitized and in the Feldberg to Dosso dei Galli direction it was left in analogue form. All ring-down and signaling functions leaving Feldberg were digitized by the 64-kbit/s CVSD orderwire units. The digital orderwire, which functioned

without failure throughout the test period, was invaluable for the operation of the tests and also permitted the normal flow of system coordination traffic in that branch of ACE High which had to be maintained without interruptions. Rapid cut-over from digital to analogue operations of the link was exercised on a number of occasions at the request of the AFCENT Primary Control Centre (PCC). No problems were encountered in restoring the analogue traffic at short notice.

As described in Chapter 4, the Data Acquisition System (DAS) contained a considerable amount of redundancy to minimize the possibility of loss of data due to test-equipment malfunction. Initially, all data was recorded both manually via test logs and automatically via the digital tape recorder. Later in the programme, after the first batch of tapes had been successfully read and verified, most of the data collection during night hours and weekends was done automatically.

Strip-chart recordings of certain early test runs were not obtained, partly due to recorder ink supply malfunctions and partly due to chart paper delivery problems. The time history of runs for which the strip chart recorder was unavailable is, however, still preserved on the digital tape. The only significant problems with the digital tape recording facility were that a number of runs were lost due to errors in the setting of the label switches on the tape recorder interface and that static discharges from test operations personnel caused occasional erroneous commands to be transmitted to the tape recorder. Due to another static discharge problem that gave rise to false triggering of the loss of bit count integrity (LBCI) indicators, no reliable loss-of-synchronization indications were available until after 12 February. However, use of the manual logs and correlation with other measurements such as error rate enabled determination of most LBCI events.

The only hard failure experienced in the DAS, apart from the strip chart recorder, was in the spectrum analyzer. Both failures were cleared by replacing the failed units.

10.3 EXPERIENCE WITH THE REL 2600 TROPOSCATTER RADIOS

Interfaces between the digital modems and the radio equipment were established at the 70-MHz IF frequency, as described in Chapter 3. The following parameters of the radio equipment were of special importance for the tests:

- (a) Gain stability
- (b) Frequency response (IF to RF and RF to IF)
- (c) Spurious signals.

10.3.1 Gain stability

The gain stability of the REL 2600 radio was found to be excellent, with the exception of the low-noise parametric pre-amplifiers used on the UHF link. Two of these amplifiers exhibited random gain variations of several dB per minute, thus presenting calibration difficulties. As a result, the parametric amplifiers were replaced with transistor amplifiers for the duration of the tests.

10.3.2 Frequency response

RF to IF frequency responses were measured for all diversity receivers on the two links (see Fig. 84 and 85). The 3-dB bandwidths were found to exceed 8 MHz for the UHF link and 20 MHz for the C-band link.

Broadband tuning of the UHF klystron amplifiers was found to require considerable attention although, once tuned, the frequency response was stable. The two digital troposcatter modems used for the tests did not have the same requirement for power amplifier broadband response and so broadbanding was accomplished separately for the MDTS and DAR modems.

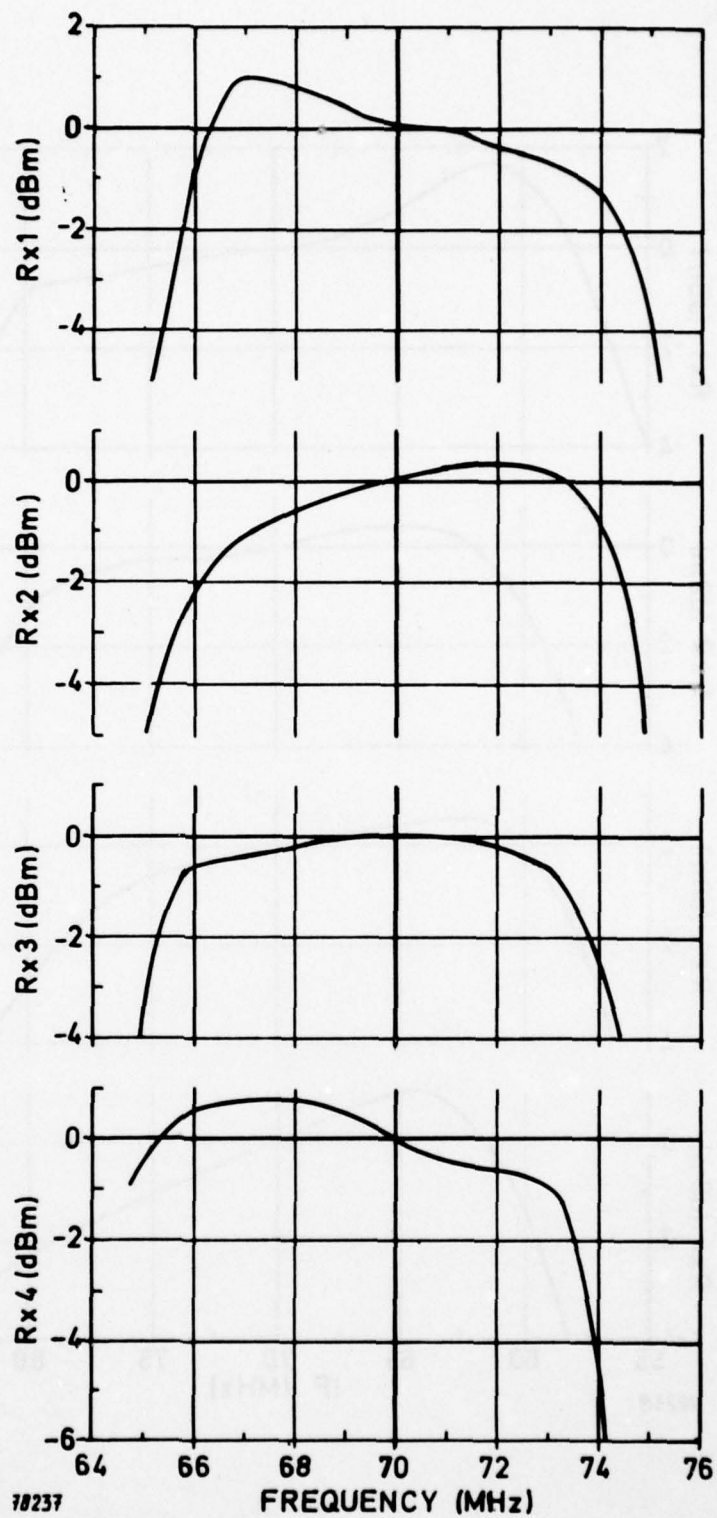


Fig. 84 UHF receiver responses

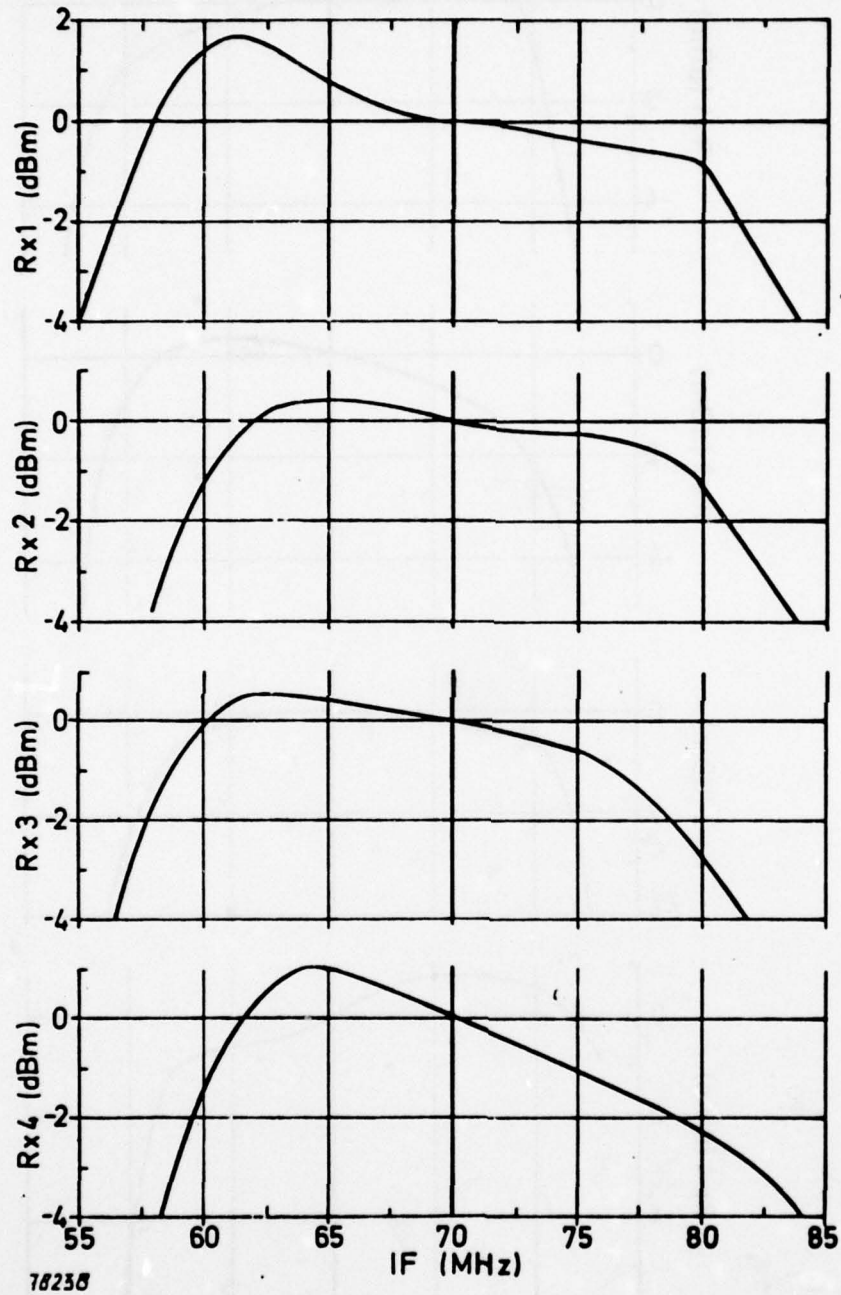
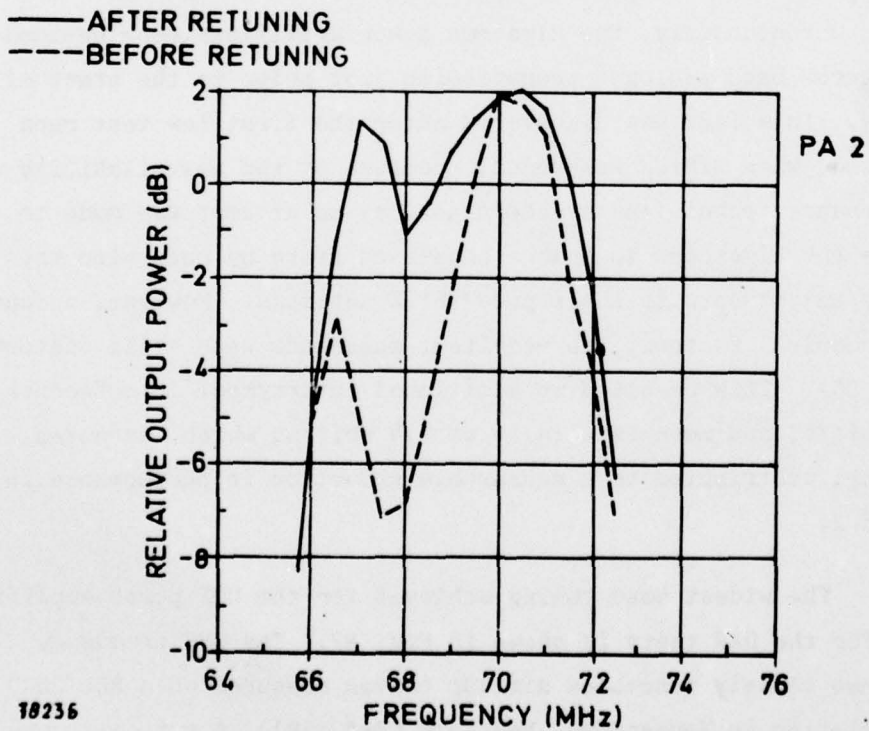
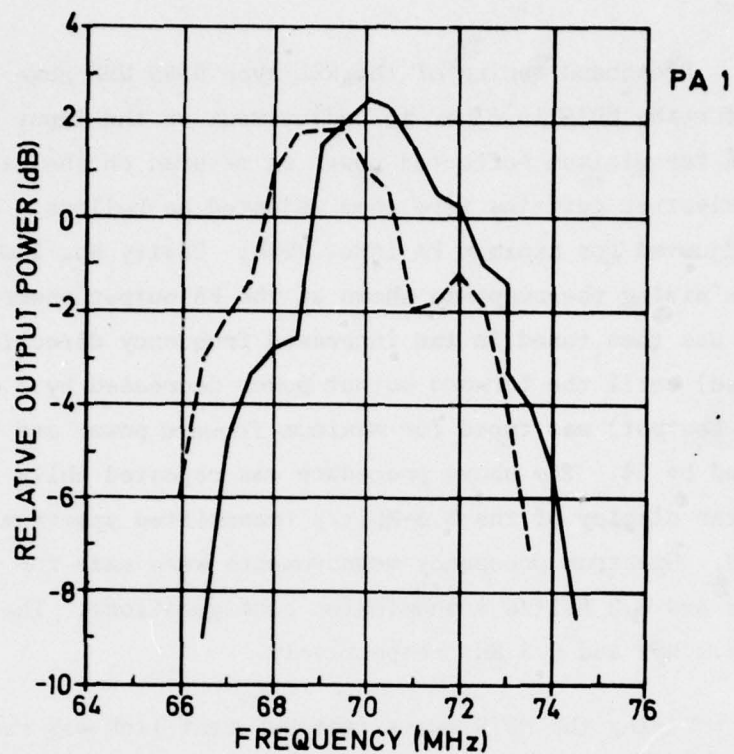


Fig. 85 C-band receiver responses

Broadband tuning of the REL type 954D UHF power amplifiers (PA) for the MDTs involved the adjustment of the input coupling to the PA for minimum reflected power as metered on the exciter. The four klystron cavities were then adjusted as follows: Cavity No. 1 was adjusted for minimum PA input VSWR; Cavity No. 2 was adjusted by maximizing the response shown on the PA output power. Cavity No. 3 was then tuned in the increased frequency direction (over-coupled) until the forward output power decreased by 3 dB. Cavity No. 4 (output) was tuned for maximum forward power and then under-coupled by 5%. The above procedure was repeated while a spectrum analyzer display of the 6.3-Mbit/s transmitted spectrum was monitored. Spectrum occupancy measurements were made for the 3.2 Mbit/s and 6.3 Mbit/s transmission configurations. The results were 5.2 MHz and 6.9 MHz respectively.

During the MDTs tests, the UHF test link was returned to its operational analogue configuration for the WINTEX NATO exercise. Unfortunately, the klystron power amplifiers were retuned for narrow band analogue transmission just prior to the start of WINTEX. This fact was discovered after the first few test runs were made when WINTEX was ended. Because of the unavailability of maintenance technicians at short notice, an attempt was made to retune the klystrons to a more broadband state by returning the cavity adjustments to their pre-WINTEx settings. However, because of mechanical factors, the resultant passbands were still distorted (Fig. 86). This resulted in additional intersymbol interference at 6.3 Mbit/s, and more especially at 9.4 Mbit/s, which, as noted earlier, contributed to a measurable reduction in performance in Period 2.

The widest band tuning achieved for the UHF power amplifiers used for the DAR tests is shown in Fig. 87. The UHF frequency response closely resembles similar curves measured on a REL 2600 installation in Youngstown, New York (Ref. 18). A typical curve taken on the US installation is shown in Fig. 88.



10236

Fig. 86 Measured frequency responses for UHF transmitters at IDGZ

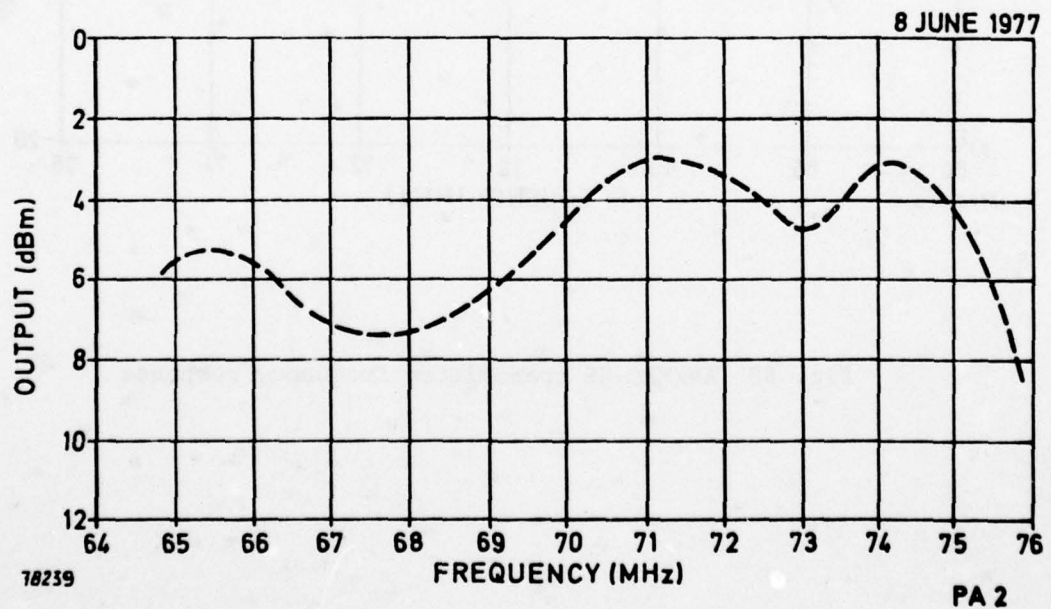
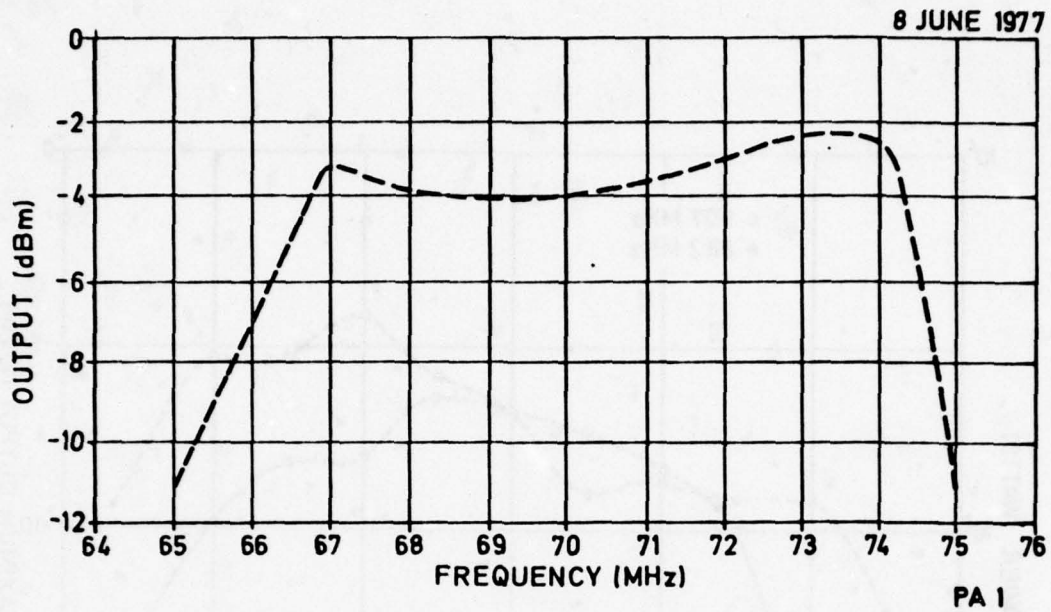


Fig. 87 Measured broadband response of PA No. 1 and 2
(used for DAR UHF test)

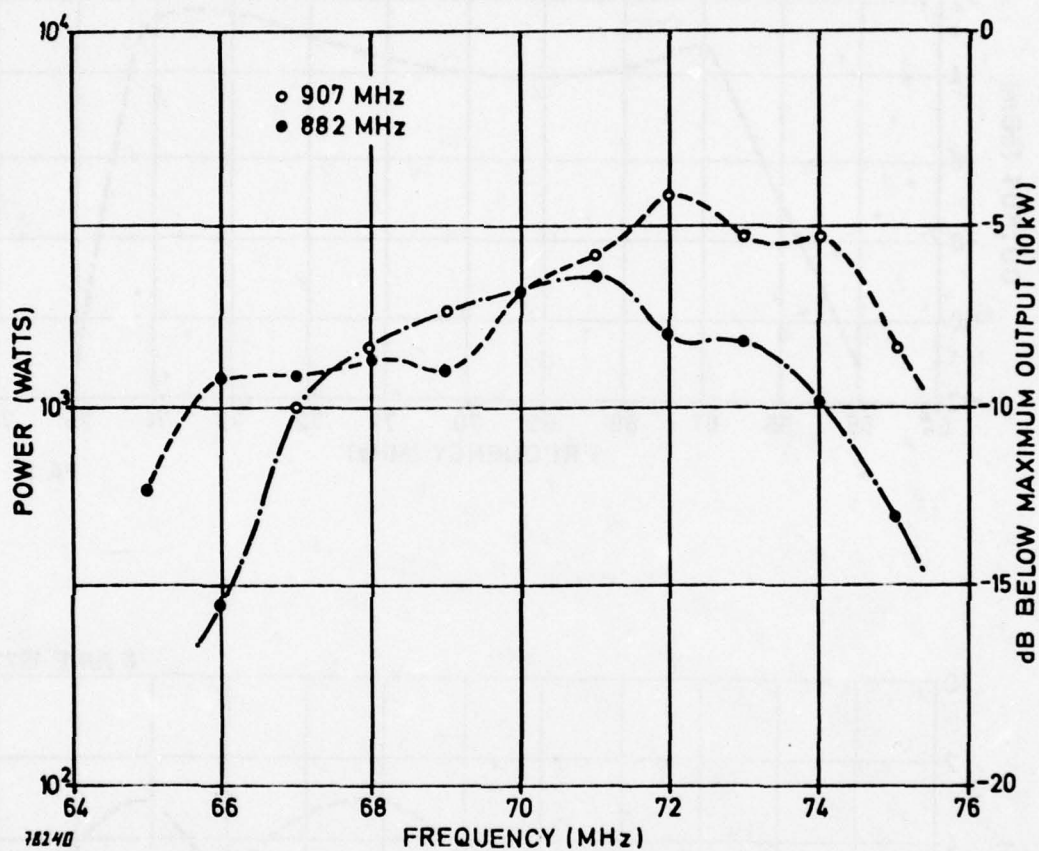


Fig. 88 AN/MRC-98 transmitter frequency response

Wideband tuning of the C-band power amplifiers was much less difficult. Frequency response plots for the C-band exciters and amplifiers are shown in Fig. 89. Figures 90 to 99 represent IF and RF transmitted spectra at all data rates tested for both the DAR and MDTs configurations.

Of special interest is the effect of the intrinsic broadband limitations of the UHF radios as reflected in the observed RF waveforms and measured performance of the DAR modem. As noted earlier, the widest tuning achieved with UHF power amplifiers exhibited a 3-dB bandwidth of 8 MHz. The significance of this bears directly on the measured performance of the DAR on the UHF link.

At 3.5 Mbit/s, which corresponds to about 48 PCM voice channels, the transmitter time gate impressed on the RF symbol waveform by the DAR modem was seen to be moderately reduced. Figure 98 shows the resultant RF symbol waveforms obtained at the 3.5-Mbit/s rate. For reference purposes, the time gate measured prior to the high power amplifiers (HPA) was of the order of 0.44 of an RF symbol or approximately 251 ns at 3.5 Mbit/s. As seen in Fig. 98, the resultant time gate, after bandlimiting by the UHF HPA, was of the order of 100 ns.

At 7.0 Mbit/s, which corresponds to 96 PCM channels (64 Kbit/s), the intrinsic UHF RF equipment limitations noticeably affected DAR performance. This effect was described briefly in Chapter 8. Figure 99 shows the relevant RF symbol waveforms observed at the output of the UHF power amplifiers at a transmitted rate of 7.0 Mbit/s under the broadband conditions shown in Fig. 88. As with the 3.5-Mbit/s DAR configuration, a 0.44 time gate was used. At 7 Mbit/s, this results in a time gate measured at the input of the HPA of 126 ns. From Fig. 99, it can be seen that the resultant time gate measured after the HPA is less than 50 ns. This would

cause the DAR performance to be extremely vulnerable to multipath dispersion, causing intersymbol interference in addition to the normal thermal noise effects. The median UHF test link dispersion measured under diversity conditions of well over 200 ns, together with the above comments and the measured DAR performance, strongly suggests that use of a transmitter time gated modem would be limited to data rates of about 3.5 Mbit/s on medium length UHF forward scatter links.

10.3.3 Spurious signals

Examination of the received spectra at the IF outputs of UHF diversity receivers at Feldberg (AFEZ) revealed that a number of spurious signals existed within the receiver IF passband. An investigation showed that these spurious signals were caused by the leakage of the UHF transmit frequencies into the mixer cavities of the diversity receivers. In one case, the difference frequency between a transmitter and a receiver was 69 MHz, causing spurious signals to appear only one megahertz from the IF centre frequency. The highest of these spurious signals was more than 40 dB below the main signal. Although there was no indication that the spurious components catastrophically affected modem performance, they may have been responsible for some random error events which occurred occasionally throughout the test for no conclusively known reasons. It is felt that these spurious problems are caused by faulty RF equipment installations and could be eliminated, or significantly reduced, if required.

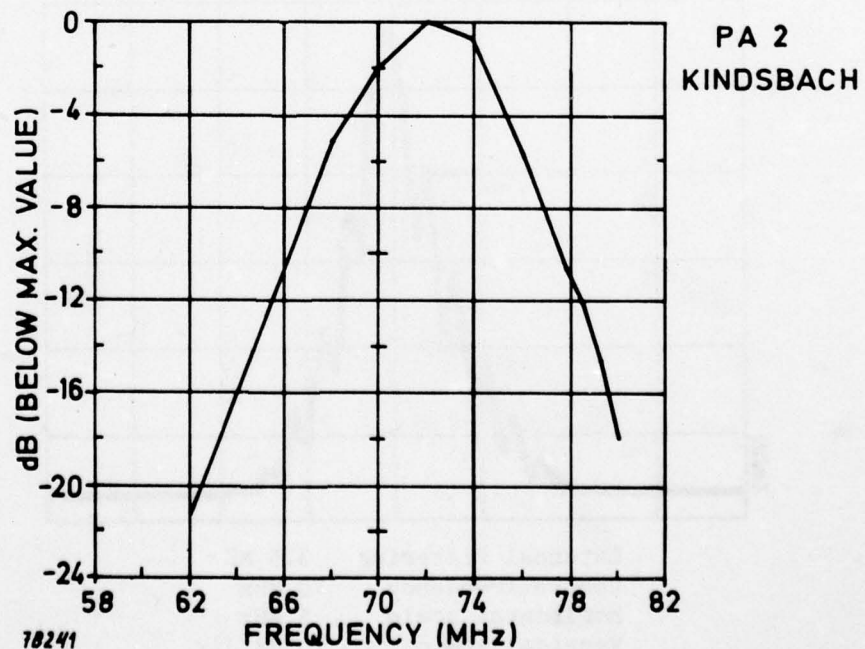
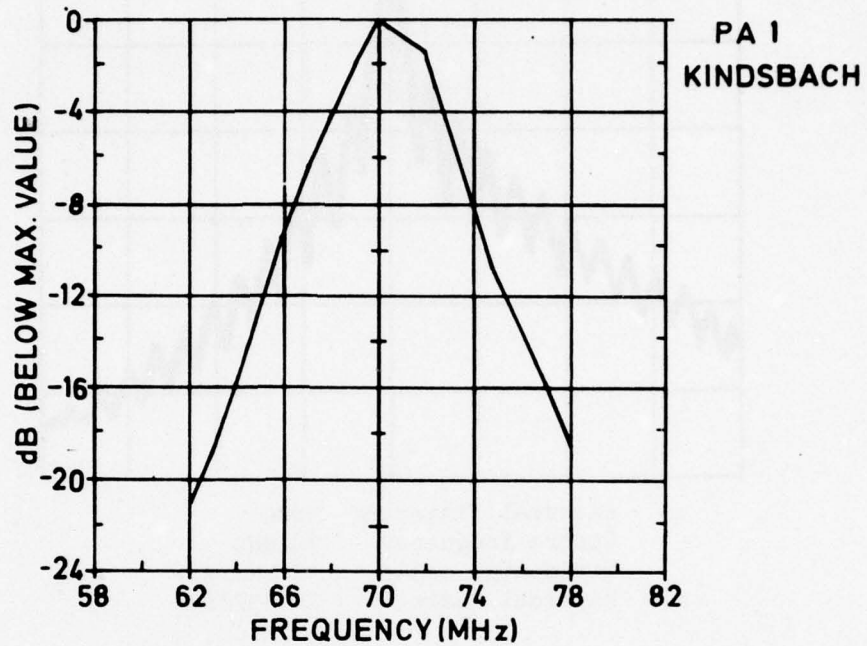
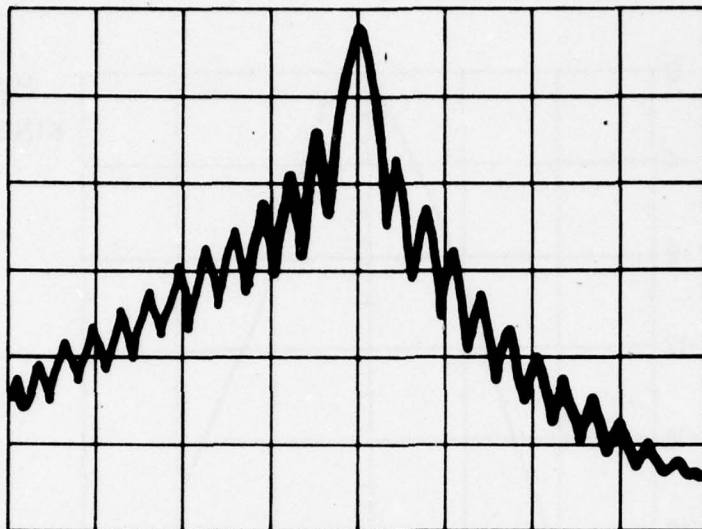
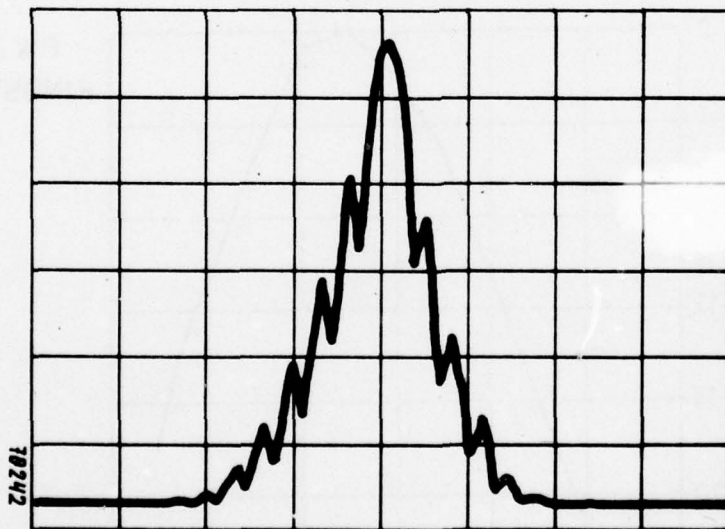


Fig. 89 Measured broadband responses (used for C-band test)



External filtering None
Centre frequency 70 MHz
Horizontal scale 5 MHz/div
Vertical scale 10 dB/div



External filtering 3.5 MHz
Centre frequency 70 MHz
Horizontal scale 5 MHz
Vertical scale 10 dB/div

Fig. 90 MDTs modem output spectra (3.2 Mbit/s)

AD-A066 380

SHAPE TECHNICAL CENTER THE HAGUE (NETHERLANDS)
THE COMBINED US/NATO DIGITAL TROPOSCATTER TEST PROGRAMME OVER T--ETC(U)
DEC 78 P NIELSEN, J OSTERHOLZ, E PUSONE

F/G 17/2.1

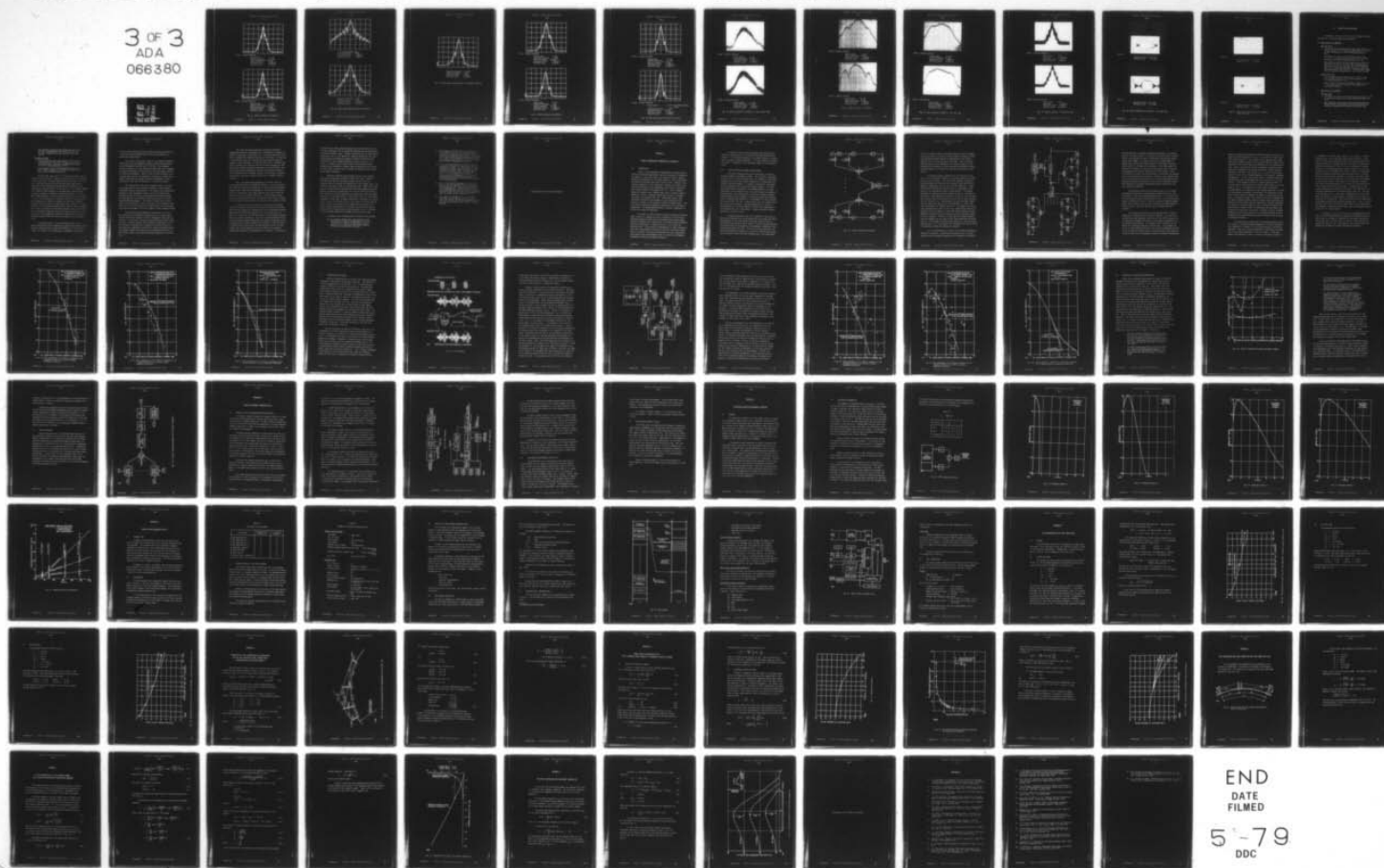
UNCLASSIFIED

STC-CR-NICS-38

DCEC-TR-12-78

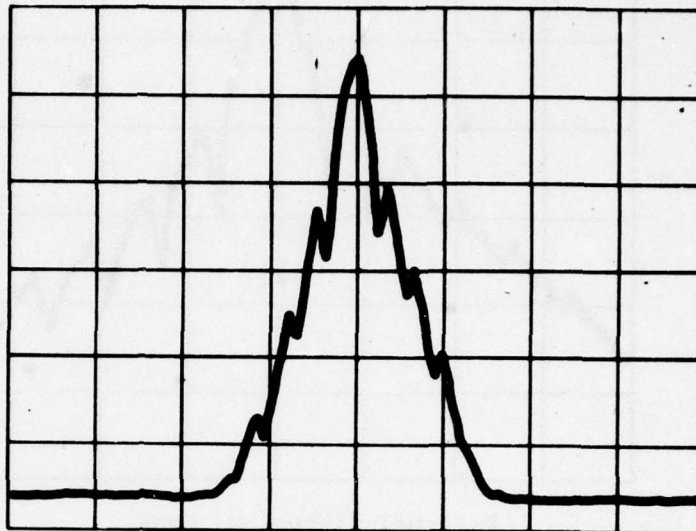
NL

3 OF 3
ADA
066380



END
DATE
FILMED

5-79
DDC



PA No. 1 output spectrum

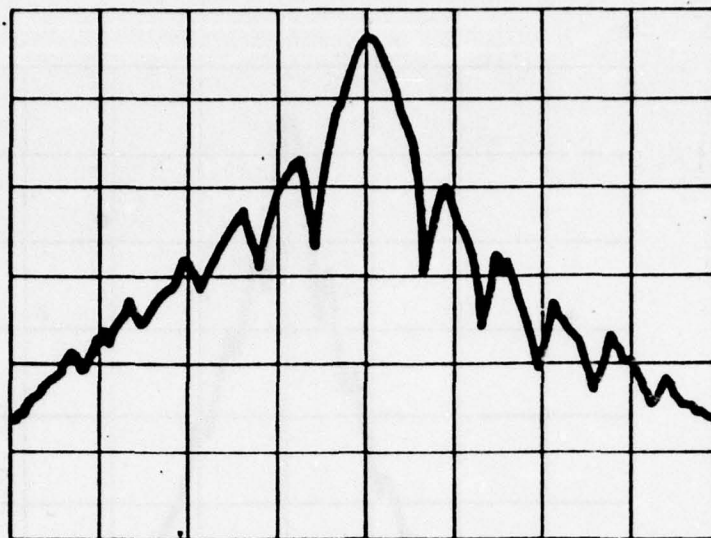
Output power	5.0 kW
External filtering	3.5 MHz
Centre frequency	923 MHz
Horizontal scale	5 MHz/div
Vertical scale	10 dB/div



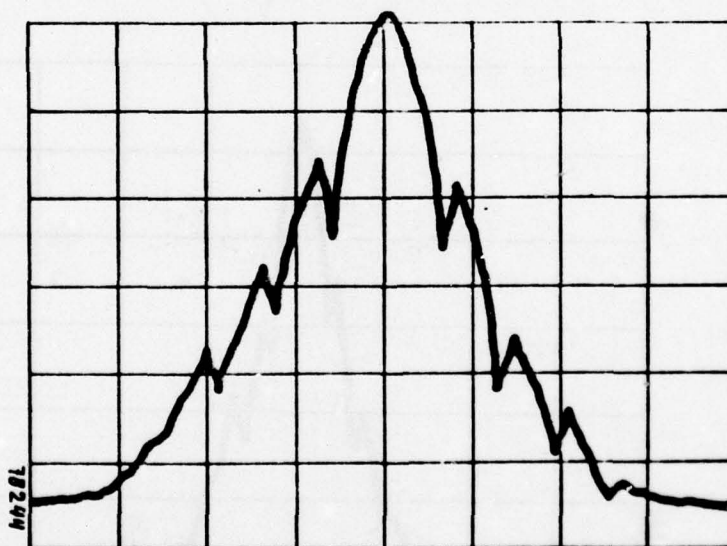
PA No. 2 output spectrum

Output power	4.2 kW
External filtering	3.5 MHz
Centre frequency	957 MHz
Horizontal scale	5 MHz/div
Vertical scale	10 dB/div

Fig. 91 MDTS RF spectra (3.2 Mbit/s)

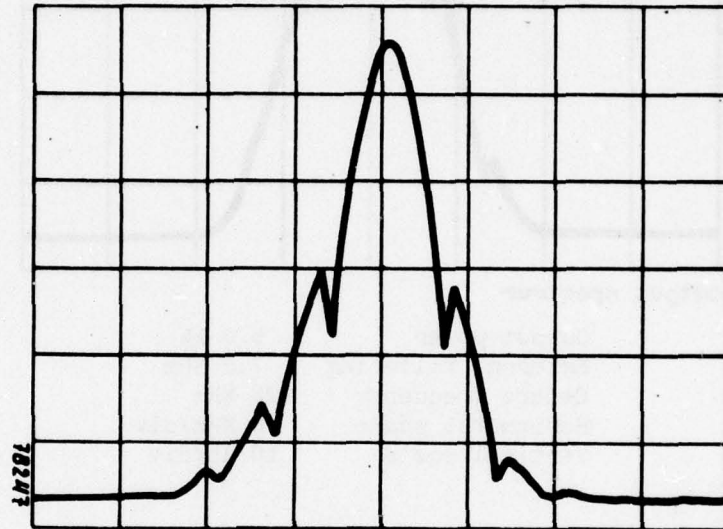


External filtering None
Centre frequency 70 MHz
Horizontal scale 5 MHz/div
Vertical scale 10 dB/div



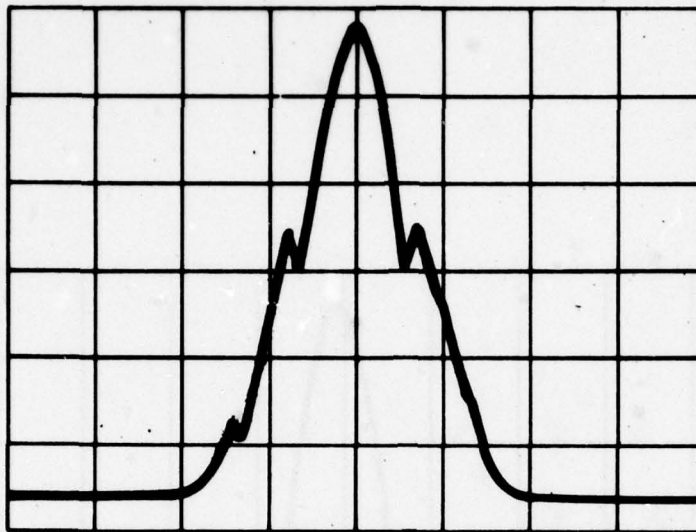
External filtering 7 MHz
Centre frequency 70 MHz
Horizontal scale 5 MHz/div
Vertical scale 10 dB/div

Fig. 92 MDTS modem output spectra (6.4 Mbit/s)



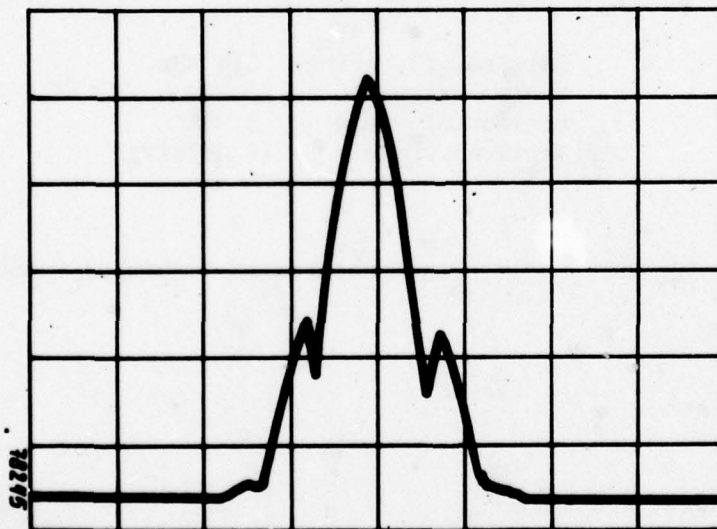
External filtering 5.4 MHz
Centre frequency 70 MHz
Horizontal scale 5 MHz
Vertical scale 10 dB/div

Fig. 92 MDTs modem output spectra (6.4 Mbit/s) (cont'd)



PA No. 1 output spectrum

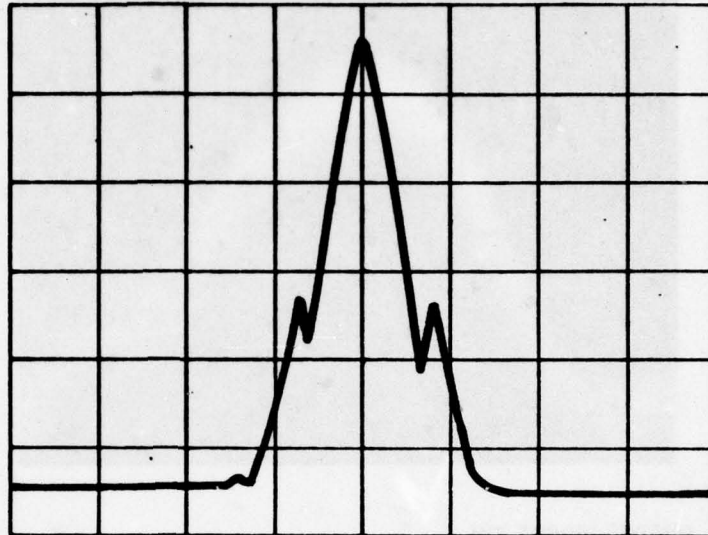
Output power	5.0 kW
External filtering	7.0 MHz
Centre frequency	923 MHz
Horizontal scale	5 MHz/div
Vertical scale	10 dB/div



PA No. 2 output spectrum

Output power	4.2 kW
External filtering	7 MHz
Centre frequency	957 MHz
Horizontal scale	5 MHz/div
Vertical scale	10 dB/div

Fig. 93 MDTS RF spectra (6.4 Mbit/s)



PA No. 2 output spectrum

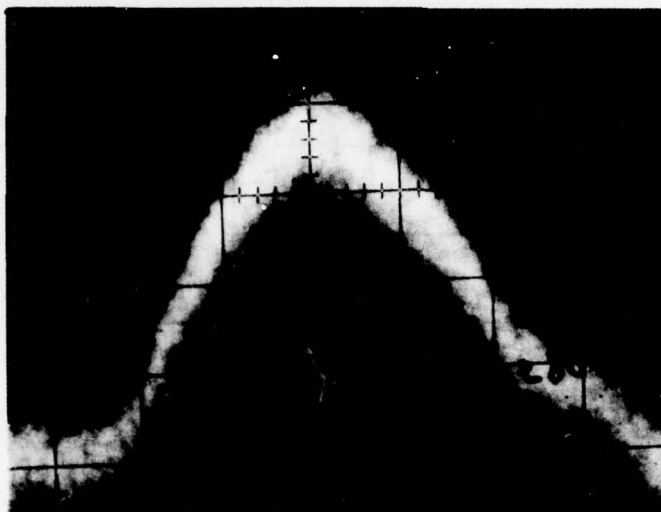
Output power	4.2 kW
External filtering	3.5 MHz
Centre frequency	957 MHz
Horizontal scale	5 MHz/div
Vertical scale	10 dB/div



PA No. 2 output spectrum

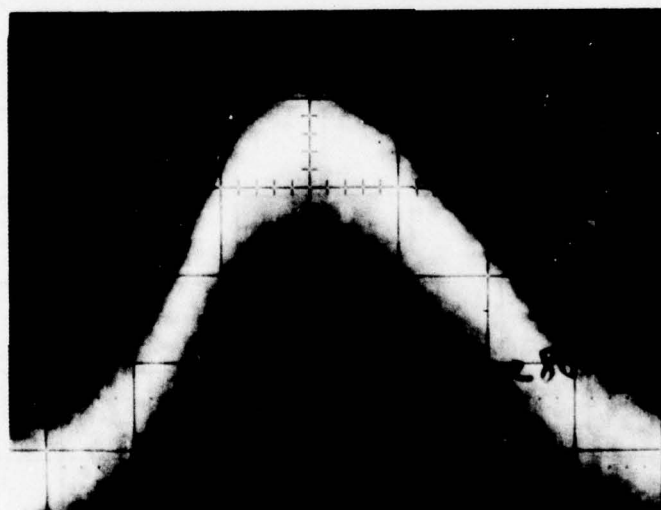
Output power	1.8 kW (3-dB reduced drive to PA)
External filtering	3.4 MHz
Centre frequency	957 MHz
Horizontal scale	5 MHz/div
Vertical scale	10 dB/div

Fig. 93 MDTS RF spectra (6.4 Mbit/s) (cont'd)



PA No. 1 output spectrum

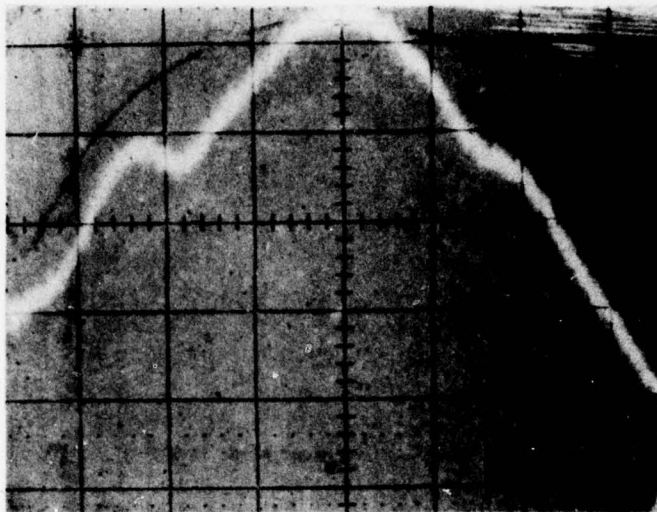
Output power 4 kW
Centre frequency 923 MHz
Horizontal scale 5 MHz/div
Vertical scale 10 dB/div



PA No. 2 output spectrum

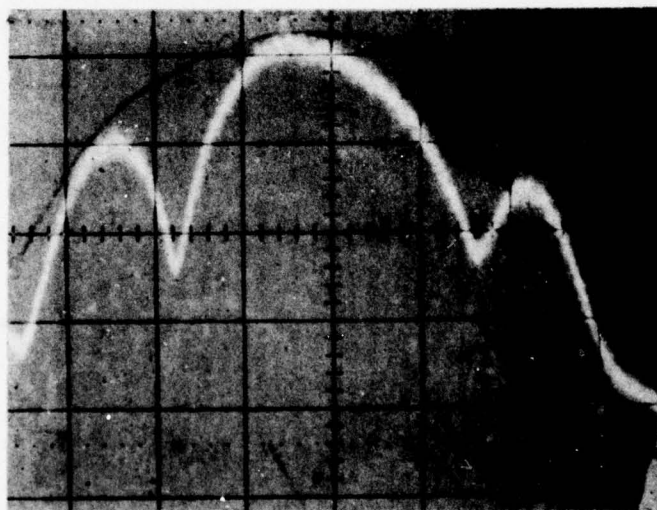
Output power 4.6 kW
Centre frequency 957 MHz
Horizontal scale 5 MHz/div
Vertical scale 10 dB/div

Fig. 94 MDTs RF spectra (9.4 Mbit/s) - trans-alpine link



PA No. 1 output spectrum

Output power 1.5 kW
Centre frequency 923 MHz
Horizontal scale 2 MHz/div
Vertical scale 10 dB/div



PA No. 2 output spectrum

Output power 700 kW
Centre frequency 957 MHz
Horizontal scale 2 MHz/div
Vertical scale 10 dB/div

Fig. 95 DAR RF spectra - 3.5 MBit/s



PA No. 2 output spectrum

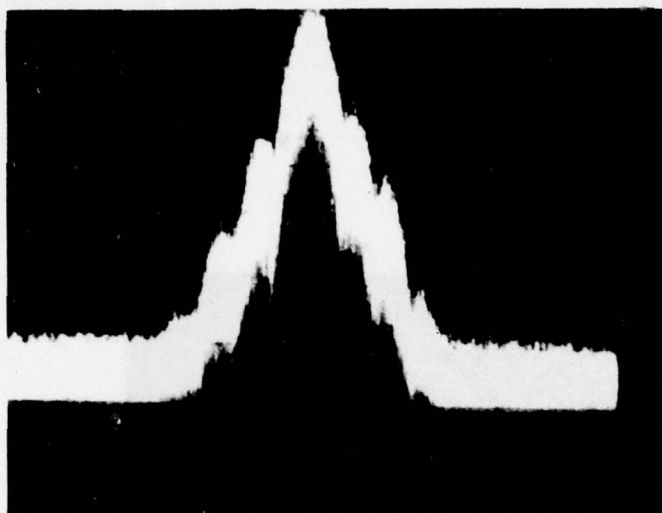
Output power 1.5 kW
Centre frequency 923 MHz
Horizontal scale 2 MHz/div
Vertical scale 10 dB/div



PA No. 2 RF spectrum

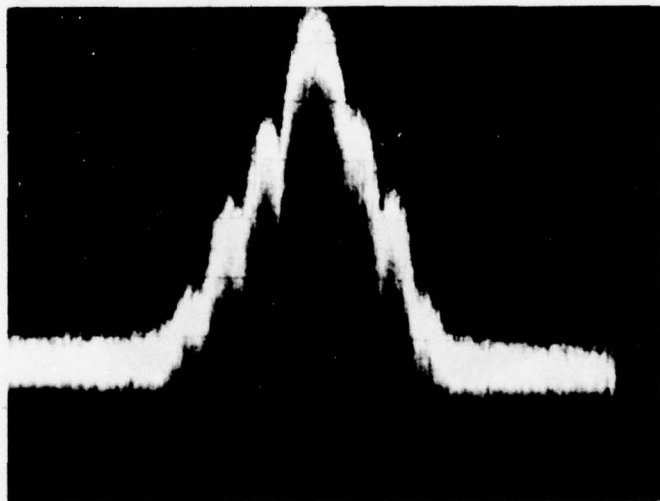
Output power 1.5 kW
Centre frequency 957 MHz
Horizontal scale 2 MHz/div
Vertical scale 10 dB/div

Fig. 96 DAR RF spectra (7 Mbit/s) - UHF test link



PA No. 1 output spectrum

Output power	60 W
Data rate	6.3 Mbit/s
Horizontal scale	5 MHz/div
Vertical scale	10 dB/div



PA No. 2 output spectrum

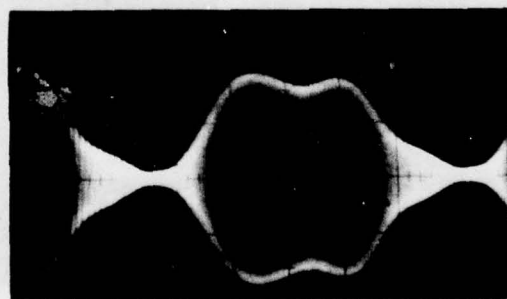
Output power	60 W
Data rate	6.7 Mbit/s
Horizontal scale	5 MHz/div
Vertical scale	10 dB/div

Fig. 97 MDTs RF spectra - C-band test link



PA No. 1

Horizontal scale 50 ns/div
Vertical scale 0.2 V/div



PA No. 2

Horizontal scale 50 ns/div
Vertical scale 0.2 V/div

Fig. 98 DAR RF waveforms (3.5 Mbit/s) - UHF test link



PA No. 1

Horizontal scale 50 ns/div
Vertical scale 0.2 V/div



PA No. 2

Horizontal scale 50 ns/div
Vertical scale 0.2 V/div

Fig. 99 DAR RF waveforms (data rate 7 Mbit/s)
- UHF test link

11. SUMMARY AND CONCLUSIONS

A summary of the major test results relating to digital performance on the test links is given below:

A. MDTS modem at 6.3 Mbit/sUHF test link

- For 90% of the time the mean bit error rate (BER) was better than 3×10^{-8} in quadruple diversity and 4×10^{-5} in dual diversity, at a mean transmitted power of 4 kW.
- For 99% of the time, the mean BER was better than 3×10^{-5} in quadruple diversity and 2×10^{-3} in dual diversity, at a mean transmitted power of 4 kW.
- The quadruple diversity fade outage rate was zero for 95% of all the runs. The mean fade outage duration measured over all the runs was 370 ms, excluding the worst-case outage (lasting approximately 20 minutes), which occurred in Test Period 2. The mean fade outage duration measured during Period 1 was 100 ms or less.

C-band test link

- The mean BER was never worse than 1×10^{-6} in quadruple diversity and 3×10^{-8} in dual diversity, at a transmitted power of 50 W.
- Fade outage occurred with negligible frequency and its duration was less than 100 ms on the C-band link in quadruple diversity.

B. DAR modem at 7.0 Mbit/sUHF test link

- For 90% of the time the mean BER was better than 1×10^{-2} in quadruple diversity at a mean transmitted power of 1 kW.
- Dual diversity tests were limited by the inability of the DAR modem to accommodate the RF bandlimiting and multipath dispersion encountered on the test link.

- The quadruple diversity fade outage rate was better than 10^{-2} outages/second for 90% of the test runs. The mean outage duration was typically less than 500 ms.

C-band test link

- The mean BER was never worse than 3×10^{-7} in quadruple diversity and 2×10^{-2} in dual diversity (for one period only; otherwise the BER was less than 10^{-3}) at a transmitted power of 50 W.
- Fade outages occurred with negligible frequency and with a typical duration of 300 ms or less on the C-band link in quadruple diversity.

Low bit error rates (10^{-10} to 10^{-8}) were achieved over the majority of the tests at 6.3 Mbit/s on the UHF link and 9.4 Mbit/s on the C-band link. However, when bit errors occurred, they occurred at carrier-to-noise ratios (CNR) which were significantly higher than those measured during previous media simulator and troposcatter link tests (Ref. 19, 20 and 21). For 9.4-Mbit/s (MDTS) and 7.0-Mbit/s (DAR) operation on the UHF link, relatively high multipath dispersion undoubtedly affected performance. For 6.3-Mbit/s MDTS operation, it was concluded that bit errors, when they occurred, were frequently not caused by low CNR or excessive multipath dispersion but rather by various test and radio equipment problems often encountered in operational test situations. A temporarily out-of-tolerance frequency source used to time the digital data source on the UHF link and minor frequency stability problems with a frequency synthesizer used in the local oscillators on the C-band test link probably contributed to many of the error events measured during the UHF test and in Test Period 4 of the C-band tests.

In UHF Test Period 2, the most probable cause of the higher-than-expected error frequency was the distorted UHF klystron frequency response which occurred after WINTEX as a result of mistuning. As a result of the additional intersymbol interference

caused by this situation and the multipath dispersion measured on the UHF test link, the MDTs modem occasionally operated in a dispersion-limited manner.

As noted in the previous chapters, the inherent bandwidth limitations of the RF equipment severely limited the performance of the DAR modem on the UHF link at 7 Mbit/s. The frequency response measured on the UHF high power amplifiers after broadband tuning was consistent with the technical data previously reported for similar RF equipment. Based on the test data obtained, it is concluded that the use of transmitter time gating to combat inter-symbol interference for megabit digital transmission over UHF troposcatter links must be reviewed on a link-by-link basis.

The maintenance of bit count integrity (BCI) is of paramount importance for the successful operation of time division multiplexed digital communications. The system test configuration employed in this programme included one level of asynchronous multiplexing and two levels of synchronous multiplexing between the radio and the voice channels terminated in the US- and NATO-supplied PCM/TDM equipment. Test results showed that for quadruple diversity operation, loss of BCI was a very infrequent event and that, in fact, BCI losses were responsible for only an exceedingly small percentage of the total number of fade outages measured.

While the measured propagation characteristics of the C-band diffraction link agreed with predictions, the trans-alpine UHF link was found to exhibit a mode of propagation which was unexpected. In particular, variable-intensity specular signal components were received together with troposcatter components in certain diversity receivers for a substantial fraction of the test. These specular components, attributed to double knife-edge diffraction along the great circle path and off-boresight diffraction or reflections, added to the overall multipath dispersion of the UHF link.

Since the increased dispersion associated with mixed propagation modes can potentially have a significant influence on digital troposcatter transmission, it is extremely important to be able to predict the possible occurrence of such modes. In the case of the UHF test link, the normally-used path profile proved inadequate for this purpose. It was not until after a detailed topographic analysis was completed that the observed propagation characteristics could be explained from physical considerations. The use of fine-grained topographic analyses and available analogue link performance data is deemed valuable to the design of digital troposcatter links that traverse large areas of highly irregular terrain.

Due to the mixed mode propagation on the UHF link and to the unavailability of a multipath analyser, it was not possible to confirm the accuracy of prediction of the multipath dispersion. However, data taken in this programme is consistent with measurements on troposcatter links which display very similar long-term variations of the multipath dispersion around the median value. The exact prediction of medium- and long-term variations of dispersion may require additional test data beyond that obtained to date.

A comparison between predicted and measured fade outage statistics was made only for dual diversity operation, since only very few fade outages were normally observed in quadruple diversity MDTs operation (with the exception of a one-hour period at 6.3 Mbit/s). For most of the UHF test periods, the DAR modem displayed dispersion limited operation. Since the current performance model for these modems assumes negligible intersymbol interference, none of these periods could be used in the comparison. With the MDTs at 6.3 Mbit/s in dual diversity, the measured mean duration of fade outages was in good agreement with the predicted value during periods when troposcatter propagation was strongest. The measured

distribution of fade outage durations under this condition was in excellent agreement with the predicted distribution plotted around the measured median value. However, during periods of high relative dispersion, e.g., at 9.4 Mbit/s in 7 MHz and during the above mentioned periods of dispersion limited 6.3 Mbit/s operation, the prediction of fade outage statistics was less accurate. As a result, it appears that a modification of existing prediction methods may be required to predict more accurately the performance of those links on which most bit errors are expected to be caused by multipath dispersion.

Markedly different median signal levels on the various diversity branches were observed on both test links. Moreover, the difference between the median signal levels of any two receivers was not constant but varied over a wide range, e.g., 0 to 25 dB for receivers 3 and 4 on the UHF test link. While this condition is unusual and not representative of normal troposcatter propagation, asymmetrical propagation can occur on diffraction links with variable terrain and possibly on troposcatter links with angle diversity. In the MDTs modem, a reduction of diversity improvement probably occurred under strongly asymmetrical conditions due to the specific choice of automatic gain control (AGC) circuitry implementation. While this effect did not catastrophically affect the overall digital performance of the MDTs, the use of this type of AGC should be reviewed, based on the assessment of the occurrence of time-variable asymmetrical propagation on specific links.

In summary, the following major conclusions were reached:

- (a) No technical difficulties are expected in the application of digital transmissions of up to 9.4 Mbit/s in 7 MHz of RF bandwidth to the C-band link or to similar links using quadruple diversity and narrow beam antennas.

- (b) With regard to the UHF link, it is difficult to extend the test results to the performance to be expected during the entire year. However, based on the measured data, reliable transmission at 6.3 Mbit/s would probably be possible, given the continued availability of the test RF bandwidth (7 MHz) and quadruple diversity.
- (c) It is unconfirmed whether 9.4 Mbit/s could be transmitted reliably in 7 MHz on the UHF link throughout the year. The performance of this configuration varied from a generally low BER (10^{-7}) for the first period to higher BER (10^{-5} to 10^{-3}) during the second period. It is felt that the combination of a distorted RF passband and the multipath dispersion contributed significantly to the high BER measured in the second period.
- (d) Due to the mixed-mode propagation on the UHF link, little new information was obtained for the planning of links with purely tropospheric scatter propagation. However, measured multipath dispersion data and its lack of correlation with median CNR was consistent with measurements taken by others on pure troposcatter links.
- (e) Test results confirmed that, for quadruple diversity, loss of BCI was a very infrequent event and that BCI losses were responsible for a very small percentage of the number of outages measured.

N A T O U N C L A S S I F I E D

-196-

This page is left blank intentionally

APPENDIX A

DIGITAL TROPOSCATTER TRANSMISSION TECHNOLOGY

A1 INTRODUCTION

Prior to the development of modulation techniques specifically for military application, digital troposcatter transmission was limited to less than 3 Mbit/s on almost all paths. Digital modulation techniques such as binary frequency shift keying (BFSK) and phase shift keying (PSK) were typically used. Because of the relative simplicity of the nonadaptive receiver structures utilizing these techniques, their performance was sharply curtailed by even a modest amount of multipath (Ref. 24). Later, compound modulation schemes (e.g., FSK/PSK) were used to separate adjacent symbols in time in a bandwidth-inefficient attempt to mitigate the effects of multipath (Ref. 25). Bandspread systems using correlation receivers were designed to take advantage of the diversity inherent in the frequency selective fading channel. However, while combatting intersymbol interference due to multipath propagation, the bandspreading approach is grossly inefficient in its use of transmitted bandwidth.

The advent of channel adaptive signal processing techniques (Ref. 19 and 20), together with the utilization of intrinsically efficient modulation forms such as quaternary phase shift keying (QPSK) and minimum shift keying (MSK), have made possible bandwidth efficient transmission at digital rates up to four times the previous limit. The successful implementation of these techniques, with their near-optimum utilization of implicit diversity, should result in thermal noise limited performance for most troposcatter links rather than in performance which is limited by intersymbol interference caused by multipath dispersion.

Currently, there are two techniques being developed for potential implementation in US National Military Communications Systems. The following discussion will briefly explore the underlying concepts of these techniques. For a more rigorous treatment, the reader is commended to the references given in the discussion below.

A2 ADAPTIVE DECISION FEEDBACK EQUALIZATION

The first technique which will be discussed is adaptive decision feedback equalization (ADFE). This technique, described in some detail in the literature (Ref. 19), embodies a transversal equalizer structure where channel adaptation is accomplished via decision directed feedback. In general, equalization techniques can be categorized into linear and feedback classes. For diversity troposcatter transmission, the implementation of a linear equalizer, as illustrated in Fig. A1, would utilize an ensemble of linear filters, each operating on a particular diversity branch. The equalized diversity signals could then be additively combined prior to sampled data detection. A requirement for linear modulation such as PAM, FSK, PSK, or MSK exists due to the linear nature of the receiver structure. Equalizer adaptation is typically accomplished via a training sequence or pilot tone, depending on the implementation of the equalizer. However, decision directed adaptation can also be used.

A feedback equalizer (Fig. A2) is similar in structure to the linear equalizer with the exception that it provides data feedback through a return path where a filtered version of the reconstructed data sequence can be added to the data decision process. This permits partial cancellation of intersymbol interference from previously-detected data bits. As with the linear equalizer, its optimum implementation consists of a series of combination matched and transversal filters for each diversity path. The transversal

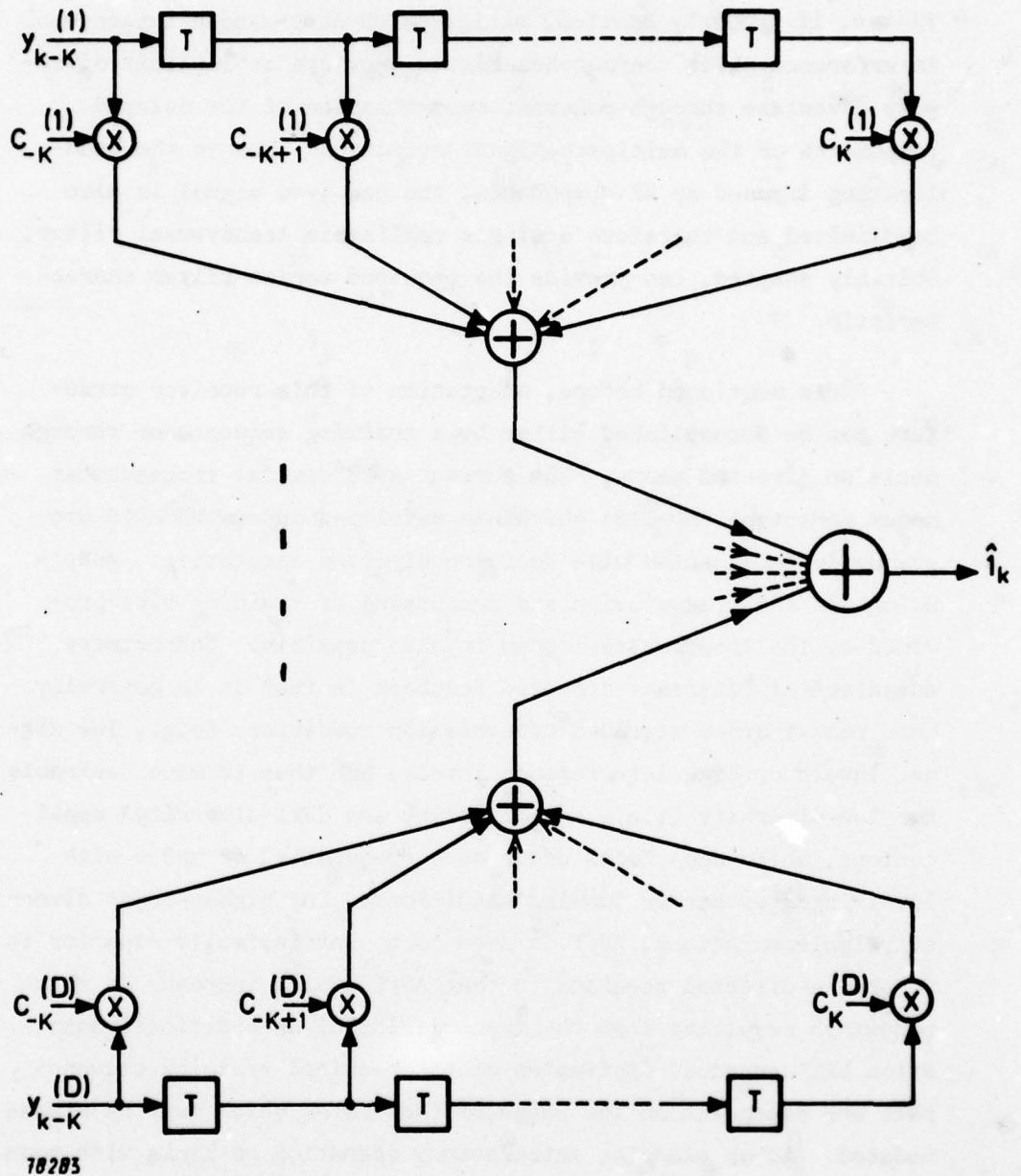


Fig. A1 Linear transversal equalizer

filter, if properly adapted, mitigates channel-caused intersymbol interference while the matched filter provides an implicit diversity advantage through coherent recombination of the delayed components of the multipath signal structure. Due to the band-limiting imposed by RF components, the received signal is also bandlimited and therefore a single realizable transversal filter, suitably adapted, can provide the required series filter characteristic.

As mentioned before, adaptation of this receiver structure can be accomplished either by a training sequence or through decision directed means. The current ADFE digital troposcatter modem prototype (MD-918) which was developed under the MDTs programme is implemented with decision directed adaptation. Adaptation via the transmission and processing of training bits provided by the troposcatter modem is also possible. The primary advantage of reference directed feedback is that it is generally more robust under degraded transmission conditions (e.g., low signal levels or high interference levels) and thus is more desirable for low diversity (i.e., non-diversity and dual-diversity) applications, where deep fades occur more frequently, or under high level interference or jamming conditions. For higher-order diversity implementations, ADFE is seen to be intrinsically superior to reference directed feedback in that ADFE avoids increase in noise bandwidth resulting from the transmission of an additional adaptation bit sequence. Estimates of the required training sequence rate are dependent on the range of fade rates which must be accommodated. As an example, satisfactory operation on links with mean fade rates of 1 to 10 Hz requires the transmission of 150-200 kbit/s of additional overhead for adaptation purposes.

It is now appropriate to outline the currently implemented adaptation technique. As mentioned previously, both the linear equalizer and the feedback equalizer can be adapted, via decision

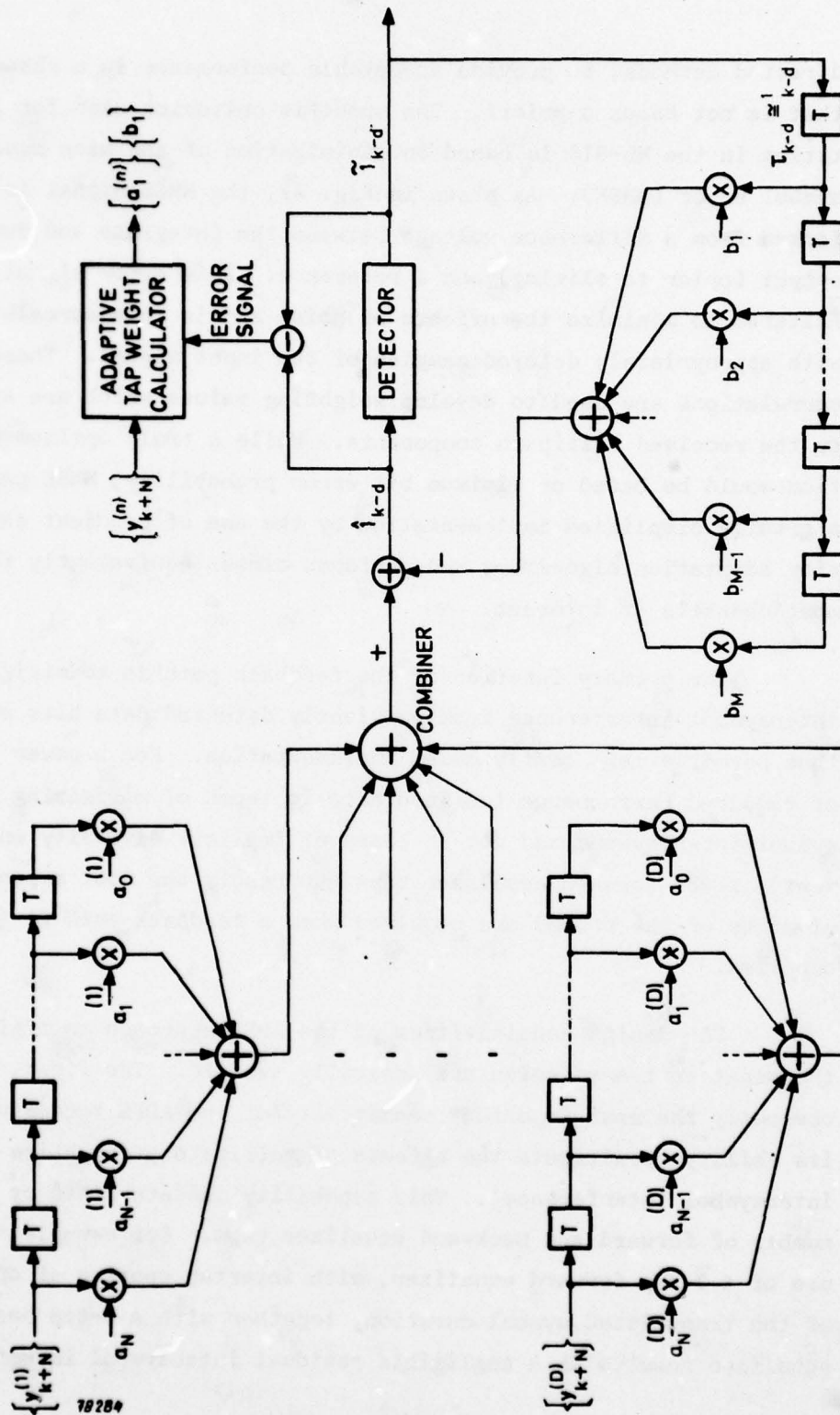


Fig. A2 Decision feedback equalizer with diversity reception

directed methods, to provide acceptable performance in a channel that is not known a-priori. The specific criterion used for adaptation in the MD-918 is based on minimization of the mean square symbol error (MMSE). As shown in Fig. A2, the MMSE signal is formed from a difference voltage between the integrate and dump output (prior to slicing) and a reference. This error signal is filtered to minimize the effects of noise and is then correlated with appropriately delayed samples of the input signal. These correlations are used to develop weighting values which are applied to the received multipath components. While a truly optimum criterion would be based on minimum bit error probability, MMSE permits a greatly simplified implementation by the use of gradient estimation adaptation algorithms and performs almost equivalently for most channels of interest.

The primary function of the feedback path is to mitigate intersymbol interference from previously detected data bits and thus permit a less costly modem implementation. For a given level of required performance (defined here in terms of minimizing intersymbol interference and not in terms of implicit diversity enhancement), fewer forward equalizer taps (currently the most expensive elements of the modem) are required when a feedback path is supplied.

The design sensitivities of the ADFE approach to digital troposcatter transmission are basically twofold. The first, and obviously the most important sensitivity of the ADFE technique, is its ability to mitigate the effects of multipath propagation (i.e., intersymbol interference). This capability is determined by the number of forward and backward equalizer taps. For example, the use of a 3-tap forward equalizer, with intertap spacing of one half of the transmitted symbol duration, together with a 3-tap backward equalizer results in a negligible residual intersymbol interference

penalty on troposcatter paths with diversity reception and a δ_s , or double-sided RMS dispersion, of up to $1.0T_s$ where T_s is the transmitted symbol duration. For channels with δ_s greater than $1.0T_s$, correction voltages obtained in the backward equalizer begin to be significant and tend to reduce the efficiency of the detection process. This is necessary to prevent intersymbol interference from becoming the dominant error-causing mechanism. However, the performance of the ADFE in the region of $\delta_s > 1.0T$ is not discontinuous and is seen to be strongly dependent on the explicit diversity configuration. In fact, the present ADFE in a quadruple diversity implementation will accommodate paths with a δ_s of up to $2T_s$ with little (≈ 2 dB) degradation from its optimum operating point. A 300-mile smooth earth troposcatter link at 6 Mbit/s has a δ_s of the order of $2T_s$ ns. Eventually, as the RMS channel dispersion increases beyond the capability of the backward equalizer to correct for the estimated intersymbol interference, the performance of the ADFE structure begins to degrade and exhibits an irreducible error rate. To extend the range of the equalizer to permit accommodation of larger multipath spreads caused by seasonal path variations, the addition of more forward equalizer taps may be indicated (although an increase of backward equalizer taps to develop correction voltages based on a greater number of previously detected symbols may suffice and is obviously less costly). Another solution, although probably the most costly, would be to increase the system order of diversity by providing additional explicit diversity such as angle or frequency diversity.

The second design sensitivity of the ADFE technique lies in its ability to utilize multipath propagation as implicit diversity. This capability is related to the intertap spacing of the forward equalizer. This can be easily visualized by considering the operation of the forward equalizer in the time domain. In the time domain, the equalizer is seen to be able to coherently combine "m"

of a possible "n" scatter paths, where m is the number of forward equalizer taps. For a particular RMS channel dispersion, extension of overall delay capability beyond the expected range of RMS dispersion does not in general provide any significant additional implicit diversity gain. This is due to the extremely low power contained in scattered components received outside twice the RMS dispersion (δ_s) of the particular channel. However, a significant number of partially correlated paths arriving within an interval bounded by twice the RMS dispersion are present (the exact number of paths is functionally dependent on the composition and dynamics of the scatter volume). These paths can be optimally combined only if the intertap spacing is of the order of the granularity of the multipath structure of the channel. Although many of these scatter components are partially correlated, they nevertheless can contribute effectively in a diversity manner (Ref. 26). The span of the equalizer (i.e., total delay or aggregate sum of the individual tap delays) of course remains constrained by the maximum δ_s which must be accommodated. The present ADFE structure implemented in the MDTS includes three forward equalizer taps. Thus, it can be expected that no more than three inband paths can be recognized by the equalizer, implying a similar upper limit in achievable implicit diversity (i.e., three orders).

Although it is only a prototype, the implementation of the ADFE in the MDTS has demonstrated significant performance gains to date, based on a number of simulated link multipath profiles and actual link tests at rates up to 12.6 Mbit/s. These results are typified by Fig. A3 to A5. The positive test results support the feasibility of ADFE as a viable troposcatter technique.

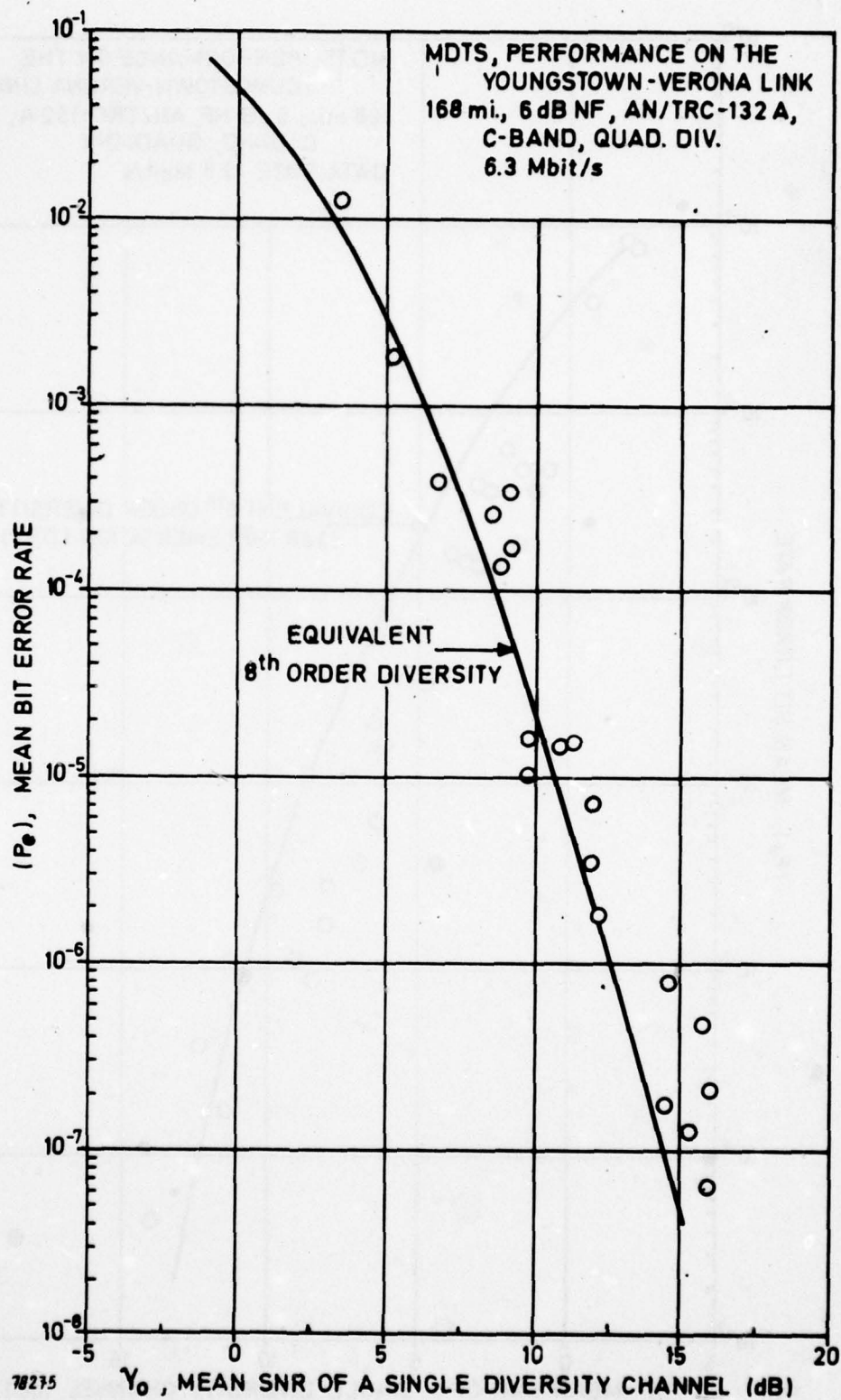


Fig. A3 MDTS performance at 6.3 Mbit/s, measured on the Youngstown-Verona link (168 mi, C-band, quadruple diversity)

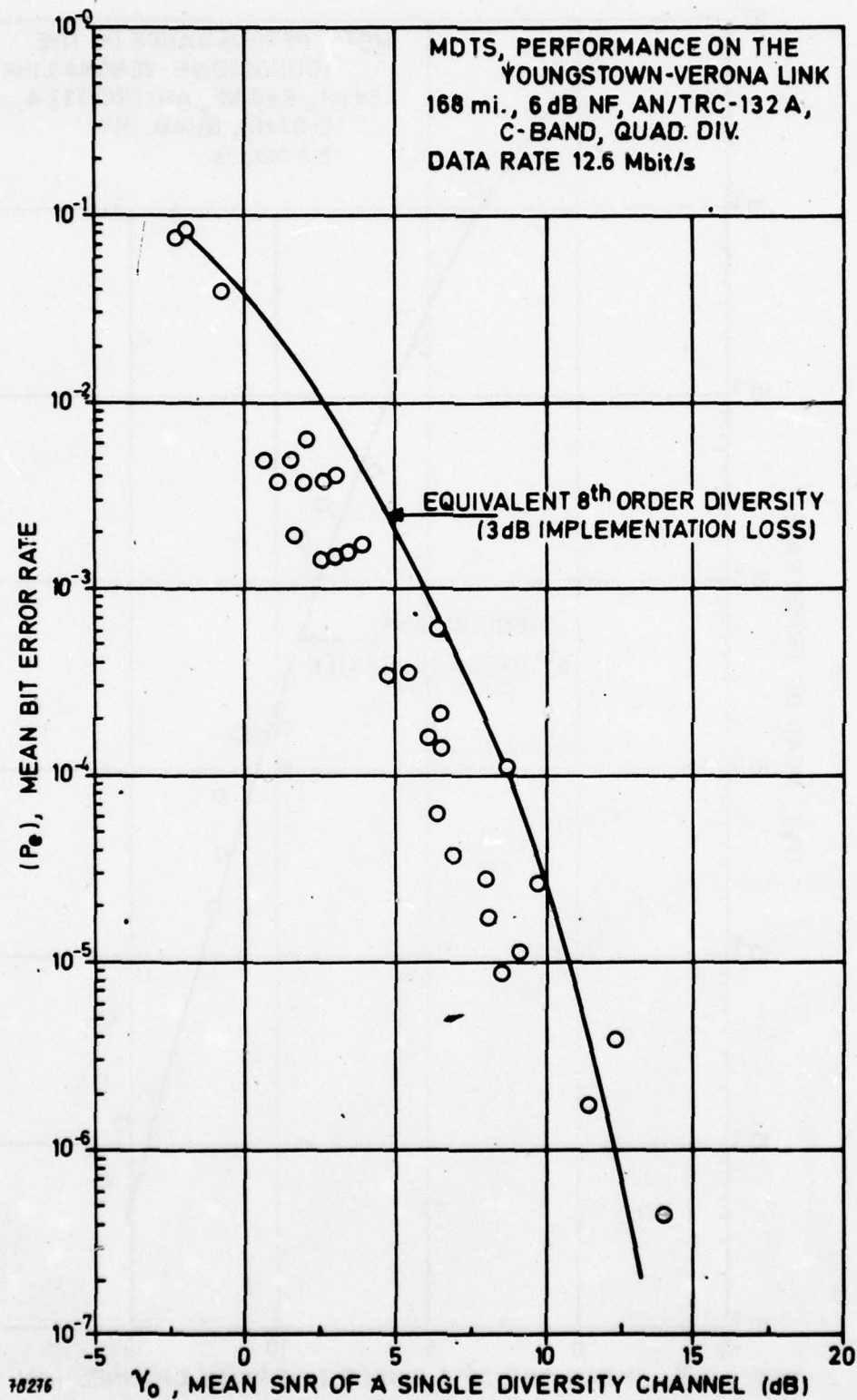


Fig. A4 MDTS performance at 12.6 Mbit/s, measured on the Youngstown-Verona link (168 mi, C-band, quadruple diversity)

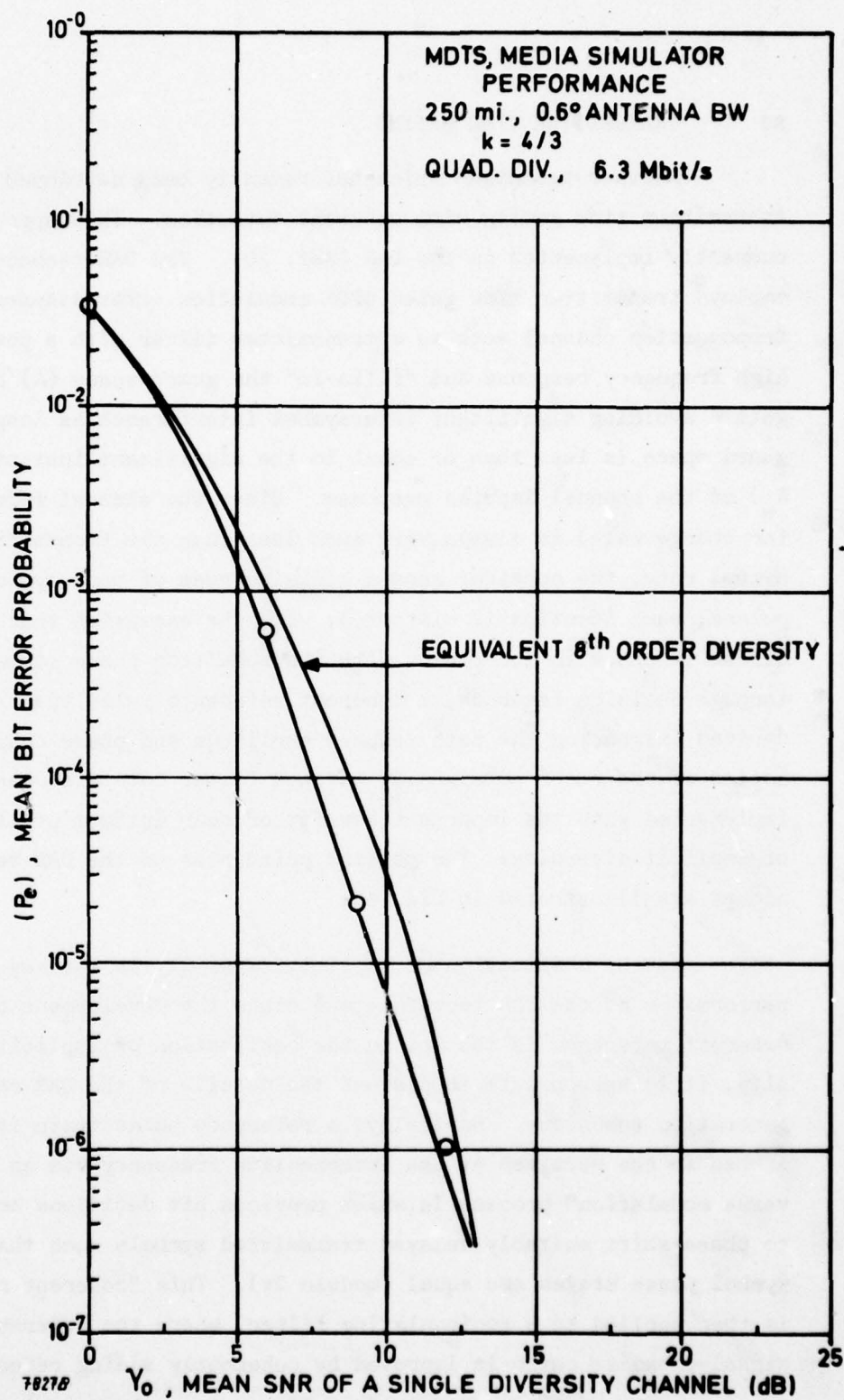


Fig. A5 MDTS performance at 6.3 Mbit/s, measured on the median simulator (250 mi, quadruple diversity)

A3 TRANSMITTER TIME GATING

Another technique which has recently been developed employs transmitter time gating with coherent detection. This approach is currently implemented in the DAR (Ref. 20). The DAR technique employs transmitter time gated QPSK modulation. The dispersive troposcatter channel acts as a transmitter filter with a power high frequency response and "fills-in" the guard space (Δ) or time gate - avoiding significant intersymbol interference as long as the guard space is less than or equal to the significant instant (i.e., δ_s) of the channel impulse response. Since the channel fade rate (or change rate) is always very much less than the transmitted symbol rate, the receiver sees a serial stream of many symbol pulses, each identically distorted, with the exception that they differ in phase in accordance with the modulator phase state. If, through decision feedback, a coherent reference pulse train can be derived (mirroring the path induced amplitude and phase characteristics of the received signal), matched filter detection can be implemented with the important benefit of near optimum utilization of implicit diversity. The salient principles of the DAR techniques are illustrated in Fig. A6.

As the utilization of implicit diversity is the key to the performance of the DAR technique and since the development of a coherent reference is the key to the realization of implicit diversity, it is appropriate to discuss the details of the DAR reference generation technique. Basically, a reference pulse train is generated in the receiver at the intermediate frequency via an "inverse modulation" process in which previous bit decisions are used to phase-shift suitably delayed transmitted symbols such that all symbol phase states are equal (modulo 2π). This "coherent reference" is then applied to a recirculating filter, where the reference signal-to-noise ratio is improved by coherently adding reference

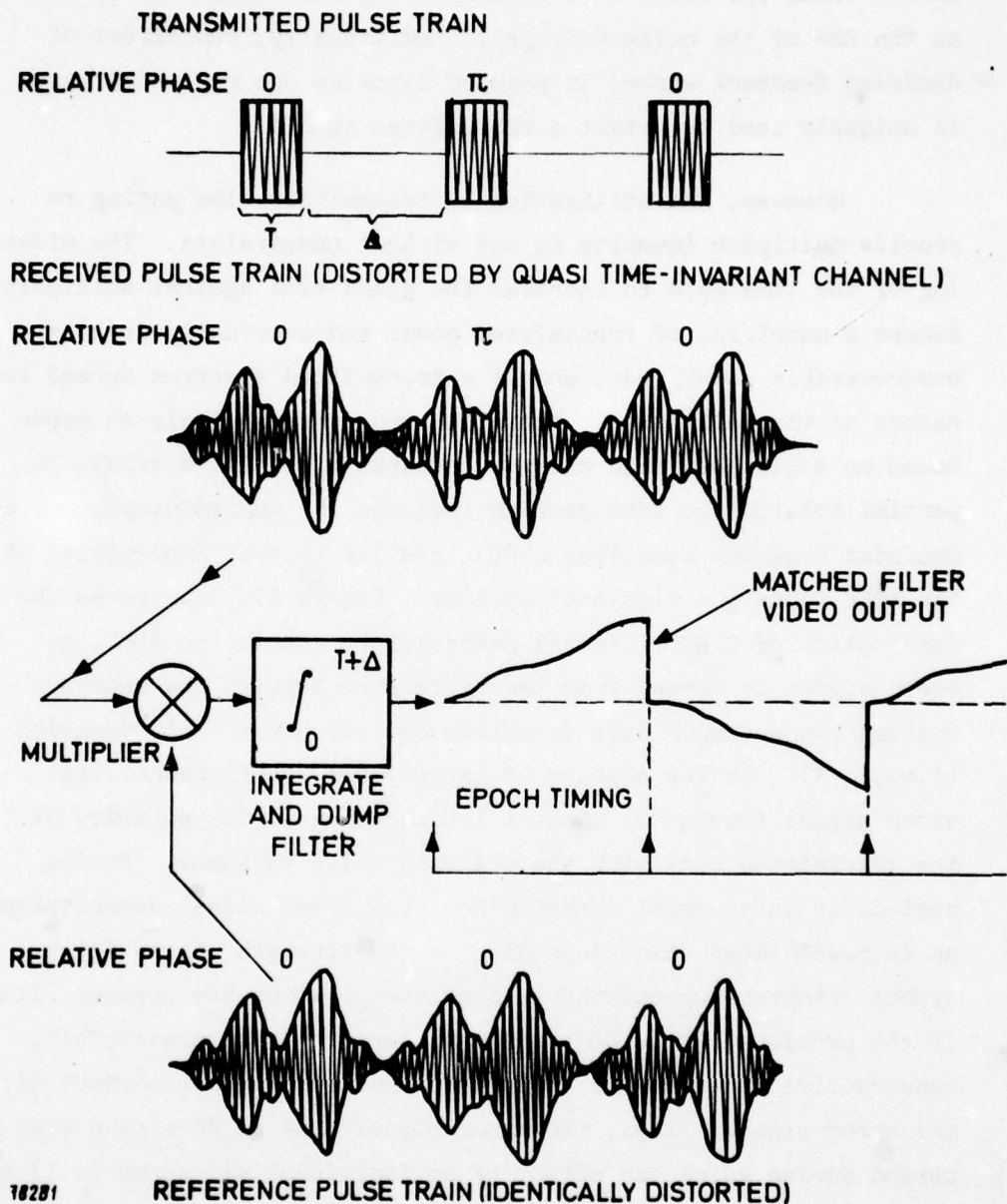


Fig. A6 DAR waveforms

pulses while the noise in the filter loop adds incoherently (i.e., as the RMS of the noise voltage). Additionally, the effect of decision feedback errors is reduced since no one reference pulse is uniquely used to detect a transmitted symbol.

However, the utilization of transmitter time gating to provide multipath immunity is not without constraints. The widening of the time gate to increase the guard time against multipath causes a sacrifice of transmitted power and eventually in 1) an unrecoverable power loss, and 2) a transmitted spectrum spread in excess of that allocated. These factors strongly imply an upper bound on achievable data rate or acceptable multipath delay. A partial solution to this problem involves the implementation of a decision feedback equalizer (DFE), similar to that implemented in the ADFE technique discussed earlier. Figure A7 illustrates the application of DFE to the DAR demodulator. As in the ADFE, an error signal is formed from the difference between the analogue voltage present upon data detection and the present bit decision (i.e., ± 1). In the absence of intersymbol interference, the error signal fluctuates about ± 1 (according to the polarity of the transmitted bit) with the standard noise variance. During periods of intersymbol interference, the error signal demonstrates an increased mean value depending on the strength of the intersymbol interference and the sign of the previous and present bits. If the previous bit is of the same polarity as the present bit, constructive interference occurs and obscures the development of the error signal. Thus, the error signal must be developed over a period during which the effect of an individual bit sense (± 1) can be averaged out. The averaged error signal is multiplied by the interfering previous bit amplitude, inverted in polarity, and added at the output of the integrate and dump filter prior to detection. This interactive process continues until the RMS error signal is forced near zero. The utilization of the DFE in the DAR should

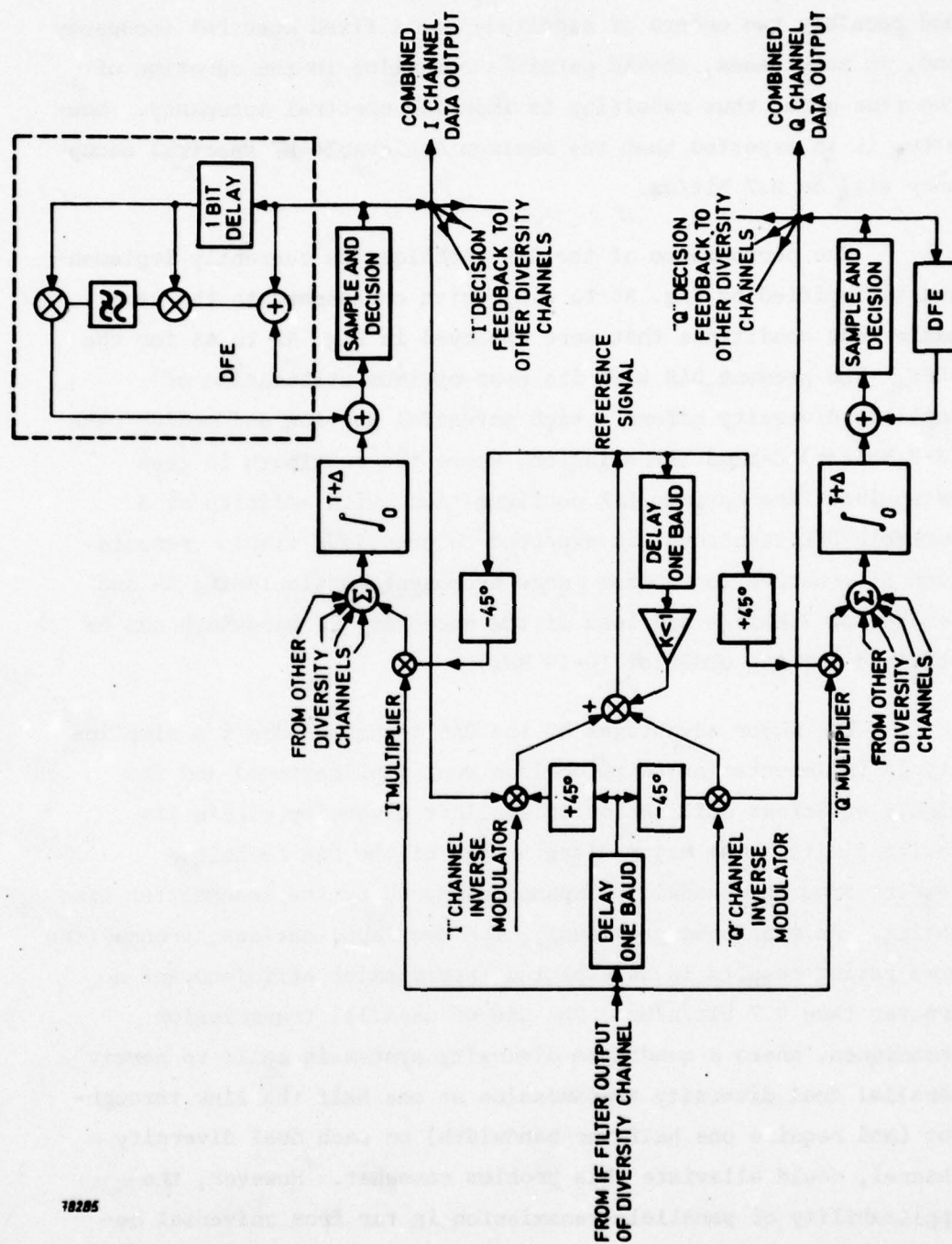


Fig. A7 Functional block diagram of DAR in QPSK receiver

allow a reduction of the irreducible bit error rate limit by one and possibly two orders of magnitude for a fixed spectral occupancy and, in many cases, should permit a reduction in the duration of the time gate, thus resulting in improved spectral occupancy. However, it is expected that the maximum achievable RF spectral occupancy will be 0.7 bit/Hz.

The performance of the DAR technique as currently implemented is typified by Fig. A8 to A10, which correspond to the same basic test conditions that were employed in Fig. A3 to A5 for the ADFE. The present DAR with its near-optimum utilization of implicit diversity offers a high potential for low and medium rate (3-7 Mbit/s) C-band transmission, where the multipath is less extensive. The optimum DAR configuration, with addition of a workable DFE structure, is expected to provide a viable transmission alternative for medium range troposystems (including L- and S-band) of 7 Mbit/s and less if the necessary RF bandwidth can be obtained (of the order of 10-14 MHz).

The major advantages of the DAR technique are its simplicity in implementation (with obvious cost implications) and its highly efficient utilization of implicit diversity within its design limits. The major disadvantage of the DAR technique results from the bandwidth expansion caused by the transmitter time gating. As mentioned previously, for most applications, transmitter time gating results in an expected transmission efficiency of no greater than 0.7 bit/s/Hz. The use of parallel transmission techniques, where a quadruple diversity system is split to permit parallel dual diversity transmission at one half the link throughput (and require one half the bandwidth) on each dual diversity channel, could alleviate this problem somewhat. However, the applicability of parallel transmission is far from universal because of its necessary dependence on extremely favourable link geometry to provide the needed implicit diversity conditions.

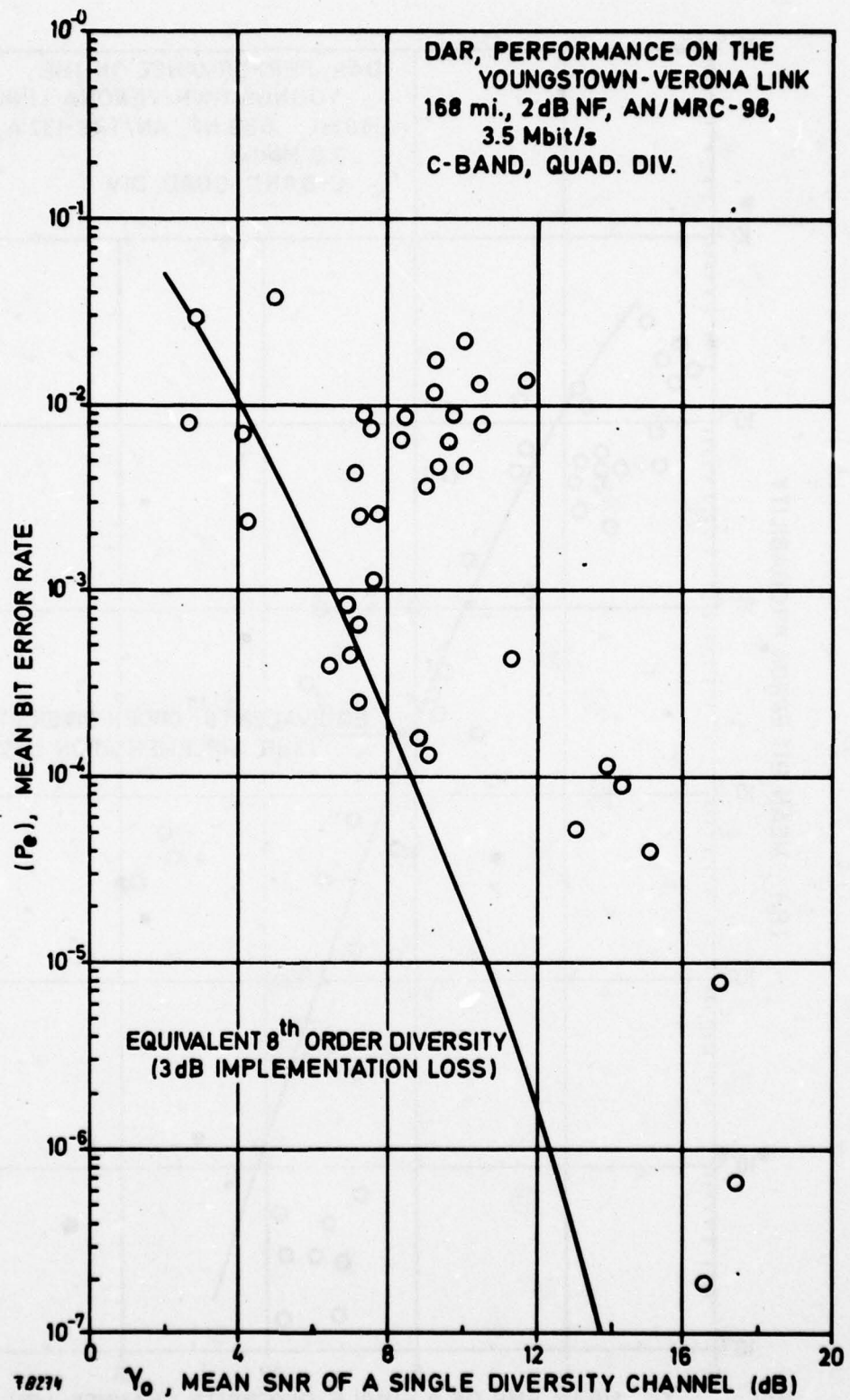


Fig. A8 DAR performance at 3.5 Mbit/s, measured on the Youngstown-Verona link (168 mi, C-band, quadruple diversity)

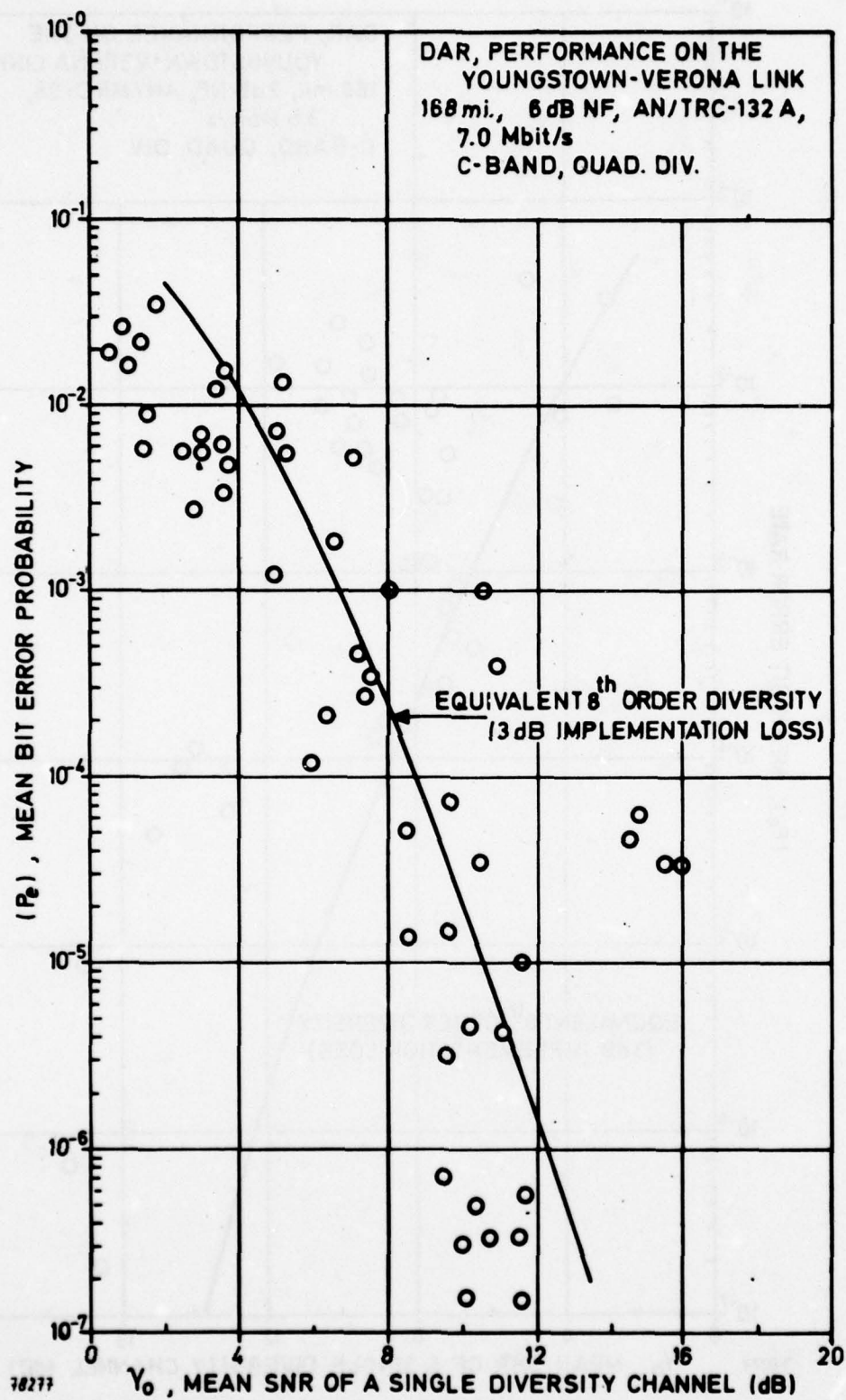


Fig. A9 DAR performance at 7.0 Mbit/s, measured on the Youngstown-Verona link (168 mi, C-band, quadruple diversity)

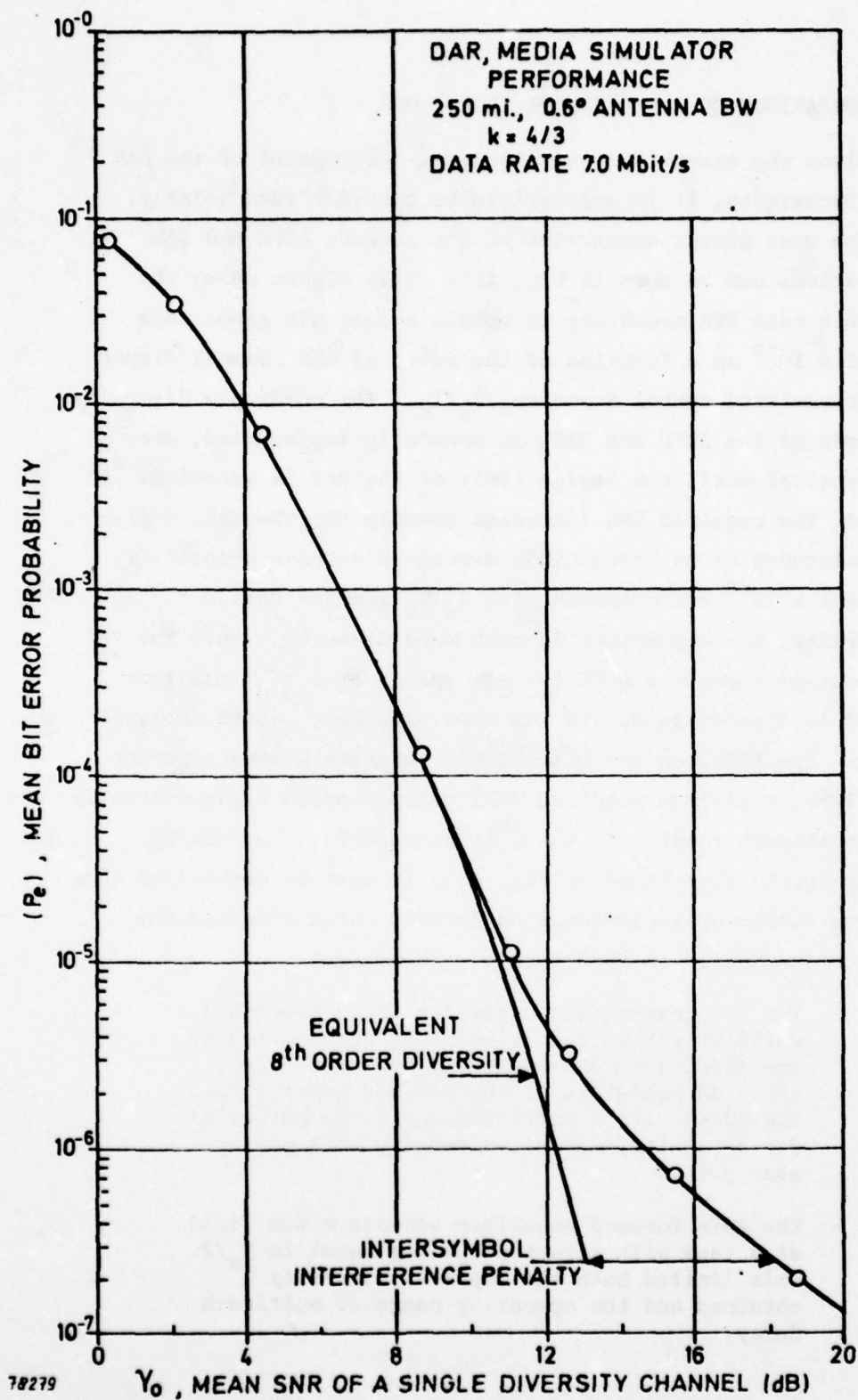


Fig. A10 DAR performance, measured on the media simulator at 7.0 Mbit/s (250 mi, quadruple diversity)

A4 COMPARISON OF ADFE AND DAR TECHNIQUES

Given the essentially simultaneous development of the DAR and ADFE techniques, it is appropriate to consider them jointly. Perhaps the most direct comparison of the current ADFE and DAR implementations can be seen in Fig. A11. This figure shows the required bit rate SNR necessary to obtain a mean bit error rate (BER) of 1×10^{-5} as a function of the ratio of RMS channel dispersion to transmitted symbol duration, δ_s/T_s . The quadruple diversity performances of the ADFE and DAR, as presently implemented, are almost identical until the design limit of the DAR is exceeded. At this point, the required SNR increases sharply for the DAR, implying the existence of an irreducible average bit error probability worse than 1×10^{-5} for channels with δ_s/T_s greater than 0.5. In dual diversity, the comparison is much more dramatic. Here the DAR actually out-performs the ADFE for all values of δ_s/T_s less than 0.5. This is apparently due to its more efficient use of implicit diversity. The ADFE, on the other hand, exhibits a less apparent optimum (i.e., a minimum required SNR) but possesses a significantly enhanced multipath range over which it is capable of operating. In drawing conclusions based on Fig. A11, it must be emphasized that there are a number of implementation factors which affected the performance summarized in this figure. These were:

- The DAR transmitted bandwidth (0.99 power BW), while only 1 to 1.25 times that transmitted by the ADFE, was more uniformly occupied (i.e., the 3-dB bandwidth of the DAR was greater than the ADFE). This permitted a greater potential for obtaining implicit diversity on a particular path.
- The ADFE forward equalizer structure was fixed at 3 taps with intertap spacing equal to $T_s/2$. This limited both the implicit diversity obtained and the operating range of multipath delay.

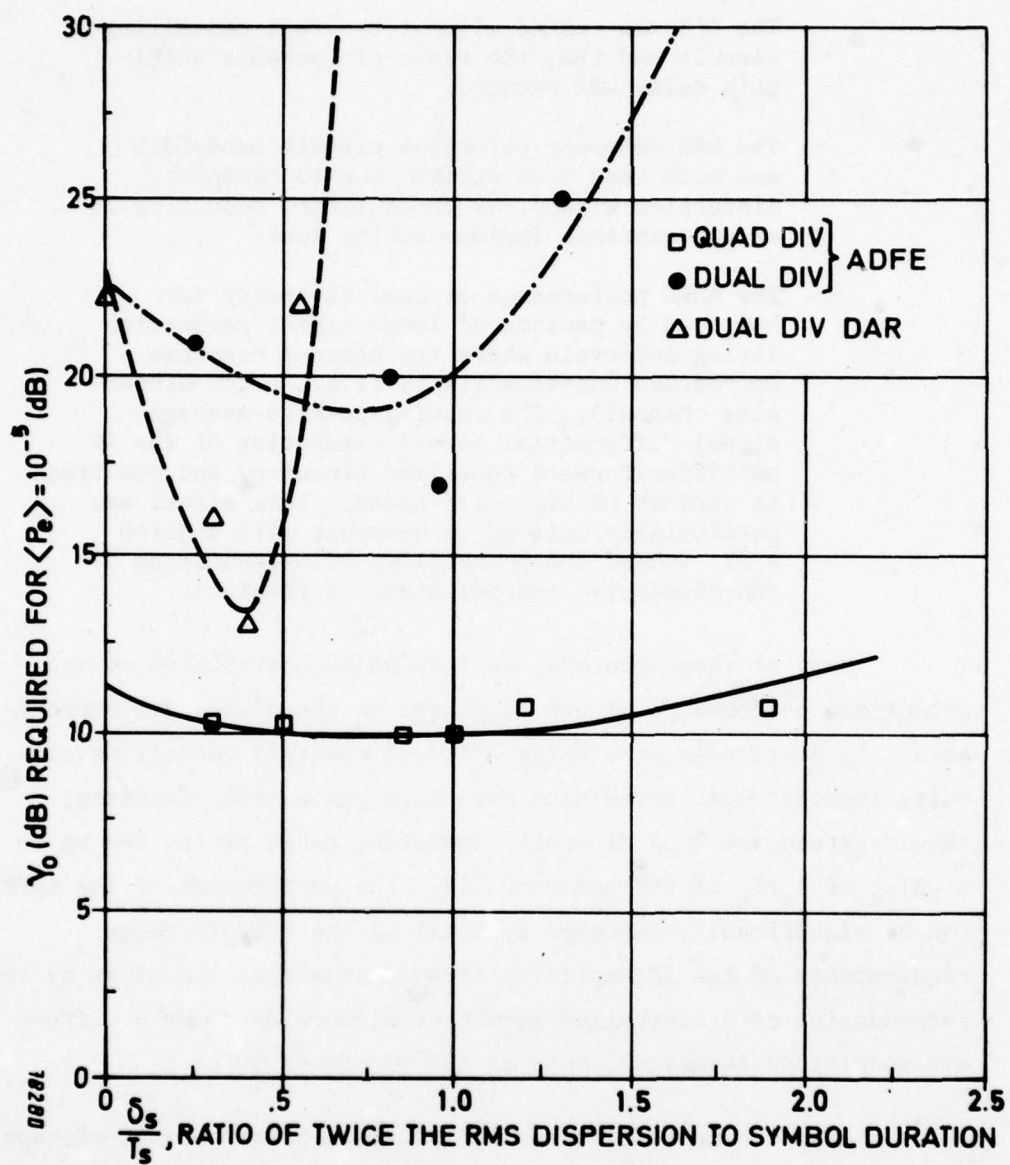


Fig. A11 Digital troposcatter modem performance summary

- The DAR was tested without the tail cancelling circuit and thus the range of operable multipath delay was reduced.
- The DAR coherent reference circuit bandwidth was much less than optimum due to bandpass distortion within the demodulator, resulting in an unacceptable implementation loss.
- The ADFE performance at dual diversity was hampered by periods of large signal saturation during intervals where the channel response approached non-selectivity (i.e., a non-dispersive channel). The ensuing peak-to-average signal differential caused saturation of the IF amplifier/forward equalizer circuitry and resulted in periods of high self-noise. This effect was particularly noticed on channels with smaller δ_s/T_s (where the probability of experiencing a non-dispersive channel state is greater).

Many of these factors, each of which contributed to the suboptimum performance of one technique or the other, are correctable. In particular, the integration of the tail cancelling circuit, together with broad band reference generation circuitry, should extend the dual diversity operating range of the DAR up to a value of δ_s/T_s of the order of 0.7. The performance of the ADFE can be significantly improved by limiting the dynamic range requirements of the IF amplifier forward equalizer circuitry by the introduction of a controlled amount of dispersion or by a different modulation technique, such as MSK or offset QPSK.

Also, in principle, the modification of the number of taps and their intertap spacing in the ADFE to permit additional implicit diversity utilization would result in a dual diversity performance approaching that of the DAR while retaining the same superior δ_s/T_s operating range. In actuality, however, the difficulties in assuring minimal crosstalk in densely tapped delay line structures will not permit absolute convergency by an improved ADFE, in low

diversity configurations, to the performance of the DAR (within its design limit). However, the ADFE will continue to operate over more dispersive channels.

Optimization arguments aside, the ultimate results of both the DAR and ADFE development programmes clearly support the technological feasibility of digital troposcatter transmission. The real questions lie in whether the DAR technique can provide the multipath protection required even with the addition of a DFE and also whether wider band allocations (i.e., resulting in 0.5 - 0.7 bit/cycle) can be obtained in the appropriate frequency bands to support application of the DAR.

A5 OTHER TECHNIQUES

Other techniques such as the Viterbi algorithm (Ref. 27) and independent sideband detection (Ref. 28) have been proposed. However, fabrication of the adaptation circuitry for the Viterbi algorithm implementation proposed for digital troposcatter, as functionally illustrated in Fig. A12, currently has a significant implementation risk at rates greater than 5 Mbit/s. Independent sideband detection is relatively inefficient in its use of transmitted power due to the necessity for a complex modulation scheme (PSK/FDM/FM). Studies (Ref. 28) have indicated that, if the Viterbi algorithm is successfully implemented at high rates, its performance should compare favourably with that of the ADFE technique and probably be less costly due to its lack of dependence on discrete analogue circuitry.

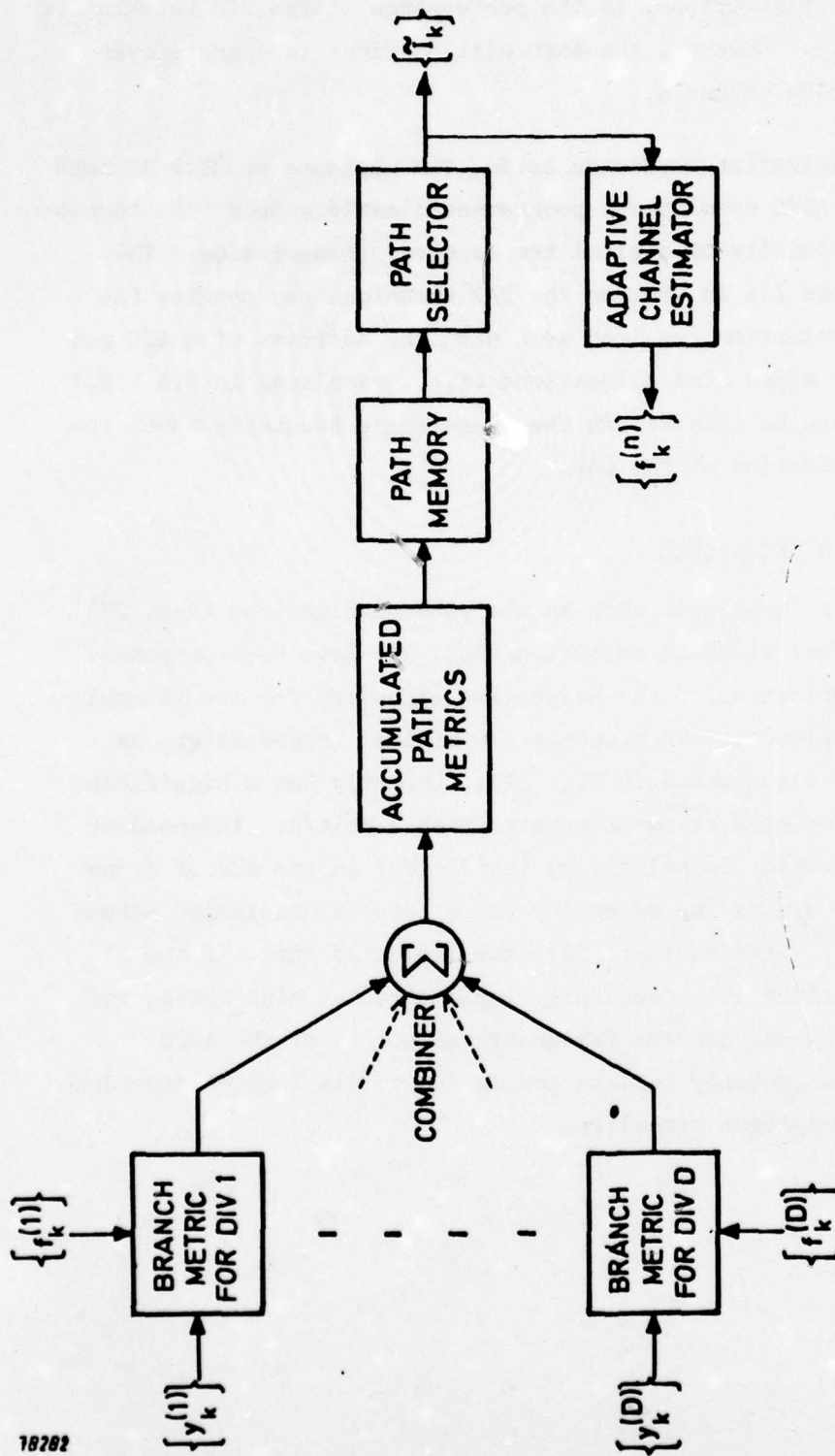


Fig. A12 Viterbi algorithm decoder with diversity reception

APPENDIX B

DIGITAL EQUIPMENT CHARACTERISTICS

B1 MEGABIT DIGITAL TROPOSCATTER SUBSYSTEM (MDTS)

The Megabit Digital Troposcatter Subsystem (MDTS) is a high rate digital modem developed to convert existing analogue troposcatter links to digital operation. The MDTS design is implemented as a multi-diversity 4-PSK modulator/demodulator utilizing adaptive-feedback equalizers to combat the intersymbol interference caused by troposcatter propagation.

The MDTS modulator performs four basic functions (Fig. B1). The video interface function accepts a serial input stream of up to 12.556 Mbit/s or two parallel non-synchronous data streams of up to 6.276 Mbit/s each. The transmit data mix and transmit timing function synchronizes the incoming data and timing to a station frequency reference with a short-term stability of at least 1 part in 10^8 . If input timing signals are not available, they can be generated from the incoming data. Data rate changes are accommodated by changing pluggable VCXO units and moving straps in the digitally implemented backward equalizer.

Differentially encoded quaternary PSK is used as the modulation method. The modulator uses a 5-MHz station clock to generate the 70-MHz IF signal and provides a switchable loopback signal to the demodulator baseband converter for maintenance purposes.

The 70-MHz spectrum controller and driver function provides two adjustable 0 to 50 mV outputs to the transmitter exciter and limits 99% of the transmitted power to a bandwidth corresponding

to either 1.0 or 1.3 bit/Hz by means of pluggable filters. The spectrum controller also provides four controlled level loopback signals to the demodulator IF amplifier for test purposes.

The MDTS demodulator in block diagram form is shown in Fig. B2. Four identical IF amplifiers with AGC accept receiver output signals from -70 to -20 dBm and provide a -10 dBm signal to the adaptive forward filter. These amplifiers operate in such a manner that the largest AGC voltage (receiver with the strongest signal) always controls the other three amplifiers. Bandwidth limiting is accomplished by a pluggable filter which is changed for each data rate change.

The adaptive forward filter is a three-tap transversal filter operating at 70 MHz. The function of the filter is to diversity-combine, remove Doppler effects, and eliminate future digit intersymbol interference. The transversal filter weights are updated by correlation of the IF signals with a decision-directed error signal. The signals on the side taps of the three-tap transversal filter are used to form a discriminator characteristic for tracking the symbol rate clock.

The baseband converter provides the inverse function of the 4-PSK modulator, i.e., it mixes the equalized input 70-MHz signal with a 70-MHz reference. The output of the converter provides both the in-phase (I) and quadrature (Q) baseband signals. Each signal is passed through a finite integrator and detector. The I and Q channels are maintained separately up to the data demultiplex operation.

The backward filter is a transversal filter having up to five taps spaced at the symbol interval. This filter removes past digit inter-symbol interference. The backward filter weights are updated by correlation of delayed data with the decision directed error signal. The backward filter is digitally implemented.

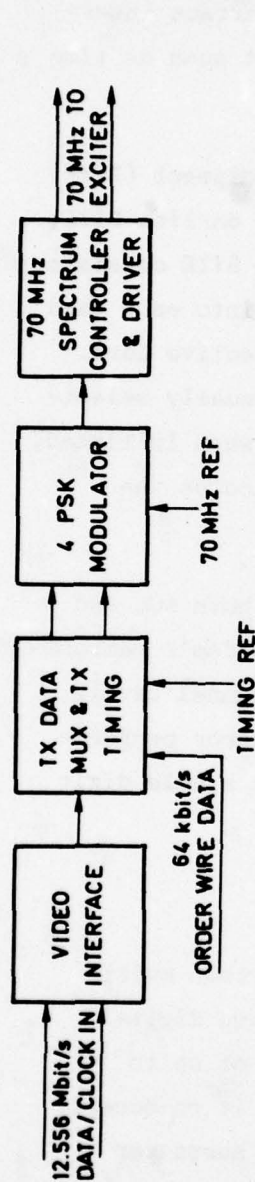


Fig. B1 MDTs modulator

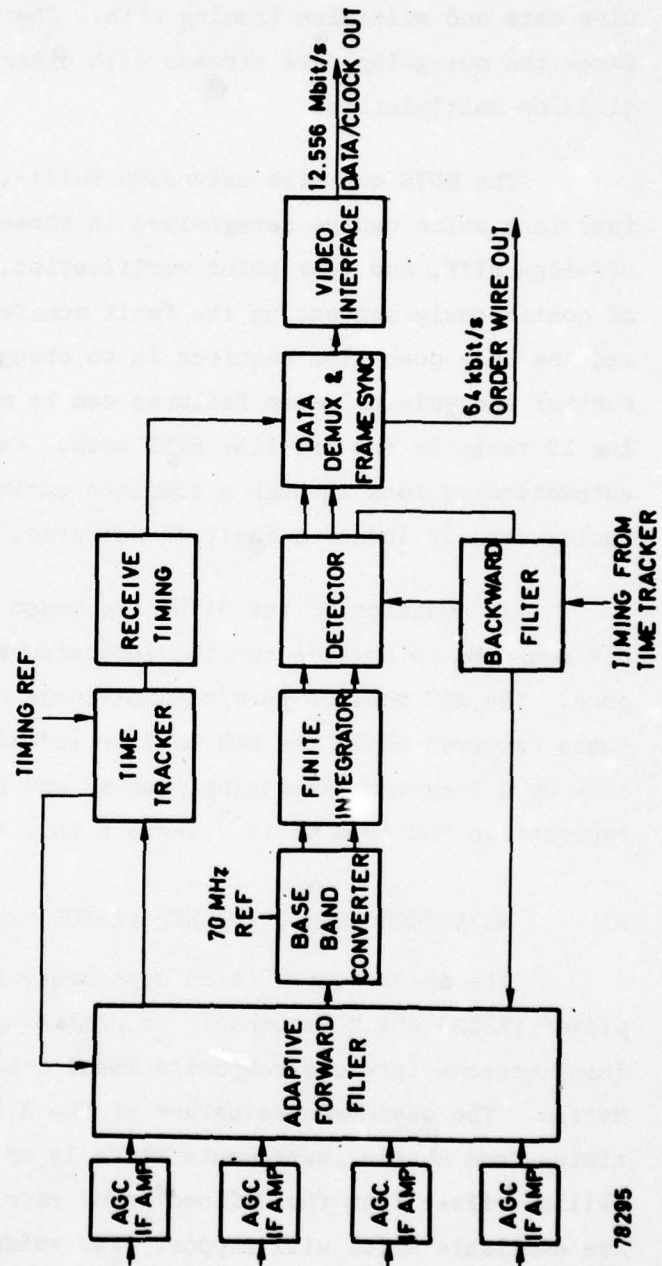


Fig. B2 MDTs demodulator

78295

The data demultiplex and frame synchronization functions provide for extraction of the one or two data streams, the order-wire data and multiplex framing bits. The video interface interfaces the out-going data streams with other equipment such as time division multiplexers.

The MDTs contains extensive built-in-test-equipment (BITE) functions which can be categorized in three levels - on-line BITE, off-line BITE, and test point verification. On-line BITE consists of continuously sequencing the fault monitors built into each card and the only down time required is to change the defective card. Further analysis of modem failures can be made by manually selecting 12 tests in the off-line BITE mode. Each test, when initiated, automatically runs through a complete cycle and indicates the faulty card if indeed a fault is detected.

In addition to the BITE, the modem contains both AGC and BER monitors to provide on-line indications of the modem's performance. The AGC monitor permits individual receive channel levels to be observed while the BER monitor indicates bit error performance by a long-term averaging process and provides a single digit exponent in the form of 10^{-x} where x is 1 to 9.

B2 ASYNCHRONOUS MULTIPLEXER (AN/GSC-24)

The AN/GSC-24(V) is an asynchronous time division multiplexer (ATDM) which is capable of combining multi-rate digital input streams into one composite mission bit stream of up to 10 Mbit/s. The asynchronous nature of the ATDM allows it to accept timing from source instruments which is up to ± 250 parts per million offset from the defined input rate. Optional channel cards are available which will support CVSD voice, teletype, or signals which provide only data (no timing). The standard channel cards support devices which supply both timing and data at any rate within the range of 45 bit/s to 3 Mbit/s. The standard and optional channel cards can be intermixed in any combination to support

a wide range of system requirements. The prototype ATDM allows thirty-one input channels, and the production unit allows up to fifteen. The prototype and production models are electrically compatible and interoperable.

All signal interfaces support ± 3 volt balanced lines of 78 ohm impedance. Control lines are provided by relay contact closure.

B3 PRIMARY MULTIPLEXER (TD-968)

The TD-968 pulse code modulation multiplexer is capable of digitizing and combining up to twenty-four 300-3000 Hz voice channels. Each channel is sampled at 8000 samples per second where each sample contains 8 significant bits. This results in 64 Kbit/s per channel and output rates of 192, 384, 768, and 1536 Kbit/s for 3, 6, 12, or 24 channel operation. Additionally, it is possible to output 1544 Kbit/s when in the 24-channel mode. At all rates synchronization can be provided by the Williard code. This code replaces the least significant bit in one of the channels on a periodic basis and therefore requires no additional bandwidth. At 1544 Kbit/s, either the Williard code or the Bell code can be selected. The use of the Bell code makes the TD-968 compatible with standard D2 channel bank equipments.

Signal interfaces support ± 3 volt balanced lines of 78 ohm impedance. The loss of frame output is provided as a 5 volt level.

APPENDIX C

DISPERSION MONITOR MEASUREMENT TECHNIQUE

C1 GENERAL

As indicated in Chapter 4 of this report, the use of digital troposcatter modems as real-time or near-real-time indicators of the RMS channel dispersion was investigated. The approach taken was to evaluate the adaptive backward equalizer (ABE) control voltages (which are in theory monotonically related to the RMS dispersion) developed in each of the troposcatter modems for linearity, dynamic range, and resolution. Figure C1 is a generic block diagram of the multipath monitor circuitry which was used in the Combined US/NATO Troposcatter Test Programme.

A troposcatter media simulator was used to calibrate the dispersion monitor circuits of the DAR and MDTs under known and controlled conditions where the RMS dispersion could be varied over a broad range. This approach was considered more appropriate than an attempt to observe the performance of the monitors over a more restricted dispersion range encountered on an actual test link using RAKE multipath analyzer measurements as a reference. Further, since simultaneous RAKE and digital modem operation over the same transmission channel is not possible, simultaneous correlation between RAKE and the multipath monitor would also not be possible. Since the RMS dispersion can be more accurately controlled in the media simulator than measured via the RAKE on an actual link, evaluation of the multipath monitor function using the media simulator was felt to be more appropriate.

C2 DISPERSION CALIBRATION

The dispersion calibration was in two parts. The first part centred about a determination of the multipath monitor dynamic range, linearity, and resolution under essentially normal channel conditions. For this test, a mean E_b/N_o of 15 dB (per explicit diversity branch) and an RMS fade rate of 2 Hz were used. A number of multipath profiles, and their associated tap settings, are shown in Fig. C2 to C5. The MDTs calibration was accomplished at 6.3 Mbit/s since the two MDTs modems which were available were configured at that data rate. Although MDTs testing on ACE High was also accomplished at other data rates, the calibration curve was affected only slightly by a data rate change. The DAR calibration was accomplished at 7 Mbit/s, which represented the highest data rate achievable with the DAR technique.

Figure C6 plots the output of the MDTs multipath monitor for various values of δ_s , or 2σ dispersion. The variance of this voltage is indicative of the short-term variation in dispersion which can be expected to be observed on an actual troposcatter link.

Figure C6 shows that the 1-s time constant low pass filtered monitor output is reasonably linear and exhibits a usable dynamic range of the order of 300 ns.

The second part of the dispersion monitor evaluation centred about a determination of the sensitivity of monitor performance to variations in transmission conditions. The MDTs dispersion monitor was shown to provide different performance in non, dual, or quadruple diversity and at mean E_b/N_o of from 4 dB to 40 dB (per diversity branch). Therefore, three relationships between monitor output and dispersion were developed and are given in Table C1. At values of E_b/N_o less than 4 dB, the voltage output

of the MDTS dispersion monitor decreased (thereby decreasing the resolution of the monitor) until it reached a level slightly less than the non-fading reference at 0 dB mean E_b/N_o .

Table C1

$$\delta_s = \frac{V-I}{S} \text{ (ns)}$$

Diversity	I	S
Non	0.75	1.10×10^{-2}
Dual	1.10	3.67×10^{-3}
Quadruple	1.10	1.04×10^{-3}

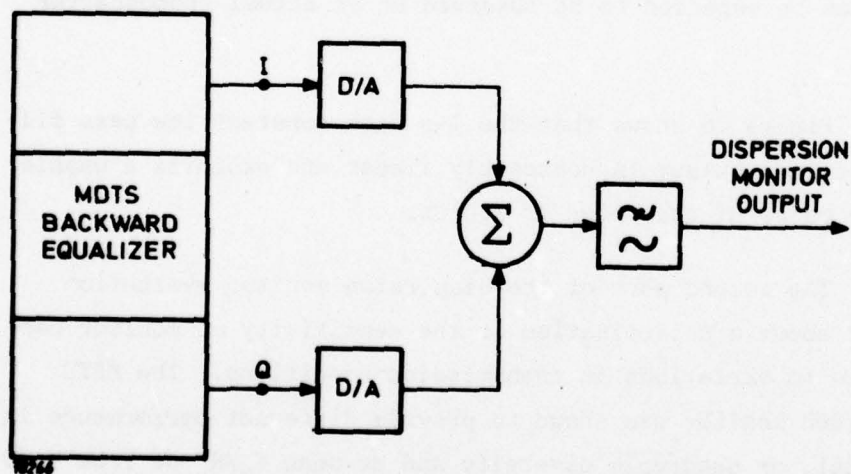


Fig. C1 MDTS dispersion monitor

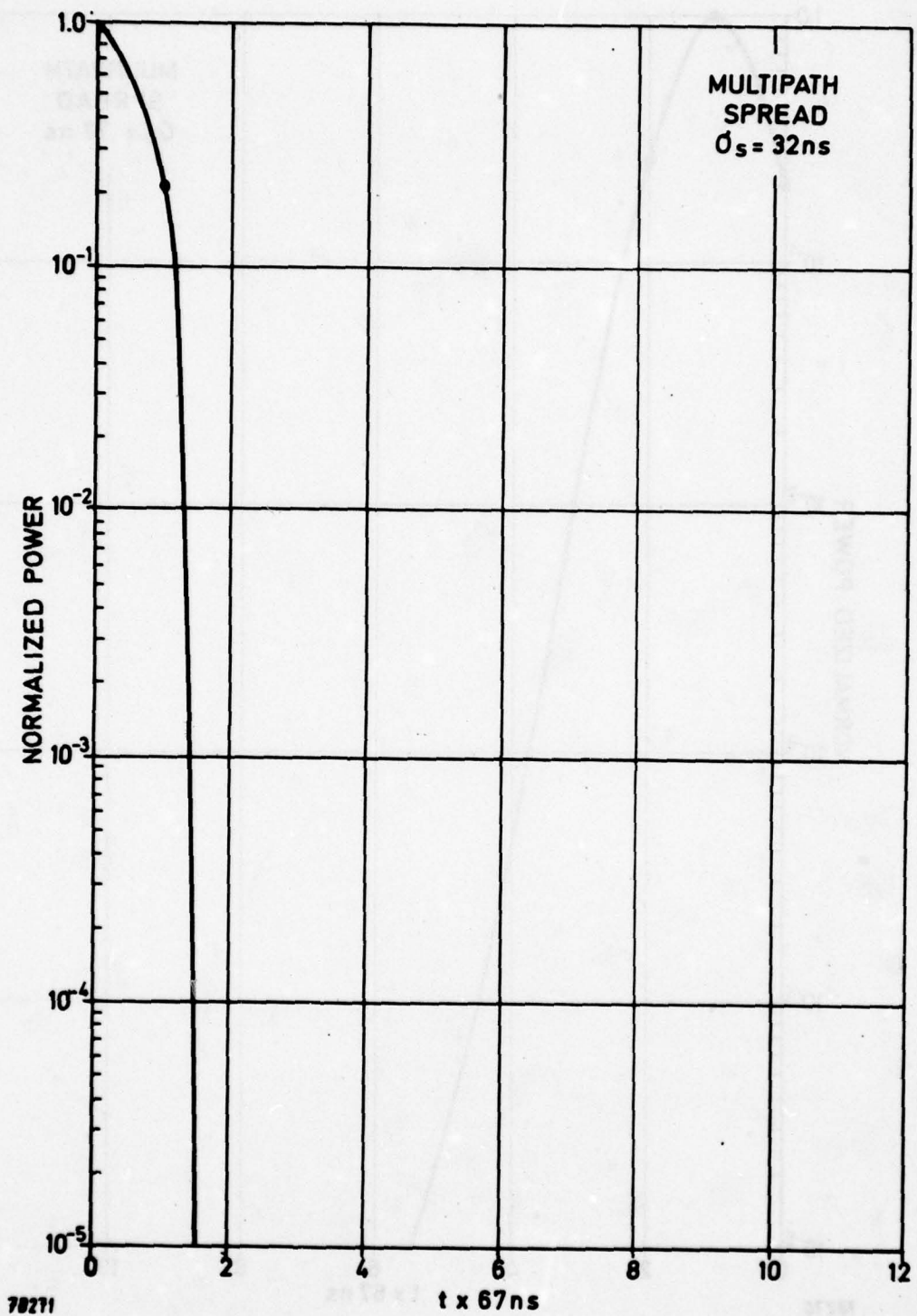


Fig. C2 Multipath profile 1

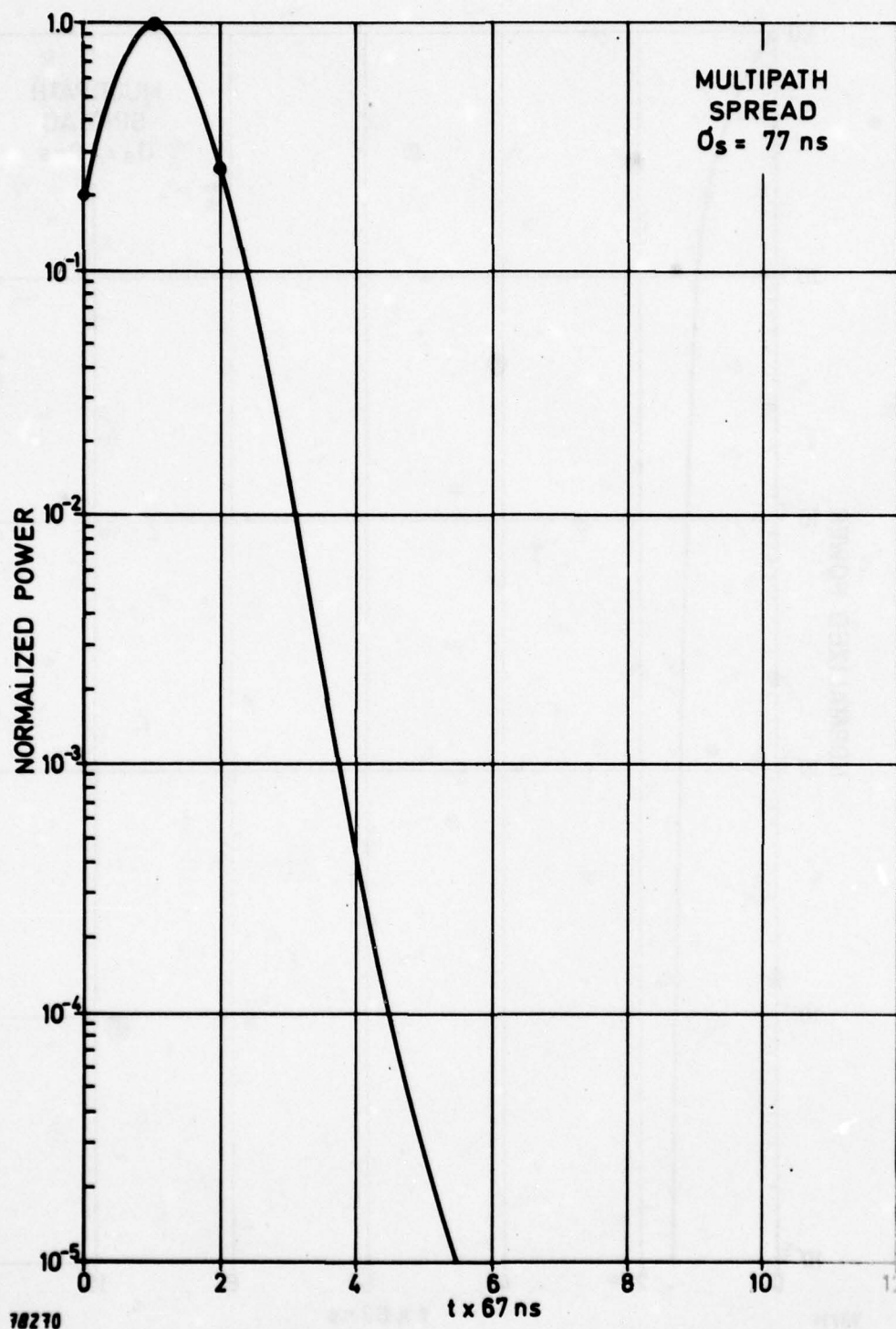


Fig. C3 Multipath profile 2

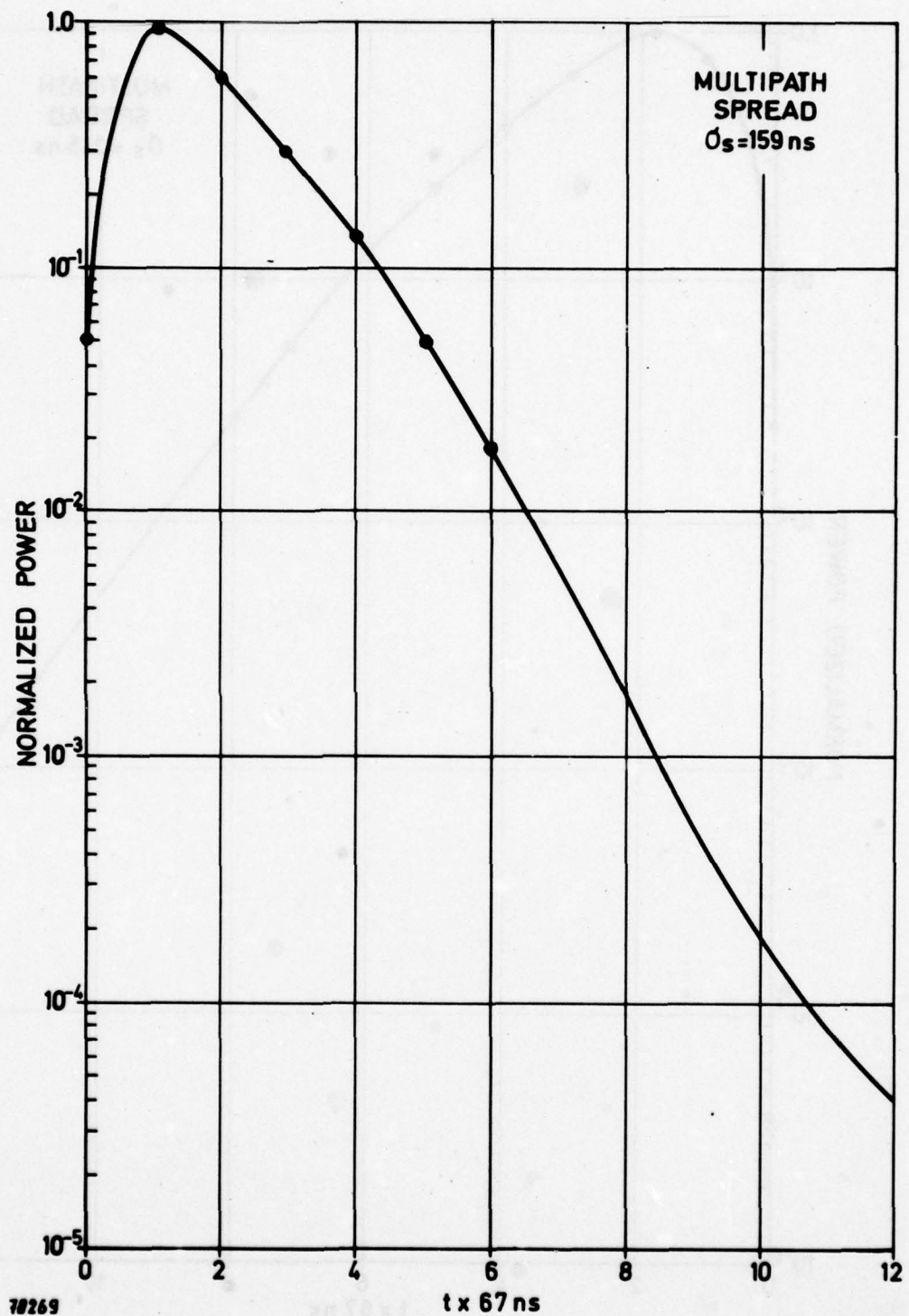


Fig. C4 Multipath profile 3

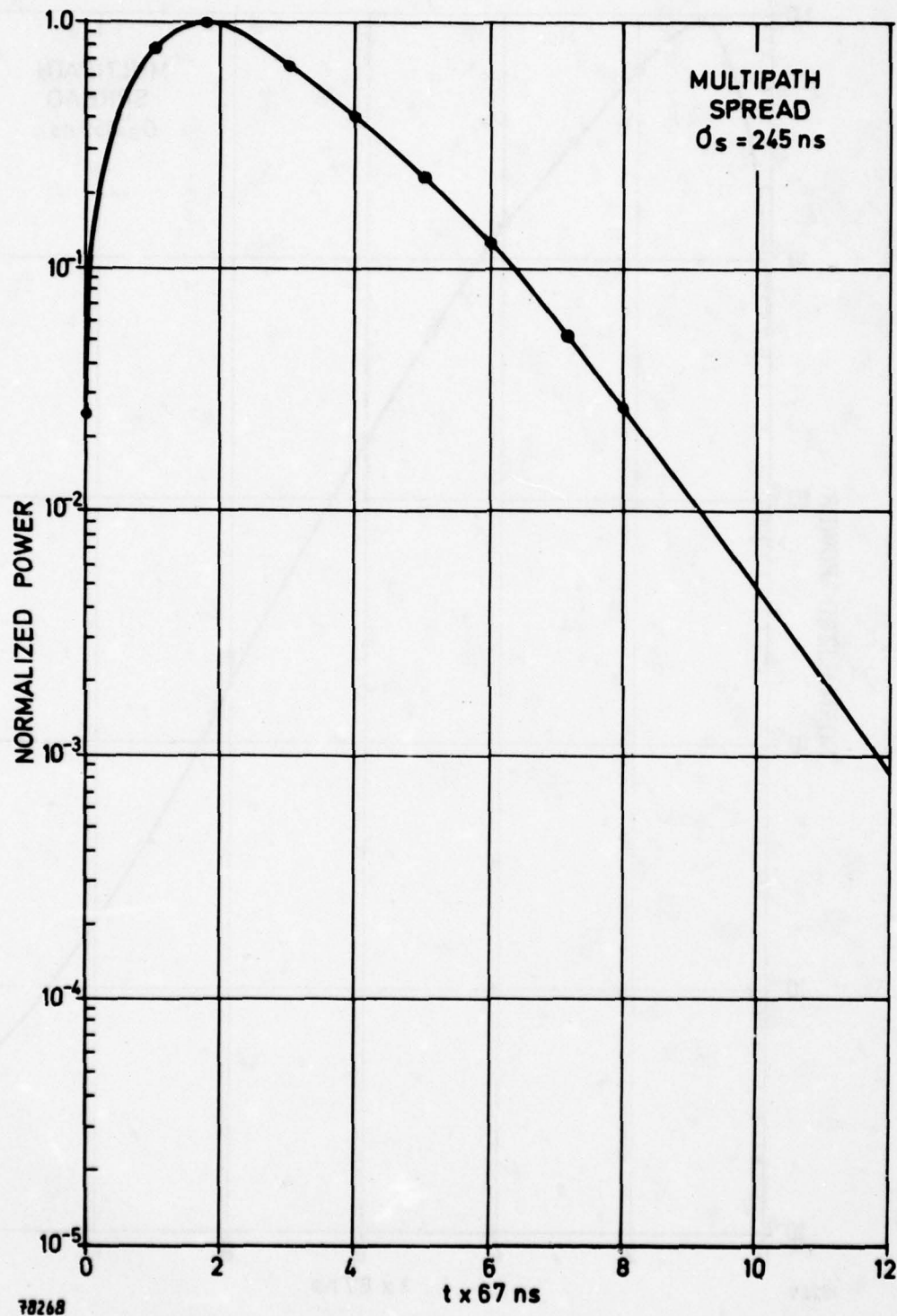


Fig. C5 Multipath profile 4

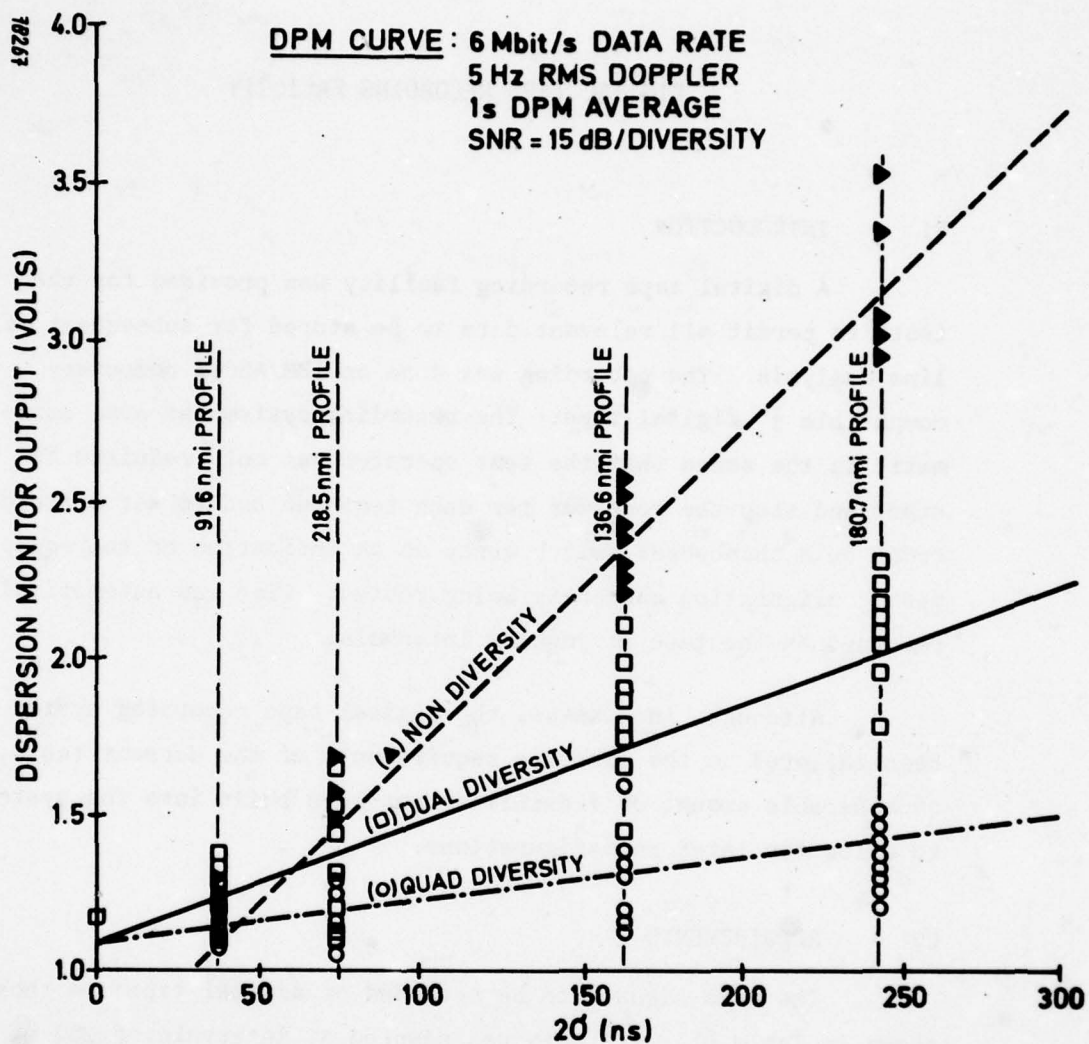


Fig. C6 Dispersion monitor calibration

APPENDIX D

DIGITAL TAPE RECORDING FACILITY

D1 INTRODUCTION

A digital tape recording facility was provided for the tests to permit all relevant data to be stored for subsequent off-line analysis. The recording was done on IBM/ASCII computer-compatible $\frac{1}{2}$ " digital tape. The recording system was semi automatic in the sense that the test operator was only required to start and stop the recorder for each test run and to set certain codes on a thumbwheel switch array as an indication of the equipment configuration currently being tested. Time was automatically recorded on the tape at regular intervals.

Although, in a sense, the digital tape recording system has been tailored to the specific requirements of the current tests, a considerable amount of flexibility has been built into the system to allow for later reconfigurations.

D2 REQUIREMENTS

The data signals to be recorded on digital tape are those shown in Table D1. All data was sampled at intervals of 100 ms to permit resolution of most fast fading phenomena. Time recordings were accurate enough to allow individual samples to be identified unambiguously against absolute time.

It is considered that 8-bit resolution is adequate for all analogue channels, provided the gain and bias of the A/D converters are adjusted individually for each channel to permit good utilization of the available dynamic range.

Table D1

Test data to be recorded

Data source	Analogue (A) or Digital (D)	No. of bits required
RSL amplifier No. 1	A	8
RSL amplifier No. 2	A	8
RSL amplifier No. 3	A	8
RSL amplifier No. 4	A	8
Multipath indicator	A	8
Modem BITE SNR	A	8
Error counter	D	24
Loss of sync. indicators	D	8

D3 CHARACTERISTICS OF THE TAPE RECORDER

The 9-track digital tape recorder used for the recording facility has built-in data buffers and control circuitry for formatting the tape in a computer-compatible format. The maximum physical record size is 2048 characters but, due to the buffers, data can be fed continuously to the recorder at a maximum speed of about 15000 8-bit characters per second. Inter-record gaps are written automatically and imperfections in the tape that might cause a loss of data are avoided by means of read-after-write checks during recording.

Because of the many built-in facilities of the tape recorder the design of the associated interface unit is greatly simplified. The interface unit is thereby essentially reduced to a data conversion and multiplexing device.

The essential technical characteristics of the digital tape recorder are given in Table D2.

Table D2

Summary of technical characteristics

Digital tape recorder:

Standards	:	IBM, ASCII
No. of tracks	:	9
Data density	:	800 bytes/inch
Tape format	:	NRZ 1
Maximum record length	:	2048 characters
Maximum average synchronous data rate:		15000 characters/ second
Maximum peak data transfer rate	:	200000 characters/ second
Reel size	:	8½ inch (1200 ft)

Interface unit

No. of inputs	:	16
Types of inputs	:	Analogue or digital
Analogue inputs	:	Bipolar or unipolar, 2.5 V, 5 V, or 10 V
Digital inputs	:	TTL
Clock outputs	:	TTL
Channel enable/disable	:	Any combination
Sampling rate	:	10 samples/second (other rates may be selected)
Frame preamble	:	16 characters
Frame length	:	127 sub-frames (other lengths may be selected)
Sub-frame length	:	Equal to number of enabled chan- nels
External frequency input	:	5 MHz, 0 dBm into 50 ohms
Clock reference output	:	5 MHz, TTL

D4 OUTLINE OF TAPE RECORDER INTERFACE UNIT

The interface unit sequentially samples up to 16 input ports at a rate selected by the test operator via a front plate control. The input interface circuitry is arranged in four groups of four channels. Each group can be configured for either analogue or digital inputs. For the current tests the interface unit is equipped for eight analogue and eight digital channels.

Channels can be enabled/disabled in any combination by means of 16 two-position switches on the front plate. Disabled channels are omitted from the sampling cycle, and they do not occupy space on the tape.

At regular intervals, a time indication is recorded on the tape, together with the status of eight hexadecimal thumbwheel switches on the front plate. These switches allow the test operator to record a certain amount of side information describing the precise test conditions, thereby facilitating cross-reference between the test log and the tape recordings. Examples of such information are:

- Modem under test
- Data rate
- Diversity configuration
- Test run number
- Calibration run.

Time indications are in the form: day, hour, minute, second, tenth-of-a-second.

D5 TAPE FORMAT DEFINITION

The tape is arranged in a frame format in which each frame consists of a preamble followed by a variable number of sub-frames (selectable by a front plate switch). Each sub-frame consists of

one 8-bit character from each enabled input port. This basic format is illustrated in Fig. D1(a).

The frame preamble consists of 16 characters, assigned as follows:

- 1- 4 : Pseudorandom sync pattern
- 5- 9 : Time
- 10-11 : Port status information (enabled/disabled)
- 12 : Sampling rate/frame length
- 13-16 : Operator codes.

For character no. 12, the relation between the hexadecimal codes and the actual sampling rate/frame length is defined by means of a PROM^{*}. In this context, the frame length is taken to mean the number of sub-frames per frame, since the length of a sub-frame is uniquely determined by the number of enabled channels.

Details of the preamble and of one sub-frame are shown in Fig. D1(b).

For normal test operation, the number of sub-frames per frame is set equal to 127 and one frame corresponds to one physical record on the tape.

During off-line processing of the tapes, a search for a particular data sub-set can be based either on the time indications or on specific operator codes which characterize that sub-set.

D6 INTERFACE UNIT IMPLEMENTATION

A functional block diagram of the interface unit is shown in Fig. D2. The interface unit consists of four functional sub-units:

^{*}Programmable Read Only Memory

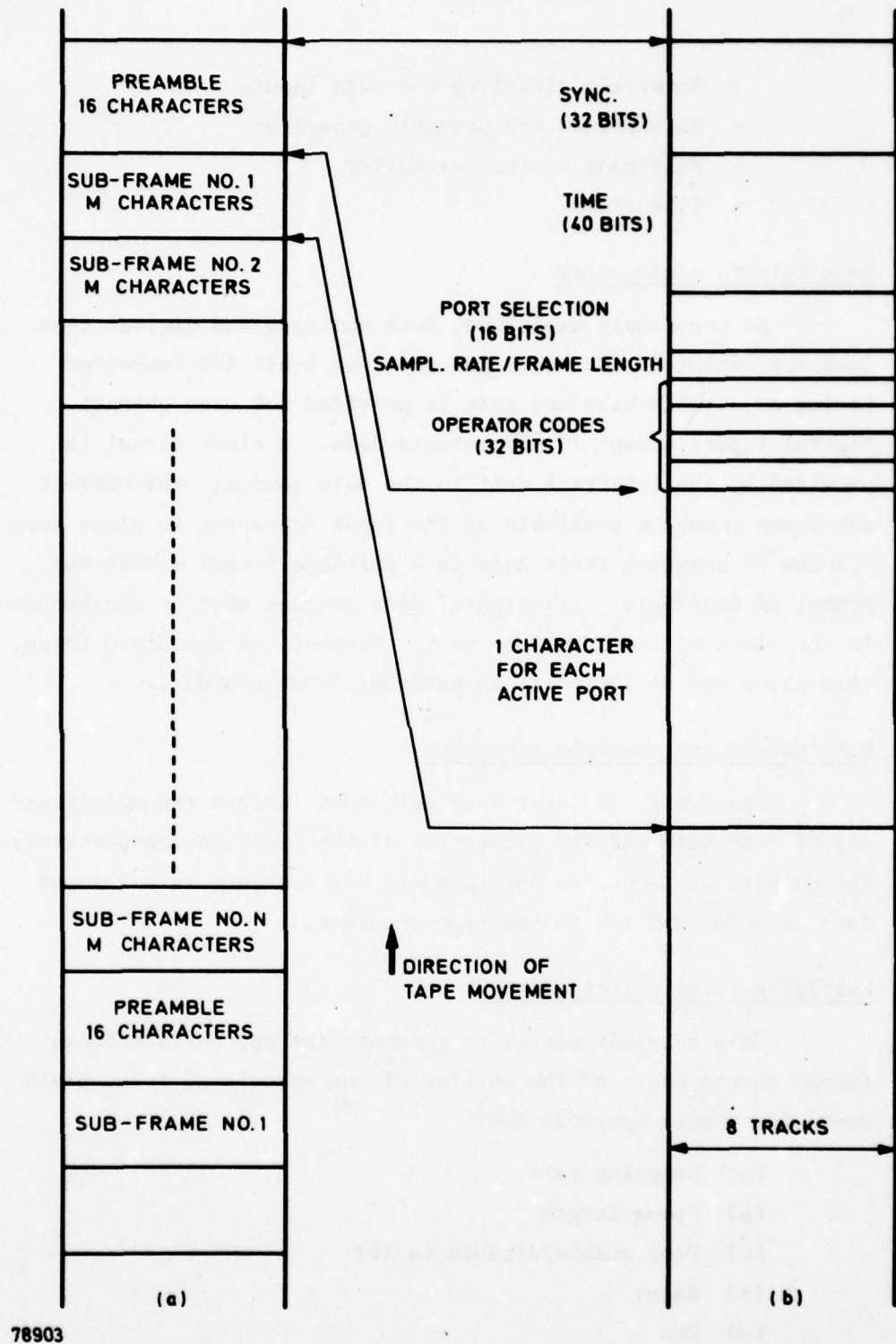


Fig. D1 Tape format

- Interface circuitry for data inputs
- Multiplexer and preamble generator
- Multiplex control circuitry
- Time clock.

Data interface circuitry

As previously explained, both analogue and digital test data are accepted. For analogue data, an 8-bit A/D converter having adjustable bias and gain is provided for each channel. Digital inputs accept TTL-compatible data. A clock signal is provided by the interface unit to the data source; the current sub-frame count is available at the input connector to allow data sources to sequence their data in a suitable format within the frame, if desirable. All digital data sources must be synchronized to the clock of the interface unit. However, as explained below, this clock can be locked to an external 5-MHz standard.

Multiplexer and preamble generator

Two 8-bit, 16-input data selectors perform the multiplexing of test data and the generation of the preamble, respectively. The outputs of these two multiplexers are combined in a 2-input data selector and fed to the tape recorder.

Multiplexer control circuitry

This sub-unit serves to generate the appropriate frame format on the basis of the setting of the associated front plate controls. These controls are:

- (a) Sampling rate
- (b) Frame length
- (c) Port enable/disable (x 16)
- (d) Reset
- (e) Run
- (f) Hold
- (g) Record single frame.

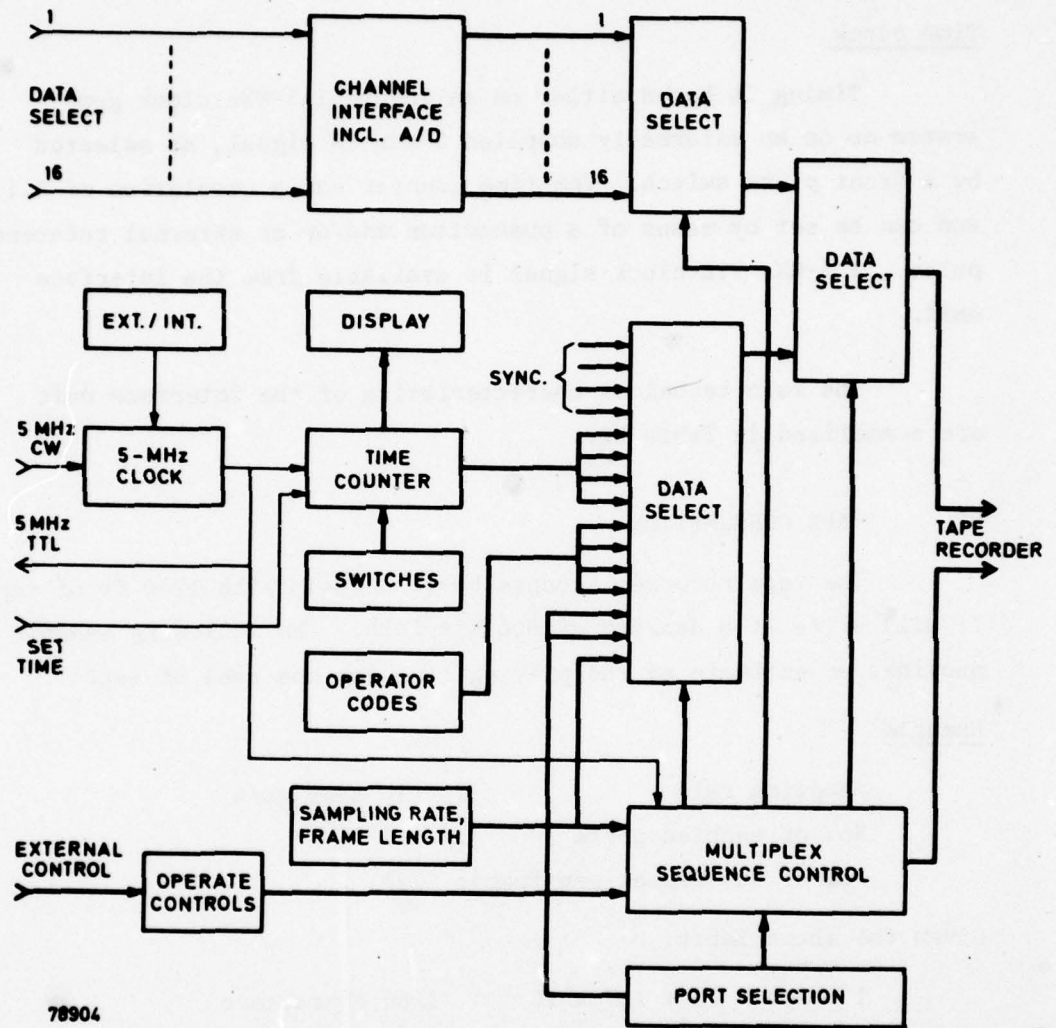


Fig. D2 Tape recorder interface unit

Remote control is possible for the four operating controls (d) through (g).

Time clock

Timing is based either on an internal 5-MHz clock generator or on an externally supplied 5-MHz CW signal, as selected by a front plate switch. The time counter has a resolution of 0.1 s and can be set by means of a pushbutton and/or an external reference pulse. A 5-MHz TTL clock signal is available from the interface unit.

The main technical characteristics of the interface unit are summarized in Table D2.

D7 TAPE CONSUMPTION

The tape recorder accepts 8 $\frac{1}{2}$ -inch reels with 1200 ft of tape. It will write at a density of 800 bit/inch. The following example provides an estimate of the playing time for one reel of tape:

Example

Sampling rate	:	10 samples/s
No. of enabled ports	:	10
No. of sub-frames per frame:		127

Given the above facts:

1 frame = 16 + 127 x 10	=	1286 characters
Frame repetition rate	=	10/127 frames/s
Length of tape per frame	=	1286/800 = 1.6075 in
Inter-record gap	=	0.6 inch
Average tape consumption per second	=	10 x (1.6075 + 0.6)/127 = 0.174
Playing time for 1200 ft	=	1200 x 12/(0.174 x 3600) hours = 23 hours

This example demonstrates that a full day's measurements can be stored on a single reel of tape.

APPENDIX E

CCIR TROPOSCATTER PATH LOSS PREDICTIONS

E1 GENERAL

The predictions outlined in this appendix are based upon CCIR Report 244-2, New Delhi, 1970, the notation of which is used in the following calculations. Climate type 6 (continental temperate) with $N_s = 320$ is assumed for both test links.

E2 C-BAND TEST LINK

To evaluate the annual median transmission loss (Section 2 of Ref. 5), the following parameters are obtained from the link characteristics given in Chapter 2 of the main text:

$$\begin{aligned} f &= 4500 \text{ MHz} \\ d &= 170 \text{ km} \\ h_{te} &= 36 \text{ m} \\ h_{re} &= 1370 \text{ m} \\ \theta &= 3.24 \text{ mrad} \\ G_t + G_r &= 81 \text{ dB} \end{aligned}$$

The effective antenna heights, h_{te} and h_{re} , above the foreground terrain have been estimated from the path profile. From these estimates, the effective distance (as defined in Ref. 5) is found to be 86.7 km. The two correction terms required in the path loss calculation are $V(d_e) = 0 \text{ dB}$ and $F(\theta d) = 126 \text{ dB}$. A significant uncertainty arises from the estimate of aperture-to-medium coupling loss: while the value given in Chapter 2 is only 0.3 dB, the CCIR prediction is 6 dB. In the following, aperture-to-medium

coupling loss for this link has been neglected. The annual median transmission loss is then found to be:

$$\begin{aligned} L(50) &= 30 \log f - 20 \log d + F(\theta d) - G_p - V(d_e) \\ &= 109.6 - 44.6 + 126 - 81 - 0 = 110 \text{ dB} \end{aligned}$$

The long-term variability of path loss is estimated by the procedure given in Section 4 of Ref. 5. For $g(f) = 1.0$, the departures from the median path loss are found to be:

$$\begin{array}{ll} Y(1\%) &= 10 \text{ dB} & Y(99\%) &= -7 \text{ dB} \\ Y(0.01\%) &= 20 \text{ dB} & Y(99.9\%) &= -11 \text{ dB} \end{array}$$

The predicted annual RSL distribution, corresponding to a nominal transmit power of 1 kW, is shown in Fig. E1. The median RSL is determined as follows:

$$\begin{aligned} \text{Median RSL (dBm)} &= \text{Tx power (dB)} - \text{Feeder loss (dB)} \\ &\quad - \text{Median path loss (dB)} \end{aligned}$$

From Section 5 of CCIR Report 238-2, the transmission loss not exceeded for 99% of the worst month is determined to be 14 dB higher than the annual value.

The standard error of prediction is indicated on Fig. E1 as determined from the relation

$$\sigma(q) = \sqrt{13 + 0.12Y^2(q)} \text{ dB}$$

where q is the percentage of time.

Note that if the CCIR prediction of aperture-to-medium coupling loss is used, the RSL distribution shown in Fig. E1 is shifted down by 6 dB.

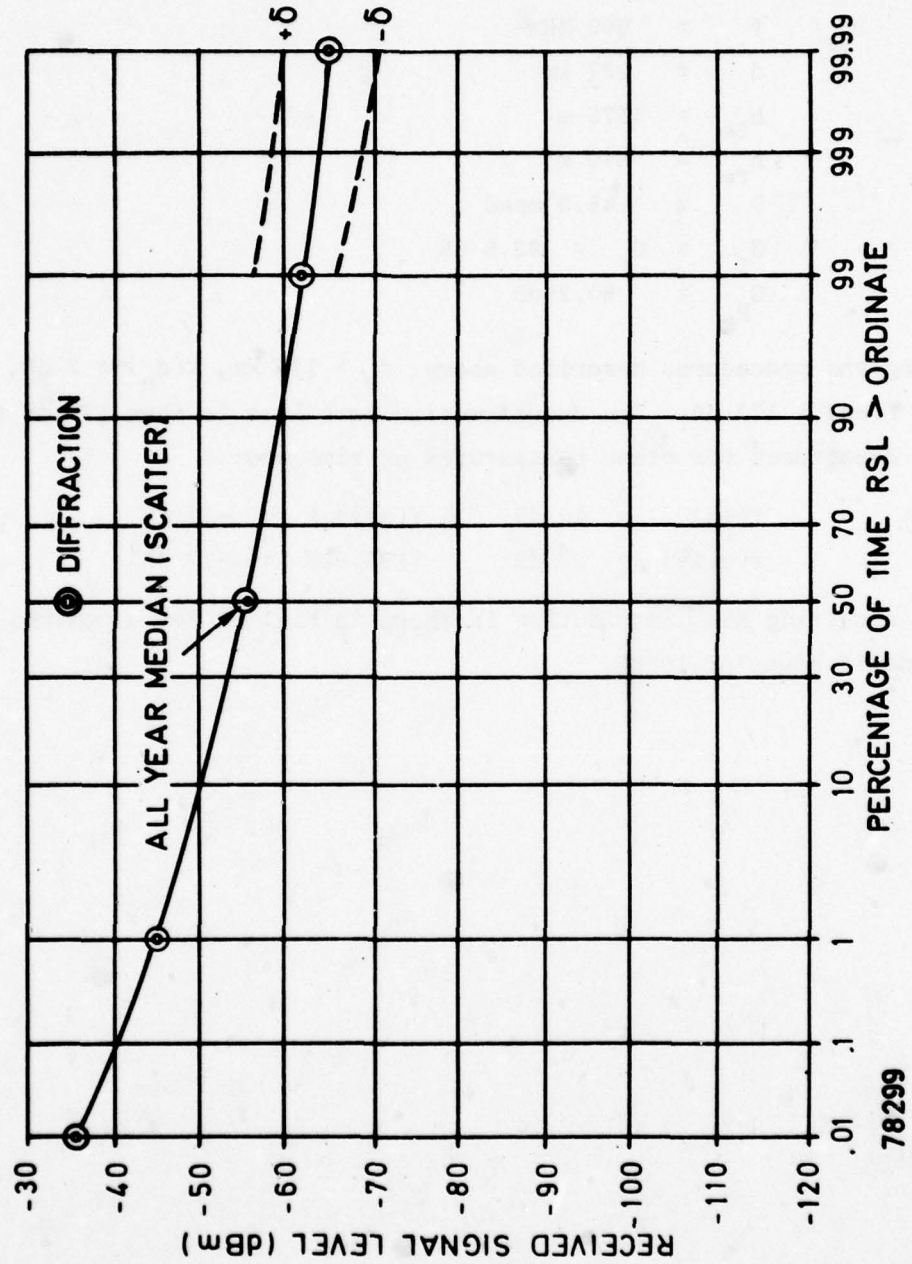


Fig. E1 CCIR prediction of path loss for link ABHZ-AFEZ; nominal transmit power of 1 kW

E3 UHF TEST LINK

The parameters used for the UHF link are:

$f = 900 \text{ MHz}$
 $d = 287 \text{ km}$
 $h_{te} = 1575 \text{ m}$
 $h_{re} = 870 \text{ m}$
 $\theta = 45.3 \text{ mrad}$
 $G_t = G_r = 92.6 \text{ dB}$
 $G_p = 80.2 \text{ dB}$

Using the procedures described above, $d_e = 115 \text{ km}$, $V(d_e) = 2 \text{ dB}$, and $F(\theta d) = 172 \text{ dB}$. The annual median path loss is then 129 dB and the departures for other percentages of time are:

$Y(1\%) = 16 \text{ dB}$ $Y(99\%) = -11 \text{ dB}$
 $Y(0.1\%) = 27 \text{ dB}$ $Y(99.9\%) = -17 \text{ dB}$

The resulting RSL distribution is shown in Fig. E2 for a nominal transmit power of 10 kW .

E3 UHF TEST LINK

The parameters used for the UHF link are:

$f = 900 \text{ MHz}$
 $d = 287 \text{ km}$
 $h_{te} = 1575 \text{ m}$
 $h_{re} = 870 \text{ m}$
 $\theta = 45.3 \text{ mrad}$
 $G_t = G_r = 92.6 \text{ dB}$
 $G_p = 80.2 \text{ dB}$

Using the procedures described above, $d_e = 115 \text{ km}$, $V(d_e) = 2 \text{ dB}$, and $F(\theta d) = 172 \text{ dB}$. The annual median path loss is then 129 dB and the departures for other percentages of time are:

$Y(1\%) = 16 \text{ dB}$ $Y(99\%) = -11 \text{ dB}$
 $Y(0.1\%) = 27 \text{ dB}$ $Y(99.9\%) = -17 \text{ dB}$

The resulting RSL distribution is shown in Fig. E2 for a nominal transmit power of 10 kW .

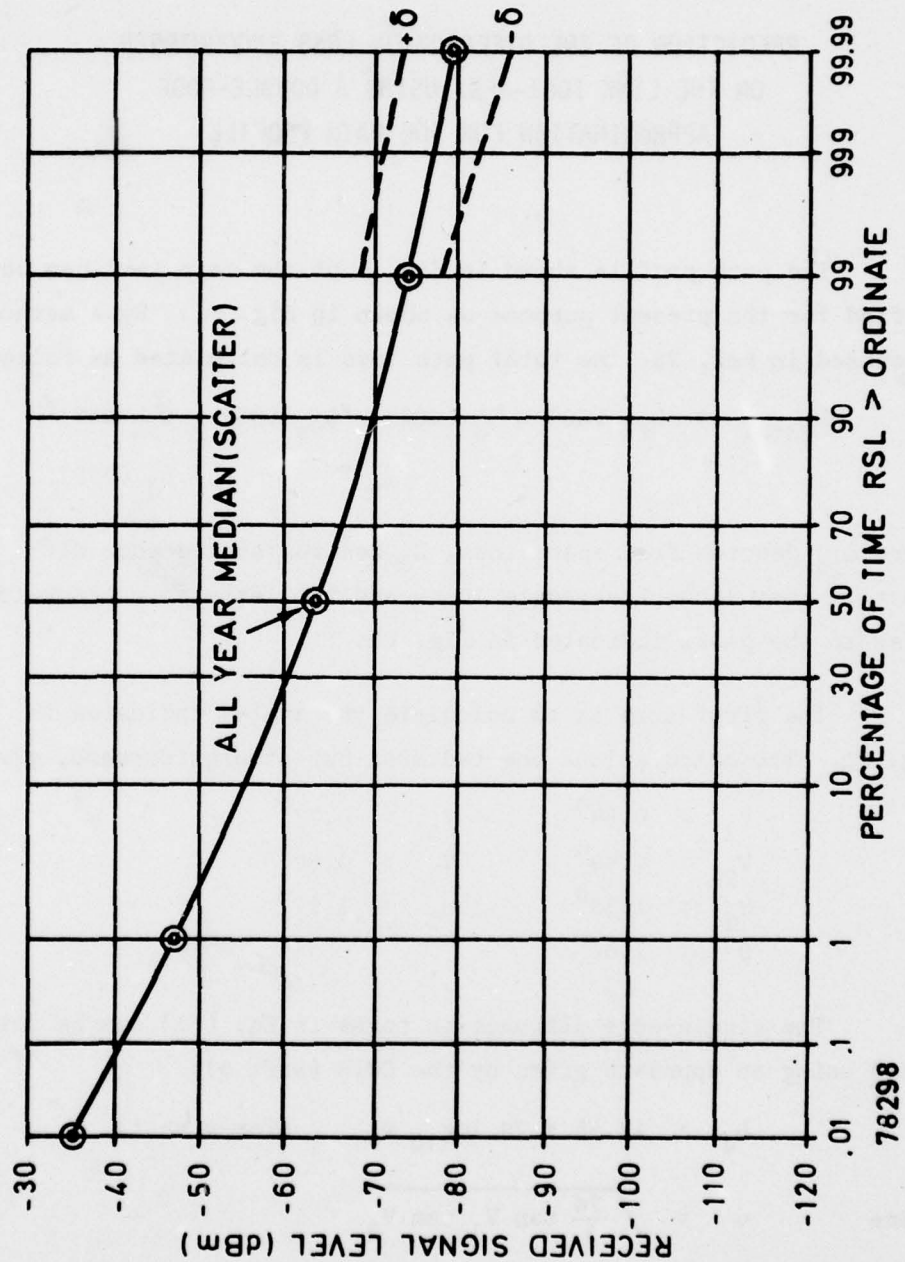


Fig. E2 CCIR prediction of path loss for link IDGZ-AFEZ; nominal transmit power of 10 kW

APPENDIX F

PREDICTION OF THE DIFFRACTION LOSS ENCOUNTERED
ON THE LINK IDGZ-AFEZ USING A DOUBLE-EDGE
APPROXIMATION FOR THE PATH PROFILE

The path profile shown in Fig. 4 of the main text can be simplified for the present purpose as shown in Fig. F1. By a method discussed in Ref. 23, the total path loss is calculated as follows:

$$L_{\text{total}} = L_{\text{fs}}(\text{AC}) + L_{\text{d}}(\text{ABC}) - L_{\text{fs}}(\text{BC}) + L_{\text{fs}}(\text{BD}) + L_{\text{d}}(\text{BCD}) \quad (\text{F1})$$

where L_{fs} denotes free space loss, L_{d} denotes single-edge diffraction loss above free space loss, and the letters in brackets refer to the peaks indicated in Fig. F1.

The first step is to calculate the angles indicated in Fig. F1. The calculations are tedious, but straightforward, giving:

$$\begin{aligned} V_1 &= 0.84^\circ & V_3 &= 0.77^\circ \\ V_2 &= 0.49^\circ & V_4 &= 0.50^\circ \\ U_1 &= 1.33^\circ & U_2 &= 1.27^\circ \\ \theta &= 2.60^\circ \end{aligned} \quad (\text{F2})$$

The single-edge diffraction terms in Eq. (F1) can be determined using an approach given by the CCIR (Ref. 5):

$$L_{\text{d}} = 12.95 + 20 \log_{10} v \quad (\text{for } v \gg 1) \quad (\text{F3})$$

where $v = \sqrt{\frac{2d}{\lambda} \tan V_1 \tan V_2}$

d is the total distance of the single-edge path considered

λ is the wavelength.

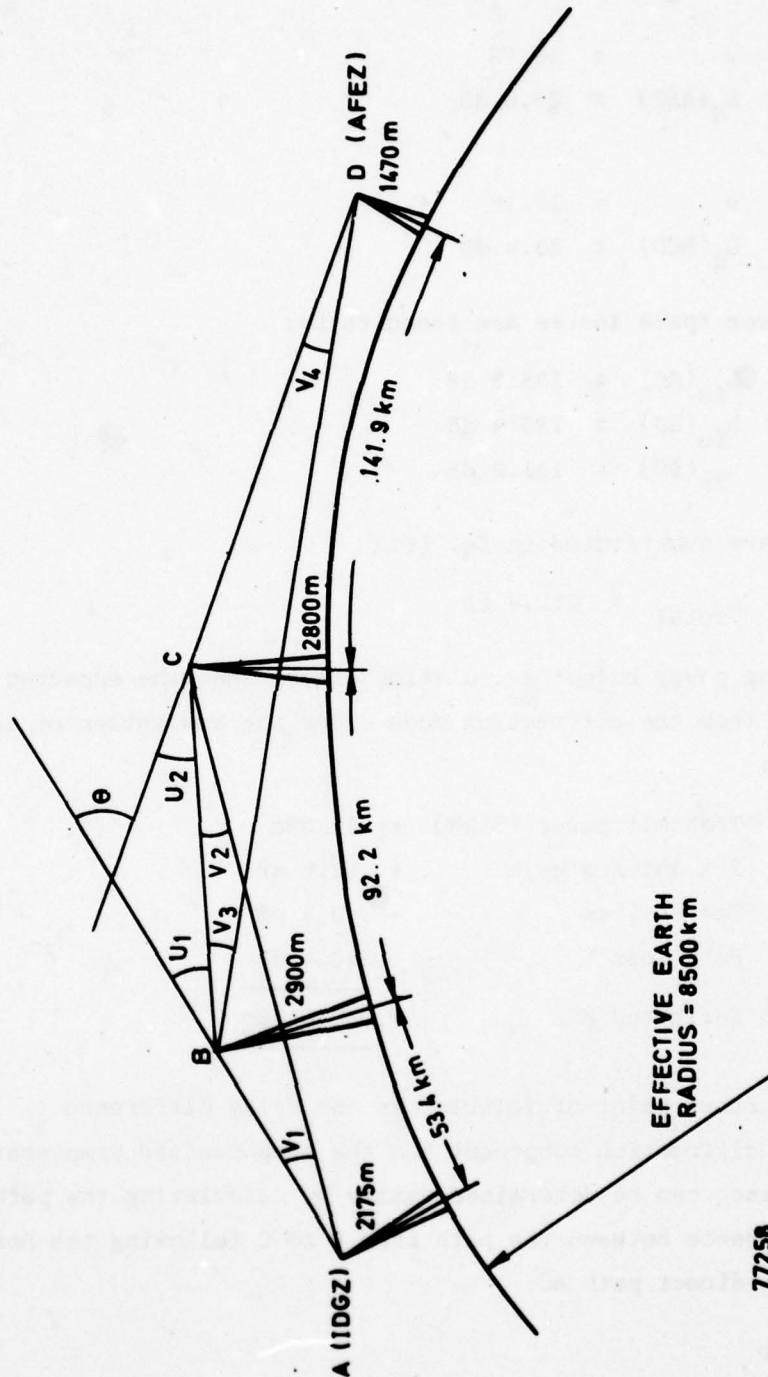


Fig. F1 Double knife-edge path profile approximation for the UHF link

For $L_d(ABC)$ and $L_d(BCD)$ respectively:

$$\begin{aligned} v &= 10.75 \\ L_d(ABC) &= 33.6 \text{ dB} \end{aligned} \quad (F5)$$

and

$$\begin{aligned} v &= 13.18 \\ L_d(BCD) &= 35.4 \text{ dB} \end{aligned} \quad (F6)$$

The three free space losses are found to be:

$$\begin{aligned} L_{fs}(AC) &= 135.3 \text{ dB} \\ L_{fs}(BD) &= 139.4 \text{ dB} \\ L_{fs}(BC) &= 131.3 \text{ dB} \end{aligned} \quad (F7)$$

when these are substituted in Eq. (F1)

$$L_{total} = 212.4 \text{ dB} \quad (F8)$$

The following power budget calculation establishes the expected RSL at AFEZ from the diffraction mode under the assumption of ideal knife edges:

Transmit power (5 kW)	+	67 dBm	
2 x antenna gain	+	92.6 dB	
Feeder loss	-	3.4 dB	
Path loss	-	212.4 dB	
Estimated RSL	-	56.6 dBm	(F9)

A further point of interest is the delay difference between the diffraction component and the troposcatter component. This difference can be determined easily by calculating the path length difference between the path from B to C following the horizon rays and the direct path BC:

$$\begin{aligned}\Delta \ell &= BC \left[\frac{\cos(U_1 - U_2)/2}{\cos(U_1 + U_2)/2} - 1 \right] \\ &\approx BC 2 \sin(U_1)/2 \sin(U_2)/2 = 23.7 \text{ m}\end{aligned}\quad (F10)$$

So the corresponding path length difference is:

$$t = \frac{\Delta \ell}{c} = \frac{23.7 \text{ m}}{3.10^8 \text{ m/s}} = 79 \text{ ns}\quad (F11)$$

APPENDIX G

SHORT-TERM DISTRIBUTION OF RSL
FOR A WIDEBAND SIGNAL SUBJECT TO FREQUENCY SELECTIVE FADING

G1 FLAT FADING RAYLEIGH CHANNEL

Consider a signal having an ideal Rayleigh fading envelope with the probability distribution function:

$$P_x(X) = \frac{x}{\sigma^2} \exp\left[-\frac{x^2}{2\sigma^2}\right] U(X) \quad (G1)$$

where $U(X)$ is the unit step function,

$$U(X) = \begin{cases} 0 & x < 0 \\ 1 & x \geq 0 \end{cases} \quad (G2)$$

The power of the signal, $Z = X^2$, has an exponential probability distribution,

$$P_z(Z) = \frac{1}{2\sigma^2} \exp\left(-\frac{Z}{2\sigma^2}\right) U(Z) \quad (G3)$$

From (G3) it follows directly that,

$$E(Z) = 2\sigma^2 \quad (G4)$$

$$\text{Var}(Z) = 4\sigma^4 \quad (G5)$$

$$\text{and Median}(Z) = 2\sigma^2 \ln 2 \approx 0.693E(z) \quad (G6)$$

Equations (G4) and (G5) show that the standard deviation of the power equals the mean power, while (G4) and (G6) establish the well-known result that the median power is smaller than the mean power by a factor of 0.693 or approximately 1.6 dB.

Y is defined to be the power expressed in decibels, i.e.,

$$Y = 10 \log_{10} Z \quad (G7)$$

The distribution of Y is easily shown to be:

$$P_Y(Y) = \frac{\ln 10}{20} \frac{Z}{\sigma^2} \exp\left(-\frac{Z}{2\sigma^2}\right) \quad (G8)$$

where Z is given by the inverse of (G7). This distribution is plotted in Fig. G1. A feeling for the dynamic range of the distribution can be obtained from observing that the difference between the 10% and 90% percentiles is 13.4 dB.

G2 FREQUENCY SELECTIVE FADING

Assume for simplicity that the power of a wideband signal subject to frequency selective fading can be represented by the sum of the powers of η independent, Rayleigh-fading signal components of equal powers. In precise terms, (η) is the ratio of signal bandwidth to channel correlation bandwidth. The channel correlation bandwidth, Ω_c , is related to the 2σ dispersion, δ_s , since the frequency correlation function and the delay power spectrum are Fourier duals. Thus, given a value of δ_s , which can be calculated from the delay power spectra itself, an estimate of Ω_c can be obtained from:

$$\Omega_c \approx \sqrt{\frac{2}{\pi}} \cdot \frac{1}{\delta_s} \quad (G9)$$

Figure G2 shows exact calculations of Ω_c and δ_s based on the modified Bellow model with the approximate relationship given in (G9). Based on (G3) and (G9), the probability distribution of the total power, Z, of a frequency selective fading signal can be shown to be:

$$P_Z(Z) = A Z_s^{\eta-1} \exp\left[-\frac{Z_s}{2\sigma^2}\right] U(Z) \quad (G10)$$

where

$$A = \frac{1}{(2\sigma^2)^\eta \Gamma(\eta)} \quad \text{and} \quad Z_s = \frac{Z}{\eta}$$

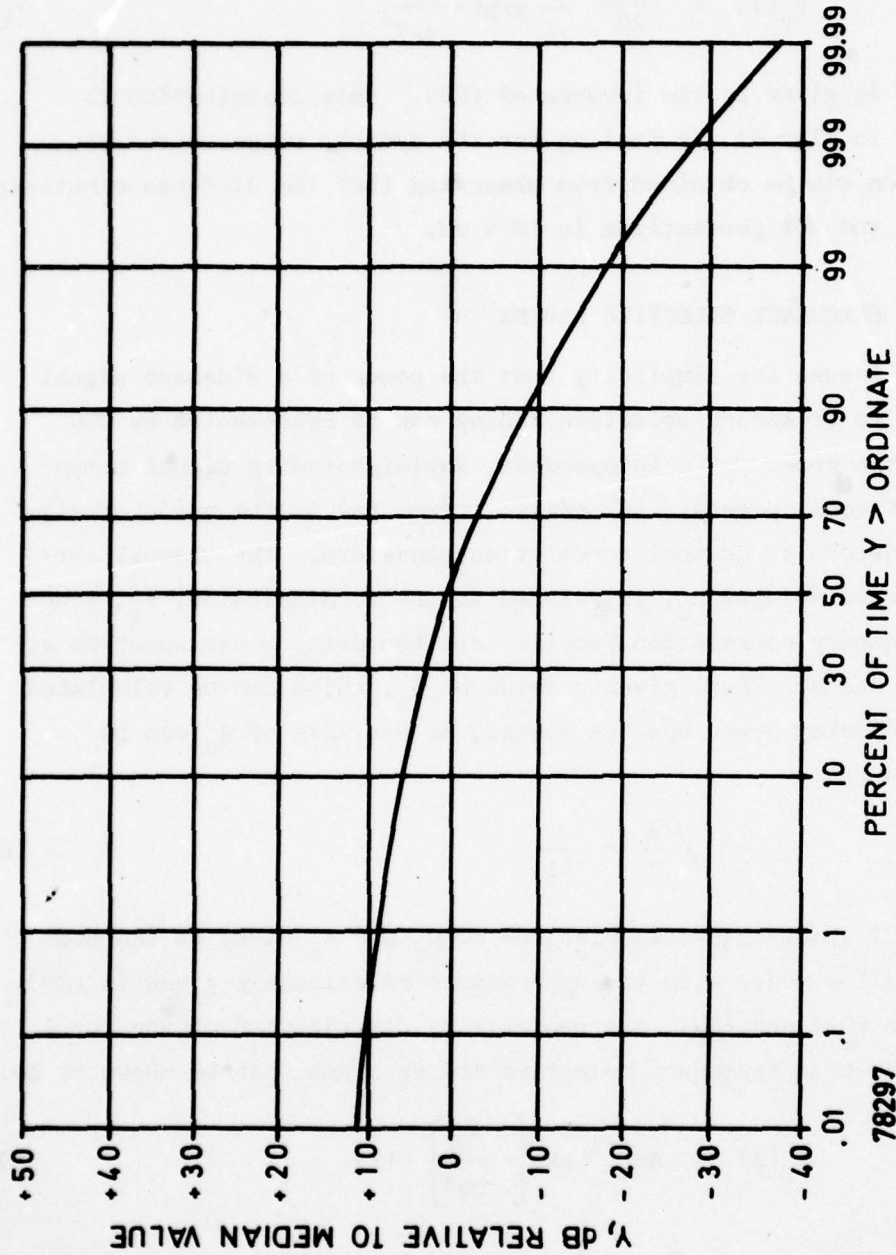
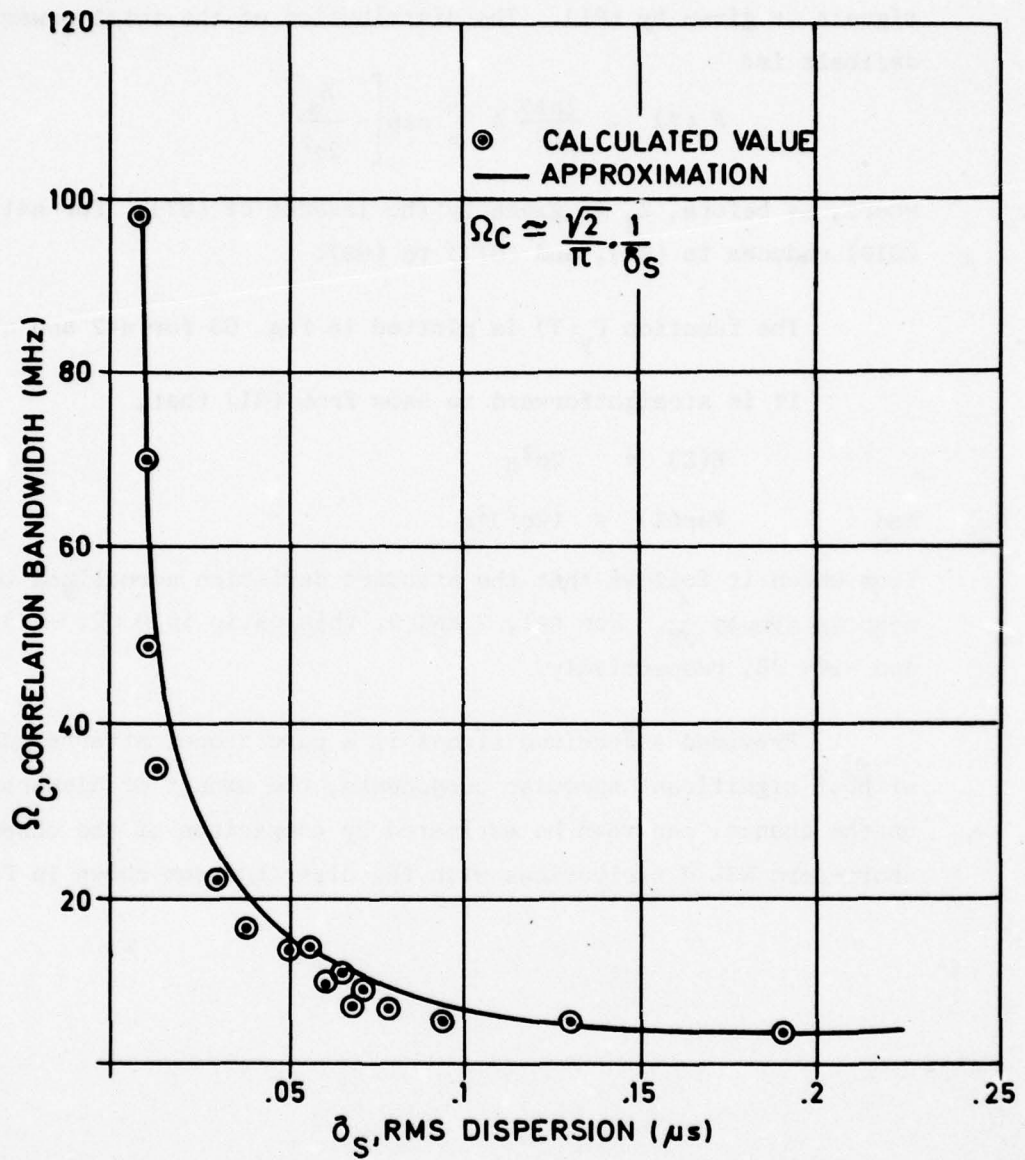


Fig. G1 Rayleigh distribution



78302

Fig. G2 Relationship between multipath dispersion and correlation bandwidth

Note that σ^2 is the variance associated with each of the component signals as given by (G1). The distribution of the total power in decibels is:

$$P_y(Y) = \frac{\ln 10}{10} A Z_s^\eta \exp \left[-\frac{Z_s}{2\sigma^2} \right] \quad (G12)$$

where, as before, Z_s is given by the inverse of (G7). For $\eta=1$, (G10) reduces to (G3), and (G11) to (G8).

The function $F_y(Y)$ is plotted in Fig. G3 for $\eta=2$ and $\eta=3$.

It is straightforward to show from (G1) that,

$$E(Z) = 2\sigma^2\eta$$

and
$$\text{Var}(Z) = (2\sigma^2)^2\eta$$

from which it follows that the standard deviation normalized to the mean is simply $\frac{1}{\sqrt{\eta}}$. For $\eta=1, 2$ and 3 , this ratio is 0 dB, -1.5 dB, and -2.4 dB, respectively.

Provided a received signal is a pure troposcatter signal without significant specular components, the amount of dispersion on the channel can then be estimated by comparison of the observed short-term RSL distributions with the distributions shown in Fig. G3.

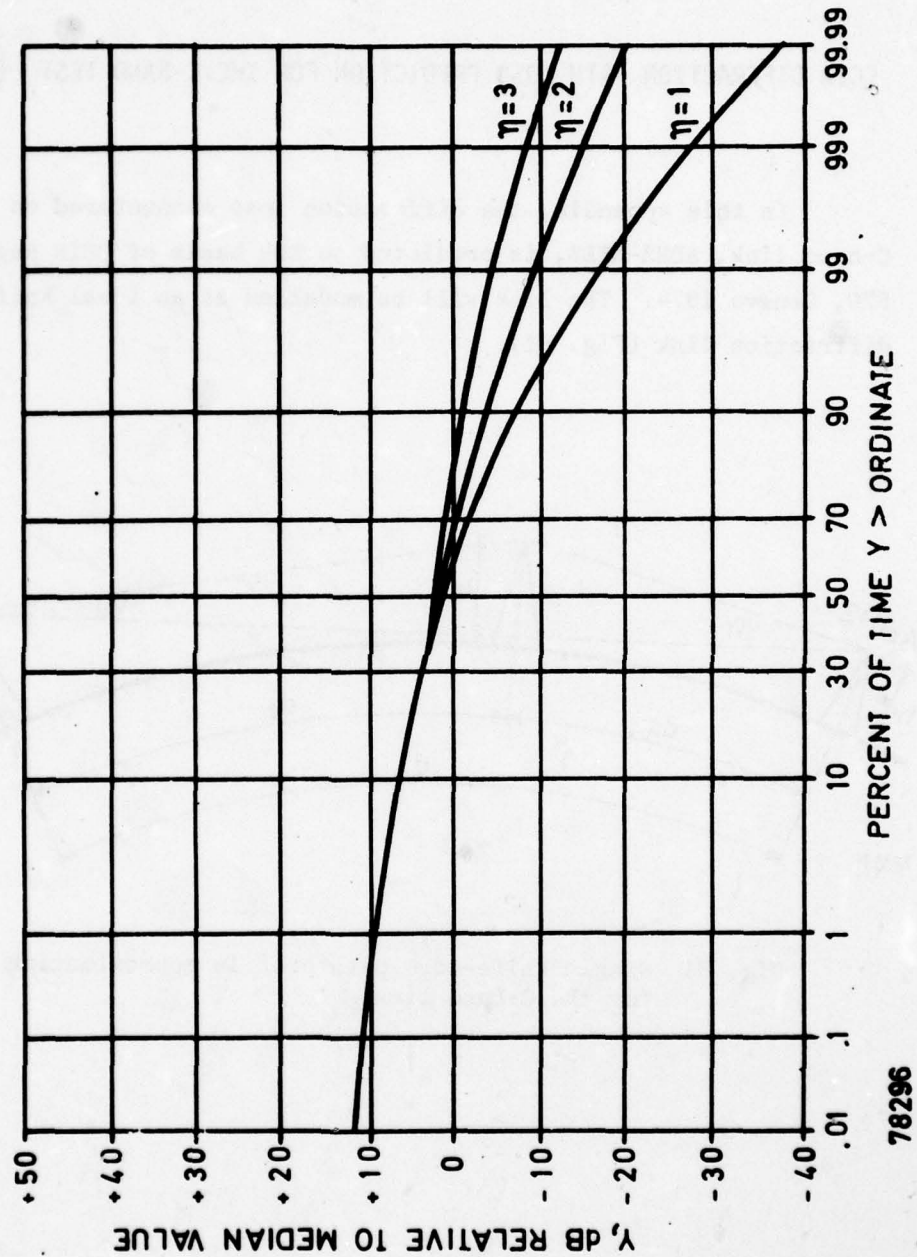


Fig. G3 Signal distribution for different orders of diversity

APPENDIX H

CCIR DIFFRACTION PATH LOSS PREDICTION FOR THE C-BAND TEST LINK

In this appendix, the diffraction loss encountered on the C-band link, ABHZ-AFEZ, is predicted on the basis of CCIR Report 570, Geneva 1974. The link will be modelled as an ideal knife-edge diffraction link (Fig. H1).

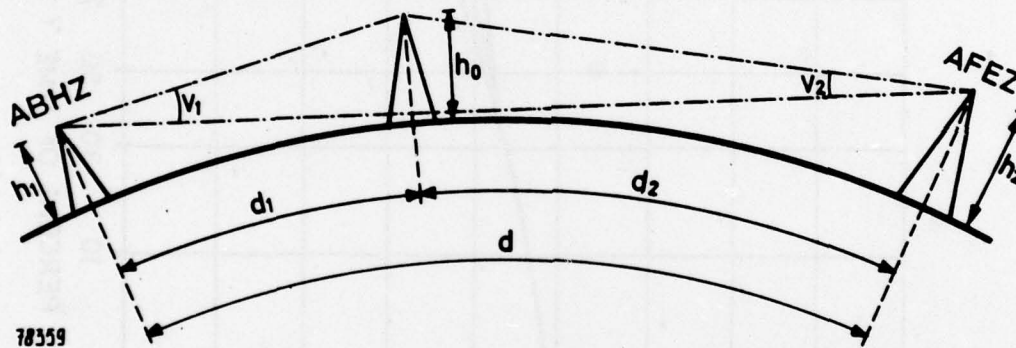


Fig. H1 Single knife-edge path profile approximation for the C-band link

The pertinent link parameters are taken from Chapter 2 of the main text:

$$\begin{aligned}d_1 &= 43.2 \text{ km} \\d_2 &= 127 \text{ km} \\h_1 &= 459 \text{ m} \\h_2 &= 1470 \text{ m} \\u_1 &= -1.57 \text{ mrad} \\u_2 &= -14.2 \text{ mrad}\end{aligned}$$

where u_1 and u_2 are the horizon angles. The angles v_1 and v_2 are determined as follows:

$$v_1 = u_1 + \left[\frac{h_1 + h_2}{d} + \frac{d}{2a} \right] = 2.48 \text{ mrad}$$

$$v_2 = u_2 + \left[\frac{h_1 - h_2}{d} + \frac{d}{2a} \right] = 0.77 \text{ mrad}$$

where a is the effective earth radius, 8500 km. The variable v , defined in Report 570, becomes

$$\sqrt{\frac{2d}{\lambda} \tan v_1 \tan v_2} = 3.18$$

from which the resulting basic transmission loss is 173 dB. The corresponding RSL value is shown in Fig. E1, together with the troposcatter predictions.

APPENDIX I

ON THE SEPARATION OF A RICE-FADING CHANNEL
INTO A RAYLEIGH-FADING AND A NON-FADING COMPONENT

This appendix derives a relationship that permits the power ratio between the non-fading and the Rayleigh-fading components of a Rician-fading signal to be determined given a knowledge of the ratio of standard deviation to the mean of the composite signal.

The output signal of a Rician channel may be thought of as consisting of two quadrature Gaussian signals plus a constant signal which for convenience may be taken to be in phase with one of the Gaussian components (Ref. 17). If the two quadrature components of the Rician signal are denoted X_1 and X_2 , it follows that X_1 and X_2 are independent random variables with density functions:

$$f_1(X_1) = \frac{1}{\sigma\sqrt{2\pi}} \exp\left[-\frac{X_1^2}{2\sigma^2}\right] \quad (I1)$$

$$f_2(X_2) = \frac{1}{\sigma\sqrt{2\pi}} \exp\left[-\frac{(X_2-m)^2}{2\sigma^2}\right] \quad (I2)$$

where it can be assumed without loss of generality that $m \geq 0$.

The powers of the two quadrature signals, defined as $Z_1 = X_1^2$ and $Z_2 = X_2^2$, are also statistically independent random variables. The total output power of the Rician channel is $Z = Z_1 + Z_2$.

By simple transformations, the density functions for Z_1 and Z_2 can be shown to be:

$$P_1(Z_1) = \frac{1}{\sigma\sqrt{2\pi Z_1}} \exp\left(-\frac{Z_1}{2\sigma^2}\right) U(Z_1) \quad (I3)$$

$$P_2(Z_2) = \frac{1}{2\sigma\sqrt{2\pi}Z_2} \left[\exp\left(-\frac{(\sqrt{Z_2}-m)^2}{2\sigma^2}\right) + \exp\left(-\frac{(\sqrt{Z_2}+m)^2}{2\sigma^2}\right) \right] U(Z_2) \quad (I4)$$

where $U(Z)$ is the unit step function,

$$U(Z) = \begin{cases} 0 & Z \leq 0 \\ 1 & Z > 0 \end{cases} \quad (I5)$$

From (I3), it is easy to show that

$$E\{Z_1\} = \sigma^2 \quad (I6)$$

$$\text{Var}\{Z_1\} = 2\sigma^4 \quad (I7)$$

The same results follow as special cases of the following calculations for Z_2 .

The evaluation of the moments of Z_2 involves the following integral:

$$I = \int_0^\infty \frac{Z^n}{2\sigma\sqrt{2\pi}Z} \left[\exp\left(-\frac{(\sqrt{Z}-m)^2}{2\sigma^2}\right) + \exp\left(-\frac{(\sqrt{Z}+m)^2}{2\sigma^2}\right) \right] dZ \quad (I8)$$

which, after the substitution $t = \sqrt{Z}$, becomes

$$\begin{aligned} I &= \int_0^\infty \frac{t^{2n}}{\sigma\sqrt{2\pi}} \left[\exp\left(-\frac{(t-m)^2}{2\sigma^2}\right) + \exp\left(-\frac{(t+m)^2}{2\sigma^2}\right) \right] dt \\ &= \int_0^\infty \frac{t^{2n}}{\sigma\sqrt{2\pi}} \exp\left(-\frac{(t-m)^2}{2\sigma^2}\right) dt \\ &\quad + \int_m^\infty \frac{t^{2n}}{\sigma\sqrt{2\pi}} \exp\left(-\frac{(t-m)^2}{2\sigma^2}\right) dt \\ &\quad + \int_0^\infty \frac{t^{2n}}{\sigma\sqrt{2\pi}} \exp\left(-\frac{(t+m)^2}{2\sigma^2}\right) dt \end{aligned} \quad (I9)$$

After another substitution in which the arguments of the exponentials are denoted $-u$, the following expression results:

$$I = \int_0^{\infty} \frac{(m + \sqrt{2\sigma^2 u})^{2n} + (m - \sqrt{2\sigma^2 u})^{2n}}{2\sqrt{\pi}\sqrt{u}} du \quad (I10)$$

This integral is easy to evaluate for n equal to 1 and 2. The results are:

$$\begin{aligned} n &= 1: \\ E\{Z_2\} &= m^2 + \sigma^2 \end{aligned} \quad (I11)$$

$$\begin{aligned} n &= 2: \\ E\{Z_2^2\} &= m^4 + 6m^2\sigma^2 + 3\sigma^4 \end{aligned} \quad (I11)$$

so that

$$\text{Var}\{Z_2\} = 2\sigma^4 + 4m^2\sigma^2 \quad (I13)$$

Since Z_1 and Z_2 are independent, the mean and variance of Z are simply:

$$E\{Z\} = E\{Z_1\} + E\{Z_2\} = 2\sigma^2 + m^2 \quad (I14)$$

$$\text{Var}\{Z\} = \text{Var}\{Z_1\} + \text{Var}\{Z_2\} = 4\sigma^4 + 4m^2\sigma^2 \quad (I15)$$

The ratio $\frac{1}{R}$ of standard deviation to mean of the Rician signal is therefore

$$\frac{1}{R} = \frac{2\sigma\sqrt{m^2 + \sigma^2}}{2\sigma^2 + m^2} \quad (I16)$$

$$\text{or} \quad \frac{1}{R} = \frac{\sqrt{1+2y}}{1+y} \quad (I17)$$

$$\text{where} \quad y = \frac{m^2}{2\sigma^2} \quad (I18)$$

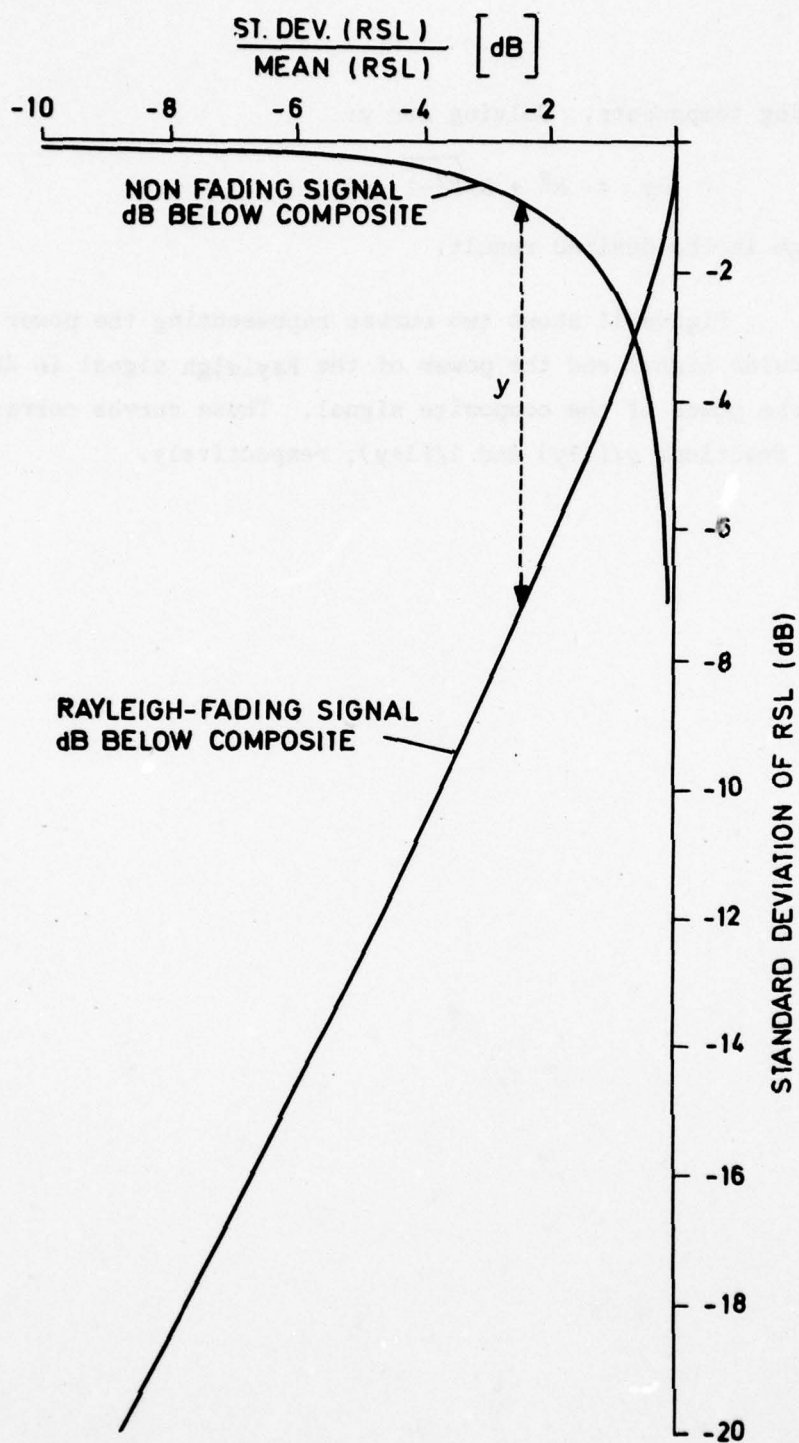
is the desired power ratio between the non-fading and the Rayleigh-

fading components. Solving for y:

$$y = R^2 + R\sqrt{R^2 - 1} - 1 \quad (I19)$$

which is the desired result.

Figure 11 shows two curves representing the power of the specular signal and the power of the Rayleigh signal in dB relative to the power of the composite signal. These curves correspond to the fractions $y/(1+y)$ and $1/(1+y)$, respectively.



78301

Fig. 11 Separation of scatter and specular components

APPENDIX J

MULTIPATH DISPERSION FOR MIXED-MODE PROPAGATION

On the UHF link the received signal was composed of a scatter component and a specular component. The path delay difference, τ , between the two components has been shown to be 79 ns (see Appendix F).

The multipath dispersion, δ_s , (2σ value of the delay power spectrum) for the combined signal depends on the ratio of specular to scatter component. δ_s can be calculated, if a particular shape of the delay power spectrum is assumed for the scatter signal.

The delay power spectrum $D(x)$, predicted by the Bello model can be closely approximated by:

$$D(x) = \frac{2x}{\sigma^2} \exp(-\sqrt{2}x/\sigma) \quad (J1)$$

where 2σ is the multipath dispersion of the scatter signal.

The mean m of x is given by:

$$m = \int_0^{\infty} \frac{2x^2}{\sigma^2} \exp(-\sqrt{2}x/\sigma) dx = \sqrt{2} \sigma \quad (J2)$$

The delay power spectrum, $D_c(x)$, of the combined signal is composed of $D(x)$ multiplied by the power, P_{sc} , of the scatter signal and a delta function at $x = -\tau$ with the power, P_{sp} , of the specular component (with $P_{sc} + P_{sp} = 1$).

The mean, m_c , and the standard deviation, σ_c , are then given by:

$$m_c = P_{sc} m - P_{sp} \tau \quad (J3)$$

$$\sigma_c^2 = P_{sc}(\sigma^2 + m^2) + P_{sp}\tau^2 - m_c^2 \quad (J4)$$

The combination of Eq. (J3) and (J4) gives:

$$\sigma_c^2 = \sigma^2(1+2P_{sp})P_{sc} + 2\sqrt{2} \sigma \tau P_{sp} P_{sc} + \tau^2 P_{sc} P_{sc} \quad (J5)$$

$$\text{Let } y = P_{sp}/P_{sc} \quad (J6)$$

$$\text{then } P_{sp} = y/(1+y) \quad (J7)$$

$$P_{sc} = 1/(1+y) \quad (J7)$$

With these values for the specular and the scatter components, σ_c^2 becomes:

$$\sigma_c^2 = \frac{1}{(1+y)^2} \{ (1+3y)\sigma^2 + 2\sqrt{2} \sigma \tau y + \tau^2 y \} \quad (J8)$$

The multipath dispersion, $\delta_c = 2\sigma_c$, has been calculated for the range of multipath dispersion expected on the UHF-link and is shown in Fig. J1.

It can be seen that the maximum increase in multipath dispersion caused by the specular component is about 70 ns. As expected, the multipath dispersion of the combined signal is actually less than that of the scatter component for large ratios of P_{sp}/P_{sc} .

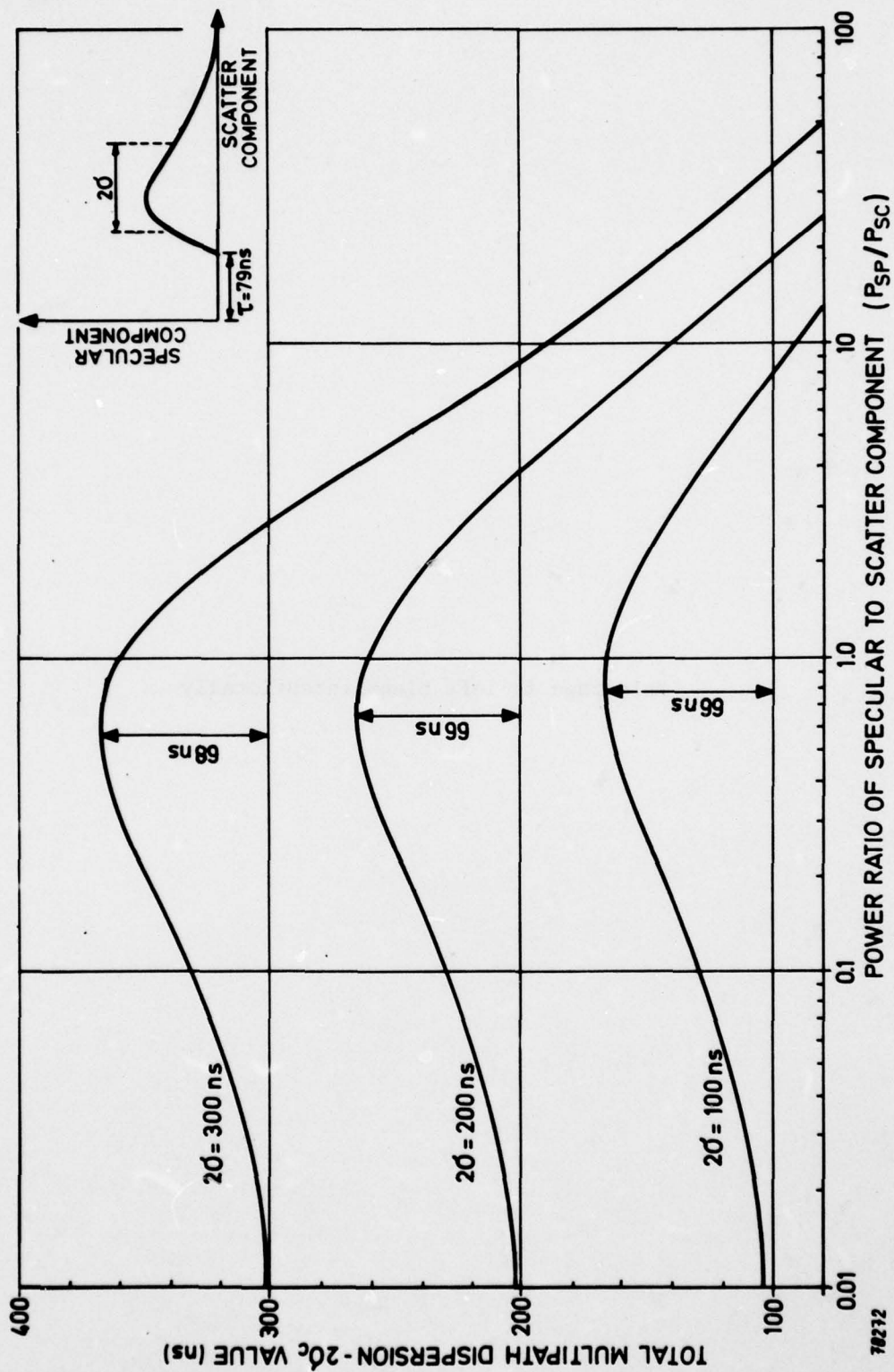


Fig. J1 Multipath dispersion for mixed mode propagation

This page is left blank intentionally

REFERENCES

1. P.T. Nielsen, J.L. Osterholz, "A test plan for the combined US/NATO digital troposcatter tests over ACE High", STC Consultant Report CR-NICS-23, October 1976 (NATO Unclassified)
2. K.W. Kirk, J.L. Osterholz, "DCS digital transmission system performance", DCEC Technical Report No. 12-76, November 1976
3. Sylvania Electronic Systems, "Troposcatter multipath analyzer", RADC-TR-70-155, August 1970
4. P.L. Rice, et al., "Transmission loss predictions for tropospheric communications systems", NBS 101 Vol. 1 & 2, May 1965
5. CCIR Report 224-1, "Estimation of tropospheric-wave transmission loss", Vol. 2, October 1966
6. S.O. Rice, "Statistical fluctuations in radio field strength far beyond the horizon", Proc. IRE Vol. 41, pp. 274-281, February 1953
7. P.A. Bello, "A troposcatter channel model", IEEE Trans. on Communications Technology, Vol. COM.17, No. 2, pp. 130-137, April 1969
8. P. Monsen, et al., "Interim technical report - adaptive antenna control", DAABO 7-76-C-8085, Signatron Inc., pp. 3.1 ff, December 1976
9. P.F. Panter, "Communications system design", New York, McGraw Hill, pp. 390-392, 1973
10. J.L. Osterholz, "Design considerations for digital troposcatter systems", AGARD Symposium on Scatter Communications, 3-5 October 1977
11. Signatron Inc., "Digital troposcatter experiments", RADC-TR-72-350, pp. 11-56, January 1973
12. K. Bullington, "Radio propagation fundamentals", BSTJ, Vol. 36 No. 3
13. A.R. Sherwood, I.A. Fantera, "Multipath measurements over troposcatter paths with application to digital transmission", NTC-75, pp. 28-1 to 28-9, December 1975

14. J. Grosskopf, "Statistische Ermittlung der Krümmungsfaktors K im äquivalenten Erdradius aus Radiosondenaufstiegen", Fernmeldetechnisches Zentralamt der Deutschen Bundespost, Technischer Bericht, Nr. 5528, April 1957
15. A.N. Ince, H.P. Williams, "Final report on UHF/VHF communications for SILK PURSE", STC Technical Report TR-42, October 1964
16. D.T. Gjessing, "Atmospheric structure deduced from forward-scatter wave propagation experiments", Radio-Science, Vol. 4, No. 12, pp. 1195-1201, December 1969
17. S.O. Rice, "Statistical properties of a sine wave plus random noise", BSTJ, Vol. 27, January 1948
18. D.R. Kern, P. Monsen, et al., "Megabit Digital Troposcatter Subsystem (MDTS) - Final Report", page 58, April 1977
19. G.T.E. Sylvania, "Megabit Digital Troposcatter Subsystem (MDTS) Research and Development Report", ECOM-0040-F, July 1976
20. Raytheon Inc., "Hybrid tropo transmission system", RADC-TD-76-250, August 1976
21. P.A. Bello, D. Chase, "A Combined Coding and Modulation Approach for High Speed Transmission over Troposcatter Channels", NTC 75 Conference Record, pp. 28-20 to 28-24, December 1975
22. F.D. Sunde, "Digital troposcatter transmission and modulation theory", BSTS Vol. 43, pp. 143-214, Part 1, January 1964
23. G. Millington, et al., "Double knife-edge diffraction in field strength predictions", Proc. of IEE Vol. 109, Part C No. 16, pp. 419-429, September 1962
24. G L. Turin, "Communications through noise, random-multipath channels", IRE National Convention Record, Part 4, pp. 154-166, March 1956
25. Signatron Inc., "Troposcatter multimode FSK/PSK modem", RADC-TR-70-175, September 1970
26. A. Sherwood, L. Suyemoto, "Multipath measurements over tropo-scatter paths, "Mitre Corp. MTP-170, April 1976

27. M.M. Goutman, "Intersymbol interference as a natural code", IEEE Transactions on Communications, Vol. Com-20, pp. 1033-1038, November-October 1976
28. R.C. Fitting, H. Weber, "Sideband diversity modem for digital transmission", Proceedings of the EASCON '74, pp. 430-433